

# **Synthesis and Characterisation of a New Class of Alkene Polymers Bearing Nucleotide Functionality**

by

**Michael Wilson**

*Thesis  
Submitted to Flinders University  
for the degree of*

**Doctor of Philosophy**

Science and Engineering

December 2020

---

# Table of Contents

Table of Contents .....	ii
Table of Figures.....	xiii
List of Tables.....	xxv
Abstract .....	xxvi
Declaration .....	xxix
Acknowledgements .....	xxx
1 Chapter 1: Introduction and Literature Review.....	1
1.1 Synopsis.....	1
1.2 Nucleotides .....	2
1.2.1 Nucleobases.....	3
1.2.2 Sugar.....	4
1.2.3 Phosphate.....	5
1.2.4 Specific Binding Between Nucleobases.....	6
1.2.4.1 Watson-Crick Binding between Nucleobases.....	7
1.2.5 Non-canonical Binding Between Nucleobases. ....	8
1.2.5.1 G-quartets.....	10
1.2.6 Nucleic Acids .....	11
1.3 Secondary Structures of DNA .....	12
1.3.1 The DNA Double Helix .....	12
1.3.1.1 $\pi$ - $\pi$ stacking of nucleobases within dsDNA.....	13

1.3.2	Forms of the DNA Double Helix .....	14
1.3.3	G-quadruplexes .....	18
1.3.4	Nucleic Acid Wires .....	20
1.3.5	Xeno Nucleic Acids.....	22
1.4	Synthesis of DNA .....	24
1.4.1	Enzymatic Synthesis of DNA.....	24
1.4.1.1	The Polymerase Chain Reaction .....	24
1.4.2	Chemical Synthesis of DNA .....	26
1.4.2.1	H-Phosphonate Method for the Chemical Synthesis of DNA .....	27
1.4.2.2	Phosphoester Approaches for the Chemical Synthesis of DNA .....	27
1.4.3	Phosphoramidite Method for the Chemical Synthesis of Nucleic Acids .....	28
1.4.3.1	Activators .....	30
1.4.3.2	Non-nucleotide Additions .....	32
1.4.3.3	Oxidation.....	33
1.4.3.4	Deprotection.....	33
1.4.4	Modified Nucleic Acids .....	34
1.4.5	Visualisation of Nucleic Acids Using Fluorescent Dyes .....	35
1.5	Synthetic Polymers .....	38
1.5.1	Types of Polymers.....	38
1.5.2	Describing Synthetic Polymerisations.....	39
1.5.3	Free Radical Polymerisations .....	41

1.5.4	Controlling Polydispersity of Living Radical Polymers .....	42
1.6	Reversible Addition-Fragmentation Chain Transfer Polymerisations (RAFT).....	43
1.6.1.1	Monomers .....	44
1.6.1.2	Chain Transfer Agents (CTAs).....	45
1.6.1.3	Kinetics of RAFT Polymerisation.....	48
1.7	Synthetic Polymer DNA Analogues.....	49
1.8	Conclusions.....	55
1.9	References.....	57
2	Chapter 2: Methods and Materials .....	82
2.1	Synopsis.....	82
2.2	Abbreviations for Nucleotide Derivatives.....	83
2.2	Materials.....	86
2.2.1	Table of Chemicals and Reagents .....	86
2.2.2	Table of DNA Sequences .....	88
2.3	Preparations.....	88
2.3.1	Recrystallisation of AIBN .....	88
2.3.2	Generation of Molecular Sieves.....	89
2.3.3	Preparation of HPMA and DCI solutions.....	89
2.4	Synthetic Procedures.....	90
2.4.1	Chapter 3 Methods.....	90

2.4.1.1	Synthesis of 5'-dimethoxytrityl- <i>N</i> -benzoyl-2'-deoxycytosine,3'-[(2-cyanoethyl)-(oxyethyl methacrylate)]-phosphate monomer.....	90
2.4.1.2	Polymerisation of 5'-dimethoxytrityl- <i>N</i> -benzoyl-2'-deoxycytosine,3'-[(2-cyanoethyl)-(oxyethyl methacrylate)]-phosphate monomer.....	90
2.4.2	Chapter 4 Methods.....	91
2.4.2.1	Coupling: Synthesis of 5'-dimethoxytrityl- <i>N</i> -isobutyryl-2'-deoxyguanosine,3'-[(2-cyanoethyl)-(oxypropyl methacrylate)]-phosphate monomer .....	91
2.4.2.2	Polymerisation of 5'-dimethoxytrityl- <i>N</i> -isobutyryl-2'-deoxyguanosine,3'-[(2-cyanoethyl)-(oxypropyl methacrylate)]-phosphate monomer.....	91
2.4.2.3	Deprotection of poly(2-(5'-dimethoxytrityl- <i>N</i> -isobutyryl-2'-deoxyguanosine-monophosphate)oxypropyl methacrylate).....	92
2.4.2.4	Detritylation of poly(2-(5'-dimethoxytrityl-2'-deoxyguanosine-monophosphate)oxypropyl methacrylate).....	92
2.4.3	Chapter 6 Methods.....	92
2.4.3.1	Synthesis of poly(dT-P-PMA) .....	92
2.5	Characterisation.....	93
2.5.1	Chapter 3 Characterisation .....	93
2.5.1.1	Nuclear magnetic resonance (NMR) spectroscopy of DMT-dC-CE-P-PMA phosphate .....	93
2.5.1.2	Quantitative Solvent-Gel Analysis.....	94
2.5.1.3	Attenuated Total Reflectance-Fourier Transform Infrared (ATR-FTIR) Spectroscopy .....	94

2.5.2	Chapter 4 Characterisation .....	94
2.5.2.1	Electrospray Ionisation- Mass Spectrometry (ESI-MS) .....	94
2.5.2.2	Size-exclusion chromatography (SEC).....	95
2.5.2.3	Kinetics Measurements .....	95
2.5.2.4	Solubility of poly(dG-P-PMA) .....	97
2.5.3	Chapter 5 Characterisation .....	98
2.5.3.1	SEM .....	98
2.5.3.2	UV-visible (UV-vis) single sample.....	98
2.5.3.3	UV-vis Measurement of TMB Oxidation Using Well Plate Reader.....	98
2.5.3.4	Dynamic Light Scattering (DLS).....	99
2.5.3.5	Circular Dichroism (CD).....	99
2.5.3.6	Melting Measurements Using Fluorescence of ATTO 550 Dye.....	100
2.5.3.7	Fluorescence Measurements .....	100
2.5.4	Chapter 6 .....	101
2.5.4.1	UV-vis Spectroscopy of Poly(dT-P-PMA) Interactions with dA ssDNA .. .....	101
2.5.4.2	Effect of Annealing on Fluorescence of Poly(dT-P-PMA) Dye Interactions .....	101
2.5.4.3	Effect of Sodium Concentration on the Interaction of the SYBR Dye...	101
2.5.4.4	Complementary Dye Interactions .....	102
2.6	References.....	102

3	Chapter 3: Synthesis of Poly(2-(5'-dimethoxytrityl- <i>N</i> -benzoyl-2'-deoxycytosine-monophosphate)oxyethyl methacrylate): a Cytosine Rich Methacrylate Polymer .....	103
3.1	Synopsis .....	103
3.1	Introduction.....	104
3.1.1	Choice of Phosphoramidite Coupling Method.....	106
3.1.2	Selection of Compatible Vinyl Moiety.....	108
3.1.3	Activation of the Nucleotide Phosphoramidite .....	111
3.1.3.1	Quenching the Activator .....	112
3.1.3.2	Oxidation.....	112
3.2	Synthesis of HEMA-Nucleotide Bioconjugate.....	114
3.2.1.1	Proton Nuclear Magnetic Resonance ( <sup>1</sup> H NMR) Spectroscopy .....	115
3.2.1.2	Phosphorous Nuclear Magnetic Resonance ( <sup>31</sup> P NMR) Spectroscopy... ..	119
3.3	Polymerisation of the DMT-dC-CE-EMA Phosphate Monomer .....	121
3.3.1.1	Selection of RAFT Agent .....	123
3.3.2	Polymerisation of DMT-dC-CE-EMA Phosphate Monomer.....	124
3.3.3	Investigating Solvent Effect on Poly(DMT-dC-CE-P-EMA).....	127
3.3.3.1	Quantitative Solvent-Gel Analysis.....	128
3.3.3.2	ATR-FTIR Spectroscopy .....	131
3.3.4	Determining the Structure of the Poly(DMT-dC-CE-P-EMA) Gel .....	133
3.4	Conclusion .....	134
3.5	References.....	135

4	Chapter 4: Synthesis of The Poly(2-(2'-deoxyguanosine-monophosphate)oxypropyl methacrylate): a Guanine Rich Methacrylate Polymer .....	142
4.1	Synopsis .....	142
4.2	Introduction.....	143
4.2.1	Maintaining the Use of the Phosphoramidite Coupling Method.....	144
4.2.2	Determining the Phosphoramidite Isomer to be Used.....	145
4.2.3	Preventing the Formation of a Gel .....	146
4.2.4	Changing the Nucleobase .....	147
4.2.5	Changing the Vinyl Moiety .....	147
4.3	Analysis of DMT-dG-CE-P-PMA Phosphite and Phosphate .....	149
4.3.1	Electrospray Ionisation Mass Spectrometry (ESI-MS).....	149
4.3.2	Nuclear Magnetic Resonance (NMR) Spectroscopy.....	152
4.3.2.1	Proton Nuclear Magnetic Resonance ( <sup>1</sup> H NMR) Spectroscopy .....	152
4.3.2.2	Phosphorous Nuclear Magnetic Resonance ( <sup>31</sup> P-NMR) Spectroscopy...	155
4.4	Polymerisation of DMT-dG-CE-PMA phosphate monomer.....	157
4.4.1	Preliminary Testing for RAFT Polymerisation of DMT-dG-CE-PMA Phosphate Monomer .....	158
4.4.2	Confirmation of polymerisation of DMT-dG-CE-P-PMA Phosphate by <sup>1</sup> H NMR .....	161
4.4.3	Solvent Effect on Polymerisation of DMT-dG-CE-PMA Phosphate Monomer.. .....	163
4.5	Kinetics for the Polymerisation of DMT-dG-CE-PMA Phosphate Monomer .....	166



4.5.1	<i>In-situ</i> <sup>1</sup> H Nuclear Magnetic Resonance (NMR) Spectroscopy Kinetic Measurements.....	167
4.5.2	<i>Ex-situ</i> Kinetics Determined by Size Exclusion Chromatography.....	172
4.6	Activation of the Guanine Nucleobase in Poly(DMT-dG-CE-P-PMA).....	175
4.6.1	Deprotection .....	176
4.6.2	Detritylation.....	177
4.6.2.1	Neutralisation Agents.....	178
4.6.3	Isolation .....	178
4.6.4	Confirmation of Nucleobase Activation.....	179
4.7	Conclusion.....	181
4.8	References.....	182
5	Chapter 5: Formation of G-quartets Utilising Nucleotide Functionalised Synthetic Polymers.....	184
5.1	Synopsis.....	184
5.2	Introduction.....	185
5.2.1	Size Exclusion Chromatography (SEC) of Poly(dG-P-PMA) .....	186
5.3	Formation of Poly(dG-P-PMA) Particles .....	187
5.3.1	Scanning Electron Microscopy (SEM) of Poly(dG-P-PMA) Particles .....	190
5.3.2	Particle Sizing of Poly(dG-P-PMA) Particles by Dynamic Light Scattering (DLS) .....	194
5.4	Determining the Presence of G-quartets and the G-quadruplex Structure. ....	195
5.5	Testing for DNAzyme Properties with TMB Oxidation .....	198

5.5.1	Bulk testing of DNAzyme Activity .....	200
5.5.2	Analysis of DNAzyme activity using UV-Vis spectroscopy .....	202
5.6	Properties of Poly(dG-P-PMA) Particles.....	205
5.6.1	Particle Sizing by Dynamic Light Scattering (DLS).....	205
5.6.2	Melting Behaviour of poly(dG-P-PMA) Particles. ....	206
5.7	ATTO 550 Fluorescence Measurements .....	208
5.7.1	Melting Behaviour of Poly(dG-P-PMA) as measured with ATTO 550 .....	209
5.7.2	Optical Imaging of Poly(dG-P-PMA) with ATTO 550 .....	211
5.8	Conclusion .....	214
5.9	References.....	214
6	Chapter 6: Interactions of Nucleotide Functionalised Synthetic Polymers with DNA Using Poly(2-(2'-deoxythymine-monophosphate)oxypropyl methacrylate) as a Model System. .....	218
6.1	Synopsis.....	218
6.2	Introduction.....	219
6.2.1	Choice of Nucleobases .....	219
6.3	Synthesis of Target T6.....	221
6.3.1	Synthesis of T3 Monomer .....	221
6.3.2	Synthesis of Polymer.....	223
6.4	Computer Modelling of T6.....	225
6.4.1	Modelling of Selective Binding Interactions Between T6 and dA ssDNA....	226

6.4.2	Modelling of Long-strand T6 .....	228
6.5	Analysis by UV-Vis spectroscopy of DNA.....	229
6.6	Determination of Duplex Formation Using Fluorescent Dyes .....	231
6.6.1	Binding and Properties of SYBR Safe® DNA stain.....	232
6.6.2	Optimisation of T6 Concentration for Investigation of Dye Binding .....	233
6.6.3	Optimisation of the SYBR Safe Concentration.....	235
6.6.4	Effect of Sodium Chloride on SYBR Interaction.....	237
6.6.5	Effect of Pre-annealing on Fluorescence.....	239
6.7	Comparison of Binding Interactions of dA ssDNA with Complementary Polymers.. .....	240
6.7.1	Interactions with SYBR Safe Dye.....	240
6.7.2	Interactions with dsGreen.....	242
6.7.3	Interactions with Yo-Pro-1 Dye .....	244
6.7.4	Interactions with SYBR Green II .....	246
6.8	Structural Hypothesis.....	248
6.9	Conclusion .....	248
6.10	References .....	249
7	Chapter 7: Conclusion .....	253
7.1	Synopsis.....	253
7.2	Concluding Remarks and Future Work.....	254
7.3	Future Work.....	257

7.4	References.....	258
	Appendix 1: C3 <sup>1</sup> H NMR Peak Attributions .....	259
	Apendix 2: G3 <sup>1</sup> H NMR Peak assignments.....	260
	Appendix 3: Example DRI chromatograms for the polymerisation kinetics of C3. ....	261
	Apendix 4: T3 <sup>1</sup> H NMR Peak Attributions .....	268

## Table of Figures

Figure Number	Caption	Page
1.1	Structure and subunits of nucleic acids, called nucleotides, indicating the numbering scheme for constituent carbons. Also shown are the nucleobase (green), the sugar (blue), and the phosphate (red) moieties. The directionality of the nucleic acid is indicated in purple.	3
1.2	The five natural nucleobases guanine (G), adenine (A), cytosine (C), thymine (T) and uracil (U) showing their carbon numbering.	4
1.3	The ribose unit showing the carbon numbering. Note the functionality attached to the 2' carbon determines if the nucleotide is for deoxyribose nucleic acid (DNA) or ribose nucleic acid (RNA).	5
1.4	Adenosine 5' triphosphate.	6
1.5	Binding faces of nucleobases using guanine as an example.	6
1.6	Standard bonding of nucleobase pairs; electron donors are marked in red, receptors are marked in blue.	7
1.7	Non-canonical binding of nucleobases (a) through the Watson-Crick face, and (b) through other faces. Image adapted from Sivakova <i>et al.</i>	9
1.8	The G-quartet as it forms around a cation.	11
1.9	Simplified structure of a DNA double helix showing the geometric definitions.	14
1.10	(a) helical structures and (b) top down structures of A-, B-, and Z-DNA each 13 nucleotides in length. Provided by Mauroesgueroto, adapted from Ussery.	15
1.11	The conformations of the deoxyribose change between the B-form and A-form DNA.	16
1.12	Di-nucleotide structure of adjacent nucleotides in Z-DNA.	17

<b>1.13</b>	<i>Syn</i> - and <i>anti</i> -conformations of deoxyguanosine based on the relative location of the protons highlighted in green. Image adapted from Stegle <i>et al.</i>	19
<b>1.14</b>	The stacking of G-quartets, and their relationship to the circular dichroism (CD) spectra. The number of <i>syn</i> - and <i>anti</i> -guanines in each quartet determine resulting effect on circular dichroism, not the specific arrangement of these guanines relative to one another. The effect on the resulting spectra is shown in the table, inset. Image adapted from Tóthová <i>et al.</i>	19
<b>1.15</b>	(a) complementary dsDNA with variation to prevent non-specific binding and (b) complementary dsDNA without variation and the resulting nucleic acid wire.	20
<b>1.16</b>	Tapping mode atomic force microscopy images of G-wires treated with salt solutions as indicated. Imaged by Marsh <i>et al.</i>	21
<b>1.17</b>	Gel electrophoresis of G-wires formed with metallic cations as imaged by Marsh <i>et al.</i> <sup>86</sup> Note the high weight fractions at the top of the gels, attributed to G-wires.	21
<b>1.18</b>	Locked nucleic acid, LNA, one of the xeno nucleic acids.	23
<b>1.19</b>	An example of a simple PNA dimer. <sup>87</sup> Nucleobases abbreviated adenine (A), cytosine (C), thymine (T) and guanine (G) with . Image adapted from Nielsen <i>et al.</i>	23
<b>1.20</b>	Outline of the steps in the polymerase chain reaction (PCR). Adapted from Gill <i>et al.</i>	26
<b>1.21</b>	Phosphotriester method for the addition of a nucleotide to the growing oligomer. Adapted from Reese <i>et al.</i> <sup>107</sup> Here the 5' position is protected by monomethoxytrityl (MMT) moiety and the coupling agent is triisopropylbenzenesulfonyl chloride (TPSCl).	28
<b>1.22</b>	Outline of the phosphoramidite method for DNA synthesis. Adapted from DNA Oligonucleotide Synthesis.	30
<b>1.23</b>	Formation of the active intermediate phosphoramidite cation, and conversion to the coupled phosphite via the	31

	phosphoramidite method. The R-group is the propagating chain or surface to be grafted from.	
<b>1.24</b>	Diagram demonstrating the structural similarities of (a) 1 <i>H</i> -tetrazole, (b) 4,5-dicyanoimidazole and (c) 5-(ethylthio)-1 <i>H</i> -tetrazole. Modified groups are shown in red.	32
<b>1.25</b>	Oxidative mechanism of the phosphoramidite method for DNA synthesis using pyridine/I <sub>2</sub> .	33
<b>1.26</b>	Sites of binding of fluorescent dyes in the DNA double helix.	35
<b>1.27</b>	Radical Polymerisation, mechanisms and processes. The initiator (I) creates radicals that react with monomer units (M) to propagate the polymer. Adapted from Living Radical Polymerization by the RAFT Process – A Second Update.	41
<b>1.28</b>	RAFT mediation mechanism, adapted from Moad <i>et al.</i> <sup>173</sup> Verticle arrows indicate the polymer exiting the RAFT mediation as dead polymers through termination (combination or disproportionation).	44
<b>1.29</b>	Some examples of monomers for reversible-addition fragmentation chain transfer polymerisations, shown on a scale from least to most activated from left to right.	45
<b>1.30</b>	RAFT agent structures. Note: the dithioester groups, marked in green, are consistent between all of the RAFT agents.	46
<b>1.31</b>	Switchable polymerisation of styrene and vinyl acetate using sodium carbonate as a ‘switch’. Modified from Thang <i>et al.</i>	49
<b>1.32</b>	Poly( <i>p</i> -phenylenebutadiynylene) polymer and it’s interaction with polyadenine DNA. Taken from Lo <i>et al.</i>	50
<b>1.33</b>	Overview of the Sonogashira polymerisation method for the templated synthesis of Poly( <i>p</i> -phenylenebutadiynylene). Taken from Lo <i>et al.</i>	51
<b>1.34</b>	Mechanism for ring opening metathesis polymerisation. Adapted from Bielawski <i>et al.</i>	52
<b>1.35</b>	Formation of the adenine methacrylate (AMA) and thymine methacrylate (TMA) monomers by nucleophilic substitution using alkylhalides. Taken from O'Reilly <i>et al.</i>	53

1.36	Formation of the non-conjugated polymer dots. Taken from O’Rielly <i>et al.</i>	55
2.1	Overview of polymer synthesis from protected nucleotide phosphoramidite to the final deprotected polymer bioconjugate.	83
2.2	ChemSpeed Swing XL showing (a) syringe pump, (b) syringes, and racks for (c) reagents, (d) reactions, and (e) collected samples.	96
3.1	Overview for the conversion of C1 starting material through the activation with tetrazole to form (i) the activated C1 intermediate. This in turn was coupled to HEMA to form C2 and subsequently oxidised to form C3. The tetrazole required for the activation (step 1) was regenerated during the coupling step (step 2) allowing it to act as a catalyst.	105
3.2	(i) 2’deoxyadenosine 5’ monophosphate and (ii) 2’deoxyadenosine 3’ monophosphate. Green arrows indicate sites that could be used for conjugation of the vinyl moiety using the phosphoramidite coupling method.	107
3.3	Coupling of the protected C1, (i) the activated phosphoramidite intermediate to (ii) HEMA resulting in the C3 monomer.	110
3.4	Mechanism for the activation of (i) a phosphoramidite, substituting the diisopropylamine (blue) with tetrazole (pink) resulting in (iii) an activated phosphoramidite. <sup>7</sup> The tetrazole is subsequently regenerated when it is substituted with the monomer, completing the coupling.	111
3.5	(i) Oxidation of phosphite to phosphate using I <sub>2</sub> /pyridine/H <sub>2</sub> O <sub>2</sub> (ii) the halide addition to an alkene, and (iii) oxidation of phosphite by ozone present in air.	113
3.6	<sup>1</sup> H NMR spectra of (i) C1 and (ii) C3 monomer, showing the appearance of peaks (a-e) associated with HEMA and the disappearance of peak (f) associated with the diisopropyl amine (inset (i, red)) Spectra acquired in deuterated	116



	acetonitrile at 600 MHz. Full peak attributions can be found in Appendix 1.	
<b>3.7</b>	<sup>1</sup> H NMR spectra of the <b>C1</b> (red), and <b>C3</b> monomer (blue), showing the region from 1 ppm to 1.25 ppm. Spectra acquired in deuterated acetonitrile at 600 MHz.	117
<b>3.8</b>	<sup>1</sup> H NMR spectra of the 5.5 ppm to 6.5 ppm region of <b>C1</b> (red) and <b>C3</b> monomer (blue), showing the appearance of peaks (a and b) associated with the <i>cis</i> and <i>trans</i> protons of the alkene (inset). In addition the peak associated with the 1' proton on the ribose is also visible in this region. Spectra acquired in deuterated acetonitrile at 600 MHz.	118
<b>3.9</b>	<sup>31</sup> P NMR spectra of the -10 ppm to 160 ppm region of <b>C1</b> (red, P(III)) and <b>C3</b> monomer (blue, P(V)) Spectra acquired pulse decoupled in deuterated acetonitrile at 600 MHz.	120
<b>3.10</b>	Thermal decomposition of AIBN into N <sub>2</sub> and the isobutyronitrile radical.	122
<b>3.11</b>	General scheme for the polymerisation of (i) <b>C3</b> monomer to (ii) <b>C4</b> using the RAFT agent 4-cyano-4-(phenylcarbonothioylthio)pentanoic acid <i>N</i> -succinimidyl ester and AIBN (ii) showing the active vinyl group (red) converted to the alkyl backbone (blue).	125
<b>3.12</b>	<b>C4</b> gel swollen with (a) water or (b) DMSO and, (b) dried at 60 °C.	126
<b>3.13</b>	Structure of the <b>C4</b> , indicating hydrophobic moieties in red.	128
<b>3.14</b>	Normalised ATR-FTIR spectrum of the <b>C4</b> gel.	131
<b>3.15</b>	ATR-FTIR spectra of <b>C4</b> gel in the fingerprint region 500-2000 cm <sup>-1</sup> .	132
<b>3.16</b>	Proposed by-product reaction caused by the solvation of vinyl-nucleotide bioconjugate for extended periods, resulting in the diene impurity that would act as the cross linking agent and subsequently leading to the gel formation.	134
<b>4.1</b>	Overview for the conversion of <b>G1</b> starting material through the activation with DCI to form the activated <b>G1</b> intermediate.	144

	This in turn was coupled to HPMA to form a <b>G2</b> monomer and then oxidised to form the <b>G3</b> monomer. The DCI required for the activation (step 1) is regenerated during the coupling step (step 2) allowing it to act as a catalyst.	
<b>4.2</b>	(i) 3'-deoxy guanosine monophosphate and (ii) 5'-deoxy guanosine monophosphate isomers.	146
<b>4.3</b>	Formation of the diene impurity from <b>G3</b> monomer in solution, followed by polymerisation creating the first addition, and leading to cross-linking with the second addition. For clarity active vinyl groups are shown in red. Polymerised vinyl groups shown in blue.	148
<b>4.4</b>	ESI-MS spectrum of the final product showing the following peaks: (a) <b>G2</b> (molecule shown inset), (b) <b>G2</b> sodium adduct, (c) <b>G3</b> monomer sodium adduct, and (d) <b>G3</b> monomer disodium + acetonitrile adduct.	151
<b>4.5</b>	<sup>1</sup> H NMR spectra of (i) <b>G1</b> starting material and (ii) the bioconjugate <b>G3</b> monomer. Spectra acquired in deuterated acetonitrile at 400 MHz, with triethylamine residue (TEA). Full peak attributions can be found in Appendix 2.	153
<b>4.6</b>	<sup>1</sup> H NMR spectra region from 3 ppm to 2 ppm showing the <b>G1</b> (black) and the <b>G3</b> monomer (blue). Spectra acquired in deuterated acetonitrile at 400 MHz.	154
<b>4.7</b>	<sup>1</sup> H NMR of the 6.3 ppm to 5.3 ppm region for <b>G1</b> (black) <b>G3</b> (blue). Spectra acquired in deuterated acetonitrile at 400 MHz.	155
<b>4.8</b>	<sup>31</sup> P NMR spectra of (i) <b>G1</b> starting material and (ii) <b>G3</b> monomer with (inset) the 6 ppm to 1 ppm region. Spectra acquired in deuterated acetonitrile at 400 MHz.	156
<b>4.9</b>	Polymerisation of <b>G3</b> monomer showing the starting vinyl group (red) converted to the alkyl group (green) and the incorporation of the NHS-RAFT agent (purple).	157
<b>4.10</b>	(i) Photo showing the phase separation of <b>G4</b> upon cooling of the polymerisation mixture, and (ii) DRI chromatogram and results of the 24 h polymerisation of <b>G4</b> , showing the	159

	formation of a polymer, 6750 Da. at 27.5 min attributed to the <b>G4</b> . Additional peaks at 31 min is attributed to the monomer and 32.5 min to DMT residue in solution.	
4.11	Structure of the <b>G4</b> heptamer. Note that following polymerisation it has not been treated in a way that would remove the NHS protecting group.	161
4.12	<sup>1</sup> H NMR spectra of <b>G4</b> in deuterated acetonitrile with majority noted peak allocation indicating (a) polymerisation, (b) nucleobase retention and, (c) the ribose connection between them. Spectra acquired in deuterated acetonitrile at 400 MHz	162
4.13	Difference in solution hue of the <b>G5</b> reaction mixture with (i) DMF and, (ii) acetonitrile as solvent after 2 h.	164
4.14	DRI chromatograms of <b>G4</b> polymerised for 2 h using either (i) acetonitrile, or (ii) dimethylformamide as the solvent. Numbers shown indicate the $M_w$ at maximum.	165
4.15	(i) Waterfall graph showing the decrease in magnitude of the 5.6 ppm peak associated with the vinyl proton as the polymerisation of DMT-dG-CE-P-PMA phosphate with stacked spectrums (inset) and, (ii) kinetic measurements of the conversion of <b>G3</b> monomer, calculated using the peak ratio of the 5.6 ppm peak associated with the vinyl proton, blue, average of 4 samples. Linear fit from 147.5 minutes shown in red. Spectra acquired in deuterated acetonitrile at 400 MHz.	171
4.16	Stages in the first addition during the RAFT polymerisation of <b>G3</b> monomer through the stages of initiation, addition, and fragmentation. This process is reversible as the radical group created by the transferred chain can recombine with the dormant chain, the one not containing the radical. The transfer of the thiol to the propagating chain generates the macro-RAFT agent.	172
4.17	(i) $M_w$ of <b>G4</b> (square) and the corresponding $\mathcal{D}$ (diamond) over time calculated from SEC and, (ii) example DRI	174

	chromatogram for the 240 min sample of <b>G4</b> . Further example DRI chromatograms can be found in Appendix 3.	
<b>4.18</b>	Process for the conversion of <b>G4</b> into <b>G6</b> through (i) deprotection removing the CE protecting groups shown in red and, (ii) detritylation removing the groups shown in orange.	176
<b>4.19</b>	(i) Mechanism for the removal of the cyanoethyl protecting group by ammonia resulting in acrylonitrile and <b>G5</b> and (ii) mechanism for the removal of isobutyryl protection from guanine using ammonia (iii) the white colloidal suspension of <b>G5</b> generated.	177
<b>4.20</b>	The orange colour produced as a result of the acetic acid addition to the <b>G5</b> from (i) immediately after addition to (ii) 5 min after addition with (iii) the mechanism for this conversion.	178
<b>4.21</b>	<sup>1</sup> H NMR spectra of (i) <b>G4</b> in deuterated acetonitrile and (ii) <b>G6</b> in deuterated DMSO. Spectra acquired in deuterated acetonitrile at 400 MHz.	180
<b>5.1</b>	DRI chromatogram of <b>G4</b> hexamer prior to deprotection, with specific results inset. Note, the large peaks at 30.5 min and 32 min were attributed to cleaved DMT and residual monomer, respectively, based on their elution time and the corresponding M <sub>w</sub> .	186
<b>5.2</b>	Sample of <b>G6</b> following deprotection and detritylation as isolated using NaOAc in propan-2-ol:water (a) 5:1 and (b) 1:15 (v/v).	189
<b>5.3</b>	Structure of <b>G6</b> showing the hydrophilic nucleotide based region known to be water soluble in isolation (green) and the comparatively hydrophobic region known to be water insoluble in isolation (red).	190
<b>5.4</b>	SEM images of the <b>G6</b> isolated in propan-2-ol:water 5:1 (v/v) at various magnification.	191
<b>5.5</b>	Non-grafted polymer monoliths of poly(2-(2-methoxyethoxy)ethyl methacrylate (MEO2MA)-co-	192

	oligo(ethylene glycol) methacrylate at differing magnification. Taken from Li <i>et al.</i>	
<b>5.6</b>	SEM images of the <b>G6</b> isolated in propan-2-ol:water 1:15 (v/v) at various magnifications.	193
<b>5.7</b>	Proposed general structure of <b>G6</b> in propan-2-ol:water 1:15 (v/v) (a) sheet ‘unit’ and (b) sheet cross section of polymersome wall.	193
<b>5.8</b>	DLS measurements showing the particle size of <b>G6</b> in 15:1 (v/v) water:propan-2-ol as isolated with NaOAc.	195
<b>5.9</b>	The stacking of G-quartets to form a G-quadruplex. Image adapted from Tóthová <i>et al.</i>	196
<b>5.10</b>	Circular dichroism measurements of <b>G6</b> in 10:1 (v/v) water:propan-2-ol as isolated with LiOAc (red) and with added NaOAc (green) and KOAc (blue) normalised to the 325 nm peak.	197
<b>5.11</b>	Structure of ferric chloride heme (Hemin)	199
<b>5.12</b>	Oxidation of TMB caused by the G-quadruplex/Hemin DNAzyme with absorption wavelengths shown. Adapted from Stefan <i>et al.</i>	199
<b>5.13</b>	UV-Vis measurements at 450 nm for acceleration in the oxidation of TMB by hemin/G-quadruplex complex. Positive controls of TMB/Hemin/GQ DNA (blue) and negative control of TMB/Hemin (black) with non-linear behaviour (red arrows). Samples measured in triplicate.	203
<b>5.14</b>	UV-Vis measurements at 450 nm for TMB oxidation of the positive GQ DNA control (blue), poly(HPMA) (orange), negative control (grey) and <b>G6</b> (yellow).	204
<b>5.15</b>	DLS measurements of Z-average particle diameter of <b>G6</b> (blue), and its protected form <b>G4</b> (orange).	205
<b>5.16</b>	Circular dichroism measurement at 261 nm of <b>G6</b> samples in 10:1 (v/v) water:propan-2-ol as isolated in LiOAc (black) and with 25 $\mu$ M KOAc (red), normalised. Heating indicated by orange, and cooling with blue.	207

5.17	Change in fluorescence intensity of ATTO 550 treated <b>G6</b> measured with heating, average of 4 samples. Particles isolated with LiOAc (solid blue) and treated with 25 $\mu\text{M}$ $\text{K}^+$ ions (solid orange), normalised to the 95 $^{\circ}\text{C}$ untreated maximum fluorescence and the derivative of the melting curves (dashed).	210
5.18	Optical and CLSM images of ATTO 550 stained (a and b) poly(HPMA), (c and d) <b>G6</b> as isolated with LiOAc, and (e and f), as isolated with LiOAc and added $\text{Na}^+$ ions and (g and h) and as isolated with LiOAc and added $\text{K}^+$ ions (25 mM), respectively. Note the excitation laser output for poly(HPMA) had been amplified 10x. Scale bars indicate 20 $\mu\text{m}$ .	212
5.19	Proposed pathway for the formation of <b>G6</b> particles and their interactions with $\text{K}^+$ ions. Starting with the polymer, forming sheets, becoming micelles with G-quartets on the surface, and forming inter-particle G-quartets.	213
6.1	Proposed binding of <b>T6</b> 23-mer (blue) interacting with dA ssDNA 23-mer (red).	220
6.2	ESI-MS spectrum of <b>T2</b> monomer showing the following peaks: (i) <b>T2</b> monomer (molecule shown inset), (ii) <b>T3</b> monomer, (iii) <b>T2</b> monomer sodium adduct, (iv) <b>T3</b> monomer water adduct, and (v) DMT-dT-CE-PMA sodium adduct.	221
6.3	$^1\text{H}$ NMR of the 6.5 ppm to 5.5 ppm region for <b>T3</b> (inset). Spectra acquired in deuterated acetonitrile at 600 MHz.	223
6.4	DRI chromatogram of <b>T6</b> following 4 h polymerisation, showing the formation of a polymer, 9364 Da.	224
6.5	Optimised structural model of <b>T6</b> and dA ssDNA pentamers following 100,000 iterations. Directionality of the dA ssDNA shown. Angles provided are (i) groove, (ii) <b>T6</b> front, (iii) top, and (iv) dA ssDNA front.	227
6.6	Molecular structure of the <b>T6</b> 21-mer following optimisation, (a) at $0^{\circ}$ and (b) $90^{\circ}$ rotation around the vertical axis, with light green bars indicating linearly aligned nucleobases.	229

<b>6.7</b>	The absorbance with increasing ratio of <b>T6</b> to dA ssDNA at 260 nm, average of 4 samples.	230
<b>6.8</b>	Structure of SYBR Safe dye.	233
<b>6.9</b>	Normalised fluorescence of 5X SYBR Safe (blue) and with <b>T6</b> at 1 mM (orange), 100 $\mu$ M (grey), 10 $\mu$ M (yellow) and 1 $\mu$ M (green). Samples run in quadruplicate at gain 10.	234
<b>6.10</b>	Normalised fluorescence of SYBR Safe with 10 $\mu$ M <b>T6</b> (blue) and without (orange) at (a) 25 $^{\circ}$ C and (b) 99 $^{\circ}$ C. Samples run in quadruplicate at gain 10, error bars are displayed in both plots though fit within the marker for some data points.	236
<b>6.11</b>	Normalised fluorescence of 2.5X SYBR Safe with 10 $\mu$ M <b>T6</b> with the addition of different loadings of NaCl ; 5 mM (purple), 10 mM (blue), 20 mM (green), 50 mM (yellow), and 100 mM (red). Samples run in quadruplicate at gain 10. Error bars included for the 10 mM NaCl sample are similarly representative of all samples.	238
<b>6.12</b>	Normalised fluorescence of SYBR Safe with <b>T6</b> following annealing at temperatures indicated.	239
<b>6.13</b>	Background corrected fluorescence of samples treated with SYBR Safe containing ssDNA and <b>T6</b> in combinations shown. Samples normalised to dA ssDNA and run in quadruplicate at gain 10, 25 $^{\circ}$ C.	241
<b>6.14</b>	Structure of dsGreen.	243
<b>6.15</b>	Background corrected fluorescence of samples treated with dsGreen containing ssDNA and <b>T6</b> in combinations shown. Samples normalised to dA ssDNA and run in quadruplicate at gain 10 at 25 $^{\circ}$ C. Samples marked * indicate oversaturation of the detector	243
<b>6.16</b>	Structure of Yo-Pro iodide.	245
<b>6.17</b>	Background corrected fluorescence of samples treated with Yo-Pro iodide ssDNA and <b>T6</b> in combinations shown. Samples normalised to dA ssDNA and run in quadruplicate at gain 2.67, 25 $^{\circ}$ C.	245

<b>6.18</b>	Background corrected fluorescence of samples treated with SYBR Green II containing ssDNA and <b>T6</b> in combinations shown. Samples normalised to dA ssDNA and run in quadruplicate at gain 10, 25 °C.	247
<b>6.19</b>	Proposed screw-like helix formed around <b>T6</b> by dA ssDNA	248



## List of Tables

<b>Table</b>	<b>Page</b>
Table 1.1 Binding energy and strength of base pairs.	7
Table 1.2: Dimensions of selected DNA forms.	15
Table 1.3: Fluorescent intercalating DNA dyes. Data provided by Thermo Fisher Scientific.	36
Table 1.4: Compatibility of dithioester derivatives, RAFT agents, with monomers by class. Taken from Living Radical Polymerization by the RAFT Process— A Third Update.	46
Table 2.1: Scientific names, abbreviations and structures for the molecules synthesised in this thesis.	83
Table 3.1: Solubility of the poly(DMT-dC-CE-P-EMA) gel in different solvents compared to the DNA and poly(HEMA).	125
Table 3.2: IR peak correlations. Molecular structure of idealised poly(DMT-dC-P-EMA) included for reference.	128
Table 4.1: Results of polymerisation of DMT-dG-CE-PMA phosphate monomer over 24 h.	154
Table 4.2: Results of polymerisation in different solvents over 2 h.	157
Table 5.1: Results of TMB oxidation tests, all samples contain hemin, TMB, 10 mM TRIS-HCl in addition to the listed reagent.	190
Table 5.2: Fluorescent properties of ATTO 550	198
Table 6.1: SEC results for the measurement of poly(dT-P-PMA).	213

## **Abstract**

DNA is a fundamental compound in biology and, from a polymer science perspective, exceeds most synthetic polymers in terms of size and composition. This thesis outlines a synthetic method for an alkene polymer bearing nucleotide functionality and its subsequent properties.

Alkene polymers are built on the radical polymerisation of alkenes leading to long chain alkyl backbones and are known to be stable for long periods. Combining the selectivity and control of DNA with the rapid synthesis and stability of living radical techniques will allow applications of DNA nanotechnologies in environments where DNA is currently unsuitable.

The background and information relevant to a thorough understanding of this thesis is presented in Chapter 1. This includes discussion of the nature of DNA and variants of its structure, methods for its synthesis, and analysis of the subsequent products. Further, information essential to understanding the polymerisation methods utilised in this work such as the radical polymerisation and the reversible addition-fragmentation chain-transfer method are also discussed. Existing literature discussing the convergence of these two fields is also covered, with the specific methods and materials as they relate to this work presented in the following Chapter 2.

Chapter 3 outlines the initial method developed for the synthesis of a nucleotide functionalised polymer using the phosphoramidite method. This method has been reported previously for the synthesis of DNA and other nucleic acids (broadly poly(ribose-phosphates)). The phosphoramidite method was altered to generate a nucleotide-alkene monomer using a protected cytosine phosphoramidite. This was possible through careful selection of the alkene moiety (hydroxyethyl methacrylate (HEMA)) and the optimisation of experimental parameters. This method was found to successfully generate the polymer as confirmed with proton and <sup>31</sup>phosphorus nuclear magnetic resonance (NMR) spectroscopy.

The synthesised HEMA-cytosine monophosphate bioconjugate monomer was polymerised using reversible addition-fragmentation chain-transfer (RAFT) polymerisation. The resulting polymers were limited in their applications as interconversion of the monomer appeared to form a diene that caused the polymer to be cross-linked, resulting in the formation of an insoluble gel. This gel was found to retain the nucleobase functionality and demonstrated the interaction of the nucleotide-alkene with solvents consistent with a hybrid polymer system.

Chapter 4 builds upon Chapter 3, presenting an improved method for the synthesis of a nucleotide-alkene bioconjugate by changing the alkene source from HEMA to 2-hydroxypropyl methacrylate (HPMA) and the nucleotide source to guanosine monophosphate. The HPMA was chosen as the presence of an additional methyl group explicitly prevented the formation of the diene impurity in the monomer. This improved method was shown to result in the HPMA-protected guanosine monophosphate through proton and  $^{31}\text{P}$  phosphorus NMR spectroscopy along with electrospray ionisation mass spectrometry.

The compatibility of the synthesised HPMA-guanosine monophosphate with RAFT polymerisation was then demonstrated through both *in-situ* and *ex-situ* techniques. Samples measured *in-situ* utilised NMR spectroscopy, with *ex-situ* measurements using size exclusion chromatography. The poly(HPMA-guanosine monophosphate) formed colloidal suspensions during isolation which lead to further analysis in the following chapter.

Chapter 5 investigated the formation of particles from the poly(HPMA-guanosine monophosphate). It was shown that the polymer was able to replicate the formation of G-quartets normally formed in guanine-rich DNA systems. Through the use of fluorescent dye binding, circular dichroism and fluorescence microscopy, the general structure of these particles was determined to be similar to vesicles or micelles with surfaces covered in active

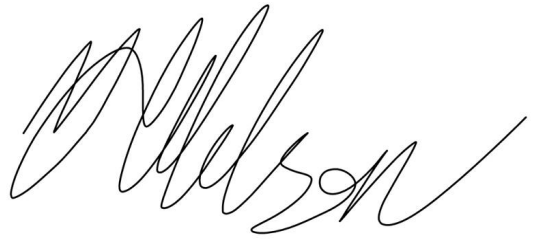
guanine moieties. The aggregation of the particles could be adjusted by the addition of potassium chloride to stabilise the formation of G-quartets between particles.

Finally, Chapter 6 demonstrated the successful synthesis of poly(HPMA-thymine monophosphate) by utilising the synthetic method developed in Chapter 4, thereby demonstrating the flexibility of the synthesis for creating a library of nucleotide-alkene bioconjugate compatible with RAFT polymerisation.

Following this successful synthesis of poly(HPMA-thymine monophosphate), its interactions with single stranded DNA were investigated with the aid of computer modelling and the use of nucleic acid binding dyes. This led to the determination that the poly(HPMA-thymine monophosphate) does bind to a complementary single stranded DNA sequence, but that the structure formed was conformationally distinct to classical double stranded DNA.

## **Declaration**

I certify that this thesis does not incorporate without acknowledgment any material previously submitted for a degree or diploma in any university; and that to the best of my knowledge and belief it does not contain any material previously published or written by another person except where due reference is made in the text.

A handwritten signature in black ink, appearing to read "M. Wilson", written in a cursive style.

Michael James Wilson

## **Acknowledgements**

To begin I thank my supervisors Professor Amanda Ellis and Professor Joe Shapter for their support and encouragement throughout the project, and Dr Elizabeth Williams of CSIRO for their collaboration and funding support especially in the early stages of the project. Further funding support was provided by ARC Future Fellowship FT130100211.

Further thanks are well deserved for Dr Renzo Fenati for his support and lending expertise to the DNA and biological components of the thesis. Sharing a lab and office with someone as proficient and skilled as Dr Fenati significantly helped me to improve my own work.

The most supportive group of friends anyone could ask for. Wingar, Fay St Clair-Burke, and Catherine Alekseenko for being my rocks, without them I would have given up a long time ago. Nobody could ask for better people in their life than those I've been fortunate enough to find.

Finally, I wish to thank the people who have contributed the most to this effort over the longest time, my family; parents Jim and Colleen, brother Ryan and sister Jamie. From an early age they fostered my inquisitive nature and always pushed me to question the world around me. Further their sacrifices to support my various academic endeavours throughout the years have pushed me to all of my greatest achievements and helped me recover when I have fallen. I can never fully express how lucky and fortunate I am to have such supportive parents.

# Chapter 1: Introduction and Literature Review

## 1.1 Synopsis

*This chapter will focus on the two classes of polymers used in the project: nucleic acid biopolymers and synthetic vinyl-based polymers. It will discuss the composition and structures of nucleic acids as well as used methods of analysis; this includes the selective bonding of complementary nucleotides and the resulting secondary structures and some of the relevant biological processes they undergo. The discussion of vinyl-based polymers will focus on the formation using reversible addition-fragmentation chain transfer (RAFT) polymerisations as this was the selected method of polymerisation used in this project. A brief overview of other polymerisation techniques is given as a means to justify the selection of this polymerisation method.*

## 1.2 Nucleotides

Nucleotides are the individual repeating units that form larger molecules called nucleic acids. These acids are found in many biological systems where they direct the synthesis of proteins<sup>1,2</sup> and regulate cell processes<sup>3</sup> by the means of using enzymes which translate the sequences of nucleotide units into amino acids and, in turn, proteins.<sup>4</sup>

Each nucleotide comprises 3 subunits: nucleobase, ribose, and phosphate; as shown in Figure 1.1. The nucleobase is the active unit and is used to give the nucleotide its name, while the sugar (ribose) and the phosphate form the 'backbone' of the molecule when multiple nucleotides are joined together. When several nucleotides connect, they form nucleic acid polymers which are covered in Section 1.2.6. Understanding of the structure and function of these molecules forms the foundation of the work performed for the purpose of and covered in this thesis. The incorporation of nucleotides into synthetic polymers is only useful if the binding function of the nucleobase is maintained, and the full nucleotides were used to provide for the best chance at enzymatic compatibility in the future work.



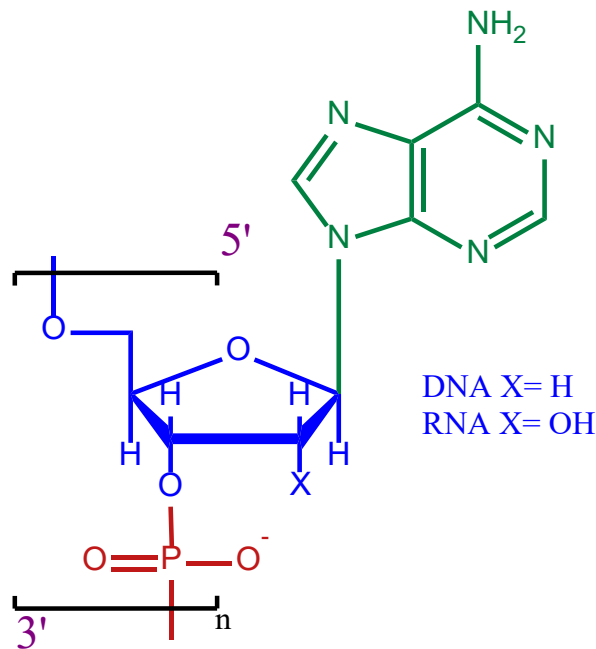


Figure 1.1 Structure and subunits of nucleic acids, called nucleotides, indicating the numbering scheme for constituent carbons. Also shown are the nucleobase (green), the sugar (blue), and the phosphate (red) moieties. The directionality of the nucleic acid is indicated in purple.

### 1.2.1 Nucleobases

The active unit of the nucleotide in regard to its biological application is the nucleobase. There are 5 natural nucleobases: adenine (A) and guanine (G) make up the pyrimidines; cytosine (C), thymine (T) and uracil (U) make up the pyrimidines, as shown in Figure 1.2. The chemical distinction between T and U is due to the presence of the methyl group on the 5th carbon atom, and these two nucleobases are typically found in DNA and RNA, respectively. The sequential order of these nucleobases within the nucleic acid biopolymer is what provides for the coding functionality of nucleic acids.<sup>5-6</sup>

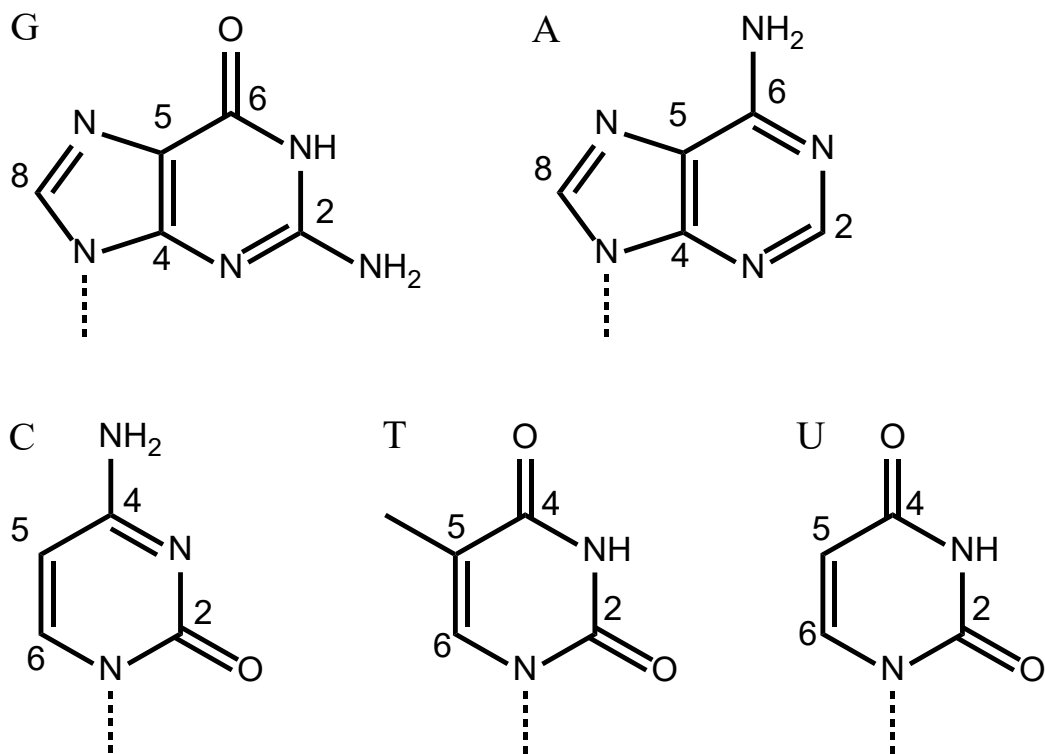


Figure 1.2 The five natural nucleobases guanine (G), adenine (A), cytosine (C), thymine (T) and uracil (U) showing their carbon numbering.

### 1.2.2 Sugar

The sugar (ribose) links the nucleobase to the sugar phosphate backbone formed in nucleic acid polymers. The numbering for the ribose ring includes the prime (') notation to distinguish it from the numbering of the carbons in the nucleobase, as shown in Figure 1.3. This numbering is important as it provides an orientation to the formed biopolymers and clarifies any alterations to the sugar moiety. Most commonly, the presence of a hydroxyl moiety on the 2' carbon is used to distinguish between the deoxyribose nucleic acid (DNA) and ribose nucleic acid (RNA).<sup>7</sup>

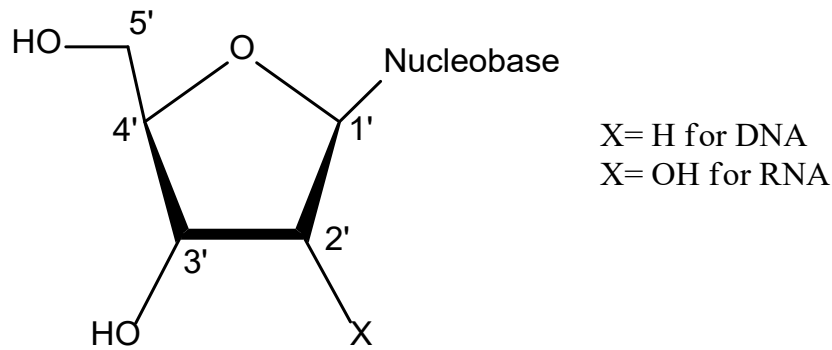


Figure 1.3 The ribose unit showing the carbon numbering. Note the functionality attached to the 2' carbon determines if the nucleotide is for deoxyribose nucleic acid (DNA) or ribose nucleic acid (RNA).

### 1.2.3 Phosphate

The phosphate acts as a link between the ribose and helps form the sugar phosphate backbone. It is the unit responsible for the acidic properties of nucleic acids as a result of the deprotonation of the hydroxyl moiety that is resonantly stabilised by the  $sp^3$ -hybridised phosphate and oxygens.<sup>8</sup> In a singular, free nucleotide the phosphate can be attached at either the 3' or 5' carbon. Within a biological system it is normally attached to the 5' position and contains a chain of phosphates, either the pyrophosphate or triphosphate, until they are cleaved when the nucleotide is added to the nucleic acid. For example, the adenosine triphosphate, see Figure 1.4, is used to transfer energy as part of the citric acid cycle.<sup>9</sup> During nucleic acid synthesis, the nucleoside triphosphate is split which generates the nucleotide and a pyrophosphate molecule; the energy released during this process is used to power the enzyme.<sup>10</sup>

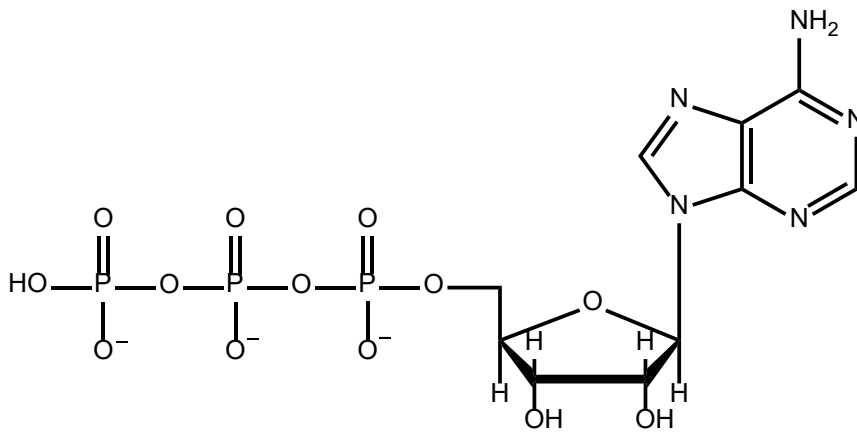


Figure 1.4 Adenosine 5' triphosphate.

### 1.2.4 Specific Binding Between Nucleobases

Nucleotides undergo specific binding as a result of H-bonding between nucleobases. Broadly speaking, this interaction between the nucleotides is classified as either canonical, more commonly known as Watson-Crick base pairing, or non-canonical.<sup>11</sup> Watson-Crick binding is considered canonical because it is the predominant interaction within nucleic acids in natural systems. It occurs through the Watson-Crick face of the nucleotide, Figure 1.5. Any other hydrogen bonding between nucleotides is non-canonical binding.

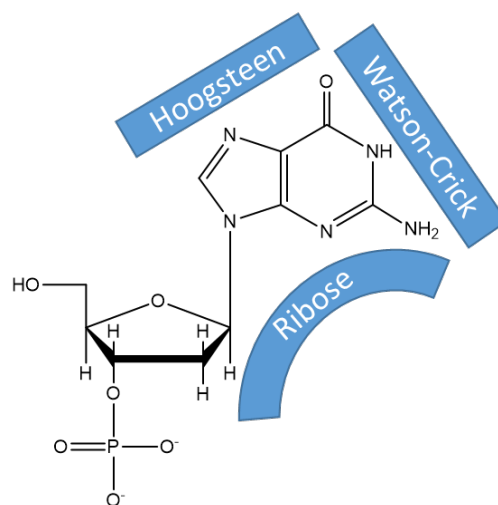


Figure 1.5 Binding faces of nucleobases using guanine as an example.

For the purpose of this project, the main binding of interest is Watson-Crick base pairing and the formation of the non-canonical G-quartet, covered in Sections 1.2.4.1 and 1.2.5.1 respectively. Select other non-canonical bindings are covered briefly in the following chapters as part of experimental design considerations.

#### 1.2.4.1 Watson-Crick Binding between Nucleobases

Although the presence of DNA had been known since the late 1860s,<sup>12</sup> its structure was not determined until Watson and Crick published their work in 1953.<sup>13</sup> Their findings described the double helix structure within DNA that had been discovered through X-ray crystallography.<sup>13</sup> The authors showed that nucleobases underwent selective hydrogen bonding, as shown in Figure 1.6, with AT and AU having two binding sites and GC having three binding sites.<sup>14</sup>

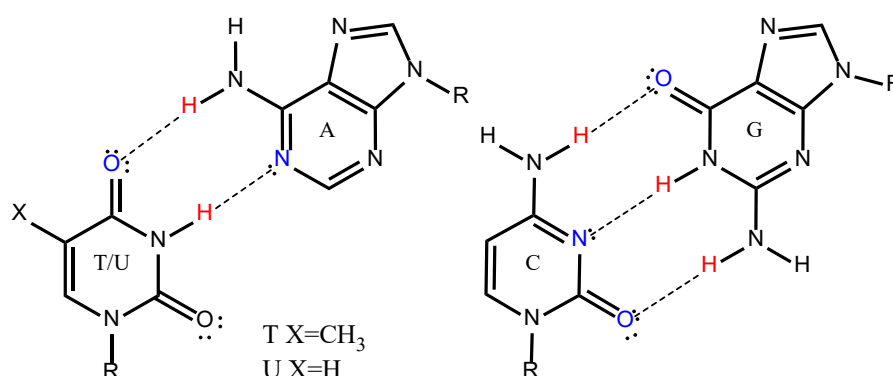


Figure 1.6 Standard bonding of nucleobase pairs; electron donors are marked in red, receptors are marked in blue.

The additional bonding site for GC pairing increases the binding strength of the base pair, as shown by Breslauer *et al.*<sup>15</sup> They showed that DNA with a higher proportion of GC base pairs had a significantly higher  $\Delta H$  compared to similar sequences of AT. The magnitude of these binding strengths are shown in Table 1.1.

**Table 1.1:** Binding energy and strength of base pairs.

Base Pair	Calculated $\Delta G_{\text{assoc(aq)}}$ contributions at 300 K (kcal/mol) <sup>16</sup>		Total force required to separate bound pair (pN) <sup>17</sup>
	H-Bonding	Base Stacking	
A-T	0.18	-1.86	14.0 $\pm$ 0.3
G-C	-0.91	-2.22	20.0 $\pm$ 0.2

### 1.2.5 Non-canonical Binding Between Nucleobases.

The hydrogen bonding between the bases, while considered selective to AT and GC, has some variance referred to as non-canonical binding. These binding structures can occur through the same Watson-Crick face as canonical binding, but may be differently orientated or form between other combinations of bases that are not AT and GC.

Aside from Watson-Crick base pairs, there are other combinations of nucleobases that can form similar electron pair donor-acceptor relationships. In total there are a further 26 stable combinations that may possibly form between the four natural nucleobases found in deoxyribose nucleotides, as reported by Sivakova *et al.*<sup>18</sup> Their works demonstrated that exposure of the amine and ketone groups from non-canonical bonding can also support the formation of tertiary structures.

Where a comparatively stable binding pair forms, but it is not the canonical Watson-Crick pair, it is called a mismatch.<sup>19</sup> Some examples are shown in Figure 1.7(a). Ebel *et al.* have shown that the GA mismatch is more stable than other nucleic acid mismatches,<sup>20</sup> which means they can drive the formation of stabilised tertiary structures as the result of the now exposed amine and ketone groups.<sup>21,22</sup> This work was further supported by Pan *et al.* who demonstrated that the GA and other mismatches remained stable enough due to solvent interactions so that they

could be analysed using electrospray without separating.<sup>23</sup> Further, they demonstrated that certain mismatches, GG, AC, TC and CC specifically, are destabilised in solution.<sup>23</sup>

Reverse Watson-Crick binding is the binding of a canonical nucleobase pair through the Watson-Crick face in a non-canonical orientation.<sup>24</sup> When formed in some RNAs, they are referred to as a Levitt base pairs; an example of this is shown in Figure 1.7(a). Though not preferred over canonical binding, Sharma *et al.*<sup>25</sup> showed through simulation that the formation of this type of pair can allow for distant regions of a nucleic acid to interact with one another. This was further supported by Shawla *et al.*<sup>26</sup> who concluded that these regions participate in binding with non-nucleic acids such as metabolites.

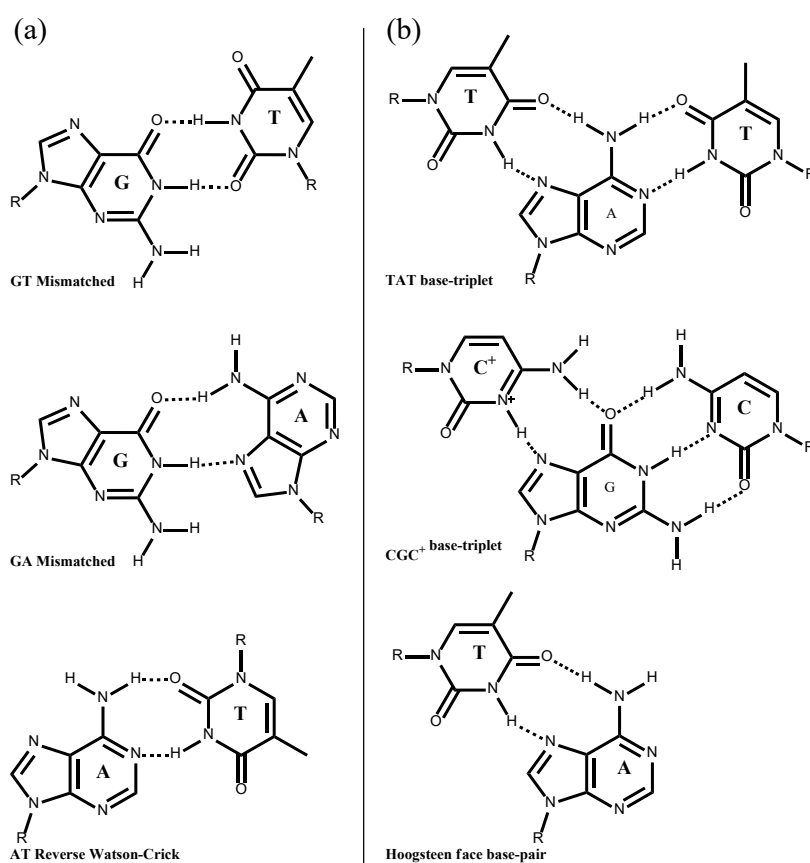


Figure 1.7 Non-canonical binding of nucleobases (a) through the Watson-Crick face, and (b) through other faces. Image adapted from Sivakova *et al.*<sup>18</sup>

The formation of non-canonical structures in DNA does not inherently require non-canonical binding or synthetic DNA sequences. For example, G-quadruplex and *i*-motif are present in natural DNA systems and can form together from DNA in a high potassium concentration environment.<sup>27</sup> The formation of DNA triplexes, shown in Figure 1.7 (b), have also been shown to act as a regulator for gene expression.<sup>28</sup>

For this project it is important to consider these non-canonical binding structures as they affect experimental decisions and what combinations of polymer and DNA should be used for binding studies and polymerisation. This gives insight into the interactions between polymers and any resulting structures formed; for example, combining non-complementary base pairs such as G and T may result in the formation of secondary structures, which might not be desirable for the purpose of the experiment.

#### 1.2.5.1 G-quartets

G-quartets are tetramers of guanine, as shown in Figure 1.8. They form as a result of binding of the Hoogsteen face to the Watson-Crick face and are normally stabilised around a cation.<sup>29</sup> Ivar Bang in 1910 was able to show through observations of how guanylic acid solutions formed gels that G-quartets may form from single nucleotides without the need for additional quartets to be present.<sup>30</sup> This work went relatively unknown until publication by Davies *et al.* in 1962 where they demonstrated using x-ray crystallography that the guanylic acid was made up of fibres formed from the stacking of these G-quartets.<sup>31</sup>



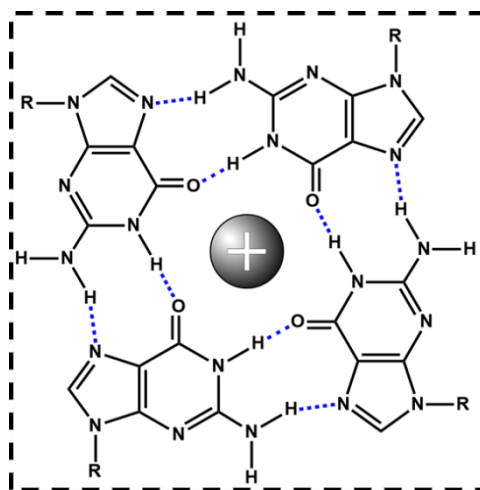


Figure 1.8 The G-quartet as it forms around a cation.<sup>32</sup>

Later work by Becker *et al.*<sup>33</sup> demonstrated for the first time that the presence of metallic cations stabilised the formation of the G-quartet. The degree to which they were stabilised by the cation was dependent on its diameter and charge. It has also been shown that there was a preference for monovalent cations and in most work the alkali metals have been used. Williamson reported on the binding preferences of guanidic acid for these Group I cations as  $K^+ > Na^+ > Cs^+ > Li^+$ .<sup>34</sup> When multiple quartets are coordinated together they form the more stable G-quadruplex, explored further in Section 1.3.3.

### 1.2.6 Nucleic Acids

Nucleic acids are the biopolymers formed by chains of nucleotides. They derive their name from their acidic properties and their presence in the nucleus of the cell. The two naturally occurring nucleic acid biopolymers, deoxyribose nucleic acid (DNA) and ribose nucleic acid (RNA) are the most commonly used.<sup>35</sup> These linear polymers form from the connection of the phosphate to the ribose building a linear polymer, as shown earlier in Figure 1.1, with the nucleobases coming off as pendant groups.

It is the sequence of the nucleobase groups that gives the nucleic acid its coding functionality. For consistency, the sequences of nucleobases are listed in terms of direction along the nucleic acid chain. This directionality is provided in relation to the ribose subunit of the nucleotide in terms of 3' and 5' based on the carbons as shown in Figure 1.3. This is important since synthetic DNA is typically synthesised in the 3' to 5' direction, while enzymatically it is generated in the 5' to 3' direction.<sup>36</sup> This nomenclature is consistent for eukaryotic cells, such as those in mammals.<sup>37</sup> In prokaryotic cells the DNA is a continuous loop and as a result does not have a terminus.<sup>2</sup> In these cases, the 3' and 5' are a reference to directionality within each ssDNA.

These nucleic acids are multiply charged anions due to the negatively charged phosphate and the positive charge on the nucleobase amines, however their actual charge is pH dependent.<sup>38</sup> Under neutral and basic conditions the DNA molecule takes on a negative charge due to the higher pH of the phosphate relative to the nucleobase. It then only takes on a positive charge at low pH, as reported by Guo *et al.*<sup>39</sup> These charges can be used for the isolation of DNA through pH based precipitation, solvent extraction or electrophoresis.<sup>40</sup>

### **1.3 Secondary Structures of DNA**

DNA can form a number of secondary structures; most recognised is the DNA double helix reported by Watson and Crick,<sup>13</sup> however, there are many other variations and alternatives. This thesis focuses on the formation and stability of the DNA double helix and the G-quadruplex as covered in the following sections.

#### **1.3.1 The DNA Double Helix**

Natural DNA is stored as a duplex or dimer structure called a double helix. These consist of two strands of ssDNA running in opposite directions and designated as double stranded DNA, dsDNA. Each of the two ssDNAs that form the duplex are read in opposite directions, leading

to the 3' and 5' notation based on the ribose component of the backbone. Where ssDNA is amorphous dsDNA forms a defined helix shape with a major and minor groove, as shown in Figure 1.9. This behaviour is not as common in RNA which typically exists only in its single stranded form, although double stranded RNA has been found in some viruses.<sup>41</sup>

#### 1.3.1.1 $\pi$ - $\pi$ stacking of nucleobases within dsDNA

The presence of multiple nucleotides in a nucleic acid contributes to additional stability of the overall duplex. This is a result of the nucleobases containing conjugated ring structures with overlapping  $\pi$ -orbitals between the adjacent nucleobases.<sup>42</sup> This means that the presence of adjacent nucleotides has a strong stabilising effect on the nucleic acid as a whole and in turn is a major contributor to the overall stability of the DNA double helix.<sup>43</sup> These  $\pi$ -orbitals stack between nucleobases allowing the formation of other nucleobase secondary structures such as *i*-motifs and G-quartets that are covered in Section 1.1.3.5. The strength of this effect is considered to be dependent on the adjacent nucleobases within the strand and the corresponding amount of overlap; this is called 'the nearest neighbour principle'.<sup>44,45</sup>

The effect of the  $\pi$ - $\pi$  stacking is primarily observed in the macrostructure of the dsDNA. The formation of the double helix is stabilised and coordinated by the stacking with the hydrogen bonding between the base pairs binding it together, i.e., the bases hold the dsDNA together but the  $\pi$ - $\pi$  orbitals orientate them to each other along the strand, limiting their inter-chain effect.<sup>46</sup> This stacking has been shown to be the determining factor for the thermodynamic stability of the dsDNA compared to base pairing. Hydrogen bonding provides for less than half the stability, while the A-T interaction performs as a destabilising force when considered in isolation.<sup>42</sup>

### 1.3.2 Forms of the DNA Double Helix

When two strands of DNA containing complementary sequences of nucleotides bind together they form a DNA duplex, dsDNA. This binding is asymmetric around the long axis leading to the formation of the familiar DNA double helix, as shown in Figure 1.9.

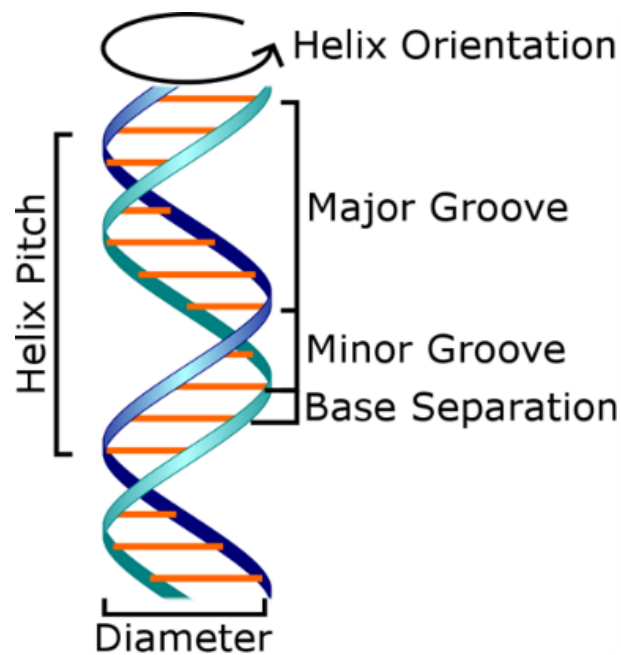


Figure 1.9 Simplified structure of a DNA double helix showing the geometric definitions.

The most common form of this helix is called B-form DNA.<sup>47,48</sup> However, it has been shown that there are additional stable forms of the DNA dimer depending on the conditions. There are three common forms of dsDNA based on conformation of the ribose ring: A-, B- and Z-form DNA. These helical forms differ only in conformation structure as a result of external conditions. Changes in conditions can lead to other forms, including C-form.<sup>49,50</sup> These structures are shown in Figure 1.10 with the dimensions outlined in Table 1.2.

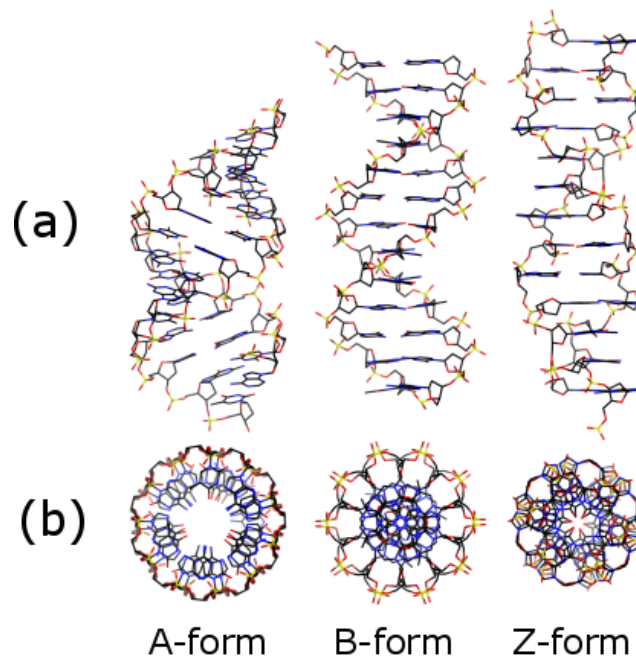


Figure 1.10 (a) helical structures and (b) top down structures of A-, B-, and Z-DNA each 13 nucleotides in length. Provided by Mauroesgueroto,<sup>51</sup> adapted from Ussery.<sup>52</sup>

B-DNA is the most common form and is found in most biological systems.<sup>58</sup> It forms a right-handed helix; the helical axis around which the DNA wraps (see Figure 1.10(a)).<sup>59</sup> This is based on DNA at standard conditions with a non-specific sequence of nucleotides.

A-DNA was discovered and named by Franklin *et al.*<sup>60</sup> and forms a tighter helix than B-DNA which leads to a shorter strand for the equivalent number of base pairs.<sup>61</sup> It forms when DNA is dried or otherwise dehydrated.<sup>62</sup> This results in a sugar pucker at the 3' carbon, shown in Figure 1.11, that reduces the separation between bases.<sup>63</sup> The axis of rotation of A-DNA is exterior to the nucleotide, generating a vertical “tunnel” through the helix. Much like B-DNA, it forms a right-handed helix.

**Table 1.2:** Dimensions of selected DNA forms.

	<b>A-DNA</b> <sup>52,53</sup>	<b>B-DNA</b> <sup>52,53</sup>	<b>C-DNA</b> <sup>54,55</sup>	<b>Z-DNA</b> <sup>52,56,57</sup>
<b>Helix Orientation</b>	Right-handed	Right-handed	Right-handed	Left-handed
<b>Diameter</b>	25.5 Å	20 Å	19 Å	18 Å
<b>Base separation by length</b>	2.3 Å	3.4 Å	3.32 Å	3.8 Å
<b>Base-ribose stereochemistry</b>	<i>anti-</i>	<i>anti-</i>	<i>anti-</i>	<i>syn-</i>
<b>Rotation per base (degrees)</b>	32.7	34.6	38.6	60 per dimer
<b>Base pair per turn</b>	11	10.5	9.33	12
<b>Helix Pitch</b>	28.2 Å	34 Å	30.97 Å	45 Å
<b>Major-minor groove</b>	Yes	Yes	No	No

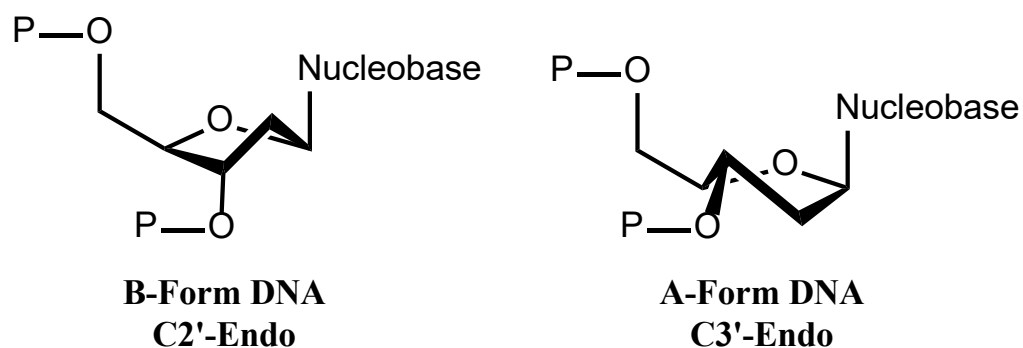


Figure 1.11 The conformations of the deoxyribose change between the B-form and A-form DNA.

Z-DNA is significantly different from A- and B- forms of DNA in terms of structure, most noticeably, it forms a left-handed helix.<sup>56</sup> This is caused by the specific sequence of repeated alternating guanine and cytosine nucleobases. This sequence causes a change in conformation of the nucleotides to form the di-nucleotide shown in Figure 1.12; here, the adjacent ribose subunits are orientated in opposite planes.

Unlike typical DNA, the Z- form is the result of a specific sequence of repeating GC nucleotides within the ssDNA which act as single unit dimers. An additional effect of this is that adjacent ribose rings are orientated in opposite directions, as shown in Figure 1.12. Due to this repeating composition and the change in orientation it acts as if it has a repeating unit consisting of 2 nucleotides.

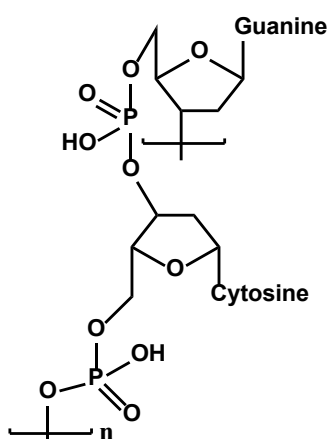


Figure 1.12 Di-nucleotide structure of adjacent nucleotides in Z-DNA.

Other conformations of DNA have also been found, typically requiring specific conditions to appear. Among these is the C-form DNA which is derived from B-form DNA as the conditions approach the lower hydration that causes the change to A-form DNA. Work by Rhodes *et al.*<sup>55</sup> showed that a change in relative humidity can also induce a change to the C-form DNA from either A- or B- form. A-form DNA can also be converted to C-form DNA with an increase in salt concentration, usually magnesium.<sup>64</sup> Portugal *et al.*<sup>54</sup> have additionally shown that the

presence of amino acids, specifically acting as counter ions, favour the conversion to C-form DNA. It may form in the presence of organic co-solvents as demonstrated by Zimmerman and Pfeiffer<sup>65</sup> who showed its formation using *tertiary*-butanol.

The existence of these stable secondary structures indicates that the formation of selective base pairing between nucleic acids of complementary sequences is highly preferred compared to simple hydrophilic interactions. This affords a degree of flexibility in the hypothesis that exotic polymers containing nucleic acid functionality can still undergo this selective binding.

### 1.3.3 G-quadruplexes

Multiple G-quartets, covered in Section 1.2.5.1, are able to form a macrostructure called a G-quadruplex which is formed when three or more quartets complex together through  $\pi$  orbital interactions, often complexing to metal ions between each quartet. They can form from one or more ssDNA sequences resulting in either inter- or intra-molecular assemblies and are typically the most stable of the secondary structures.<sup>66,67</sup>

G-quadruplexes have been shown to be formed around a number of different metallic cations including lead (II),<sup>68</sup> calcium (II),<sup>69</sup> strontium (II),<sup>70</sup> barium (II),<sup>71,72</sup> rubidium (I)<sup>73</sup> and some non-metallic cations such as  $\text{NH}_4^+$ .<sup>74</sup> It has also been shown by Kan *et al.*<sup>75</sup> that the presence of other compounds, specifically polyethylene glycol, causes molecular crowding and induces the formation without the presence of a counter ion.

Guanine nucleobases, relative to the deoxyribose, exist as either *syn*- and/or *anti*- conformations within a G-quartet, Figure 1.13. Characteristic signals in the circular dichroism (CD) spectrum enables identification of the various *syn*-/*anti*- conformations of the inter-G-quartet stacking, Figure 1.14.



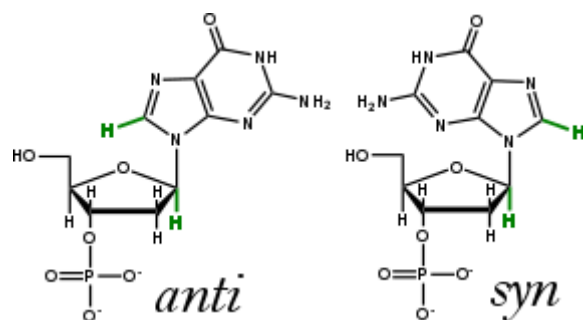


Figure 1.13 *Syn*- and *anti*-conformations of deoxyguanosine based on the relative location of the protons highlighted in green. Image adapted from Stegle *et al.*<sup>66</sup>

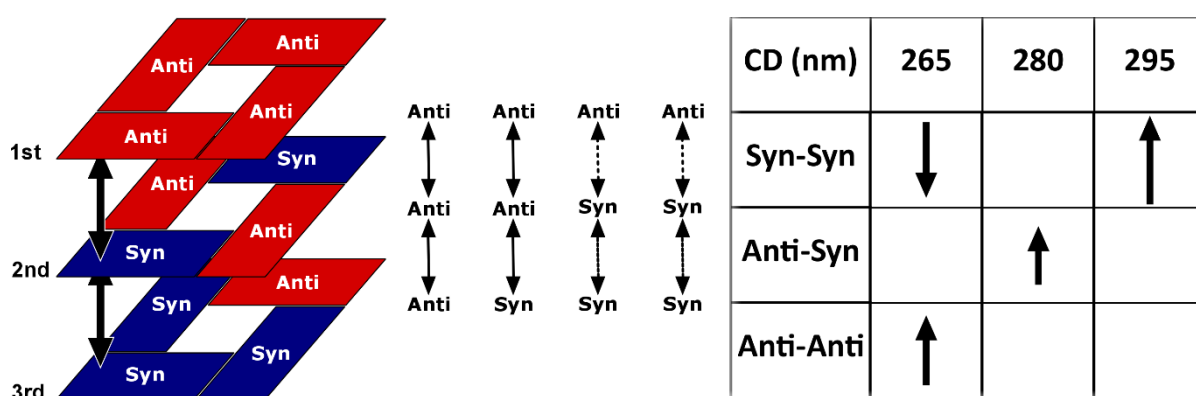


Figure 1.14 The stacking of G-quartets, and their relationship to the circular dichroism (CD) spectra. The number of *syn*- and *anti*- guanines in each quartet determine resulting effect on circular dichroism, not the specific arrangement of these guanines relative to one another.

The effect on the resulting spectra is shown in the table, inset. Image adapted from Tóthová *et al.*<sup>76</sup>

G-quadruplexes have been found to play a role in both natural DNA and RNA sequences as a regulator of cellular processes.<sup>77</sup> G-quadruplexes have additionally found uses in a multitude of disciplines from cancer biology<sup>78–80</sup> and novel therapeutics<sup>80,81</sup> through to nanoelectronics<sup>82</sup> and nanomechanical systems.<sup>83</sup> Adding G-quadruplexes into synthetic polymer-based system makes for a unique macromolecular structure suitable for a broad range of biological applications.

### 1.3.4 Nucleic Acid Wires

Nucleic acid wires are secondary structures made up of multiple shorter sequences, as shown in Figure 1.15. They can be formed by an overhang of repeated sequences or long single nucleotide sequences without an anchor sequence.<sup>84,85</sup>

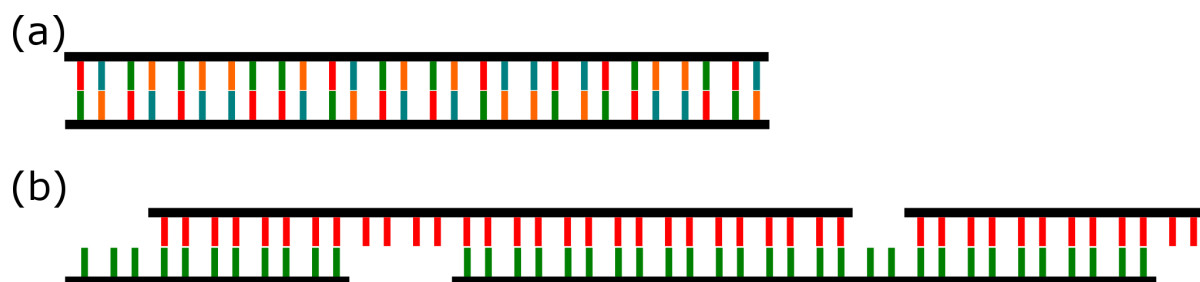


Figure 1.15 (a) complementary dsDNA with variation to prevent non-specific binding and (b) complementary dsDNA without variation and the resulting nucleic acid wire.

Of note to this thesis is the formation of G-quadruplex wires. They are formed in the same manner as dsDNA wires, where there is no anchoring sequence allowing for the formation of long stacked complexes. Work by Marsh *et al.*<sup>86</sup> showed not only the formation of G-wires, but also imaged the wires using atomic force microscopy (AFM), Figure 1.16. Here, they showed the formation of G-wires and the resulting high molecular weight that caused them to show low migration and the distinct smearing when analysed by gel electrophoresis, see Figure 1.17. When the structures were denatured, i.e., melted, they migrated as ssDNA resulting in only a single spot.

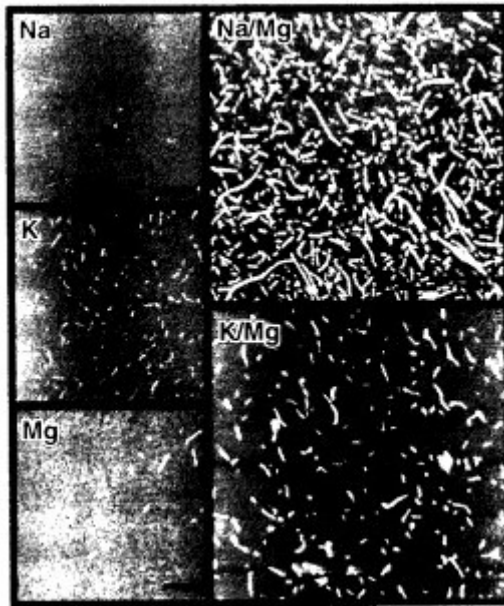


Figure 1.16 Tapping mode atomic force microscopy images of G-wires treated with salt solutions as indicated. Imaged by Marsh *et al.*<sup>86</sup>

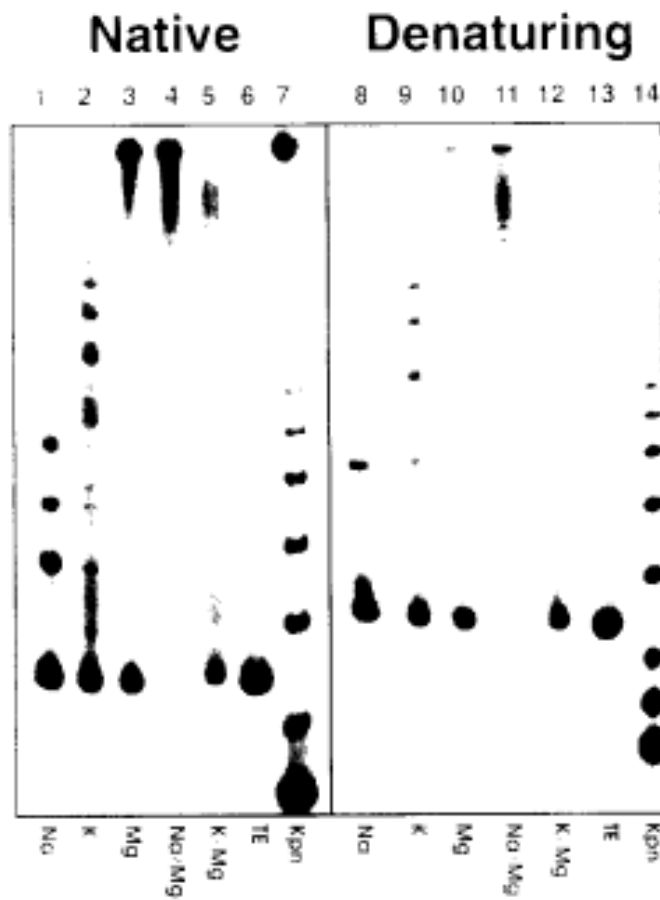


Figure 1.17 Gel electrophoresis of G-wires formed with metallic cations as imaged by Marsh *et al.*<sup>86</sup> Note the high weight fractions at the top of the gels, attributed to G-wires.

### 1.3.5 Xeno Nucleic Acids

Xeno nucleic acids, XNA, are synthetic variations on the nucleic acid structure which contain altered ribose and phosphate subunits, sometimes substituting them completely. This preserves their binding selectivity with the nucleobase moiety. Most common in XNAs are alterations to the ribose but some contain different backbones in place of the ribose phosphate found in DNA and RNA.

Demonstrating the properties and stability of XNAs is important to this work as it shows that the formation of selective binding is not isolated to natural nucleic acids. Further, variations in the composition and structure may affect structures, but do not inherently prevent the formation of Watson-Crick or other types of binding. For this project the polymers generated had a 2-carbon bond spacing between repeating units, substantially shorter than the inter-nucleotide distance of DNA.

Common among these, XNA are locked nucleic acids. They contain an additional carbon in the ribose connecting the 2' hydroxyl to the 4' carbon as shown in Figure 1.18. It is called a locked nucleic acid because it is unable to form the 2' endo conformation required in the B-form DNA helix and is therefore locked in the 2' endo conformation. This allows selective formation of the A-form without the normal hydration or salt content, described in Section 1.3.2.

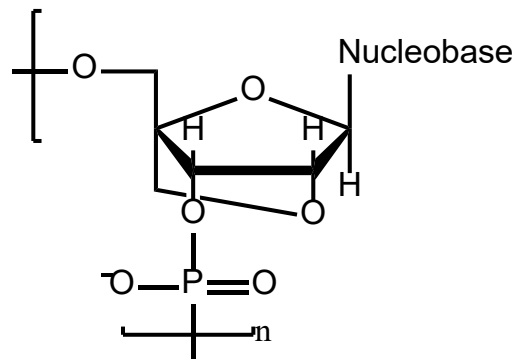


Figure 1.18 Locked nucleic acid, LNA, one of the xeno nucleic acids.

Peptide nucleic acids contain a polypeptide backbone, retaining only the nucleobase functionality as shown in Figure 1.19. The peptidic nucleic acid structure is notable to this project as it has been shown by Nielsen *et al.*<sup>87</sup> to form a helical structure similar to DNA, despite having a structurally distinct backbone with different charge and nucleobase separation compared to any naturally occurring nucleic acid.

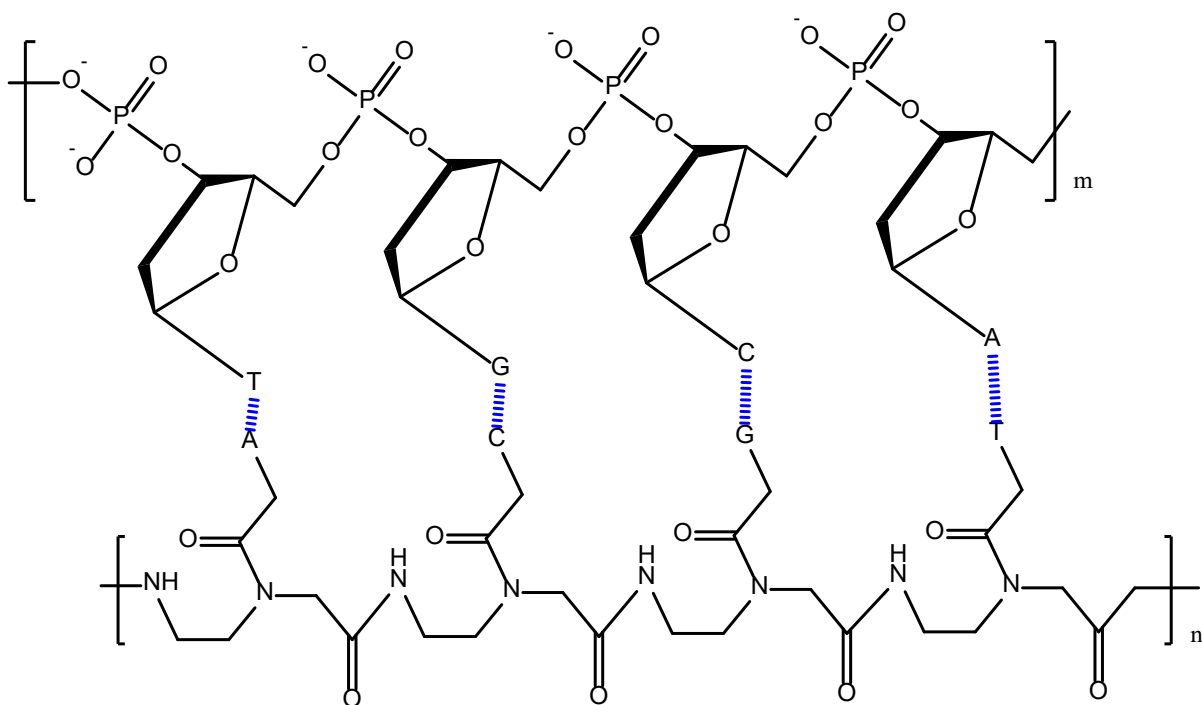


Figure 1.19 An example of a simple PNA dimer.<sup>87</sup> Nucleobases abbreviated adenine (A), cytosine (C), thymine (T) and guanine (G) with . Image adapted from Nielsen *et al.*<sup>87</sup>

## 1.4 Synthesis of DNA

### 1.4.1 Enzymatic Synthesis of DNA

DNA sequences can be copied onto a template strand through the use of enzymes called polymerases, both *in-vitro* and *in-situ*. Polymerases are a class of enzymes that transcribe DNA from a template sequence onto a new sequence doubling the volume of DNA in the solution where the subsequent templated DNA polymer is complementary to the initial template. These enzymes vary across species and cell types but can be extracted for use *in-vitro*. The most common example is *Taq* polymerase derived from the bacteria *Thermus aquaticus*.<sup>88</sup> *In-situ* DNA replication is carried out on dsDNA which interacts with enzymes and separates only in target regions.<sup>89</sup> In synthetic methods such as the polymerase chain reaction (PCR), covered in the following section, the dsDNA is heated until melting, where the nucleobase dehybridises, forming ssDNA.

The transcription process performed by these enzymes is unidirectional, typically occurring in the 5' to 3' direction as shown in Figure 1.1.<sup>90</sup> This results in the ssDNA containing phosphate functionality at the 5' terminus, and hydroxyl functionality at the 3' terminus.

#### 1.4.1.1 The Polymerase Chain Reaction

The most common method for *in-vitro* DNA synthesis is PCR. This is an amplification method whereby a sequence of DNA is repeatedly transcribed into a new sequence. It is often called an amplification process because it requires an initial template, and all DNA produced during the process is either complementary or equivalent to that original sequence. It is typically used for sequences in the range of 25 up to 2,000 bases.<sup>91</sup> The enzymatic process is preferred for many applications as the DNA is copied reliably and with virtually no error.<sup>92</sup> Under specialised conditions, reported by Cheng *et al.*,<sup>93</sup> an excess of 50,000 bases (approximately

16,350 kDa) has been recorded. The exact range for PCR is determined by the enzymes used, but the process is consistent with that shown in Figure 1.20.

To perform this synthesis, the dsDNA to be amplified is placed in a solution with free nucleotides and primers; the latter are short chain complementary DNA which defines where the transcription will begin. In a typical experiment, a dsDNA template is heated to approximately 95 °C in order to melt and separate the dsDNA into ssDNA. It is then cooled to 68 °C in order to anneal the complementary primers to the ssDNA which then allows for the binding of *Taq* polymerase. This enzyme is then activated by heating to 72 °C for the transcription. Here, the enzyme moves along the template strand drawing nucleotides from solution and extending the daughter strand.

Each cycle of this process effectively doubles the number of DNA strands in a sample. This process maintains all the properties of the original DNA and copies created this way are indistinguishable from it once the process is complete. The choice of primers determines the region of the DNA to be replicated and can be used to target specific genetic sequences,<sup>94,95</sup> or to add functionality to the 5' terminus of the ssDNA.<sup>96</sup> The major drawback of PCR is its limited scale, typically with output in the order of micrograms, as reported by Wang *et al.*<sup>97</sup>

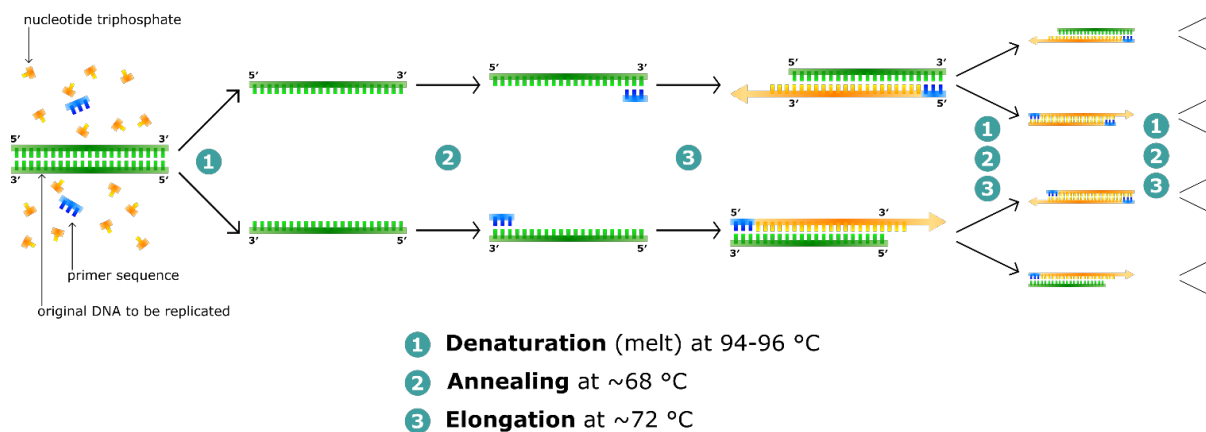


Figure 1.20 Outline of the steps in the polymerase chain reaction (PCR). Adapted from Gill *et al.*<sup>98</sup>

## 1.4.2 Chemical Synthesis of DNA

Chemically synthesised oligonucleotides are relatively short sequences of nucleic acids, compared to those found in biological systems.<sup>99,100</sup> They can vary in size from 2 to 2,000 bases in length, but for most research applications they are at the lower end of this range, typically <250 bases.<sup>101</sup> These ssDNA sequences are generated through a single addition process similar to step-growth polymerisation. Methods of chemical synthesis normally rely heavily on the use of protecting groups to prevent reaction of the non-terminal alcohol.<sup>102</sup> The earliest popular method was the H-phosphonate method developed in 1952<sup>103</sup> which was then followed by the phosphodiester and phosphotriester<sup>104</sup> techniques in the later 1950s and 1960s. These methods all relied on the coupling of the 3' hydroxyl to the 5' phosphate of individual nucleotide phosphate derivatives in much the same way as the phosphoramidite method discussed in the following section.

This thesis focuses on the coupling of nucleotides to vinyl moieties using a modified version of the phosphoramidite method. This choice of method was made due in part to the comparative difficulties of the phosphor-ester and H-phosphonate methods. Those are covered briefly in



this work as they were considered a possible alternative should the phosphoramidite method have proven unsuccessful, or for future work where their differing substrates may prove more useful.

#### 1.4.2.1 H-Phosphonate Method for the Chemical Synthesis of DNA

The H-phosphonate method uses a 3' phosphonate nucleotide and couples it to the 5' hydroxyl of the growing chain using a condensing agent such as pivaloyl chloride.<sup>105</sup> One of the major benefits to this method is that the nucleobases do not require protection, as shown by Kung *et al.*<sup>106</sup> In general it is no longer used commercially due to its lower yield, but has found application where additional functionality is needed, as the coupled phosphonate is in equilibrium between the PO<sub>3</sub>H and PO<sub>2</sub>OH.<sup>102</sup> Due to this lower yield and the reactive PO<sub>3</sub>H intermediate it was ruled out for this project.

#### 1.4.2.2 Phosphoester Approaches for the Chemical Synthesis of DNA

The phosphodiester and phosphotriester methods are condensation reactions for the chemical synthesis of DNA.<sup>107</sup> These were developed in the 1970-80s during the time between the H-phosphonate and phosphoramidite methods, but have now fallen mostly out of use due to their relatively low yields.<sup>108,109</sup> More recently they have found some new application benefiting from their comparatively simple substrates.<sup>110</sup> The reaction for the phosphotriester method is shown in Figure 1.21.

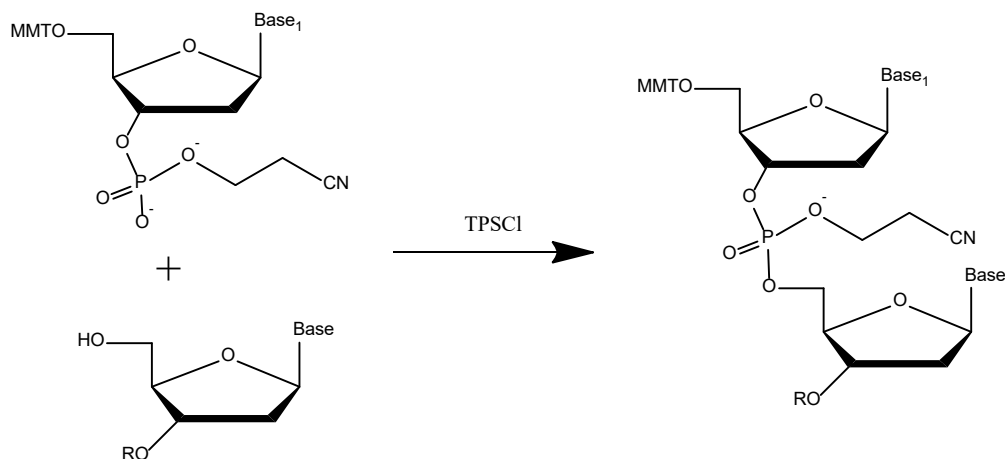


Figure 1.21 Phosphotriester method for the addition of a nucleotide to the growing oligomer.

Adapted from Reese *et al.*<sup>107</sup> Here the 5' position is protected by monomethoxytrityl (MMT) moiety and the coupling agent is triisopropylbenzenesulfonyl chloride (TPSCl).

While these methods require the same protection of the nucleobases compared to other methods described, they use the more reactive P(V) phosphate making it less suitable for coupling to small reactive hydroxyl containing molecules due to the susceptibility to ligand exchange.<sup>111</sup> Further, the activators for these reactions are benzenesulfonyl chloride derivatives which could produce undesirable competitive polymerisations if used with the bioconjugated vinyl-nucleotide intended for this project.

### 1.4.3 Phosphoramidite Method for the Chemical Synthesis of Nucleic Acids

The phosphoramidite method was developed specifically for the synthetic production of DNA; it is a process of sequence addition through the nucleophilic substitution of a phosphoramidite monomer. Due to the level of specificity required, it is typically a surface grafted technique.<sup>102</sup> The process is highly sensitive to water and the reactions are performed in acetonitrile<sup>112</sup> as a cyclic step-wise addition process, as shown in Figure 1.22, with each cycle adding another phosphoramidite monomer.

The typical phosphoramidite method for DNA synthesis utilises a 3' surface grafted nucleotide as the first nucleotide. The process begins with the removal of the 5' dimethoxytrityl protecting group using a mild acid, typically chloroacetic acid.<sup>113</sup> The next phosphoramidite to be added in the sequence is then activated with 1*H*-tetrazole or a derivative<sup>114</sup> and added to the growing oligonucleotide. Tetrazole acts as a regenerated catalyst and substitutes with the diisopropylamine, in turn substituting with the deprotected 5' hydroxyl group of the growing oligonucleotide. The surface is then washed to remove residual activated phosphoramidite and the process is repeated for each nucleotide addition. For simplicity the oxidation and final deprotection is normally conducted at the end following the complete oligonucleotide synthesis.

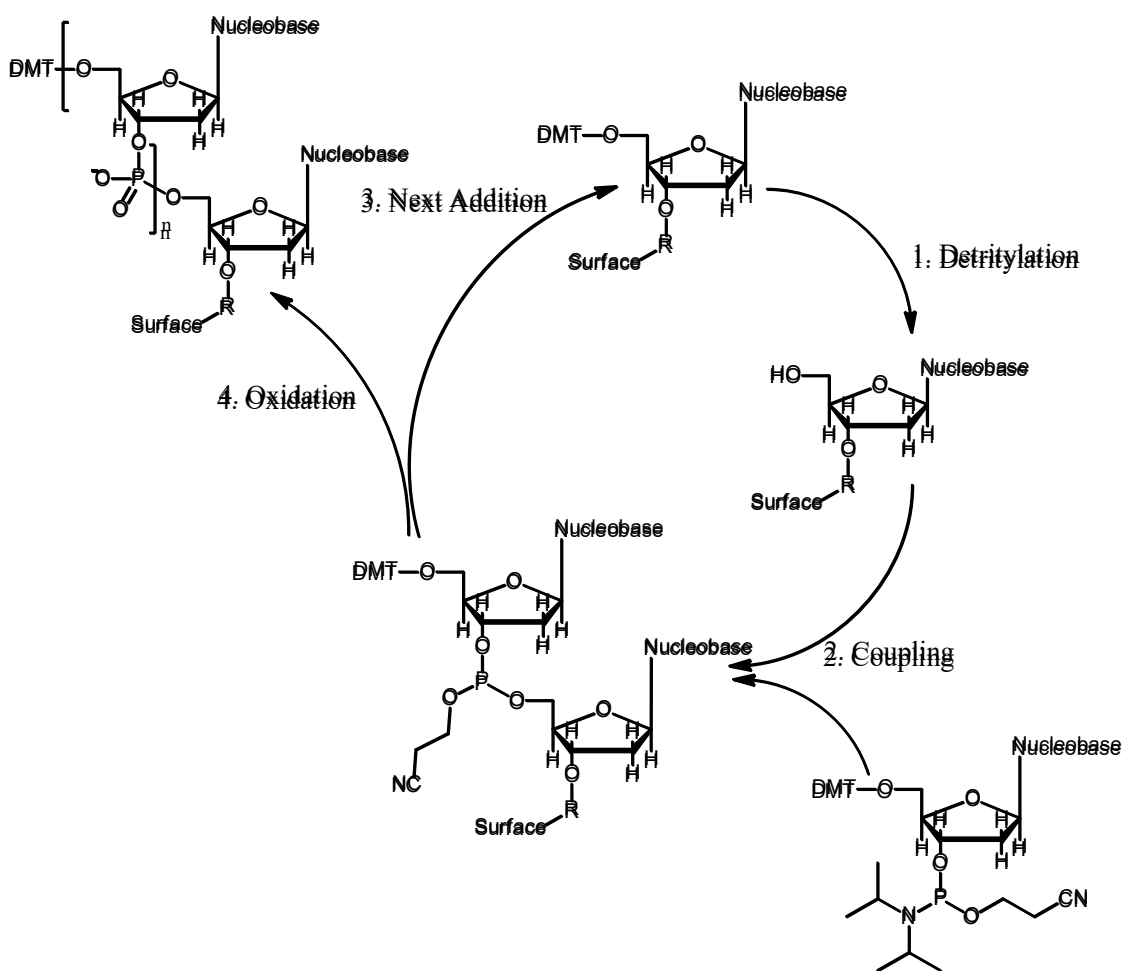


Figure 1.22 Outline of the phosphoramidite method for DNA synthesis. Adapted from DNA Oligonucleotide Synthesis.<sup>115</sup>

#### 1.4.3.1 Activators

Activators are the reagents in the coupling step, shown in Figure 1.22, that create the intermediate phosphoramidite to undergo the  $S_N2$  reaction. The most common activator is 1*H*-tetrazole. The mechanism of the coupling is debated with the activator being both an acid catalyst, and also shown to act as a nucleophile to generate a P-tetrazolyl intermediate, as outlined in Figure 1.23. Following coupling, however, the activator is regenerated so once an excess is present the reaction is typically quantitative. A variety of possible activators may be

used, with some showing improved reactions and preferences when using non-standard phosphoramidite.<sup>116,117</sup>

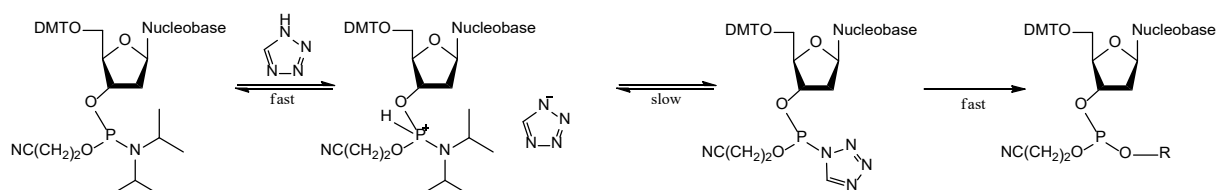


Figure 1.23 Formation of the active intermediate phosphoramidite cation, and conversion to the coupled phosphite via the phosphoramidite method. The R-group is the propagating chain or surface to be grafted from.

Berner *et al.*<sup>118</sup> investigated the properties of a number of simple azolyls, containing between one and four nitrogens, to prove the formation of the phosphate. They found that the initial protonation of the phosphorus was rapid, but the subsequent formation of the tetrazolophosphane was the rate limiting step. Further, they showed that the subsequent coupling and formation of the phosphoester linkage is irreversible.<sup>119</sup> The mechanism has been later advanced by Russell *et al.*<sup>120</sup> who further supported this hypothesis with a number of other tetrazole derivatives.

The common alternative to tetrazole is 4,5-dicyanoimidazole (DCI) (Figure 1.24(b)), proposed by Vargeese *et al.* in 1998.<sup>121</sup> Though chemically distinct from tetrazole, it shares structural similarities, as shown in Figure 1.24. Notably, the ring structure is still able to stabilise the negative charge formed during the phosphor protonation, with electron withdrawing groups in the 4 and 5 position. There are several major benefits to DCI instead of tetrazole.<sup>122</sup> Most notable is its higher coupling rate, twice that of tetrazole;<sup>123</sup> further, the higher pKa of 5.2 compared to 4.8 for tetrazole makes it better for the extended reaction times required for bulkier phosphoramidites. This allows for faster reactions with lower acidity, reducing the exposure of the phosphoramidite to the conditions that lead to its degradation.<sup>124</sup> Another alternative

activator is 5-ethylthio-1*H*-tetrazole (Figure 1.24(c)), proposed by Wincott *et al.*<sup>125</sup> which showed a higher coupling rate between free nucleotide phosphoramidites in solution and the propagating surface oligomer when compared to tetrazole.

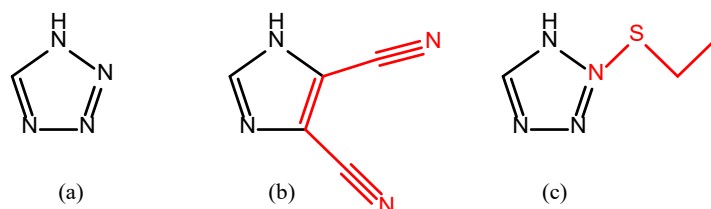


Figure 1.24 Diagram demonstrating the structural similarities of (a) 1*H*-tetrazole, (b) 4,5-dicyanoimidazole and (c) 5-(ethylthio)-1*H*-tetrazole. Modified groups are shown in red.

#### 1.4.3.2 Non-nucleotide Additions

The phosphoramidite method can be used to add other non-nucleotide phosphoramidite species, as discussed in the following section. The phosphoramidite method utilises a number of different protecting groups for the hydroxyl and amine moieties. Typically, the 5' hydroxyl is protected by a 4,4'-dimethoxytrityl regardless of the nucleotide being used.<sup>126,127</sup> Adenine and cytosine are both protected with benzoyl protecting groups on the 6 and 4 carbon amines respectively; guanine is normally protected with the isobutryl or dimethylformamide due the para-position of its amine on the nucleobase.<sup>128</sup>

Commercially there are alternative phosphoramidites used when mild conditions are required. Typically the result of additional functionality which has been incorporated into the DNA sequences that are sensitive to harsh conditions.<sup>129</sup> In these cases a trimethoxytrityl group is used on the 5' hydroxyl due to its better leaving group functionality.<sup>130</sup>

### 1.4.3.3 Oxidation

Oxidation is the step that generates the phosphate, stabilising the structure of the nucleic acid. In literature this step normally utilises a mixture containing pyridine and  $I_2$  as the active components.<sup>131</sup> This process is outlined in Figure 1.25. The  $I_2$  initially reacts with the phosphite to generate the  $P^+$  intermediate which, in turn, undergoes nucleophilic substitution with water, catalysed by the presence of the pyridine, generating pyridinium iodide as a by-product. Further reaction with pyridine at the phosphate results in complete oxidation to the P(V) state. Other oxidants have been considered for this experiment, including the comparatively gentle process demonstrated by Cvetovich<sup>132</sup> using  $H_2O_2$  as an alternative.

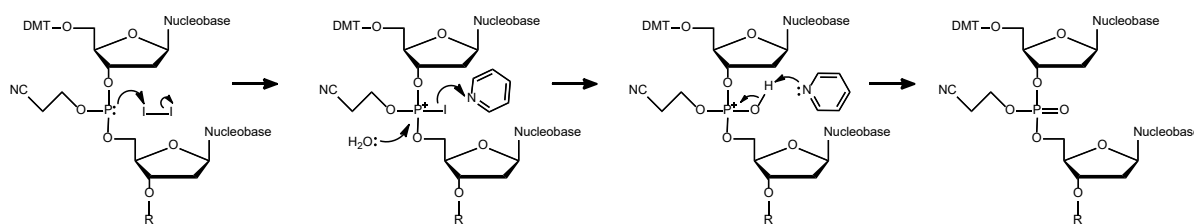


Figure 1.25 Oxidative mechanism of the phosphoramidite method for DNA synthesis using pyridine/ $I_2$ .<sup>115</sup>

### 1.4.3.4 Deprotection

During the synthesis of nucleic acids through the phosphoramidite method two deprotection steps take place. The first step is detritylation which occurs between each cycle of addition. It removes the DMT protecting group, in the process generating the alcohol required for the next nucleotide addition, as shown in Figure 1.22. Due to the dry conditions required for the coupling, it is normally conducted with trichloroacetic acid which is soluble in acetonitrile. If conducted outside of the phosphoramidite reaction however, almost any acid can be used to achieve the same outcome. One of the major benefits of this process is that it is quantitative

and can be observed thanks to the bright orange colour appearing as a result of formation of the DMT cation.

The second deprotection step is typically conducted following the complete synthesis of the nucleic acid oligomer. This step removes the protecting groups from both the phosphate and nucleobase, generating the active nucleic acid. The presence of the protecting groups on the phosphate and nucleobase prevent the nucleophilic components of the nucleobases and the hydroxyl group on the phosphate conjugate acid from reacting during the coupling step. The method for performing this step and removal of cyanoacryl protecting group is treatment with concentrated ammonia at 60 °C.

#### 1.4.4 Modified Nucleic Acids

Specific terminal functionality can be incorporated into the template DNA through the addition of moieties to the 5' end of the primer sequence. This method has been used, for example, to add fluorescent tags to detect the binding and unbinding of DNA probes for analytical applications.<sup>133</sup>

Addition of thiol moieties has been achieved by Sinha *et al.*<sup>134</sup> using a H-phosphonate derivative. This method treats DNA with a H-phosphonate salt containing thiol moiety, in the presence of a bulky acyl chloride. Further advancement of this work was recently conducted by Kupihár *et al.*<sup>135</sup> through the creation of a thiol functionalised phosphoramidite which was incorporated into DNA at the 5' terminus. The benefit of this method was that it could be included in commercial phosphoramidite-based DNA synthesisers without modification, compared to the original H-phosphonate method that was a post-synthesis addition.

Other terminal DNA moieties have also been demonstrated by Rabe *et al.*<sup>136</sup> who conjugated the streptavidin protein to thiolated DNA resulting in a protein-DNA bioconjugate. This was



done by using maleimide functionalised streptavidin and coupling it to a terminal thiol on a C<sub>6</sub> linker. The biggest drawback of this method was that the reaction resulted in only a 10% yield, although they discussed that the maleimide reacted selectively to the terminal thiol and not the thiolated DNA component.<sup>136</sup>

#### 1.4.5 Visualisation of Nucleic Acids Using Fluorescent Dyes

Fluorescent dyes have been used for the detection of nucleic acids and their binding state in many experiments. The binding of the dye causes its confinement, thus increasing its quantum yield. These dyes are classified based on their binding location and the type of interaction, as shown in Figure 1.26; most common are the intercalation between base pairs with some dyes, and bis-intercalators binding between multiple pairs.<sup>137,138</sup> Less commonly dyes may also bind externally, or in the grooves of DNA where they are selective to either the major or the minor groove, typically dependant on the size.

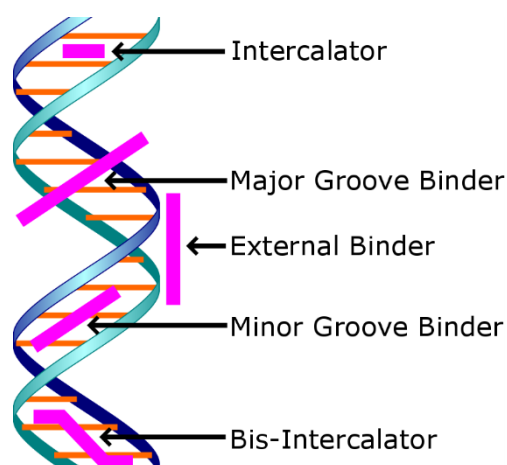


Figure 1.26 Sites of binding of fluorescent dyes in the DNA double helix.

Intercalating dyes are molecules that insert into dsDNA between the base pairs and complex to the  $\pi$ - $\pi$  orbitals. These dyes are commonly used to detect all DNA within a sample for visualisation or measuring the process of amplification, covered in Section 1.4.1.1.<sup>139</sup> The most

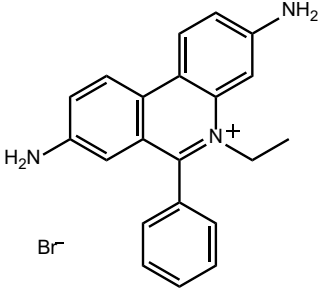
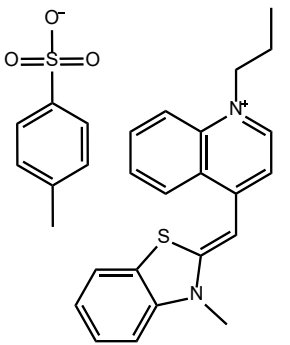
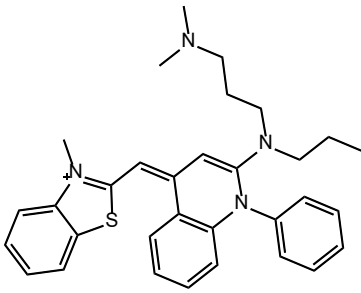
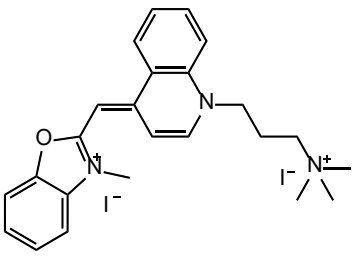
commonly used intercalator dye has been ethidium bromide.<sup>140</sup> However, due in part to its toxicity, there is now a wide range of alternative stains available, most notably the SYBR series of dyes. These dyes intercalate within the helix and are complexed to the  $\pi$ -orbitals<sup>141</sup> which prevents the heterocyclic dye systems from changing orientation, and that is what creates their fluorescent appearance.<sup>141,142</sup> Yo-Pro™ stains also fit into this category with its intercalation being the major source of their fluorescence.<sup>143</sup>

Groove binding dyes fill the vacant regions in the base pair plane and fill whichever groove they can fit in. Some of these dyes have also been shown to act as intercalating dyes.<sup>144,145</sup> Hoechst stains as a class are exclusively groove binding dyes.<sup>146</sup> Cyanine dyes, such as SYBR and dsGreen, have been shown by Vitzthum *et al.*<sup>147</sup> to bind as both intercalating dyes and groove binding dyes, with the majority of the fluorescent yield coming from the groove binding position.

External binders are a unique class of dyes as they attach through electrostatic interactions rather than selective binding to DNA<sup>148</sup> which makes them more suitable for visualisation applications. However, this type of dyes lacks specificity towards nucleic acids which makes them least suitable for the polymer-nucleic acid systems investigated in this project.<sup>149</sup>

For this project the dyes used were SYBR™ Green II, dsGREEN, Yo-Pro-1 Iodide and SYBR™ SAFE. The SYBR name is a trademark of ThermoFisher Scientific and refers to a class of mostly cyanine dyes. These dyes were chosen based on their performance extensively described in literature and their selectivity for different binding conditions, as listed in Table 1.3.

**Table 1.3:** Fluorescent intercalating DNA dyes. Data provided by Thermo Fisher Scientific.

Name	Structure	Absorption/Emission wavelength (nm)	Type of nucleic acid detected
<b>Ethidium bromide</b>		(210 and 285)/605	ssDNA, dsDNA
<b>SYBR™ Safe</b>		509/524	dsDNA, DNA and RNA in gel
<b>SYBR™ Green I dsGreen</b>		497/520 454/524	dsDNA, DNA and RNA in gel
<b>YO-PRO™-1 Iodide</b>		491/509	DNA in cells
<b>SYBR™ Green II</b>	Unknown, trade secret	(254 and 497)/520	RNA, ssDNA
<b>SYBR™ Gold</b>	Unknown, trade secret	(495 and 300)/537	ssDNA, dsDNA

## 1.5 Synthetic Polymers

This thesis covers the generation of synthetic polymers that replicate properties characteristic to nucleic acids. The replication is achieved through the incorporation of nucleotides into monomers and then subsequently polymerising them. Out of a broad range of polymerisation techniques that could be used, several are covered in this section, and then narrowed down to the method chosen: mediated living radical polymerisation.

### 1.5.1 Types of Polymers

The polymers synthesised in this project were homopolymers: polymers generated from only a single monomer, as this allowed the polymers to be interrogated while limiting their secondary effects. Existing literature that studies the synthesis and interactions of synthetic DNA analogues has frequently used heteropolymers,<sup>150</sup> polymers containing a mixture of monomers, as such an explanation of them is given here for clarity.

Block co-polymers contain discrete regions generated from each monomer. For example, ABA-type co-polymers would be made up of one block of monomer A followed by a block of polymer B and then ending in another block of polymer A. These can be made by the addition of a second monomer of significantly higher reactivity partway through the polymerisation or through pausing, cleaning, and restarting the polymerisation.<sup>151</sup> This has been demonstrated by a number of groups, though notably Manguian *et al.*<sup>152</sup> demonstrated the use of a novel first block that allowed for the synthesis of a second block that was otherwise incompatible in their solvent system.

One of the additional benefits to block co-polymers is that they can be used to combine polymerisation techniques. For example, Klaerner *et al.*<sup>153</sup> combined the formation of a radical polymerisation with a condensation polymerisation for the formation of block co-polymers. In

their work they specifically showed the concurrent formation of the two blocks, possibly because the monomers were orthogonal to the opposing techniques. The result of this work could allow for the increased speed of synthesis of mixed functionality polymers.

Typically, as no two monomers have the same reactivity, the radical will begin to propagate with the more active monomer first, effectively starting as a homopolymer. As the more reactive monomer is consumed the balance shifts and the now higher concentration of the second monomer causes it to be preferred.<sup>157,158</sup>

### 1.5.2 Describing Synthetic Polymerisations

The effectiveness of these polymerisation methods and the characteristics of the resulting polymers are measured by a number of metrics: conversion, size, composition, and dispersity index ( $\mathcal{D}$ ).

Conversion is a simple mass transfer metric and is the equivalent to extent of reaction,  $\xi$ , shown in Equation 1.1,<sup>159</sup> where  $\xi$  is a percentage value that represents the mass of monomer that has been converted to the polymer,  $\Delta n_i$  is the amount of each reagent, and  $\nu_i$  is the stoichiometric amount initially. For addition polymerisations this formula can be simplified to Equation 1.2, as there is no ejected small molecule and the stoichiometry is 1:1; here  $m_f$  is the mass of monomer remaining and  $m_i$  is the initial amount of monomer. High values are considered a better result as this indicates efficient use of the monomer reducing the amount of isolation required and unused monomer wasted.

$$\xi = \frac{\Delta n_i}{\nu_i} \quad \text{Equation 1.1}$$

$$\xi = \frac{m_f}{m_i} \quad \text{Equation 1.2}$$

Dispersity,  $D$ , represents the uniformity of the polymer chain size. It is calculated using the formula shown in Equation 1.3 to determine the distribution and uniformity of the polymer.<sup>160</sup> These equations for  $D$  determine how far the population distribution for polymer length differs from a perfect bell curve. As the value of  $D$  increases above 1, the uniformity of the polymer lengths decreases. In biological systems such as nucleic acids and proteins the value of  $D$  is 1: it means that every polymer chain is exactly the same length and of the same composition. The calculation of  $D$  uses a series of averages that describe the size of the polymer chains in terms of their mass. These are number average molecular weight ( $M_n$ ) and weight average molecular weight ( $M_w$ ). The  $M_n$  is the unweighted average molecular weight of the polymers, i.e., the total weight of the polymer chains in the sample divided by the number of polymer chains in the sample,  $N$  (Equation 1.4).  $M_w$  is the weighted-average molecular weight that preferences longer chains as shown in Equation 1.5.

$$D = \frac{M_w}{M_n} \quad \text{Equation 1.3}$$

$$\bar{M}_n = \frac{\sum_i N_i M_i}{\sum_i N_i} \quad \text{Equation 1.4}$$

$$\bar{M}_w = \frac{\sum_i N_i M_i^2}{\sum_i N_i M_i} \quad \text{Equation 1.5}$$

The dispersity is thereby related to the degree of polymerisation (DP) which indicates the average number of repeating units within a polymer chain in a given sample. As the mass of the repeating unit is generally a constant this can be described by Equation 1.6, where  $M_n$  is the number average molecular weight of the polymer and the  $M_0$  is the molecular weight of the repeating unit.

$$DP = \frac{M_n}{M_0} \quad \text{Equation 1.6}$$

### 1.5.3 Free Radical Polymerisations

Free radical polymerisation is a chain-growth polymerisation method that generates linear carbon chains resulting in polyethylene-based polymers. The formation of the polyethylene chain begins with the decomposition of an initiator, such as azobisisobutyronitrile (AIBN), to generate a radical. This radical then attacks the unsaturated carbon-carbon bond as shown in Figure 1.27; this leads to the propagation phase where the terminal radical reacts with another vinyl moiety, adding a single monomer unit which leads to the regeneration of another terminal radical.

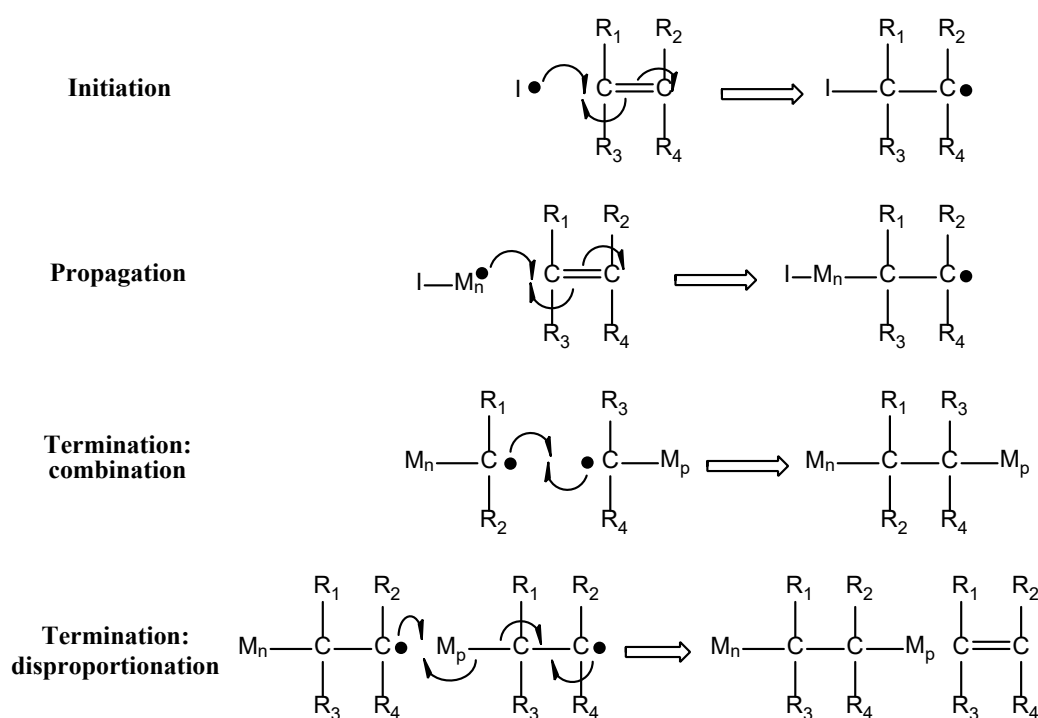


Figure 1.27 Radical Polymerisation, mechanisms and processes. The initiator (I) creates radicals that react with monomer units (M) to propagate the polymer. Adapted from Living

Radical Polymerization by the RAFT Process – A Second Update.<sup>161</sup>

This propagation phase continues until ended by a termination event that destroys the radical from the chain. This may happen with the addition of a non-propagating species to quench the

reaction, an additive, or through two propagating chains interacting. Of the latter there are two types: firstly, termination through combination where two propagating radicals react to form a single chain; secondly, disproportionation where a propagating radical reacts with another chain causing a fragmentation which can result in a small molecule being formed which may be a different monomer.<sup>161</sup>

#### 1.5.4 Controlling Dispersity of Living Radical Polymers

There are a number of methods used to lower the  $D$  of a polymer towards the ideal  $D = 1$ , all of which broadly fall into one of two categories: isolation or mediation.

Isolation means the reaction is controlled by limiting the monomers access to their initiator.<sup>162</sup>

A typical example presented for this type of control is the utilisation of step-growth condensation polymerisations where the repeating unit is comprised of two monomers, such as a dialcohol and a diisocyanate, that do not polymerise individually but will react together.<sup>163</sup> As this reaction typically proceeds to completion, stoichiometric additions of each monomer ensure single monomer addition to the terminal groups.<sup>163</sup> For radical polymerisations this is demonstrated with emulsion polymerisation;<sup>164</sup> here the monomer is encapsulated within a two-phase mixture. The bulk phase is the non-solvent within which the solvent forms an emulsion: 'capsules' of solvent contain, ideally, a single initiator and a uniform amount of monomer in each one.<sup>152</sup> These then propagate within the capsule until all of the monomer is exhausted. As all the capsules contain the same amount of monomer the resulting polymers should be of the same molecular weights and  $D$ . In practice, however, it is rarely the case that there is a perfect 1:1 ratio of initiator to particle, or that the monomer is evenly distributed.<sup>165,166</sup>

Mediation methods imply an introduction of an additional component to the reaction that controls the rate of polymerisation, typically slowing it down so that no individual polymer chain propagates significantly ahead of the others.<sup>167,168</sup>



Reversible-deactivation radical polymerisation (RDRP) is a group of these mediated polymerisation techniques that control polymer synthesis using a mediator possessing an equilibrium.<sup>169</sup> This mediator limits propagation of the polymer by activating and deactivating chains.<sup>169</sup> Compared to standard uncontrolled free radical polymerisation the process is typically slower as many chains are inactive.<sup>170</sup> As a result of the equilibrium between active and dormant polymers results in lower dispersity index and greater control over molecular weight.<sup>171</sup> Termination events are also less common as a result of the majority of chains being inactive at any given instant.<sup>161</sup> There are a number of these types of polymerisations, including atom-transfer radical polymerisation (ATRP), nitroxide-mediated (NMP) and reversible addition-fragmentation chain transfer (RAFT) polymerisation. For the purpose of this thesis RAFT was chosen and is covered in the following section.

## **1.6 Reversible Addition-Fragmentation Chain Transfer Polymerisations (RAFT)**

Reversible addition-fragmentation chain transfer polymerisation is a technique developed by the CSIRO in 1998.<sup>172</sup> The fundamental process is similar to that of a radical polymerisation. The control is provided by the presence of a chain transfer agent (CTA): these compounds are outlined in the following section, but their interactions are all similar. The RAFT agent intercepts a propagating chain and then either regenerates the chain or passes off the radical onto a secondary chain. As a result, the complete process creates a number of chains equal to the number of initiators and the number of RAFT molecules. This process is visualised in Figure 1.28.

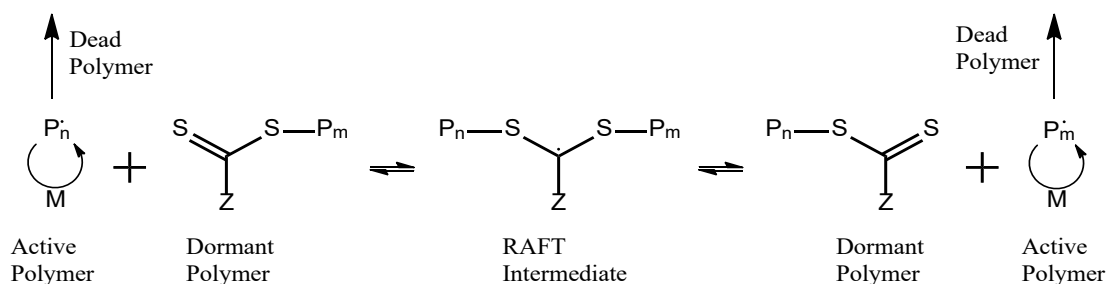


Figure 1.28 RAFT mediation mechanism, adapted from Moad *et al.*<sup>173</sup> Vertical arrows indicate the polymer exiting the RAFT mediation as dead polymers through termination (combination or disproportionation).

### 1.6.1.1 Monomers

RAFT polymerisation in principle works with all monomers compatible with radical polymerisation, for example, molecules containing an ethene functionality. In general, these monomers are divided into 2 classes: more-activated monomers (MAMs) and less-activated monomers (LAMs). This class combined with the reaction conditions required, temperature, solvent, and initiator, are the criteria used to determine a suitable RAFT agent. The following is a brief description, with more detailed explanation of their kinetics in relation to RAFT polymerisation covered in Section 1.6.1.3.

MAMs are monomers that contain an electron deficient vinyl group with radical stabilising substituents: they include those adjacent to aromatic, carbonyl or nitrile groups. Conversely, LAMs are monomers that contain an electron rich vinyl group with radical destabilising substituents: they include those adjacent to methyl, nitrogen or oxygen lone pair, or a heteroatom of a heteroaromatic ring.<sup>174</sup> Some examples are shown in Figure 1.29.

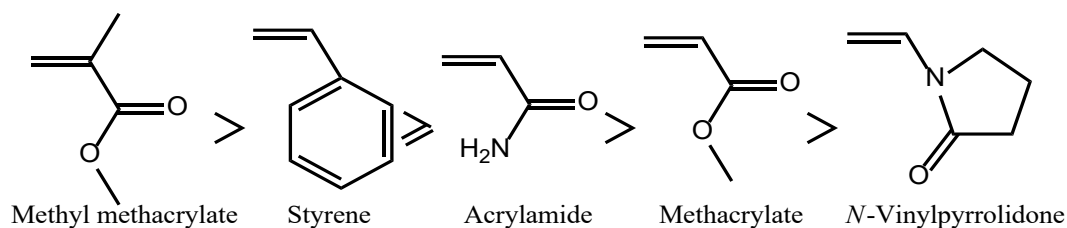


Figure 1.29 Some examples of monomers for reversible-addition fragmentation chain transfer polymerisations, shown on a scale from least to most activated from left to right.<sup>175</sup>

### 1.6.1.2 Chain Transfer Agents (CTAs)

Chain transfer agents, or RAFT agents, are the mediators in RAFT polymerisation that switch chains between the active and dormant state. The efficacy at which they do this is not universal, most CTAs would effectively control one polymerisation while retarding another similar one.<sup>176</sup> The compatibility of a CTA with any given polymerisation is affected primarily by the type of monomer used. However, it is also dependent heavily on the solvent and other reaction conditions.<sup>177–179</sup>

At their core CTAs are a dithioester; see Figure 1.30, green. There are four general classes of CTAs: dithiocarbamates, xanthates, dithioesters and trithiocarbonates, as shown in Figure 1.28. Each of these classes has different uses as determined by the solvent and monomer. Attached to the dithioester are the R and Z groups; the Z groups determine the reactivity of the agent and control the rate of addition and fragmentation; the R groups reinitiate the polymerisation and become the terminal functionality on the polymer.<sup>180</sup> A broad outline of polymer compatibility with RAFT agents is shown in Table 1.4.

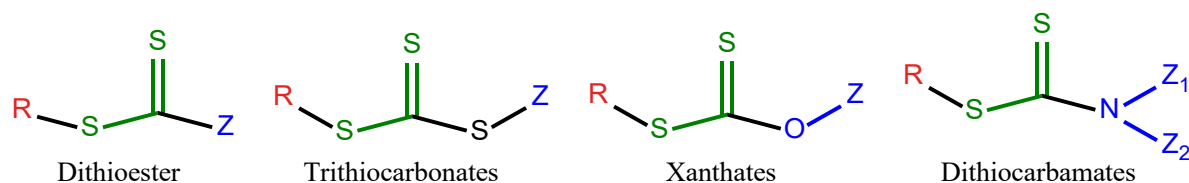


Figure 1.30 RAFT agent structures. Note: the dithioester groups, marked in green, are consistent between all of the RAFT agents.

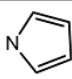
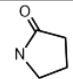
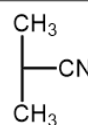
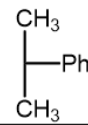
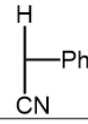
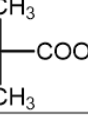
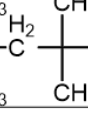
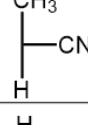
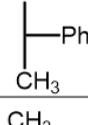
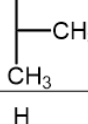
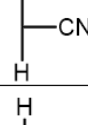
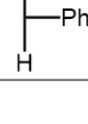
Dithioesters, specifically dithiobenzoates, were the first RAFT agents to be developed by Rutger *et al.*<sup>172</sup> and they are most effective with the use of MAMs. This efficiency is attributed to the slow rate of fragmentation of the radical intermediate as a result of LAMs being a poor homolytic leaving group.<sup>172</sup>

Trithiocarbonates are unique among RAFT agents in that the Z group can be used to determine the rate of the reaction, or as a second propagating site if R = Z. This allows for the growth of novel di-block polymers where the trithiocarbonate is in the centre, as shown by Mayadunne *et al.*<sup>181</sup> It has been further shown, however, that the predominating polymer formed in these situations is not a di-block co-polymer as the first monomer addition typically becomes a better leaving group than the second propagating group and is typically most suited for MAMs.<sup>161</sup>

Xanthates are sometimes referred to as macromolecular design by interchange of xanthate (MADIX) due to their use in polymer systems prior to the development of RAFT. A xanthate was first used as a “convenient source of alkyl and acyl radicals” for the addition of mono-adducts in 1988 by Delduc *et al.*<sup>182</sup> They are predominantly used with vinyl esters and vinyl amides<sup>174</sup> and are most suited for LAMs.<sup>161</sup>

Dithiocarbamates are more effective with LAMs; this is the result of lower transfer constants associated with radical addition from the propagating chains.<sup>180</sup> Dithiocarbamates can be designed by using cyclic systems or electron withdrawing groups on the nitrogen.

**Table 1.4:** Compatibility of dithioester derivatives, RAFT agents, with monomers by class.  
Taken from Living Radical Polymerization by the RAFT Process— A Third Update.<sup>174</sup>

Class	Aryl dithioester	Trithiocarbonate	Alkyl or aralkyl dithioester	Aromatic dithiocarbamate	Lactam dithiocarbamate	O-aryl xanthate	O-alkyl xanthate	N-alkyl-N-aryl dithiocarbamate	N,N-dialkyl dithiocarbamate
	Z R	Ph	SCH <sub>3</sub>	CH <sub>3</sub>			OPh	OCH <sub>3</sub>	NPh(CH <sub>3</sub> )
	MMA St MA VAc	MMA St MA VAc	MMA St MA VAc	MMA St MA VAc	MMA St MA VAc	MMA St MA VAc	MMA St MA VAc	MMA St MA VAc	MMA St MA VAc
	MMA St MA VAc	MMA St MA VAc	MMA St MA VAc	MMA St MA VAc	MMA St MA VAc	MMA St MA VAc	MMA St MA VAc	MMA St MA VAc	MMA St MA VAc
	MMA St MA VAc	MMA St MA VAc	MMA St MA VAc	MMA St MA VAc	MMA St MA VAc	MMA St MA VAc	MMA St MA VAc	MMA St MA VAc	MMA St MA VAc
	MMA St MA VAc	MMA St MA VAc	MMA St MA VAc	MMA St MA VAc	MMA St MA VAc	MMA St MA VAc	MMA St MA VAc	MMA St MA VAc	MMA St MA VAc
	MMA St MA VAc	MMA St MA VAc	MMA St MA VAc	MMA St MA VAc	MMA St MA VAc	MMA St MA VAc	MMA St MA VAc	MMA St MA VAc	MMA St MA VAc
	MMA St MA VAc	MMA St MA VAc	MMA St MA VAc	MMA St MA VAc	MMA St MA VAc	MMA St MA VAc	MMA St MA VAc	MMA St MA VAc	MMA St MA VAc
	MMA St MA VAc	MMA St MA VAc	MMA St MA VAc	MMA St MA VAc	MMA St MA VAc	MMA St MA VAc	MMA St MA VAc	MMA St MA VAc	MMA St MA VAc
	MMA St MA VAc	MMA St MA VAc	MMA St MA VAc	MMA St MA VAc	MMA St MA VAc	MMA St MA VAc	MMA St MA VAc	MMA St MA VAc	MMA St MA VAc
	MMA St MA VAc	MMA St MA VAc	MMA St MA VAc	MMA St MA VAc	MMA St MA VAc	MMA St MA VAc	MMA St MA VAc	MMA St MA VAc	MMA St MA VAc
	MMA St MA VAc	MMA St MA VAc	MMA St MA VAc	MMA St MA VAc	MMA St MA VAc	MMA St MA VAc	MMA St MA VAc	MMA St MA VAc	MMA St MA VAc
CH <sub>4</sub>	MMA St MA VAc	MMA St MA VAc	MMA St MA VAc	MMA St MA VAc	MMA St MA VAc	MMA St MA VAc	MMA St MA VAc	MMA St MA VAc	MMA St MA VAc

Blue=controls well    Black=controls, but not so well    Grey=Does not control.

### 1.6.1.3 Kinetics of RAFT Polymerisation

The kinetics of RAFT polymerisations are controlled by the equilibrium between the dormant and active chains within the reaction. Further, there are differences to consider with the initial rate of reaction compared to classical radical polymerisation. Key among these is the existence of an initial incubation, or inhibitory period, as the CTA is converted to the macroinitiator. The effect of this period is similar to that seen when there is an excess of oxygen in the system which retards the propagation of the radical chain.<sup>183</sup> This inhibition period has been shown to be the result of the first monomer addition changing the leaving group properties of the CTA, such that almost all of the CTA is converted to a single monomer adduct before the propagation continues.<sup>184</sup>

This issue can be overcome through the use of switchable RAFT agents which are typically pH driven changes involving the protonation of trithiocarbamate, nitrogen, or heteroaromatic nitrogen. This effect has been demonstrated by Thang *et al.*<sup>185</sup> who used a sodium carbonate ‘switch’ to change the electron withdrawing nature of the CTA and change from a styrene addition to vinyl acetate, two generally incompatible monomers. The reaction is shown in Figure 1.31.

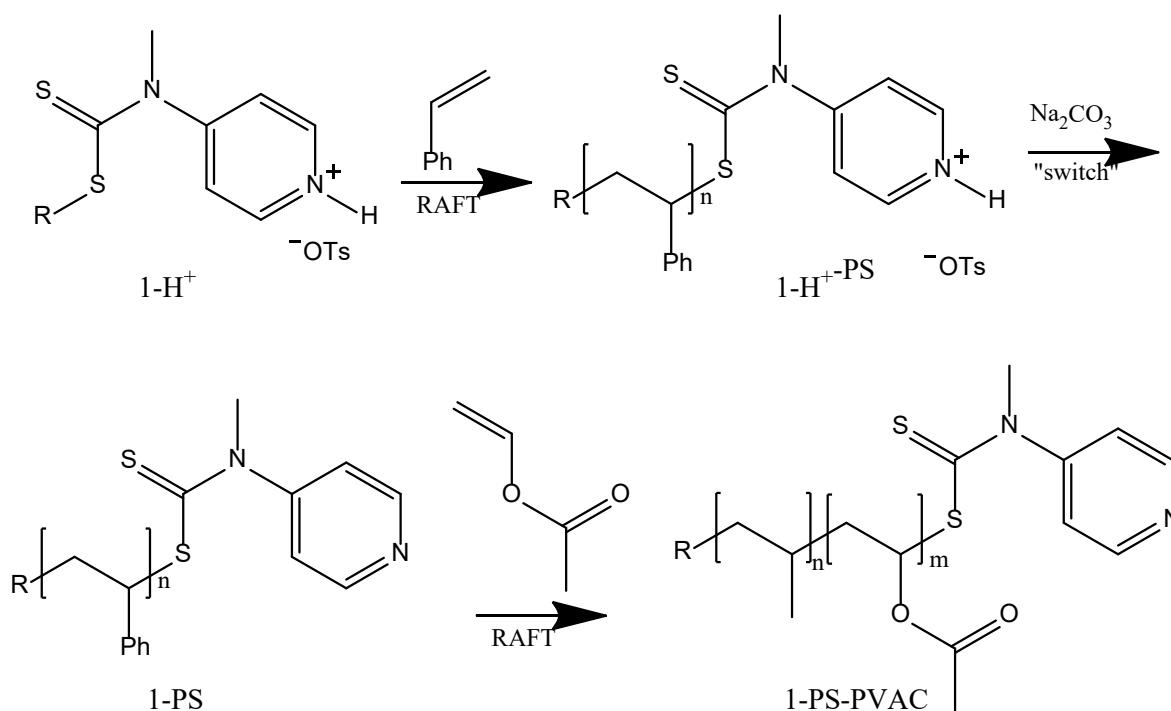


Figure 1.31 Switchable polymerisation of styrene and vinyl acetate using sodium carbonate as a 'switch'. Modified from Thang *et al.*<sup>186</sup>

## 1.7 Synthetic Polymer DNA Analogues

Polymers have been made that replicate the self-assembly of nucleic acids by incorporating nucleobases into their structure. Through extensive work it has been demonstrated by a number of groups that these polymers exhibit some DNA-like activity and are capable of selective binding. As discussed in Section 1.2.1, the nucleobase is the active unit of the nucleotide that enables this binding; as a result, there are a number of applications where nucleobases have been attached to the monomer unit for multiple polymerisation methods, including condensation and radical polymerisations.

The templating of polymers containing nucleobase functionality has been conducted by a number of groups. Of particular note is the work of Lo *et al.*<sup>187,188</sup> In this body of work Lo *et al.* first created a polymer bearing thymine functionality using the Sonogashira polymerisation method. Using this polymer the selective binding to adenine was demonstrated using free

deoxyadenosine nucleobases in solution and non-binding to thymidine in solution. In addition the presence of a complementary polyadenine DNA strand was also shown to selectively bind as measured with the change in fluorescence, Figure 1.32. It was noted the duplex formed between the polymer and ssDNA displayed similar melting behaviour to dsDNA in that there was a sharp and rapid melting of the duplex structures formed.<sup>187</sup> Further, the polyadenine ssDNA binding to the thymine polymer was measured through the structural change as determined through CD spectroscopy.<sup>187</sup>

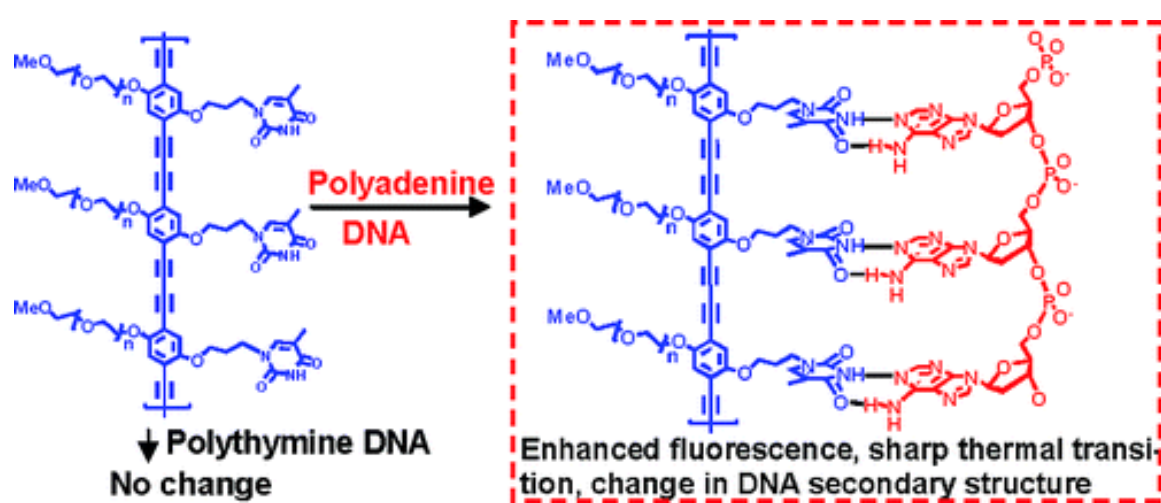


Figure 1.32 Poly(*p*-phenylenebutadiynylene) polymer and its interaction with polyadenine DNA. Taken from Lo *et al.*<sup>187</sup>

Following this work, Lo *et al.* also demonstrated the templating of one polymer's properties onto a second, daughter polymer, using nucleobase binding. The addition of nucleobase functionality to the monomers to the starting monomer in both cases was achieved through simple alkylation with a primary bromide. The template polymer containing thymine was synthesised using a ring opening metathesis polymerisation (ROMP) due to narrow  $\mathcal{D}$  shown in Figure 1.34.<sup>188</sup> The daughter polymer containing adenine was then synthesised the Sonogashira polymerisation method, outlined in Figure 1.33. Due to the low aqueous solubility of polymers generated from the Sonogashira method, most significantly due to its



phenylacetylene backbone, a PEG-3 pendant group was also incorporated to improve solubility and give space to the adenine; the resulting polymer is shown in Figure 1.33.

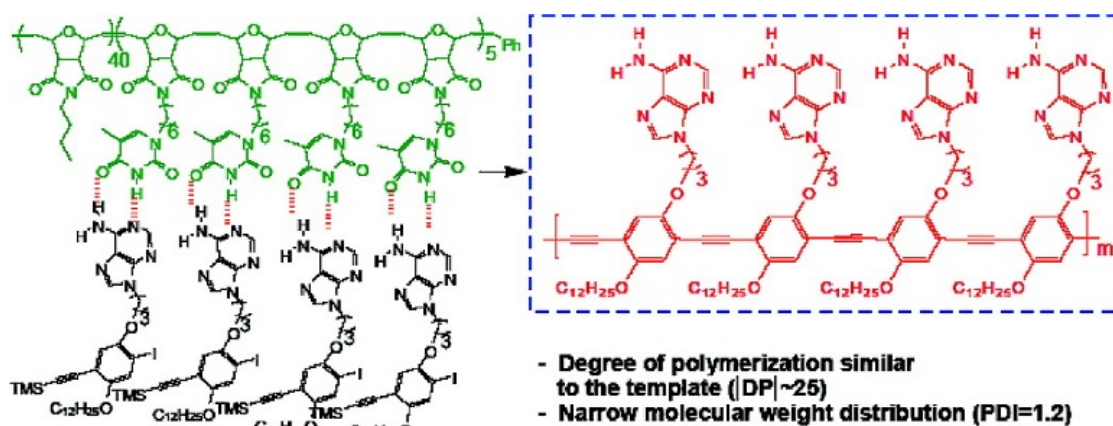


Figure 1.33 Overview of the Sonogashira polymerisation method for the templated synthesis of Poly(*p*-phenylenebutadiynylene). Taken from Lo *et al.*<sup>188</sup>

This experiment is of note as it demonstrated two achievements: firstly, the combination of a nucleobase containing polymer with an additional polymerisation technique; more importantly, however, this was the first work demonstrating enzymatic-like activity in copying the molecular properties of one polymer onto another using the addition of nucleobase functionality.<sup>188</sup>

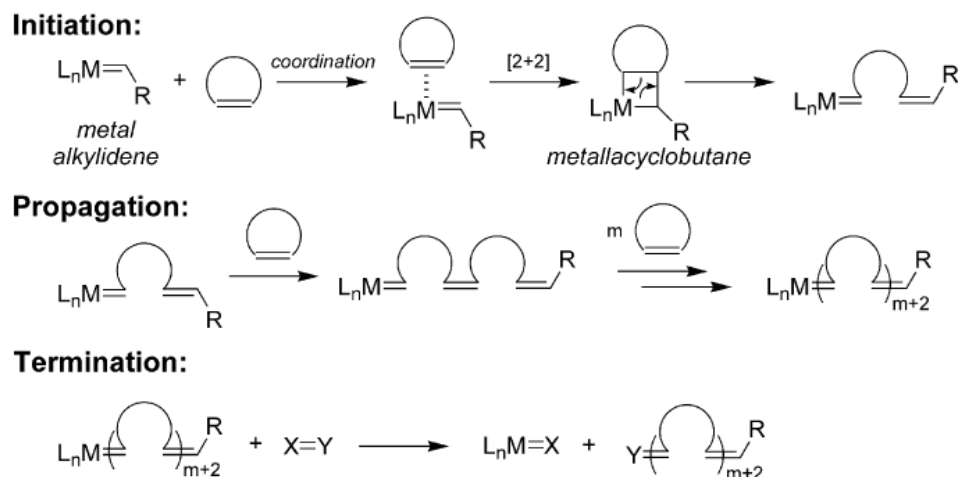


Figure 1.34 Mechanism for ring opening metathesis polymerisation. Adapted from Bielawski *et al.*<sup>189</sup>

Similar work was also conducted by South and Weck<sup>190</sup> using thymine containing monomers; they demonstrated the synthesis of two polymers. The first was a solid support-based polymer containing norbornene. It was able to selectively bind their thymine containing monomer and control its polymerisation. In the paper they do not describe the bioconjugate monomer composition beyond it containing both thymine and cyclic alkene moieties. The authors do demonstrate however control of this polymerisation, provided by the selective binding between the cyclic alkene template and the thymine containing monomer. This proximity control led to a lower extinction coefficient for the initiator and subsequently higher degree of polymerisation than would be achieved otherwise.<sup>190</sup>

Extensive work combining nucleic acids components with radical polymerisation techniques has also been conducted by the O'Reilly research group.<sup>150,191-195</sup> Primarily their work was focussed on the incorporation of nucleobases into polymers and investigating the resulting effect on morphology. They successfully demonstrated the effect of solvent on the formation of base pairs and its subsequent effect on polymerisation.<sup>191</sup> The monomers synthesised for the O'Reilly paper used a hydroxyethyl methacrylate as the vinyl source and then conjugated to

the nucleobase by first converting it into 2-(2-bromoacetoxy) ethyl methacrylate using bromoacetyl chloride which was then coupled to the nucleobase using nucleophilic substitution of the terminal bromine.<sup>191</sup> An overview of the process is shown in Figure 1.35; they demonstrated that a solvent, CHCl<sub>3</sub>, allowed for the formation of base pairs between nucleobase functionalised monomers that resulted in the formation of copolymers containing a high proportion of alternating repeating units.<sup>191</sup> When the same polymerisation was conducted with a solvent that prevented the formation of these units, dimethylformamide, the resulting polymer instead contained a statistical distribution of incorporated monomers rather than an alternating sequence.<sup>191</sup> When the solvent was changed to one that prevented the formation of these base pairs, the polymer instead appeared more consistent with a statistical copolymer. This result was not unexpected, but the successful demonstration of nucleobase containing polymers synthesised with RAFT demonstrates a compatibility further expanded in this thesis.

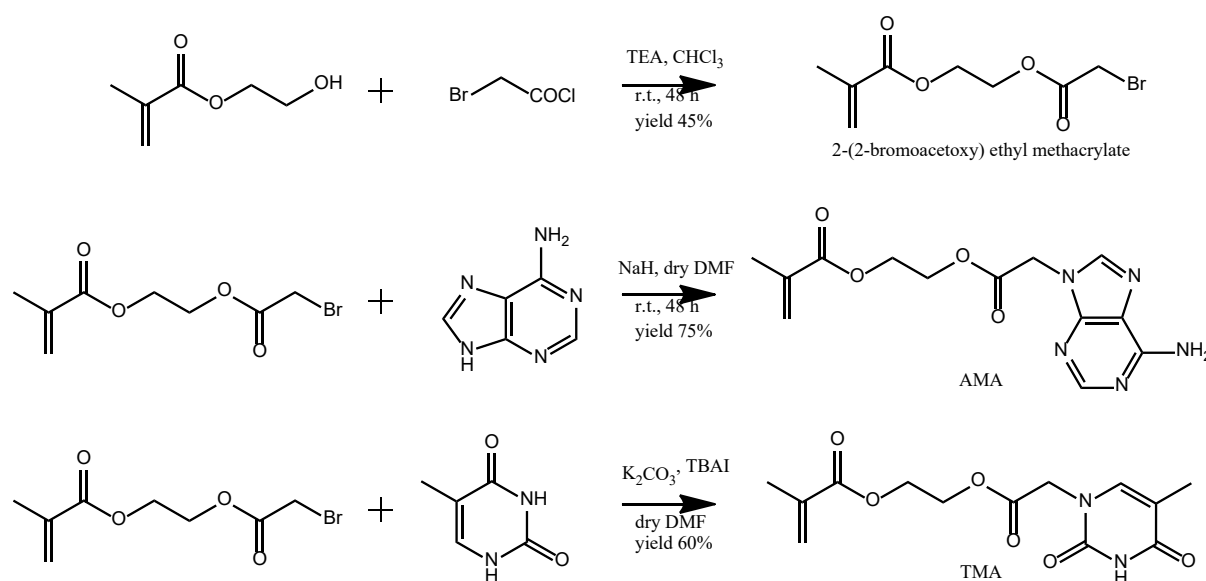


Figure 1.35 Formation of the adenine methacrylate (AMA) and thymine methacrylate (TMA) monomers by nucleophilic substitution using alkylhalides. Taken from O'Reilly *et al.*<sup>191</sup>

Most recently the O'Reilly group have focussed on using these polymers to develop tuneable morphologies through the utilisation of nucleobases as a way to direct molecular recognition.<sup>192-194</sup> An example of this was the formation of well-defined spherical micelles comprised of amphiphilic diblock copolymers.<sup>195</sup> The hydrophilic block containing the nucleobase functionality was located in the centre of the micelle; when a polymer containing the complementary nucleobase functionality was loaded into the solution containing these micelles, the added polymer was found to migrate into the centre of the micelles and change the morphology, but this transition was dependant on the initial block copolymer composition. Where the hydrophobic region of the polymer was shorter, the micelles decreased in size, although remained micelles. Where the length of the hydrophobic polymer block was larger, the micelles transitioned into cylinders before collapsing back into smaller micelles.<sup>195</sup> The transitions of these particles was determined through a number of techniques including dynamic light scattering (DLS) for determining size, and transmission electron microscopy (TEM) to image the structures.

Following formation of tuneable morphologies, the group has further expanded this work to functionalise the external surface of the particles<sup>194</sup> using thermoresponsive poly(*N*-isopropylacrylamide)-*block*-nucleobase functionalised polymers. The nucleobase monomers were adenine and thymine functionalised acrylamide which were synthesised through the same method shown in Figure 1.35, substituting an acrylamide for the acrylate. The result of this work demonstrated that the micelles formed by post-addition of the complementary block copolymer to the preformed thymine micelles created particles that would compact the surface structure upon heating. It further demonstrated the conjugation method for generating nucleobase functionalised polymers could be expanded to a wider variety of vinyl-based monomers.

This has to date culminated in the synthesis of several polymeric nanoparticles with both morphology and fluorescence controlled through the incorporation of nucleobase functionality.<sup>192</sup> One such example was using 4-acryloylmorpholine-*bloc*-vinyl nucleobase polymers containing either adenine or thymine functionality. These polymers were then combined to form the micelle-like particles, and the thymine components cross-linked. This resulted in fluorescent particles called non-conjugated polymer dots, similar to quantum or carbon dots in function. The group demonstrated that confinement of the nucleobases, particularly the adenine, results in  $\pi$ - $\pi$  stacking which creates the emission-decay pathway necessary for fluorescence. Further, it was shown that this fluorescence was generated in the core of the particles primarily from adenine that had become entrapped during the cross-linking process, see Figure 1.36.

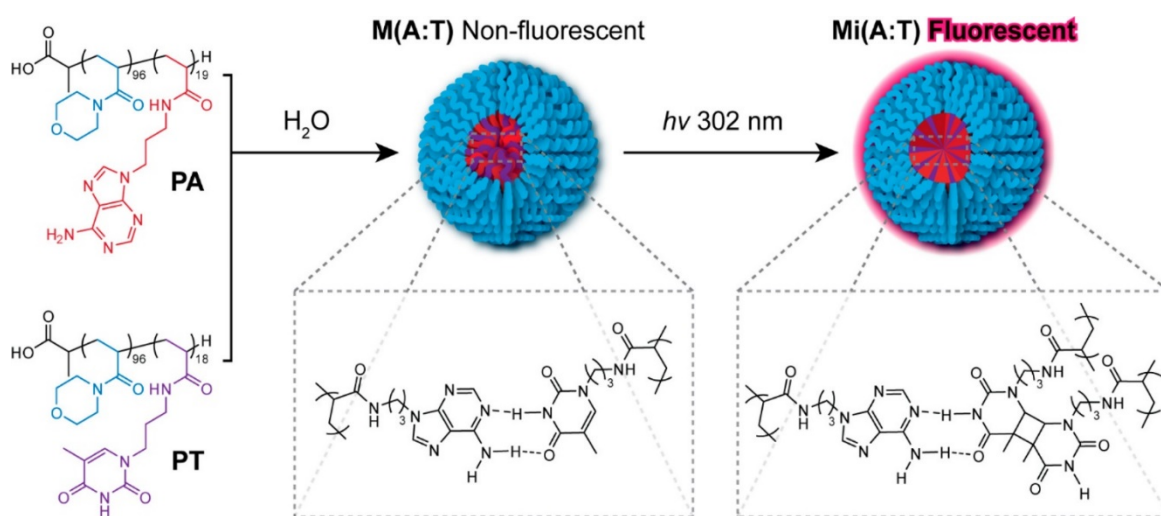


Figure 1.36 Formation of the non-conjugated polymer dots. Taken from O’Rielly *et al.*<sup>192</sup>

## 1.8 Conclusions

Notably, to date all work with radical based polymer systems has been conducted using nucleobases, rather than any larger subunit. The reasoning for this is likely the difficulty in synthesising these compounds: the additional moieties increase the chance for cleavage or

competing polymerisation systems. The major limitation, however, is that these methods will only ever be limited to synthetic systems and binding to natural DNA. The aim of this project is to develop a nucleotide functionalised synthetic polymer that not only exhibits similar binding properties but may in the future extend them to enzymatic compatibility.

There are 6 chapters that comprise the remainder of this thesis as follows:

**Chapter 2: Experimental Methods**, describes the methods and materials used to synthesise and characterise the nucleotide bioconjugates developed in this thesis.

**Chapter 3: Synthesis of poly(2-(5'-dimethoxytrityl-N-benzoyl-2'-deoxycytosine-monophosphate)oxyethyl methacrylate): a cytosine rich methacrylate polymer**, describes the synthesis and characterisation of a nucleotide functionalised monomer bearing cytosine functionality, and their subsequent polymerisation. It also includes the experimental development process and justification for the reagents used in the synthesis.

**Chapter 4: Synthesis of poly(2-(2'-deoxyguanosine-monophosphate)oxypropyl methacrylate): a guanine rich methacrylate polymer**, describes the polymerisation and isolation of the bioconjugated polymers bearing guanine functionality. This chapter improves and refines the methods presented in chapter 3. This includes detailing the deprotection and detritylation of the polymer synthesised to generate an active guanine moiety. Also covered are the competitive polymerisations and the kinetics of the polymerisation of the poly(2-(2'-deoxyguanosine-monophosphate)oxypropyl methacrylate).

**Chapter 5: Formation of G-quartets utilising nucleotide functionalised synthetic polymers**, describes the self-assembling and subsequent characterisation of G-quartets from poly(2-(2'-deoxyguanosine-monophosphate)oxypropyl methacrylate). It also covers the effect of monovalent cations,  $K^+$  and  $Na^+$ , on the formation of the G-quartets and G-quadruplex.

**Chapter 6: Interactions of nucleotide functionalised synthetic polymers with DNA using Poly(2-(2'-deoxythymine-monophosphate)oxypropyl methacrylate) as a model system,** describes the interactions of the nucleotide functionalised synthetic polymer poly(2-(2'-deoxythymine-monophosphate)oxypropyl methacrylate) with single stranded DNA.

Chapter 7 concludes the thesis, summarises its findings, and outlines potential future research based on the work presented.

## 1.9 References

- (1) Owen, B.; McMurray, C. Rapid Method for Measuring DNA Binding to Protein Using Fluorescence Anisotropy. *Protoc. Exch.* **2009**.
- (2) Seligmann, H. Codon Expansion and Systematic Transcriptional Deletions Produce Tetra-, Pentacoded Mitochondrial Peptides. *J. Theor. Biol.* **2015**, *387*, 154–165.
- (3) Kanzaki, H.; Shinohara, F.; Kanako, I.; Yamaguchi, Y.; Fukaya, S.; Miyamoto, Y.; Wada, S.; Nakamura, Y. Molecular Regulatory Mechanisms of Osteoclastogenesis through Cytoprotective Enzymes. *Redox Biol.* **2016**, *8*, 186–191.
- (4) Nirenberg, M.; Leder, P. RNA Codewords and Protein Synthesis: The Effect of Trinucleotides upon the Binding of SRNA to Ribosomes. *Science (80-. ).* **1964**, *145* (3639), 1399–1407.
- (5) Wang, J.; Liu, G.; Munge, B.; Lin, L.; Zhu, Q. DNA-Based Amplified Bioelectronic Detection and Coding of Proteins. *Angew. Chemie Int. Ed.* **2004**, *43* (16), 2158–2161.
- (6) Deleault, N. R.; Lucassen, R. W.; Supattapone, S. RNA Molecules Stimulate Prion Protein Conversion. *Nature* **2003**, *425* (6959), 717–720.

- (7) Saenger, W. Why Study Nucleotide and Nucleic Acid Structure? In *Principles of Nucleic Acid Structure*; Springer-Verlag, 1984; pp 1–8.
- (8) Thaplyal, P.; Bevilacqua, P. C. Experimental Approaches for Measuring PKa's in RNA and DNA. In *Methods in Enzymology*; NIH Public Access, 2014; Vol. 549, pp 189–219.
- (9) Thauer, R. K. Citric-Acid Cycle, 50 Years on. Modifications and an Alternative Pathway in Anaerobic Bacteria. *Eur. J. Biochem.* **1988**, *176* (3), 497–508.
- (10) Kottur, J.; Nair, D. T. Pyrophosphate Hydrolysis Is an Intrinsic and Critical Step of the DNA Synthesis Reaction. *Nucleic Acids Res.* **2018**, *46* (12), 5875–5885.
- (11) Westhof, E.; Yusupov, M.; Yusupova, G. Recognition of Watson-Crick Base Pairs: Constraints and Limits Due to Geometric Selection and Tautomerism. *F1000Prime Reports*. Faculty of 1000 Ltd 2014, p 19.
- (12) Dahm, R. Friedrich Miescher and the Discovery of DNA. *Dev. Biol.* **2005**, *278* (2), 274–288.
- (13) Watson, J. D.; Crick, F. H. Molecular Structure of Nucleic Acids. A Structure for Deoxyribose Nucleic Acid. *Nature* **1953**, *55* (2), 108–109.
- (14) Pederson, T. Molecular Biology of the Gene: By James D. Watson: W. A. Benjamin (1965): New York, New York. *FASEB J.* **2015**, *29* (11), 4399–4401.
- (15) Breslauer, K. J.; Frank, R.; Blocker, H.; Marky, L. A. Predicting DNA Duplex Stability from the Base Sequence. *Proc. Natl. Acad. Sci.* **1986**, *83* (11), 3746–3750.
- (16) Cieplak, P.; Kollman, P. A. Calculation of the Free Energy of Association of Nucleic Acid Bases in Vacuo and Water Solution. *J. Am. Chem. Soc.* **1988**, *110* (12), 3734–3739.



- (17) Zhang, T. B.; Zhang, C. L.; Dong, Z. L.; Guan, Y. F. Determination of Base Binding Strength and Base Stacking Interaction of DNA Duplex Using Atomic Force Microscope. *Sci. Rep.* **2015**, *5*, 9143.
- (18) Sivakova, S.; Rowan, S. J. Nucleobases as Supramolecular Motifs. *Chem. Soc. Rev.* **2005**, *34* (1), 9.
- (19) Rossetti, G.; Dans, P. D.; Gomez-Pinto, I.; Ivani, I.; Gonzalez, C.; Orozco, M. The Structural Impact of DNA Mismatches. *Nucleic Acids Res.* **2015**, *43* (8), 4309–4321.
- (20) Ebel, S.; Lane, A. N.; Brown, T. Very Stable Mismatch Duplexes: Structural and Thermodynamic Studies on Tandem G.Cntdot.A Mismatches in DNA. *Biochemistry* **1992**, *31* (48), 12083–12086.
- (21) Lewis, J. P.; Sankey, O. F. Geometry and Energetics of DNA Basepairs and Triplets from First Principles Quantum Molecular Relaxations. *Biophys. J.* **1995**, *69* (3), 1068–1076.
- (22) Rurack, K.; Resch-Genger, U. Rigidization, Preorientation and Electronic Decoupling - The “magic Triangle” for the Design of Highly Efficient Fluorescent Sensors and Switches. *Chem. Soc. Rev.* **2002**, *31* (2), 116–127.
- (23) Pan, S.; Sun, X.; Lee, J. K. Stability of Complementary and Mismatched DNA Duplexes: Comparison and Contrast in Gas versus Solution Phases. *Int. J. Mass Spectrom.* **2006**, *253* (3), 238–248.
- (24) Sykes, M. T.; Levitt, M. Simulations of RNA Base Pairs in a Nanodroplet Reveal Solvation-Dependent Stability. *Proc. Natl. Acad. Sci. U. S. A.* **2007**, *104* (30), 12336–12340.

- (25) Sharma, P.; Mitra, A.; Sharma, S.; Singh, H.; Bhattacharyya, D. Quantum Chemical Studies of Structures and Binding in Noncanonical RNA Base Pairs: The *trans* Watson-Crick:Watson-Crick Family. *J. Biomol. Struct. Dyn.* **2008**, *25* (6), 709–732.
- (26) Chawla, M.; Abdel-Azeim, S.; Oliva, R.; Cavallo, L. Higher Order Structural Effects Stabilizing the Reverse Watson-Crick Guanine-Cytosine Base Pair in Functional RNAs. **2014**, *42* (2).
- (27) Zemánek, M.; Kypr, J.; Vorlíčková, M. Conformational Properties of DNA Containing (CCA)<sub>n</sub> and (TGG)<sub>n</sub> Trinucleotide Repeats. *Int. J. Biol. Macromol.* **2005**, *36* (1–2), 23–32.
- (28) Peters, M.; Rozas, I.; Alkorta, I.; Elguero, J. DNA Triplexes: A Study of Their Hydrogen Bonds. *J. Phys. Chem. B* **2002**, *107* (1), 323–330.
- (29) Lane, A. N.; Chaires, J. B.; Gray, R. D.; Trent, J. O. Stability and Kinetics of G-Quadruplex Structures. *Nucleic Acids Res.* **2008**, *36* (17), 5482–5515.
- (30) Bang, I. Untersuchungen Über Die Guanylsäure. *Biochem. Z.* **1910**, *26*, 293–311.
- (31) Gellert, M.; Lipsett, M. N.; Davies, D. R.; Lim, K. W.; Mechulam, Y.; Phan, A. T. Helix Formation By Guanylic Acid. *Proc. Natl. Acad. Sci.* **1962**, *48* (12), 2013–2018.
- (32) Bhattacharyya, D.; Arachchilage, G. M.; Basu, S. Metal Cations in G-Quadruplex Folding and Stability. *Frontiers in Chemistry*. Frontiers Media SA 2016, p 38.
- (33) Pinnavaia, T. J.; Marshall, C. L.; Mettler, C. M.; Fisk, C. L.; Miles, H. T.; Becker, E. D. Alkali Metal Ion Specificity in the Solution Ordering of a Nucleotide, 5'-Guanosine Monophosphate. *J. Am. Chem. Soc.* **1978**, *100* (11), 3625–3627.

- (34) Williamson, J. R. G-Quartet Structures in Telomeric DNA. *Annu. Rev. Biophys. Biomol. Struct.* **1994**, *23* (1), 703–730.
- (35) Breaker, R. R. Natural and Engineered Nucleic Acids as Tools to Explore Biology. *Nature* **2004**, *432* (7019), 838–845.
- (36) Ellington, A.; Pollard, J. D. Synthesis and Purification of Oligonucleotides. In *Current Protocols in Molecular Biology*; Wiley-Blackwell, 2001; Vol. 42, pp 2.11.1-2.11.25.
- (37) Hance, N.; Ekstrand, M. I.; Trifunovic, A. Mitochondrial DNA Polymerase Gamma Is Essential for Mammalian Embryogenesis. *Hum. Mol. Genet.* **2005**, *14* (13), 1775–1783.
- (38) Allemand, J. F.; Bensimon, D.; Jullien, L.; Bensimon, A.; Croquette, V. PH-Dependent Specific Binding and Combing of DNA. *Biophys. J.* **1997**, *73* (4), 2064–2070.
- (39) Guo, Z.; Wang, Y.; Yang, A.; Yang, G. The Effect of PH on Charge Inversion and Condensation of DNA. *Soft Matter* **2016**, *12* (31), 6669–6674.
- (40) Miller, S. A.; Dykes, D. D.; Polesky, H. F. A Simple Salting out Procedure for Extracting DNA from Human Nucleated Cells. *Nucleic Acids Res.* **1988**, *16* (3), 1215.
- (41) Libonati, M.; Carsana, A.; Furia, A. Double-Stranded RNA. *Mol. Cell. Biochem.* **1980**, *31* (1), 147–164.
- (42) Yakovchuk, P.; Protozanova, E.; Frank-Kamenetskii, M. D. Base-Stacking and Base-Pairing Contributions into Thermal Stability of the DNA Double Helix. *Nucleic Acids Res.* **2006**, *34* (2), 564–574.
- (43) Mignon, P.; Loverix, S.; Steyaert, J.; Geerlings, P. Influence of the  $\pi$ -Interaction on the Hydrogen Bonding Capacity of Stacked DNA/RNA Bases. *Nucleic Acids Res.* **2005**, *33*

- (6), 1779–1789.
- (44) SantaLucia, J.; Allawi, H. T.; Seneviratne, P. A. Improved Nearest-Neighbor Parameters for Predicting DNA Duplex Stability. *Biochemistry* **1996**, *35* (11), 3555–3562.
- (45) Huguet, J. M.; Ribezzi-Crivellari, M.; Bizarro, C. V.; Ritort, F. Derivation of Nearest-Neighbor DNA Parameters in Magnesium from Single Molecule Experiments. *Nucleic Acids Res.* **2017**, *45* (22), 12921–12931.
- (46) Matta, C. F.; Castillo, N.; Boyd, R. J. Extended Weak Bonding Interactions in DNA:  $\pi$ -Stacking (Base–Base), Base–Backbone, and Backbone–Backbone Interactions. *J. Phys. Chem. B* **2006**, *110* (1), 563–578.
- (47) Sharma, S. Non-B DNA Secondary Structures and Their Resolution by RecQ Helicases. *Journal of Nucleic Acids*. Hindawi October 2, 2011, p 724215.
- (48) Guiblet, W. M. F.; Cremona, M. A.; Cechova, M.; Harris, R. S.; Kejnovska, I.; Kejnovsky, E.; Eckert, K.; Chiaromonte, F.; Makova, K. D. Non-B DNA Affects Polymerization Speed and Error Rate in Sequencers and Living Cells, July 16, 2017.
- (49) Wahl, M. C.; Sundaralingam, M. B-Form to A-Form Conversion by a 3'-Terminal Ribose: Crystal Structure of the Chimera d(CCACTAGTG)r(G). *Nucleic Acids Res.* **2000**, *28* (21), 4356–4363.
- (50) Vongsutilers, V.; Phillips, D. J.; Train, B. C.; McKelvey, G. R.; Thomsen, N. M.; Shaughnessy, K. H.; Lewis, J. P.; Gannett, P. M. The Conformational Effect of Para-Substituted C8-Arylguanine Adducts on the B/Z-DNA Equilibrium. *Biophys. Chem.* **2011**, *154* (1), 41–48.

- (51) Mauroesgueroto. File:Dnaconformations.png - Wikimedia Commons  
<https://commons.wikimedia.org/wiki/File:Dnaconformations.png> (accessed Jun 18, 2018).
- (52) Ussery, D. W. DNA Structure: A-, B- and Z-DNA Helix Families. In *Encyclopedia of Life Sciences*; John Wiley & Sons, Ltd: Chichester, UK, 2002.
- (53) Vargason, J. M.; Henderson, K.; Ho, P. S. A Crystallographic Map of the Transition from B-DNA to A-DNA. *Proc. Natl. Acad. Sci. U. S. A.* **2001**, *98* (13), 7265–7270.
- (54) Portugal, J.; Subirana, J. A. Counterions Which Favour the C Form of DNA. *EMBO J.* **1985**, *4* (9), 2403–2408.
- (55) Rhodes, N. J.; Mahendrasingam, A.; Pigram, W. J.; Fuller, W.; Brahms, J.; Vergne, J.; Warren, R. A. J. The C Conformation Is a Low Salt Form of Sodium DNA. *Nature* **1982**, *296* (5854), 267–269.
- (56) Rich, A.; Nordheim, A.; Wang, A. H. J. The Chemistry and Biology of Left-Handed Z-DNA. *Annu. Rev. Biochem.* **1984**, *53* (1), 791–846.
- (57) Ho, P. S. The Non-B-DNA Structure of d(CA/TG)<sub>n</sub> Does Not Differ from That of Z-DNA. *Proc. Natl. Acad. Sci. U. S. A.* **1994**, *91* (20), 9549–9553.
- (58) Srinivasan, J.; Cheatham, T. E.; Cieplak, P.; Kollman, P. A.; Case, D. A. Continuum Solvent Studies of the Stability of DNA, RNA, and Phosphoramidate-DNA Helices. *J. Am. Chem. Soc.* **1998**, *120* (37), 9401–9409.
- (59) Dickerson, R. E.; Klug, A. Base Sequence and Helix Structure Variation in B and A DNA. *J. Mol. Biol.* **1983**, *166* (3), 419–441.

- (60) Franklin, R. E.; Gosling, R. G. The Structure of Sodium Thymonucleate Fibres. I. The Influence of Water Content. *Acta Crystallogr.* **1953**, *6* (8), 673–677.
- (61) Lu, X. J.; Shakked, Z.; Olson, W. K. A-Form Conformational Motifs in Ligand-Bound DNA Structures. *J. Mol. Biol.* **2000**, *300* (4), 819–840.
- (62) Kulkarni, M.; Mukherjee, A. Understanding B-DNA to A-DNA Transition in the Right-Handed DNA Helix: Perspective from a Local to Global Transition. *Prog. Biophys. Mol. Biol.* **2017**, *128*, 63–73.
- (63) Dickerson, R. E.; Drew, H. R.; Conner, B. N.; Wing, R. M.; Fratini, A. V.; Kopka, M. L. The Anatomy of A-, B-, and Z-DNA. *Science (80-. )*. **1982**, *216* (4545), 475–485.
- (64) Van Dam, L.; Levitt, M. H. BII Nucleotides in the B and C Forms of Natural-Sequence Polymeric DNA: A New Model for the C Form of DNA. *J. Mol. Biol.* **2000**, *304* (4), 541–561.
- (65) Zimmerman, S. B.; Pfeiffer, B. H. Does DNA Adopt the C Form in Concentrated Salt Solutions or in Organic Solvent/Water Mixtures? An X-Ray Diffraction Study of DNA Fibers Immersed in Various Media. *J. Mol. Biol.* **1980**, *142* (3), 315–330.
- (66) Stegle, O.; Payet, L.; Mergny, J. L.; MacKay, D. J. C.; Huppert, J. L. Predicting and Understanding the Stability of G-Quadruplexes. *Bioinformatics* **2009**, *25* (12), 374–382.
- (67) Phan, A. T.; Kuryavyi, V.; Luu, K. N.; Patel, D. J. Structure of Two Intramolecular G-Quadruplexes Formed by Natural Human Telomere Sequences in K<sup>+</sup> Solution. *Nucleic Acids Res.* **2007**, *35* (19), 6517–6525.
- (68) Kotch, F. W.; Fettingner, J. C.; Davis, J. T. A Lead-Filled G-Quadruplex: Insight into the

- G-Quartet's Selectivity for Pb<sup>2+</sup> over K<sup>+</sup>. *Org. Lett.* **2000**, 2 (21), 3277–3280.
- (69) Lee, M. P. H.; Parkinson, G. N.; Hazel, P.; Neidle, S. Observation of the Coexistence of Sodium and Calcium Ions in a DNA G-Quadruplex Ion Channel. *J. Am. Chem. Soc.* **2007**, 129 (33), 10106–10107.
- (70) Kankia, B. I.; Marky, L. A. Folding of the Thrombin Aptamer into a G-Quadruplex with Sr<sup>2+</sup>: Stability, Heat, and Hydration. *J. Am. Chem. Soc.* **2001**, 123 (44), 10799–10804.
- (71) Shi, X.; Fetting, J. C.; Davis, J. T. Homochiral G-Quadruplexes with Ba<sup>2+</sup> but Not with K<sup>+</sup>: The Cation Programs Enantiomeric Self-Recognition. *J. Am. Chem. Soc.* **2001**, 123 (27), 6738–6739.
- (72) Zhang, D.; Huang, T.; Lukeman, P. S.; Paukstelis, P. J. Crystal Structure of a DNA/Ba<sup>2+</sup> G-Quadruplex Containing a Water-Mediated C-Tetrad. *Nucleic Acids Res.* **2014**, 42 (21), 13422–13429.
- (73) Ida, R.; Wu, G. Solid-State <sup>87</sup>Rb NMR Signatures for Rubidium Cations Bound to a G-Quadruplex. *Chem. Commun.* **2005**, No. 34, 4294–4296.
- (74) Nagesh, N.; Chatterji, D. Ammonium Ion at Low Concentration Stabilizes the G-Quadruplex Formation by Telomeric Sequence. *J. Biochem. Biophys. Methods* **1995**, 30 (1), 1–8.
- (75) Kan, Z.; Yao, Y.; Wang, P.; Li, X.; Hao, Y.; Tan, Z. Molecular Crowding Induces Telomere G-Quadruplex Formation under Salt-Deficient Conditions and Enhances Its Competition with Duplex Formation. *Angew. Chemie Int. Ed.* **2006**, 45 (10), 1629–1632.
- (76) Tóthová, P.; Krafčíková, P.; Víglaský, V. Formation of Highly Ordered Multimers in G-

- Quadruplexes. *Biochemistry* **2014**, *53* (45), 7013–7027.
- (77) Rhodes, D.; Lipps, H. J. Survey and Summary G-Quadruplexes and Their Regulatory Roles in Biology. *Nucleic Acids Research*. Oxford University Press October 15, 2015, pp 8627–8637.
- (78) Kaiser, C. E.; Gokhale, V.; Yang, D.; Hurley, L. H. Gaining Insights into the Small Molecule Targeting of the G-Quadruplex in the c-MYC Promoter Using NMR and an Allele-Specific Transcriptional Assay. In *Topics in current chemistry*; 2012; Vol. 330, pp 1–21.
- (79) Han, H.; Hurley, L. H. G-Quadruplex DNA: A Potential Target for *Anti-Cancer* Drug Design. *Trends Pharmacol. Sci.* **2000**, *21* (4), 136–142.
- (80) Balasubramanian, S.; Neidle, S. G-Quadruplex Nucleic Acids as Therapeutic Targets. *Curr. Opin. Chem. Biol.* **2009**, *13* (3), 345–353.
- (81) Bidzinska, J.; Cimino-Reale, G.; Zaffaroni, N.; Folini, M. G-Quadruplex Structures in the Human Genome as Novel Therapeutic Targets. *Molecules* **2013**, *18* (10), 12368–12395.
- (82) Livshits, G. I.; Stern, A.; Rotem, D.; Borovok, N.; Eidelstein, G.; Migliore, A.; Penzo, E.; Wind, S. J.; Di Felice, R.; Skourtis, S. S.; *et al.* Long-Range Charge Transport in Single G-Quadruplex DNA Molecules. *Nat. Nanotechnol.* **2014**, *9* (12), 1040–1046.
- (83) Alberti, P.; Mergny, J.-L. DNA Duplex-Quadruplex Exchange as the Basis for a Nanomolecular Machine. *Proc. Natl. Acad. Sci. U. S. A.* **2003**, *100* (4), 1569–1573.
- (84) Berlin, Y. A.; Burin, A. L.; Ratner, M. A. DNA as a Molecular Wire. *Superlattices*



- Microstruct.* **2000**, 28 (4), 241–252.
- (85) Catherall, T.; Huskisson, D.; McAdams, S.; Vijayaraghavan, A. Self-Assembly of One Dimensional DNA-Templated Structures. *J. Mater. Chem. C* **2014**, 2 (34), 6895–6920.
- (86) Marsh, T. C.; Vesenka, J.; Henderson, E. A New DNA Nanostructure, the G-Wire, Imaged by Scanning Probe Microscopy. *Nucleic Acids Res.* **1995**, 23 (4), 696–700.
- (87) Nielsen, P. E. Peptide Nucleic Acid. A Molecule with Two Identities. *Acc. Chem. Res.* **1999**, 32 (7), 624–630.
- (88) Chien, A.; Edgar, D. B.; Trela, J. M. Deoxyribonucleic Acid Polymerase from the Extreme Thermophile *Thermus Aquaticus*. *J. Bacteriol.* **1976**, 127 (3), 1550.
- (89) Berg, J. M.; Tymoczko, J. L.; Stryer, L. *Biochemistry*; W.H. Freeman, 2002.
- (90) Teplitz, R. R. An Introduction to Genetic Analysis. *JAMA J. Am. Med. Assoc.* **2011**, 257 (16), 2223.
- (91) PCR Selection Chart | NEB <https://www.neb.com/tools-and-resources/selection-charts/pcr-selection-chart> (accessed May 23, 2018).
- (92) Ppyun, H.; Kim, S. H.; Youn, M. H.; Cho, S. S.; Kwon, K. M.; Kweon, D. H.; Kwon, S. T. Improved PCR Performance and Fidelity of Double Mutant Neq A523R/N540R DNA Polymerase. *Enzyme Microb. Technol.* **2016**, 82, 197–204.
- (93) Cheng, S.; Fockler, C.; Barnes, W. M.; Higuchi, R. Effective Amplification of Long Targets from Cloned Inserts and Human Genomic DNA. *Proc. Natl. Acad. Sci. U. S. A.* **1994**, 91 (12), 5695–5699.

- (94) Shuber, A. P. Universal Primer Sequence for Multiplex DNA Amplification. WO1996041012A1, June 7, 1995.
- (95) Truett, G. E.; Heeger, P.; Mynatt, R. L.; Truett, A. A.; Walker, J. A.; Warman, M. L. Annealing Control Primer System for Improving Specificity of PCR Amplification. *Biotechniques* **2004**, *35* (6), 1180–1184.
- (96) Brownstein, M. J.; Carpten, J. D.; Smith, J. R. Modulation of Non-Templated Nucleotide Addition by Taq DNA Polymerase: Primer Modifications That Facilitate Genotyping. *Biotechniques* **1996**, *20* (6), 1004–1010.
- (97) Wang, Y.; Barbacioru, C.; Hyland, F.; Xiao, W.; Hunkapiller, K. L.; Blake, J.; Chan, F.; Gonzalez, C.; Zhang, L.; Samaha, R. R. Large Scale Real-Time PCR Validation on Gene Expression Measurements from Two Commercial Long-Oligonucleotide Microarrays. *BMC Genomics* **2006**, *7* (1), 59.
- (98) Gill, P.; Ghaemi, A. Nucleic Acid Isothermal Amplification Technologies - A Review. *Nucleosides, Nucleotides and Nucleic Acids* **2008**, *27* (3), 224–243.
- (99) LeProust, E. M.; Peck, B. J.; Spirin, K.; McCuen, H. B.; Moore, B.; Namsaraev, E.; Caruthers, M. H. Synthesis of High-Quality Libraries of Long (150mer) Oligonucleotides by a Novel Depurination Controlled Process. *Nucleic Acids Res.* **2010**, *38* (8), 2522–2540.
- (100) Kodumal, S. J.; Patel, K. G.; Reid, R.; Menzella, H. G.; Welch, M.; Santi, D. V. Total Synthesis of Long DNA Sequences: Synthesis of a Contiguous 32-Kb Polyketide Synthase Gene Cluster. *Proc. Natl. Acad. Sci. U. S. A.* **2004**, *101* (44), 15573–15578.
- (101) Hughes, R. A.; Ellington, A. D. Synthetic DNA Synthesis and Assembly: Putting the

- Synthetic in Synthetic Biology. *Cold Spring Harb. Perspect. Biol.* **2017**, *9* (1), a023812.
- (102) Roy, S.; Caruthers, M. Synthesis of DNA/RNA and Their Analogs via Phosphoramidite and H-Phosphonate Chemistries. *Molecules* **2013**, *18* (11), 14268–14284.
- (103) Corby, N. S.; Kenner, G. W.; Todd, A. R. Nucleotides. Part XVI. Ribonucleoside-5' Phosphites. A New Method for the Preparation of Mixed Secondary Phosphites. *Journal of the Chemical Society (Resumed)*. The Royal Society of Chemistry January 1, 1952, pp 3648–3649.
- (104) Gilham, P. T.; Khorana, H. G. Studies on Polynucleotides. I. A New and General Method for the Chemical Synthesis of the C5'-C3' Internucleotidic Linkage. Syntheses of Deoxyribo-Dinucleotides. *J. Am. Chem. Soc.* **1958**, *80* (23), 6212–6222.
- (105) Stawinski, J.; Kraszewski, A. Some Aspects of Oligoribonucleotides Synthesis via the H-Phosphonate Approach. *Acta Biochim. Pol.* **1998**, *45* (4), 907–915.
- (106) Kung, P.-P.; Jones, R. A. H-Phosphonate DNA Synthesis without Amino Protection. *Tetrahedron Lett.* **1992**, *33* (40), 5869–5872.
- (107) Reese, C. B. The Chemical Synthesis of Oligo- and Poly-Nucleotides by the Phosphotriester Approach. *Tetrahedron* **1978**, *34* (21), 3143–3179.
- (108) Cashion, P.; Porter, K.; Cadger, T.; Sathe, G.; Tranquilla, T.; Notman, H.; Jay, E. Simplification of DNA Synthesis by the Phosphotriester Method. *Tetrahedron Lett.* **1976**, *17* (42), 3769–3772.
- (109) Beaucage, S. L.; Iyer, R. P. Advances in the Synthesis of Oligonucleotides by the Phosphoramidite Approach. *Tetrahedron* **1992**, *48* (12), 2223–2311.

- (110) Efimov, V. A.; Molchanova, N. S.; Chakhmakhcheva, O. G. Approach to the Synthesis of Natural and Modified Oligonucleotides by the Phosphotriester Method Using O-Nucleophilic Intramolecular Catalysis. *Nucleosides, Nucleotides and Nucleic Acids* **2007**, *26* (8–9), 1087–1093.
- (111) Grøndahl, L.; Suzuki, S.; Wentrup-Byrne, E. Influence of a Diene Impurity on the Molecular Structure of Phosphate-Containing Polymers with Medical Applications. *Chem. Commun. (Camb)*. **2008**, No. 28, 3314–3316.
- (112) Gaytán, P. Chemical Synthesis of Oligonucleotides Using Acetone as a Washing Solvent. *Biotechniques* **2009**, *47* (2), 701–702.
- (113) Guzaev, A.; Manoharan, M. Conjugation of Oligonucleotides via an Electrophilic Tether: N- Chloroacetamidohexyl Phosphoramidite Reagent. *Bioorganic Med. Chem. Lett.* **1998**, *8* (24), 3671–3676.
- (114) Vargeese, C.; Carter, J.; Yegge, J.; Krivjansky, S.; Settle, A.; Kropp, E.; Peterson, K.; Pieken, W. Efficient Activation of Nucleoside Phosphoramidites with 4,5-Dicyanoimidazole during Oligonucleotide Synthesis. *Nucleic Acids Res.* **1998**, *26* (4), 1046–1050.
- (115) DNA Oligonucleotide Synthesis. *Sigma-Aldrich Technical Documents*. 2017, pp 5–9.
- (116) Welz, R.; Müller, S. 5-(Benzylmercapto)-1H-Tetrazole as Activator for 2'-O-TBDMS Phosphoramidite Building Blocks in RNA Synthesis. *Tetrahedron Lett.* **2002**, *43* (5), 795–797.
- (117) Froehler, B. C.; Matteucci, M. D. Substituted 5-Phenyltetrazoles: Improved Activators of Deoxynucleoside Phosphoramidites in Deoxyoligonucleotide Synthesis. *Tetrahedron*

- Lett.* **1983**, *24* (31), 3171–3174.
- (118) Berner, S.; Mühlhlegger, K.; Seliger, H. The Reaction of Tetrazole with Phosphoramidites as a Model for the Nucleotide Coupling Step. *Nucleosides and Nucleotides* **1988**, *7* (5–6), 763–767.
- (119) Berner, S.; Mühlhlegger, K.; Seliger, H. Studies on the Role of Tetrazole in the Activation of Phosphoramidites. *Nucleic Acids Res.* **1989**, *17* (3), 853–864.
- (120) Russell, M. A.; Laws, A. P.; Atherton, J. H.; Page, M. I. The Mechanism of the Phosphoramidite Synthesis of Polynucleotides. *Org. Biomol. Chem.* **2008**, *6* (18), 3270.
- (121) Vargeese, C.; Carter, J.; Yegge, J.; Krivjansky, S.; Settle, A.; Kropp, E.; Peterson, K.; Pieken, W. Efficient Activation of Nucleoside Phosphoramidites with 4,5-Dicyanoimidazole during Oligonucleotide Synthesis. *Nucleic Acids Res.* **1998**, *26* (4), 1046–1050.
- (122) Sanghvi, Y. S.; Guo, Z.; Pfundheller, H. M.; Converso, A. Improved Process for the Preparation of Nucleosidic Phosphoramidites Using a Safer and Cheaper Activator. *Org. Process Res. Dev.* **2000**, *4* (3), 175–181.
- (123) Beaucage, S. L.; Caruthers, M. H. Synthetic Strategies and Parameters Involved in the Synthesis of Oligodeoxyribonucleotides According to the Phosphoramidite Method. *Curr. Protoc. Nucleic Acid Chem.* **2000**, *00* (1), 3.3.1-3.3.20.
- (124) *DCI-A Logical Alternative Activator*; 1997.
- (125) Wincott, F.; Drenzo, A.; Shaffer, C.; Grimm, S.; Tracz, D.; Workman, C.; Sweedler, D.; Gonzalez, C.; Scaringe, S.; Usman, N. Synthesis, Deprotection, Analysis and

- Purification of RNA and Ribosomes. *Nucleic Acids Res.* **1995**, *23* (14), 2677–2684.
- (126) Iwai, S.; Shimizu, M.; Kamiya, H.; Ohtsuka, E. Synthesis of a Phosphoramidite Coupling Unit of the Pyrimidine (6-4) Pyrimidone Photoproduct and Its Incorporation into Oligodeoxynucleotides. *J. Am. Chem. Soc.* **1996**, *118* (32), 7642–7643.
- (127) Nikiforov, T. T.; Connolly, B. A. Straightforward Preparation and Use in Oligodeoxynucleotide Synthesis of 5'-O-(4,4'-Dimethoxytrityl)-4-[S-(2-Cyanoethyl)]-Thiothymidine. *Tetrahedron Lett.* **1992**, *33* (17), 2379–2382.
- (128) Vu, H.; McCollum, C.; Jacobson, K.; Theisen, P.; Vinayak, R.; Spiess, E.; Andrus, A. Fast Oligonucleotide Deprotection Phosphoramidite Chemistry for DNA Synthesis. *Tetrahedron Lett.* **1990**, *31* (50), 7269–7272.
- (129) Guzaev, A. P.; Vvedenskiy, V. V.; Khirud Gogoi. Solid Supports and Phosphoramidite Building Blocks for Oligonucleotide Conjugates. US20180016232A1, July 14, 2017.
- (130) Srivastava, S. C.; Thatikonda, S. K.; Shukla, P.; Srivastav, S. K. Synthesis of High Purity Dmt-C3-Disulfide Phosphoramidite. WO2013126034A1, February 22, 2012.
- (131) Maier, M. A.; Choi, Y.; Gaus, H.; Barchi, J. J.; Marquez, V. E.; Manoharan, M. Synthesis and Characterization of Oligonucleotides Containing Conformationally Constrained Bicyclo[3.1.0]Hexane Pseudosugar Analogs. *Nucleic Acids Res.* **2004**, *32* (12), 3642–3650.
- (132) Cvetovich, R. J. Hydrogen Peroxide Oxidation of Phosphite Triesters in Oligonucleotide Syntheses. *Org. Process Res. Dev.* **2010**, *14* (1), 295–297.
- (133) Proudnikov, D.; Mirzabekov, A. Chemical Methods of DNA and RNA Fluorescent

- Labeling. *Nucleic Acids Res.* **1996**, *24* (22), 4535–4542.
- (134) Sinha, N. D.; Cook, R. M. The Preparation and Application of Functionalised Synthetic Oligonucleotides: III. Use of H-Phosphonate Derivatives of Protected Amino-Hexanol and Mercapto-Propanol or-Hexanol. *Nucleic Acids Res.* **1988**, *16* (6), 2659–2670.
- (135) Kupihár, Z.; SchméI, Z.; Kele, Z.; Penke, B.; Kovács, L. Synthesis and Application of a Novel, Crystalline Phosphoramidite Monomer with Thiol Terminus, Suitable for the Synthesis of DNA Conjugates. *Bioorganic Med. Chem.* **2001**, *9* (5), 1241–1247.
- (136) Rabe, K. S.; Niemeyer, C. M. Selective Covalent Conjugation of Phosphorothioate DNA Oligonucleotides with Streptavidin. *Molecules* **2011**, *16* (8), 6916–6926.
- (137) Jacobsen, J. P.; Pedersen, J. B.; Hansen, L. F.; Wemmer, D. E. Site Selective Bis-Intercalation of a Homodimeric Thiazole Orange Dye in DNA Oligonucleotides. *Nucleic Acids Res* **1995**, *23* (5), 753–760.
- (138) Rye, H. S.; Yue, S.; Wemmer, D. E.; Quesada, M. A.; Haugland, R. P.; Mathies, R. A.; Glazer, A. N. Stable Fluorescent Complexes of Double-Stranded DNA with Bis-Intercalating Asymmetric Cyanine Dyes: Properties and Applications. *Nucleic Acids Res.* **1992**, *20* (11), 2803–2812.
- (139) Gudnason, H.; Dufva, M.; Bang, D. D.; Wolff, A. Comparison of Multiple DNA Dyes for Real-Time PCR: Effects of Dye Concentration and Sequence Composition on DNA Amplification and Melting Temperature. *Nucleic Acids Res.* **2007**, *35* (19), e127.
- (140) Singer, V. L.; Lawlor, T. E.; Yue, S. Comparison of SYBR® Green I Nucleic Acid Gel Stain Mutagenicity and Ethidium Bromide Mutagenicity in the Salmonella/Mammalian Microsome Reverse Mutation Assay (Ames Test). *Mutat. Res. Toxicol. Environ.*

- Mutagen.* **1999**, 439 (1), 37–47.
- (141) Olmsted, J.; Kearns, D. R. Mechanism of Ethidium Bromide Fluorescence Enhancement on Binding to Nucleic Acids. *Biochemistry* **1977**, 16 (16), 3647–3654.
- (142) Millar, D. P.; Robbins, R. J.; Zewail, A. H. Torsion and Bending of Nucleic Acids Studied by Ultrashort Time-Resolved Fluorescence Depolarization of Intercalated Dyes. *J. Chem. Phys.* **1982**, 76 (4), 2080–2094.
- (143) Biebricher, A. S.; Heller, I.; Roijmans, R. F. H.; Hoekstra, T. P.; Peterman, E. J. G.; Wuite, G. J. L. The Impact of DNA Intercalators on DNA and DNA-Processing Enzymes Elucidated through Force-Dependent Binding Kinetics. *Nat. Commun.* **2015**, 6 (1), 7304.
- (144) Armitage, B. A. Cyanine Dye-DNA Interactions: Intercalation, Groove Binding, and Aggregation. *Top. Curr. Chem.* **2005**, 253, 55–76.
- (145) Bengtsson, M.; Karlsson, H. J.; Westman, G.; Kubista, M. A New Minor Groove Binding Asymmetric Cyanine Reporter Dye for Real-Time PCR. *Nucleic Acids Res.* **2003**, 31 (8), 45e – 45.
- (146) Latt, S. A.; Stetten, G.; Juergens, L. A.; Willard, H. F.; Scher, C. D. Recent Developments in the Detection of Deoxyribonucleic Acid Synthesis by 33258 Hoechst Fluorescence. *J. Histochem. Cytochem.* **1975**, 23 (7), 493–505.
- (147) Zipper, H.; Brunner, H.; Bernhagen, J.; Vitzthum, F. Investigations on DNA Intercalation and Surface Binding by SYBR Green I, Its Structure Determination and Methodological Implications. *Nucleic Acids Res.* **2004**, 32 (12), e103–e103.



- (148) Blake, A.; Peacocke, A. R. The Interaction of Aminoacridines with Nucleic Acids. *Biopolymers* **1968**, *6* (9), 1225–1253.
- (149) Armstrong, R. W.; Kurucsev, T.; Strauss, U. P. Interaction between Acridine Dyes and Deoxyribonucleic Acid. *J. Am. Chem. Soc.* **1970**, *92* (10), 3174–3181.
- (150) McHale, R.; O'Reilly, R. K. Nucleobase Containing Synthetic Polymers: Advancing Biomimicry via Controlled Synthesis and Self-Assembly. *Macromolecules* **2012**, *45* (19), 7665–7675.
- (151) Tasdelen, M. A.; Yagci, Y.; Levent Demirel, A.; Biedron, T.; Kubisa, P. Synthesis and Characterization of Block-Graft Copolymers [Poly(Epichlorohydrin-*b*-Styrene)-Gpoly(Methyl Methacrylate)] by Combination of Activated Monomer Polymerization, NMP and ATRP. *Polym. Bull.* **2007**, *58* (4), 653–663.
- (152) Manguian, M.; Save, M.; Charleux, B. Batch Emulsion Polymerization of Styrene Stabilized by a Hydrophilic Macro-RAFT Agents. *Macromol. Rapid Commun.* **2006**, *27* (6), 399–404.
- (153) Klaerner, G.; Trollsås, M.; Heise, A.; Husemann, M.; Atthoff, B.; Hawker, C. J.; Hedrick, J. L.; Miller, R. D. Concurrent Chain and Stepwise Polymerizations for the Preparation of Block Copolymers in One Step. *Macromolecules* **1999**, *32* (24), 8227–8229.
- (154) Wang, F.; Hickner, M.; Kim, Y. S.; Zawodzinski, T. A.; McGrath, J. E. Direct Polymerization of Sulfonated Poly(Arylene Ether Sulfone) Random (Statistical) Copolymers: Candidates for New Proton Exchange Membranes. *J. Memb. Sci.* **2002**, *197* (1–2), 231–242.

- (155) Wang, F.; Hickner, M.; Ji, Q.; Harrison, W.; Mecham, J.; Zawodzinski, T. A.; McGrath, J. E. Synthesis of Highly Sulfonated Poly(Arylene Ether Sulfone) Random(Statistical) Copolymers via Direct Polymerization. *Macromol. Symp.* **2001**, *175* (1), 387–396.
- (156) Bhanu, V. .; Rangarajan, P.; Wiles, K.; Bortner, M.; Sankarpandian, M.; Godshall, D.; Glass, T. .; Banthia, A. .; Yang, J.; Wilkes, G.; *et al.* Synthesis and Characterization of Acrylonitrile Methyl Acrylate Statistical Copolymers as Melt Processable Carbon Fiber Precursors. *Polymer (Guildf)*. **2002**, *43* (18), 4841–4850.
- (157) Harwood, H. J. Structures and Compositions of Copolymers. *Makromol. Chemie. Macromol. Symp.* **1987**, *10–11* (1), 331–354.
- (158) Fineman, M.; Ross, S. D. Linear Method for Determining Monomer Reactivity Ratios in Copolymerization. *J. Polym. Sci.* **1950**, *5* (2), 259–262.
- (159) *Green Book, 2nd Ed.: IUPAC Quantities, Units and Symbols in Physical Chemistry. Second Edition, Blackwell Scientific Publications, Oxford, 1993.; 2007.*
- (160) Stepto, R. F. T. Dispersity in Polymer Science (IUPAC Recommendations 2009). *Pure Appl. Chem.* **2009**, *81* (2), 351–353.
- (161) Moad, G.; Rizzardo, E.; Thang, S. H. Living Radical Polymerization by the RAFT Process A Second Update. *Aust. J. Chem.* **2009**, *62* (11), 1402–1472.
- (162) Boyer, C.; Soeriyadi, A. H.; Zetterlund, P. B.; Whittaker, M. R. Synthesis of Complex Multiblock Copolymers via a Simple Iterative Cu(0)-Mediated Radical Polymerization Approach. *Macromolecules* **2011**, *44* (20), 8028–8033.
- (163) Huh, K. M.; Bae, Y. H. Synthesis and Characterization of Poly(Ethylene Glycol)/Poly(1-

- Lactic Acid) Alternating Multiblock Copolymers. *Polymer (Guildf)*. **1999**, 40 (22), 6147–6155.
- (164) Thickett, S. C.; Gilbert, R. G. Emulsion Polymerization: State of the Art in Kinetics and Mechanisms. *Polymer (Guildf)*. **2007**, 48 (24), 6965–6991.
- (165) Murray, M. J.; Snowden, M. J. The Preparation, Characterisation and Applications of Colloidal Microgels. *Adv. Colloid Interface Sci.* **1995**, 54 (C), 73–91.
- (166) Li, B.; Brooks, B. W. Semi-batch Processes for Emulsion Polymerisation. *Polym. Int.* **1992**, 29 (1), 41–46.
- (167) Prescott, S. W. Chain-Length Dependence in Living/Controlled Free-Radical Polymerizations: Physical Manifestation and Monte Carlo Simulation of Reversible Transfer Agents. *Macromolecules* **2003**, 36 (25), 9608–9621.
- (168) Izgorodina, E. I.; Coote, M. L. Is the Addition-Fragmentation Step of the RAFT Polymerisation Process Chain Length Dependent? *Macromol. Theory Simulations* **2006**, 15 (5), 394–403.
- (169) Jenkins, A. D.; Jones, R. G.; Moad, G. Terminology for Reversible-Deactivation Radical Polymerization Previously Called “Controlled” Radical or “Living” Radical Polymerization (IUPAC Recommendations 2010). *Pure Appl. Chem.* **2009**, 82 (2), 483–491.
- (170) Shipp, D. A. Reversible-Deactivation Radical Polymerizations. *Polymer Reviews*. Taylor & Francis Group April 22, 2011, pp 99–103.
- (171) Konkolewicz, D.; Wang, Y.; Zhong, M.; Krys, P.; Isse, A. A.; Gennaro, A.;

- Matyjaszewski, K. Reversible-Deactivation Radical Polymerization in the Presence of Metallic Copper. A Critical Assessment of the SARA ATRP and SET-LRP Mechanisms. *Macromolecules*. American Chemical Society November 26, 2013, pp 8749–8772.
- (172) Chiefari, J.; Chong, Y. K. B.; Ercole, F.; Krstina, J.; Jeffery, J.; Le, T. P. T.; Mayadunne, R. T. A.; Meijs, G. F.; Moad, C. L.; Moad, G.; *et al.* Living Free-Radical Polymerization by Reversible Addition - Fragmentation Chain Transfer : The RAFT Process We Wish to Report a New Living Free-Radical Polymer- Iization of Exceptional Effectiveness and Versatility . 1 The Living Character Is Conferred By. *Macromolecules* **1998**, *31* (16), 5559–5562.
- (173) Moad, G.; Rizzardo, E.; Thang, S. H. RAFT Polymerization and Some of Its Applications. *Chem. - An Asian J.* **2013**, *8* (8), 1634–1644.
- (174) Moad, G.; Rizzardo, E.; Thang, S. H. Living Radical Polymerization by the RAFT Process a Third Update. In *Australian Journal of Chemistry*; CSIRO PUBLISHING, 2012; Vol. 65, pp 985–1076.
- (175) Chong, B. Y. K.; Krstina, J.; Le, T. P. T.; Moad, G.; Postma, A.; Rizzardo, E.; Thang, S. H. Thiocarbonylthio Compounds [S=C(Ph)S-R] in Free Radical Polymerization with Reversible Addition-Fragmentation Chain Transfer (RAFT Polymerization). Role of the Free-Radical Leaving Group (R). *Macromolecules* **2003**, *36* (7), 2256–2272.
- (176) Chong, B. Y. K.; Le, T. P. T.; Moad, G.; Rizzardo, E.; Thang, S. H. More Versatile Route to Block Copolymers and Other Polymers of Complex Architecture by Living Radical Polymerization: The RAFT Process. *Macromolecules* **1999**, *32* (6), 2071–2074.

- (177) Perrier, S.; Davis, T. P.; Carmichael, A. J.; Haddleton, D. M. First Report of Reversible Addition–Fragmentation Chain Transfer (RAFT) Polymerisation in Room Temperature Ionic Liquids. *Chem. Commun.* **2002**, 2 (19), 2226–2227.
- (178) Barner-Kowollik, C.; Buback, M.; Charleux, B.; Coote, M. L.; Drache, M.; Fukuda, T.; Goto, A.; Klumperman, B.; Lowe, A. B.; Mcleary, J. B.; *et al.* Mechanism and Kinetics of Dithiobenzoate-Mediated RAFT Polymerization. I. The Current Situation. *J. Polym. Sci. Part A Polym. Chem.* **2006**, 44 (20), 5809–5831.
- (179) Baussard, J.-F.; Habib-Jiwan, J.-L.; Laschewsky, A.; Mertoglu, M.; Storsberg, J. New Chain Transfer Agents for Reversible Addition-Fragmentation Chain Transfer (RAFT) Polymerisation in Aqueous Solution. *Polymer (Guildf)*. **2004**, 45 (11), 3615–3626.
- (180) Moad, G.; Rizzardo, E.; Thang, S. H. Living Radical Polymerization by the RAFT Process. *Aust. J. Chem.* **2005**, 58 (6), 379–410.
- (181) Mayadunne, R. T. A.; Rizzardo, E.; Chiefari, J.; Krstina, J.; Moad, G.; Postma, A.; Thang, S. H. Living Polymers by the Use of Trithiocarbonates as Reversible Addition-Fragmentation Chain Transfer (RAFT) Agents: ABA Triblock Copolymers by Radical Polymerization in Two Steps. *Macromolecules* **2000**, 33 (2), 243–245.
- (182) Delduc, P.; Tailhan, C.; Zard, S. Z. A Convenient Source of Alkyl and Acyl Radicals. *J. Chem. Soc. Chem. Commun.* **1988**, 0 (4), 308–310.
- (183) McLeary, J. B.; McKenzie, J. M.; Tonge, M. P.; Sanderson, R. D.; Klumperman, B. Initialisation in RAFT-Mediated Polymerisation of Methyl Acrylate. *Chem. Commun.* **2004**, 10 (17), 1950–1951.
- (184) McLeary, J. B.; Calitz, F. M.; McKenzie, J. M.; Tonge, M. P.; Sanderson, R. D.;

- Klumperman, B. Beyond Inhibition: A  $^1\text{H}$  NMR Investigation of the Early Kinetics of RAFT-Mediated Polymerization with the Same Initiating and Leaving Groups. *Macromolecules* **2004**, *37* (7), 2383–2394.
- (185) Benaglia, M.; Chen, M.; Chong, Y. K.; Moad, G.; Rizzardo, E.; Thang, S. H. Polystyrene- *Block* -Poly(Vinyl Acetate) through the Use of a Switchable RAFT Agent. *Macromolecules* **2009**, *42* (24), 9384–9386.
- (186) Chiefari, J.; Chong, Y. K. B.; Ercole, F.; Krstina, J.; Jeffery, J.; Le, T. P. T.; Mayadunne, R. T. A.; Meijs, G. F.; Moad, C. L.; Moad, G.; *et al.* Living Free-Radical Polymerization by Reversible Addition - Fragmentation Chain Transfer: The RAFT Process. *Macromolecules* **1998**, *31* (16), 5559–5562.
- (187) Lo, P. K.; Sleiman, H. F. Synthesis and Molecular Recognition of Conjugated Polymer with DNA-Mimetic Properties. *Macromolecules* **2008**, *41* (15), 5590–5603.
- (188) Lo, P. K.; Sleiman, H. F. Nucleobase-Templated Polymerization: Copying the Chain Length and Polydispersity of Living Polymers into Conjugated Polymers. *J. Am. Chem. Soc.* **2009**, *131* (12), 4182–4183.
- (189) Bielawski, C. W.; Grubbs, R. H. Living Ring-Opening Metathesis Polymerization. *Progress in Polymer Science (Oxford)*. Pergamon January 1, 2007, pp 1–29.
- (190) South, C. R.; Weck, M. Template-Enhanced Ring-Opening Metathesis Polymerization. *Macromolecules* **2007**, *40* (5), 1386–1394.
- (191) Kang, Y.; Lu, A.; Ellington, A.; Jewett, M. C.; O'Reilly, R. K. Effect of Complementary Nucleobase Interactions on the Copolymer Composition of RAFT Copolymerizations. *ACS Macro Lett.* **2013**, *2* (7), 581–586.

- (192) Hua, Z.; Wilks, T. R.; Keogh, R.; Herwig, G.; Stavros, V. G.; O'Reilly, R. K. Entrapment and Rigidification of Adenine by a Photo-Cross-Linked Thymine Network Leads to Fluorescent Polymer Nanoparticles. *Chem. Mater.* **2018**, *30* (4), 1408–1416.
- (193) Fong, D.; Hua, Z.; Wilks, T. R.; O'Reilly, R. K.; Adronov, A. Dispersion of Single-Walled Carbon Nanotubes Using Nucleobase-Containing Poly(Acrylamide) Polymers. *J. Polym. Sci. Part A Polym. Chem.* **2017**, *55* (16), 2611–2617.
- (194) Hua, Z.; Keogh, R.; Li, Z.; Wilks, T. R.; Chen, G.; O'Reilly, R. K.; O'Reilly, R. K. Reversibly Manipulating the Surface Chemistry of Polymeric Nanostructures via a “Grafting To” Approach Mediated by Nucleobase Interactions. *Macromolecules* **2017**, *50* (9), 3662–3670.
- (195) Hua, Z.; Pitto-Barry, A.; Kang, Y.; Kirby, N.; Wilks, T. R.; O'Reilly, R. K. Micellar Nanoparticles with Tuneable Morphologies through Interactions between Nucleobase-Containing Synthetic Polymers in Aqueous Solution. *Polym. Chem.* **2016**, *7* (25), 4254–4262.

## **Chapter 2: Methods and Materials**

### **2.1 Synopsis**

*This chapter pertains to the materials, reagents, experimental procedures, and characterisation techniques used in this thesis.*



## 2.2 Abbreviations for Nucleotide Derivatives.

This section lists the abbreviations, names and structures for the compounds synthesised in this thesis (Table 2.1) based on the process outlined in Figure 2.1.

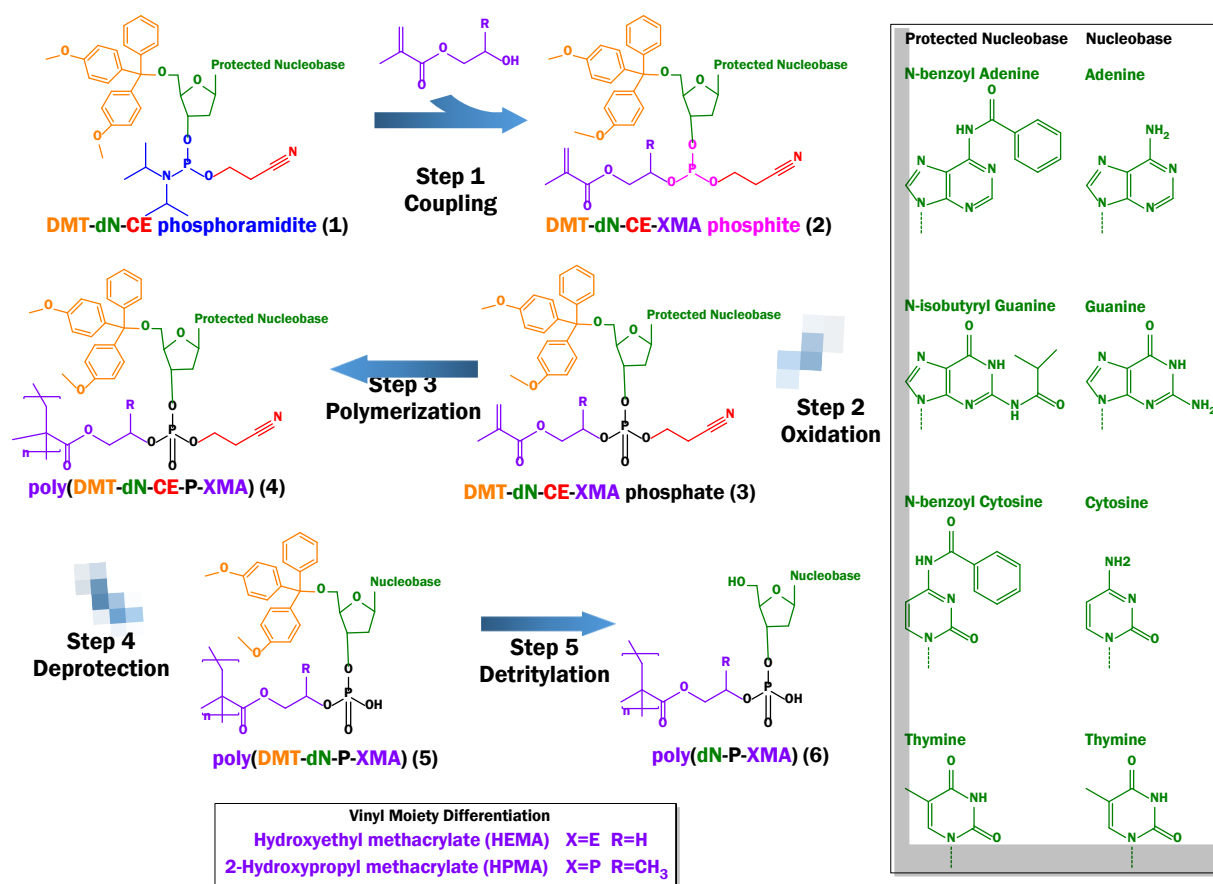


Figure 2.1 Overview of polymer synthesis from protected nucleotide phosphoramidite to the final deprotected polymer bioconjugate.

**Table 2.1:** Scientific names, abbreviations and structures for the molecules synthesised in this thesis.

<b>Process</b>	<b>Abbreviation (Figure 2.1 reference)</b>	<b>Chemical name</b>
Chapter 3		
<i>Starting material</i>	DMT-dC-CE phosphoramidite <b>(C1)</b>	5'-dimethoxytrityl- <i>N</i> -benzoyl-2'-deoxycytosine,3'-[(2-cyanoethyl)-(N,N-diisopropyl)]-phosphoramidite
<i>Coupled</i>	DMT-dC-CE-EMA- phosphite <b>(C2)</b>	5'-dimethoxytrityl- <i>N</i> -benzoyl-2'-deoxycytosine,3'-[(2-cyanoethyl)-(oxyethyl methacrylate)]-phosphite monomer
<i>Oxidized</i>	DMT-dC-CE-EMA- phosphate <b>(C3)</b>	5'-dimethoxytrityl- <i>N</i> -benzoyl-2'-deoxycytosine,3'-[(2-cyanoethyl)-(oxyethyl methacrylate)]-phosphate monomer
<i>Polymerized</i>	poly(DMT-dC-CE-P- EMA) <b>(C4)</b>	poly(2-(5'-dimethoxytrityl- <i>N</i> -benzoyl-2'-deoxycytosine-monophosphate)oxyethyl methacrylate)
Chapters 4,5		
<i>Starting material</i>	DMT-dG-CE phosphoramidite <b>(G1)</b>	5'-dimethoxytrityl- <i>N</i> -isobutyryl-2'-deoxyguanosine,3'-[(2-cyanoethyl)-(N,N-diisopropyl)]-phosphoramidite

<i>Coupled</i>	DMT-dG-CE-PMA-phosphite ( <b>G2</b> )	5'-dimethoxytrityl- <i>N</i> -isobutyryl-2'-deoxyguanosine,3'-[(2-cyanoethyl)-(oxypropyl methacrylate)]-phosphite monomer
<i>Oxidised</i>	DMT-dG-CE-PMA-phosphate ( <b>G3</b> )	5'-dimethoxytrityl- <i>N</i> -isobutyryl-2'-deoxyguanosine,3'-[(2-cyanoethyl)-(oxypropyl methacrylate)]-phosphate monomer
<i>Polymerized</i>	poly(DMT-dG-CE-P-PMA) ( <b>G4</b> )	poly(2-(5'-dimethoxytrityl- <i>N</i> -isobutyryl-2'-deoxyguanosine-monophosphate)oxypropyl methacrylate)
<i>Deprotected</i>	poly(DMT-dG-P-PMA) ( <b>G5</b> )	poly(2-(5'-dimethoxytrityl-2'-deoxyguanosine-monophosphate)oxypropyl methacrylate)
<i>Detritylated</i>	poly(dG-P-PMA) ( <b>G6</b> )	poly(2-(2'-deoxyguanosine-monophosphate)oxypropyl methacrylate)
Chapter 6		
<i>Starting material</i>	DMT-dT-CE phosphoramidite ( <b>T1</b> )	5'-dimethoxytrityl-2'-deoxythymine,3'-[(2-cyanoethyl)-(N,N-diisopropyl)]-phosphoramidite
<i>Coupled</i>	DMT-dT-CE-PMA-phosphite ( <b>T2</b> )	5'-dimethoxytrityl-2'-deoxythymine,3'-[(2-cyanoethyl)-(oxypropyl methacrylate)]-phosphite monomer

<i>Oxidised</i>	DMT-dT-CE-PMA-phosphate <b>(T3)</b>	5'-dimethoxytrityl-2'-deoxythymine,3'-[(2-cyanoethyl)-(oxypropyl methacrylate)]-phosphate monomer
<i>Polymerised</i>	poly(DMT-dT-CE-P-PMA) <b>(T4)</b>	poly(2-(5'-dimethoxytrityl-2'-deoxythymine-monophosphate)oxypropyl methacrylate)
<i>Deprotected</i>	poly(DMT-dT-P-PMA) <b>(T5)</b>	poly(2-(5'-dimethoxytrityl-2'-deoxythymine-monophosphate)oxypropyl methacrylate)
<i>Detritylated</i>	poly(dT-P-PMA) <b>(T6)</b>	poly(2-(2'-deoxythymine-monophosphate)oxypropyl methacrylate)

## 2.2 Materials

This section lists all chemicals and reagents used for the research of this thesis.

### 2.2.1 Table of Chemicals and Reagents

<b>Chemical Name</b>	<b>Supplier/Manufacturer</b>	<b>Info</b>
<b>Acetone, analytical grade</b>	Chem-Supply, Australia	Used as purchased for all cleaning
<b>Acetone, HPLC</b>	Sigma-Aldrich, Australia	Used as purchased
<b>Acetonitrile</b>	Sigma-Aldrich, Australia	Purchased dry and stored over 4 Å molecular sieves when used
<b>Acetonitrile, deuterated (CD<sub>3</sub>CN)</b>	Sigma-Aldrich, Australia	Used as purchased.
<b>Acetic acid, glacial</b>	Sigma-Aldrich, Australia	Used as purchased
<b>Ammonia, 30 %</b>	Chem-Supply, Australia	Used as purchased
<b>Azobisisobutyronitrile (AIBN)</b>	Merk, Germany	Recrystallised using the method outlined in Section 2.3.1
<b>Chloroform</b>	Sigma-Aldrich, Australia	Used as purchased
<b>Chloroform, deuterated (CDCl<sub>3</sub>)</b>	Sigma-Aldrich, Australia	Used as purchased
<b>4-Cyano-4-(phenylcarbonothioylthio)pentanoic acid <i>N</i>-succinimidyl ester (NHS-RAFT)</b>	Sigma-Aldrich, Australia	Used as purchased, stored below -20 °C.

<b>Deuterium oxide (D<sub>2</sub>O)</b>	Sigma-Aldrich, Australia	Used as purchased
<b>Deuterated chloroform</b>	Sigma-Aldrich, Australia	Used as purchased
<b>Dichloromethane (DCM)</b>	Sigma-Aldrich, Australia	Used as purchased
<b>N,N-Dimethylformamide (DMF) (99 % anhydrous)</b>	Sigma-Aldrich, Australia	Used as purchased
<b>4,5, dicyanoimidazole (DCI)</b>	Tokyo Chemical Industry, Japan	Used as purchased
<b>Ethyl acetate (EtOAc)</b>	Chem-Supply, Australia	Used as purchased
<b>Hydroxyethyl methacrylate (HEMA)</b>	Sigma-Aldrich, Australia	Used as purchased
<b>2-hydroxypropyl methacrylate (HPMA)</b>	Sigma-Aldrich, Australia	Used as purchased
<b>Lithium acetate (LiOAc)</b>	Sigma-Aldrich, Australia	Used as purchased
<b>Methanol (&gt; 99.9%) (MeOH)</b>	Sigma-Aldrich, Australia	Used as purchased
<b>Tetrazole, 0.45 M in acetonitrile</b>	Sigma-Aldrich, Australia	Used as purchased
<b>Phosphoramidites, DMT-dG-CE</b>	Glen Research, USA LGC Link Tech, UK	Transition to a LGC Link tech occurred during the work covered in chapter 4.
<b>Phosphoramidites, DMT-dA-CE</b>	Glen Research, USA LGC Link Tech, UK	Transition to a LGC Link tech occurred during the work covered in chapter 4.
<b>Phosphoramidites, DMT-dT-CE</b>	Glen Research, USA LGC Link Tech, UK	Transition to a LGC Link tech occurred during the work covered in chapter 4.
<b>Phosphoramidites, DMT-dC-CE</b>	Glen Research, USA LGC Link Tech, UK	Transition to a LGC Link tech occurred during the work covered in chapter 4.
<b>Phosphoramidites, 5' DMT-dG-CE</b>	Linktech, United Kingdom	Used as purchased
<b>Propan-2-ol</b>	Chem-Supply, Australia	Used as purchased
<b>Sodium acetate (NaOAc)</b>	Sigma-Aldrich, Australia	Used as purchased
<b>Sodium carbonate</b>	Sigma-Aldrich, Australia	Used as purchased
<b>Tetrahydrofuran (THF)</b>	Sigma-Aldrich, Australia	Used as purchased
<b>Triethylamine (TEA)</b>	Sigma-Aldrich, Australia	Used as purchased
<b>Tris(hydroxymethyl)aminomethane hydrochloride (TRIS-HCl)</b>	Sigma-Aldrich, Australia	Used as purchased
<b>Water, MilliQ</b>		Prepared by filtering through resin membrane filters to a resistivity of <18 MΩ cm. this was used for all reactions and separations.

## 2.2.2 Table of DNA Sequences

Sequence Name	Nucleobase Sequence (5'-3')	Supplier
<b>dA ssDNA</b>	AAA AAA AAA AAA AAA AAA AAA AA	IDT DNA, Iowa, United States. Provided dry and prepared to 1 $\mu$ M with 10 mM TRIS-HCl EDTA buffer and stored bellow 20 $^{\circ}$ C.
<b>dT ssDNA</b>	TTT TTT TTT TTT TTT TTT TTT TT	IDT DNA, Iowa, United States. Provided dry and prepared to 1 $\mu$ M with 10 mM TRIS-HCl EDTA buffer and stored bellow 20 $^{\circ}$ C.
<b>GQ</b>	GGG AAA GGG CAC CGG GCC GGG	IDT DNA, Iowa, United States. Provided dry and prepared to 1 $\mu$ M with 10 mM TRIS-HCl EDTA buffer and stored bellow 20 $^{\circ}$ C.

## 2.3 Preparations

This section outlines the methods used to prepare materials and reagents.

### 2.3.1 Recrystallisation of AIBN

AIBN breaks down in storage requiring it to be recrystallised before use.<sup>1</sup> This recrystallisation was conducted in batches every 3-6 months depending on usage needs. To conduct the recrystallization a batch of AIBN (~10 g) was placed into methanol (100 mL) and heated to 50  $^{\circ}$ C with vigorous stirring. During this time a vacuum filtration funnel was preheated to 50  $^{\circ}$ C. The hot AIBN solution was then vacuum filtered through a quantitative filter paper to remove the insoluble breakdown products. The eluent was then cooled to 5  $^{\circ}$ C for 24 h. Due to a lack of crystallisation the solution was then cooled to -21  $^{\circ}$ C for a further 24 h. At this point if crystals had not formed the crystallization was catalysed by the addition of a drop of MilliQ water and cooled to -21  $^{\circ}$ C for a further 24 h.

This resulted in the formation of fine crystals ~2 mm in length which were isolated by filtration. These AIBN crystals were then placed under vacuum in a desiccator until dried. Once dry the AIBN was transferred to a screw top vial and sealed with paraffin film, then stored below -10 °C until required.

### 2.3.2 Generation of Molecular Sieves

To generate the 4 Å molecular sieves, they were placed in a dry glass watch glass, and heated to 250 °C for 12 h prior to use. When not used immediately, the sieves were stored at 110 °C. Before use the 4 Å molecular sieves were placed in the desired vessel, sealed with a rubber septum, and allowed to cool to room temperature before the addition of solvents.

### 2.3.3 Preparation of HPMA and DCI solutions.

The glassware required for these solutions was first dried in an oven at 95 °C for a minimum of 24 h prior to use to ensure any surface moisture was thoroughly removed.

A solution of DCI (0.8 M, 250 mL) was prepared by adding DCI (23.62 g, 0.2 mol) to a volumetric flask and filled to the 250 mL marker with dry acetonitrile and sonicated until dissolved. The solution was then decanted into a dried bottle containing 100 g of 4 Å molecular sieves and sealed with a rubber septum. The bottle was then backfilled and degassed with dry N<sub>2</sub>, and stored at 5 °C until used.

A solution of HPMA (0.2 M, 250 mL) was prepared by adding HPMA (7.28 g, 0.05 mol) to a volumetric flask and filled to the 250 mL marker with dry acetonitrile. The solution was then sealed with a rubber septum, backfilled and degassed with dry N<sub>2</sub>, and stored at 5 °C until used.

## 2.4 Synthetic Procedures

This section outlines the specific synthesis procedures for compounds used in this thesis.

### 2.4.1 Chapter 3 Methods

#### 2.4.1.1 Synthesis of 5'-dimethoxytrityl-*N*-benzoyl-2'-deoxycytosine,3'-[(2-cyanoethyl)-(oxyethyl methacrylate)]-phosphate monomer.

To carry out the conjugation **C1** (0.17 g, 0.2 mmol) was placed into a dried 15 mL vial, sealed with a rubber septa, and backfilled with N<sub>2</sub>. Tetrazole in dry acetonitrile (0.45 M, 6 mL) was combined with HEMA (0.31 g, 2.3 mmol) and added to the **C1** using a syringe while maintaining N<sub>2</sub> atmosphere. The sample was then cooled to 4 °C for 4 h and quenched with 2 mL of 45:45:10 v/v/v, ethyl acetate (EtOAc), dichloromethane (DCM), and triethylamine (TEA) (EtOAc:DCM:TEA) solution. The resulting mixture was solvent extracted with DCM (~30 mL) to isolate the organic phase containing the **C3** monomer. This was then dried under a flow of compressed air to oxidise the P(III) phosphite to the P(V) phosphate, thereby generating the **C3** monomer. The yield was recorded as 0.14 g (76%).

#### 2.4.1.2 Polymerisation of 5'-dimethoxytrityl-*N*-benzoyl-2'-deoxycytosine,3'-[(2-cyanoethyl)-(oxyethyl methacrylate)]-phosphate monomer.

For the polymerisation, **C3** monomer (1 g, 1.1 mmol) was dissolved in dry acetonitrile (10 mL). To this azobisisobutyronitrile (AIBN) (0.2 mg, 1.2 μmol) was added as an initiator and 4-cyano-4-(phenylcarbonothioylthio)pentanoic acid *N*-succinimidyl ester (NHS-RAFT) (0.6 mg, 15 μmol) as a mediator. This resulted in a ratio of **3C**:RAFT-NHS:AIBN of 100:1.5:0.1. The resulting solution was degassed using N<sub>2</sub> for 45 min before being heated to 70 °C to activate the polymerisation and maintained at that temperature for 3.5 h resulting in **C4** which formed a gel. The exact yield could not be obtained due to the hydration of the gel but was greater than 50%.



## 2.4.2 Chapter 4 Methods

### 2.4.2.1 Coupling: Synthesis of 5'-dimethoxytrityl-N-isobutyryl-2'-deoxyguanosine,3'-[(2-cyanoethyl)-(oxypropyl methacrylate)]-phosphate monomer (G3)

HPMA (0.2 M, 6 mL) and DCI (0.8 M, 6 mL) solutions were added to **G1** (1 g, 1.1 mmol) in the sealed vial as supplied and sonicated for 1 min before being cooled to 4 °C for 4 h. The reaction was then quenched with a 45:45:10 solution of EtOAc:DCM:TEA (v/v/v, 4 mL) and left for 12 h at 0 °C. Though not vital, it was found that the addition of the HPMA solution to the reaction before adding the DCI allowed for easier solvation of the phosphoramidite.

The resulting mixture containing **G2** monomer was then phase extracted by pouring the mixture into an aqueous NaHCO<sub>3</sub> solution (0.1 M, 20 mL) and isolating the organic (DCM) phase. This phase was then washed with an equal volume of milliQ water. The organic (DCM) phase containing the **G2** monomer was then isolated.

The DCM solvent was removed under a high flow of compressed air (>5 L/min) (typically 12 h) in order to avoid the formation of any diene by-product during the isolation of the final **G3** monomer product. This also serves the secondary purpose of oxidising the phosphite into a phosphate (from the P(III) to P(V) oxidation state). The yield was recorded as 0.82 g (76%). Resulting in the formation of the **G3** monomer.

### 2.4.2.2 Polymerisation of 5'-dimethoxytrityl-N-isobutyryl-2'-deoxyguanosine,3'-[(2-cyanoethyl)-(oxypropyl methacrylate)]-phosphate monomer (G3).

The following is an example polymerisation method based on the molar ratio of 100:4:1 gives an effective ratio of 20:1 monomer to initiators and was designed to yield short polymers for easier characterisation and solubility studies. The exact amounts varied for some experiments to match the ratios presented. The **G3** monomer (1.54 g, 1.7 mmol) was combined with the

NHS-RAFT agent (27 mg, 7.1  $\mu\text{mol}$ ) and AIBN (3 mg, 1.8  $\mu\text{mol}$ ) at a molar ratio of 100:4:1 in dry acetonitrile (15 ml). The reaction mixture was put into a scintillation vial with a rubber septum seal and degassed using dry  $\text{N}_2$  for 45 min, typically resulting in a decrease in solvent volume of between 5-15 v/v, and then heated to 70  $^\circ\text{C}$  in a mineral oil bath with stirring for 24 h under a sealed  $\text{N}_2$  atmosphere. At the end of this time the reaction vessel was quenched by rapidly cooling the reaction vessel with an ice water bath and exposing it to atmosphere. This cooling caused the polymer to precipitate from solution. Samples were then freeze dried until a pressure of 0.019 mbar was attained. The yield was recorded as 0.96 g (62%).

#### 2.4.2.3 Deprotection of poly(2-(5'-dimethoxytrityl-N-isobutyryl-2'-deoxyguanosine-monophosphate)oxypropyl methacrylate).

The crude **G4** (0.8 g, 0.9 mmol) was placed in a round bottom flask with 30% ammonia in water (50 mL). The solution was heated to 50  $^\circ\text{C}$  for up to 24 h until the sample dissolved and the solution turned clear. The solution was then vacuum filtered through a quantitative filter paper and the eluent dried under  $\text{N}_2$ .

#### 2.4.2.4 Detritylation of poly(2-(5'-dimethoxytrityl-2'-deoxyguanosine-monophosphate)oxypropyl methacrylate).

**G5** (0.4 g, 0.5 mmol) was placed into 80% acetic acid in water (10 mL) for 20 min producing a bright orange colour. Lithium acetate (1.5 M, 1 mL, 1.5 mmol) was then added until the orange colour was removed. The solution was cooled to 0  $^\circ\text{C}$  for 30 min, then the solution centrifuged to isolate the final polymeric product **G6**. The yield was recorded as 0.16 g (38%).

### 2.4.3 **Chapter 6 Methods**

#### 2.4.3.1 Synthesis of poly(dT-P-PMA)

Synthesis of the starting material, **T3** monomer was conducted using the same methodology presented in Section 2.4.2.1 for the synthesis of **G3** monomer. To generate the thymine version of the bioconjugate **G1** was substituted for **T1**.

The polymerisation of the **T3** monomer was conducted using the same procedure as discussed in Section 2.4.2.2 for the polymerisation of **G3** monomer.

To adapt the method for **T3** monomer and achieve the increased  $M_w$  for the resulting polymer the ratio of monomer:NHS-RAFT:AIBN was altered to 100:4:1, an effective monomer:initiators. Therefore, **T3** (0.78 g, 0.86 mmol) was combined with NHS-RAFT (14.4 mg) and AIBN (1.95 mg) in dry acetonitrile (6 mL). The yield was recorded as 0.34 g (78%).

## 2.5 Characterisation

This section outlines the general methods for characterisation used in the following chapters.

### 2.5.1 Chapter 3 Characterisation

#### 2.5.1.1 Nuclear magnetic resonance (NMR) spectroscopy of DMT-dC-CE-P-PMA phosphate

Samples (5 mg) were placed into a single use NMR tube with deuterated acetonitrile solvent (1 mL). The sample was then sonicated until the **C3** fully dissolved.

##### 2.5.1.1.1 $^1\text{H}$ NMR Spectroscopy

Samples were measured using either a Bruker 400 MHz or 600 MHz spectrometer, as indicated in the data captions, using a 5 mm inverse multinuclear probe measuring  $^1\text{H}$ . Spectra were acquired using compilation of 32 scans.

#### 2.5.1.1.2 $^{31}\text{P}$ NMR Spectroscopy

Bruker 400 MHz spectrometer using a 5 mm inverse multinuclear probe measuring  $^{31}\text{P}$ . Spectra were acquired using 128 scans.

#### 2.5.1.2 Quantitative Solvent-Gel Analysis

Five fragments of the C4 polymer gel between 0.5 mg and 2.5 mg were placed separately into 25 mL scintillation vials and dried at 50 °C for 6 h. To each vial 10 mL one of the solvents DMSO, H<sub>2</sub>O, MeOH, THF, or acetonitrile was added. These samples were then placed in a dark cupboard for 12 h to absorb any solvent they could. Fragments were then removed and patted dry on Kimtech® Science™ Kimwipes™ to remove surface moisture before being weighed to determine their swelling ratio.

#### 2.5.1.3 Attenuated Total Reflectance-Fourier Transform Infrared (ATR-FTIR) Spectroscopy

Fragments of the poly(DMT-dG-CE-P-EMA) gel approximately 1 mg in weight were dried and placed onto the Nicolet Nexus 870 step-scan FTIR using the ATR accessory with a diamond crystal. The spectrum was acquired over the range of 525 nm to 5000 nm in transmission mode.

### 2.5.2 **Chapter 4 Characterisation**

#### 2.5.2.1 Electrospray Ionisation- Mass Spectrometry (ESI-MS)

ESI-MS contains two stages; the electrospray to ionise the analyte and the mass spectrometer to measure the resulting mass to charge ratio of the analyte. In this case the analyte was the G2 monomer solution. To start with liquid containing the analyte is positively charged through the removal of electrons by a cathode as the sample moves towards the ESI nozzle. The analyte is then exposed to both a high electric potential and vacuum. This causes the formation of a charged aerosol, electrospray, which is accelerated across the potential

towards a mass spectrometer inlet. Through a process of Coulomb fission these aerosol particles break up until only one molecule of analyte remains in each particle. Simultaneously, due to the vacuum present the solvent is removed. This spray is then analysed by the mass spectrometer.

The ESI-MS spectrum presented in this thesis were recorded on a Waters Synapt HDMS (Waters, Manchester, UK) in electrospray positive ion mode, using an infusion of 0.05 mM sodium formate solution for calibration.

#### 2.5.2.2 Size-exclusion chromatography (SEC)

The average molecular weight ( $M_n$ ) and  $D$  of **G4** synthesised via the large-scale process was determined using SEC on a Waters 2690 Separation Module using a Waters 410 differential refractometer. Two Agilent PLgel 5  $\mu$ m MiniMIX-C columns were used in series with an Agilent guard column for protection. The eluent was HPLC grade tetrahydrofuran at 5 mL/min with 5  $\mu$ L sample injection volumes. Calibration was conducted using polystyrene standards.

#### 2.5.2.3 Kinetics Measurements

##### 2.5.2.3.1 *In-situ* NMR Spectroscopy Kinetic Measurements

*In-situ* NMR spectroscopy polymerisation measurements to determine kinetics were conducted on a Bruker 400 MHz spectrometer using a 5 mm inverse multinuclear probe measuring  $^1\text{H}$  nucleus.

To acquire measurements the NMR instrument was preheated to 70 °C prior to inserting the NMR tube. A degassed solution of **G3** (1 mL, 75 mg/mL) with RAFT agent and AIBN at a molar ratio of 20:4:1 in  $d_3$ -acetonitrile was sealed in a glass NMR tube under an  $\text{N}_2$

atmosphere. The NMR tube was then inserted into the instrument and measurements were taken for 2.5 min at 10 min intervals for a total cycle time of 12.5 min and repeated for 850 min. The integration ratio of the monomer peak at 5.6 ppm was compared to the peak associated with trace TEA at 3.1 ppm to determine conversion.

#### 2.5.2.3.2 Ex-situ Kinetic Measurements with SEC

*Ex-situ* kinetic measurements were collected with the assistance of a ChemSpeed Swing XL. This is an automated sampling system that allows arrays of experiments to be conducted in a closed cabinet, as shown in Figure 2.2. The system is made of 4 major components. The syringe pump and syringes (Figure 2.2(a and b)), the reagent rack (Figure 2.2(c)), the reaction rack (Figure 2.2(d)) and the collection rack (Figure 2.2(e)). Each of these racks is mounted on a water block to allow for heating and cooling to the desired temperatures, with the reaction rack located at the opposite end of the machine to the reagent and collection racks to prevent contamination. The entire cabinet is atmospherically isolated with samples loaded through an airlock.

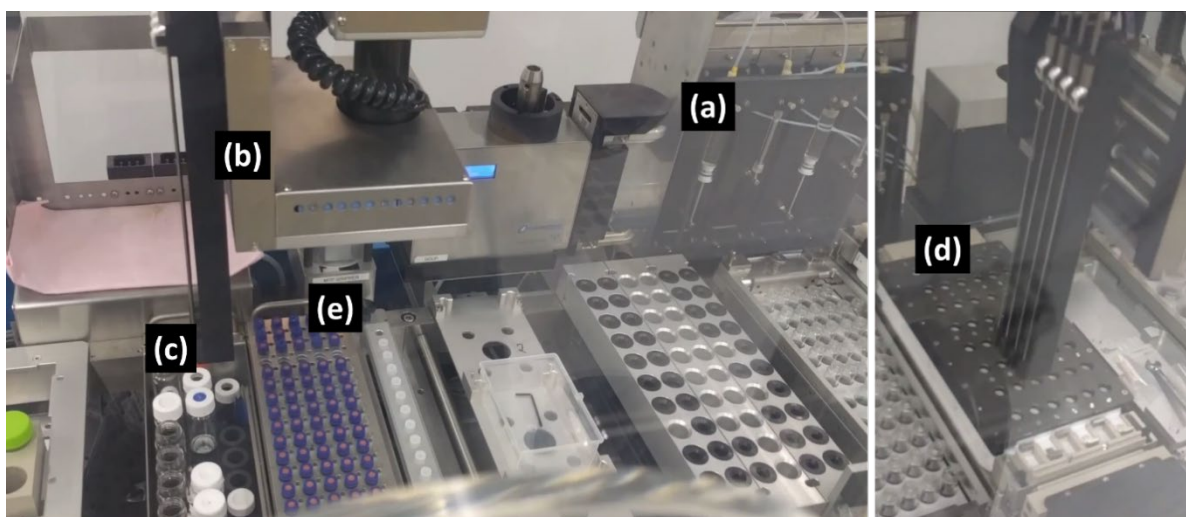


Figure 2.2 ChemSpeed Swing XL showing (a) syringe pump, (b) syringes, and racks for (c) reagents, (d) reactions, and (e) collected samples.

For kinetic measurements the ChemSpeed Swing XL chamber was first purged with dry N<sub>2</sub> and maintained under a flow of N<sub>2</sub> for the remainder of the experiment. The ChemSpeed Swing XL was loaded with a 4 x 8 vial block as the reaction rack which was heated to 110 °C to purge surface water, ensuring dry reaction vessels before the temperature was lowered back to 70 °C for conducting the polymerisation. A separate rack containing 2 mL vials was also loaded for collecting the samples as they were removed from the polymerisation. Bulk solutions of the **G3** (0.1 M) monomers with the AIBN and NHS-RAFT in a molar ratio of 100:1:0.25 were prepared in acetonitrile (25 mL) and degassed with argon (5 L/min) for 45 min. These were then loaded into the airlock and placed into a third rack, separated from the heated 4 x 8 vial block by an air gap to prevent inadvertent heating.

The ChemSpeed Swing XL then separated 3 samples, each of 7 mL, of the **G3** monomer:RAFT-NHS:AIBN solution into different vials of the 4 x 8 heated vial block. At set time increments of 30, 60, 90, 240, 300, 480, and 600 min 1 mL samples were removed and placed into separate unheated 2 mL collection vials.

These **G4** samples were then freeze-dried and solvated in THF before being analysed using SEC as outlined in Section 1.5.2.2, to determine the average molecular weight ( $M_n$ ) and  $D$  of the **G4**. Examples are presented in Appendix 3.

#### 2.5.2.4 Solubility of G6

The solubility of the final deprotected, detritylated **G6** was evaluated in a number of solvents; DMAc, chloroform, THF, and water:propan-2-ol mixtures. This was determined qualitatively by adding **G6** (10 mg) to 1 mL of solvent with sonication for 10 min. The **G6** sample was then qualitatively inspected noting transparency and clarity of the solution formed.

### 2.5.3 Chapter 5 Characterisation

#### 2.5.3.1 SEM

Silicon wafer was diced into ~5 mm squares and washed successively in MilliQ water, acetone, water, and HPLC grade ethanol. The wafers were then air dried in a covered container to prevent dust settling. Samples of the **G6** were then dropcast onto the wafer and placed into liquid nitrogen 5 min until vigorous bubbling had stopped and the samples were frozen solid. The wafers were then freeze-dried to 0.019 mbar, approximately 4 h, until dry. The dried samples were coated with 3 nm platinum using an Emitech Quorum Sputter Coater K575X and imaged on a FEI Phenom Scanning Electron Microscope under ambient atmosphere.

#### 2.5.3.2 UV-visible (UV-vis) single sample

The UV-vis spectrum of **G6** was obtained on the NanoDrop 1000 microvolume spectrophotometer. 1.5  $\mu$ L sample volumes were measured with 0.2 mm path length and 3 nm resolution.

To determine the nature of the binding within the **G6** particles, they were isolated using the method described previously, Section 1.4.2.4, using LiOAc and prepared in 10:1 (v/v) water:propan-2-ol at 10  $\mu$ g/mL loading of the **G6**. Two additional samples were prepared from this batch prepared with added NaOAc and KOAc salts. This was done as larger monovalent cations have been shown to increase the formation and stability of G-quartets.<sup>2,3</sup> The samples were then analysed using a full spectrum scan at 4 s  $\text{nm}^{-1}$  dwell-time between 180 nm and 340 nm.

#### 2.5.3.3 UV-vis Measurement of TMB Oxidation Using Well Plate Reader.



Stock solutions (1 mL each) were prepared containing analyte (0.5  $\mu$ L, 0.1 M), KCl reaction buffer (18.5  $\mu$ L, 25 mM) and TMB solution (985  $\mu$ L, 400  $\mu$ M). From these bulk solutions 4 x 100  $\mu$ L samples were taken for each analyte and placed into a 96-well microplate. Hemin solution (1  $\mu$ L, 500X) was then added to each well to catalyse the oxidation. The well plate was then immediately placed into a well plate reader measuring absorbance at 595 nm over 15 min, taking samples every 30 s for 125 min.

#### 2.5.3.4 Dynamic Light Scattering (DLS)

**G6** (1  $\mu$ M, 1 mL) was prepared in a cuvette and recorded on a Malvern high performance particle size analyser. Hemin solution (2  $\mu$ L, 500X) was added in increments and inverted for successive samples. For comparison, a solution of the protected **G4** (1  $\mu$ M, 1 mL) was used as a control.

#### 2.5.3.5 Circular Dichroism (CD)

CD spectra were recorded on an Aviv Biomedical Model 410 (Aviv, Rhode Island, USA) equipped with Peltier-controlled thermostat housing unit using a SQ-grade cuvette, with a path length of 1 mm. Spectra were obtained at 25  $^{\circ}$ C using a scanning rate of 15 nm min<sup>-1</sup>, bandwidth of 1 nm, 1 nm interval data sampling, and a single accumulation.

Samples were prepared by re-suspending the final product **G6** (0.1 M) in water:propan-2-ol (10:1 (v/v), 1 mL) with mild sonication. Multiple solutions were prepared for each instrument analysis. For experiments where **G6** was doped with KOAc or NaOAc this was performed by taking 300  $\mu$ L of the **G6** solution and adding in 3  $\mu$ L of aqueous KOAc or NaOAc (2.5 M). This resulted in a doping of 25 mM of KOAc or NaOAc.

Melting data was obtained using the same sample preparation. Measurements were taken at the 261 nm wavelength with a 1 nm slit. Samples were then heated by 1 °C at a rate of 5 °C/min and equilibrated for 30 s before recording measurements for 1 min.

#### 2.5.3.6 Melting Measurements Using Fluorescence of ATTO 550 Dye

For the **G4** analysis as isolated with lithium acetate, ATTO 550 fluorescent dye (1 µL, 500X) was added to 100 µL of **G6** in water:propan-2-ol 10:1 (v/v) a solution. Then 25 µL was transferred into each of 4 separate plastic vials for analysis. For the **G6** doped with KOAc (25 mM), ATTO 550 dye (1 µL, 500X) was added to 100 µL of the KOAc doped solution. Then 25 µL was transferred into 4 separate plastic vials for analysis.

#### 2.5.3.7 Fluorescence Measurements

Fluorescence versus temperature measurements were then conducted on each 25 µL sample simultaneously in a Rotor-Gene real-time polymerase chain reaction (PCR) thermocycler using a yellow channel (530 ± 5 nm excitation, 557 ± 5 detection) for detection. The samples were heated at 1 °C/min from 30 °C to 95 °C. The fluorescence of each of the 4 solutions of each sample were averaged.

For the **G6** samples were analysed as isolated with LiOAc. 1x ATTO 550 fluorescent dye (1 µL) was added to 100 µL of **G6** in water:propan-2-ol 10:1 (v/v) a solution. For the **G6** doped with KOAc (25 mM), 1x ATTO 550 dye (1 µL) was added to 100 µL of the KOAc doped solution. Confocal fluorescence microscope images were taken on a Nikon A1R with a 150 µm glass cover slide using a 488 nm excitation at 200x magnification and red band detection. Each sample was drop cast onto the glass cover slide and the sample imaged near the glass-solvent interface.

## 2.5.4 Chapter 6

### 2.5.4.1 UV-vis Spectroscopy of Poly(dT-P-PMA) Interactions with dA ssDNA

UV-Vis spectroscopy was used to determine if the combinations of dA ssDNA 23-mer and poly(dT-P-PMA) 21-mer when mixed caused the formation of a duplex. To do this, separate solutions of the 23-mer dA ssDNA and 21-mer poly(dT-P-PMA) were prepared at 1 ng/ $\mu$ L each in TRIS-HCl EDTA buffer. The solutions were then combined at ratios from 100% dA ssDNA through to 100% poly(dT-P-PMA). Absorption was measured using the 260 nm peak associated with free nucleotides.<sup>4</sup>

### 2.5.4.2 Effect of Annealing on Fluorescence of Poly(dT-P-PMA) Dye Interactions

For measuring dye interactions with mixtures where binding was being determined, samples were tested in quadruplicate. Samples of poly(dT-P-PMA) (100  $\mu$ L, 10  $\mu$ M) were prepared in TRIS-HCl buffer (0.01 mM) then heated to either 45 °C or 95 °C from room temperature, held at that temperature for 15 min, before being cooled. SYBR Safe 2.5X was then added. These temperatures were chosen as 45 °C was above the 35 °C seen in Chapter 6 Section 6.6.2, where the fluorescence rapidly drops. The 95 °C point was chosen as a maximum temperature control. This heating process was conducted using a generic PCR heating block before measuring the samples on the Qiagen® Rotor-Gene Q real time PCR instrument.

### 2.5.4.3 Effect of Sodium Concentration on the Interaction of the SYBR Dye

Samples of poly(dT-P-PMA) (1  $\mu$ L, 1 mM) were prepared in TRIS-HCl buffer (0.01 mM) with SYBR safe dye (5  $\mu$ L, 50X). To this 0.5, 1, 2, 5 or 10  $\mu$ L of sodium chloride solution (2.5 M) was added and the solution made up to a total of 100  $\mu$ L. The 100  $\mu$ L solution was then divided into four 25  $\mu$ L aliquots and measured on the Qiagen® Rotor-Gene Q real time PCR instrument using the default detection settings for the relevant dye.

#### 2.5.4.4 Complementary Dye Interactions

Samples were prepared in TRIS-HCl buffer (0.01 mM). To prepare each sample the relevant dye (5  $\mu$ L) was added to a vial with samples of the analyte; poly(dT-P-PMA) (10  $\mu$ L, 10  $\mu$ M), dA ssDNA (10  $\mu$ L, 10  $\mu$ M), dT ssDNA (10  $\mu$ L, 10  $\mu$ M), poly(acrylic acid) (10  $\mu$ L, 10  $\mu$ M). The solution was then made to 100  $\mu$ L. From the 100  $\mu$ L solution four 20  $\mu$ L aliquots and measured on the Qiagen® Rotor-Gene Q real time PCR instrument using the default detection settings for the relevant dye.

## 2.6 References

- (1) Bossoutrot, J.-M. Method for the Recrystallisation and/or Purification of Azo-Type Compounds. WO2006072699A1, 2005.
- (2) Nagesh, N.; Chatterji, D. Ammonium Ion at Low Concentration Stabilizes the G-Quadruplex Formation by Telomeric Sequence. *J. Biochem. Biophys. Methods* **1995**, *30* (1), 1–8.
- (3) Kaiser, C. E.; Gokhale, V.; Yang, D.; Hurley, L. H. Gaining Insights into the Small Molecule Targeting of the G-Quadruplex in the c-MYC Promoter Using NMR and an Allele-Specific Transcriptional Assay. In *Topics in current chemistry*; 2012; Vol. 330, pp 1–21.
- (4) Desjardins, P.; Conklin, D. NanoDrop Microvolume Quantitation of Nucleic Acids. *J. Vis. Exp.* **2010**, No. 45.

# Chapter 3: Synthesis of Poly(2-(5'-dimethoxytrityl-N-benzoyl-2'-deoxycytosine-monophosphate)oxyethyl methacrylate): a Cytosine Rich Methacrylate Polymer

## 3.1 Synopsis

*This chapter describes the design, synthesis and characterisation of 5'-dimethoxytrityl-N-benzoyl-2'-deoxycytosine,3'-[(2-cyanoethyl)-(oxyethyl methacrylate)]-phosphate monomer, henceforth referred to as the **DMT-dC-CE-EMA phosphate monomer**. Synthesis of the **DMT-dC-CE-EMA phosphate monomer** was achieved through the coupling of hydroxyethyl methacrylate (HEMA) with a protected 5' cytosine (C) monophosphate. Following the synthesis of the **DMT-dC-CE-EMA phosphate monomer** it was polymerised using reversible addition-fragmentation chain transfer (RAFT) polymerisation and subsequently found to form a cross-linked gel.*

### 3.1 Introduction

This chapter outlines a method for the synthesis of 5'-dimethoxytrityl-*N*-isobutyryl-2'-deoxycytosine, 3'-[(2-cyanoethyl)-(2-oxyethyl methacrylate)]-phosphate (**C3** monomer) using a phosphoramidite coupling approach. In this method hydroxyethyl methacrylate (HEMA) was coupled to a protected cytosine phosphoramidite 5'-dimethoxytrityl-*N*-benzoyl-2'-deoxycytosine,3'-[(2-cyanoethyl)-(*N,N*-diisopropyl)]-phosphoramidite (**C1**). The coupling was achieved through the substitution of the diisopropylamine (DIPA) moiety with an oxyethyl methacrylate (EMA) moiety chosen for this experiment as it contained the alkene group required for radical polymerisation. The reasoning for the choice of the phosphoramidite coupling as the polymerisation method will be discussed in Section 3.2.1., followed by the discussion of choice of specific variables as they pertain to the synthesis of a nucleotide-vinyl bioconjugate. An overview of the phosphoramidite coupling method used in this chapter is shown in Figure 3.1. This synthesis route results in a **C3** monomer.

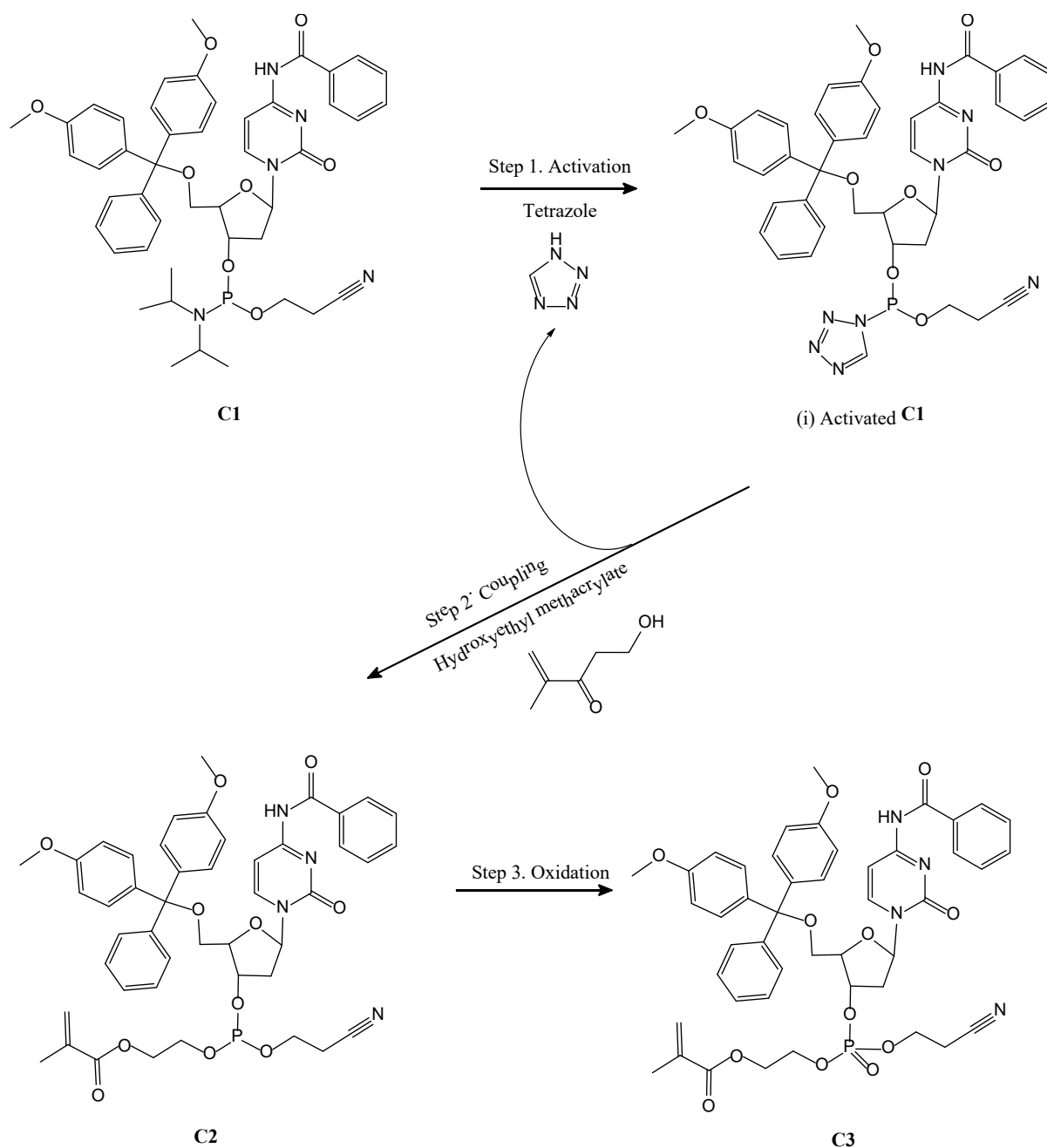


Figure 3.1 Overview for the conversion of C1 starting material through the activation with tetrazole to form (i) the activated C1 intermediate. This in turn was coupled to HEMA to form C2 and subsequently oxidised to form C3. The tetrazole required for the activation (step 1) was regenerated during the coupling step (step 2) allowing it to act as a catalyst.

Following the synthesis of the **C3** monomer, it was subsequently polymerised using the RAFT polymerisation method for radical polymerisation, resulting in poly(2-(5'-dimethoxytrityl-*N*-benzoyl-2'-deoxycytosine-monophosphate) oxyethyl methacrylate) (**C4**).

### 3.1.1 Choice of Phosphoramidite Coupling Method

Coupling of additional moieties to a nucleotide can be achieved using a number of methods, depending on the site of the attachment. The three sites where the vinyl moiety could have been attached in this case were the phosphate, 3' hydroxyl, and 5' hydroxyl moieties (Figure 3.2(green arrows)), depending on the isomer of phosphoramidite used.

For this thesis the coupling of HEMA was conducted through the phosphate site for a number of reasons: Firstly, the reactive sites on the phosphate are equivalent due to the resonance structure of the PO<sub>4</sub><sup>-</sup>; this means that the attachment does not need to consider the chirality of the binding site. Secondly, the phosphate acts as a linker in nucleic acids connecting the nucleosides together, so it was considered appropriate to mimic this in a vinyl-coupled version.

There are three coupling methods for the attachment to the phosphate: H-phosphonate, phosphoester, or phosphoramidite. These methods are discussed specifically in Chapter 1, Section 1.4.2. The phosphoramidite coupling approach was chosen due to it having the most easily accessible starting substrate, since phosphoramidites are commonly used in commercial DNA synthesisers.<sup>1</sup>

Specifically, deoxyribose nucleotide phosphoramidites, Figure 3.2(i), were chosen instead of ribose nucleotides as the presence of a hydroxyl moiety at the 2' carbon would require further protection to prevent non-specific coupling. This would have introduced an additional variable that was not necessary for this proof of concept stage.



With these criteria in mind, the choice was narrowed to two isomers of the nucleotide phosphoramidite dependent on whether the phosphorous was attached to the 3' or 5' hydroxyl moiety on the nucleoside subunit, see Figure 3.2. The largest effect this difference could have had on the coupling was the possibility of the phosphorous being cleaved from the nucleoside resulting in a vinyl phosphate monomer and free nucleoside. As a result, the 3' isomer was chosen as the secondary hydroxyl is less susceptible to hydrolysis, reducing the possibility of the cleavage occurring.

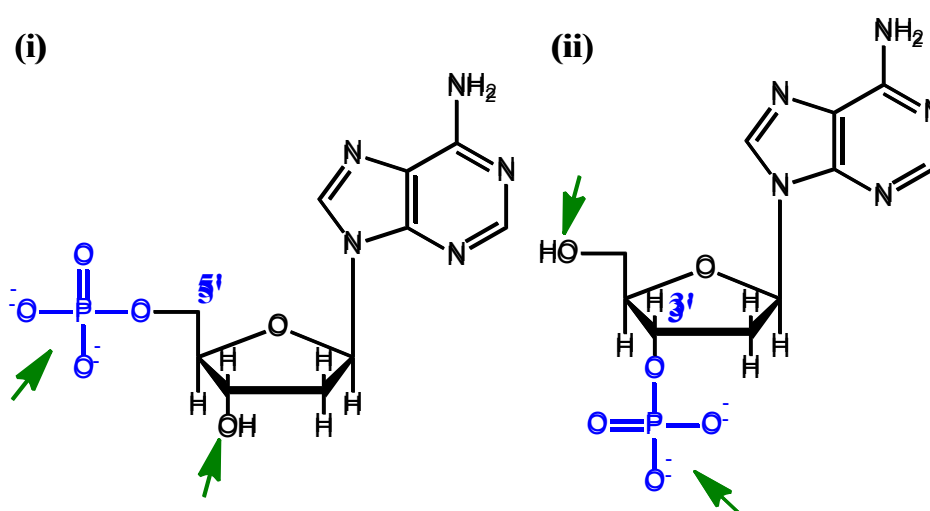


Figure 3.2 (i) 2'-deoxyadenosine 5' monophosphate and (ii) 2'-deoxyadenosine 3' monophosphate. Green arrows indicate sites that could be used for conjugation of the vinyl moiety using the phosphoramidite coupling method.

The phosphoramidite coupling method requires a polar aprotic solvent. For this thesis acetonitrile was used. Work conducted by Gaytán *et al.*<sup>2</sup> has shown that acetone could be used as an alternative. It would be preferable as acetone is easier to remove due to its higher vapour pressure. However, the conditions of the coupling require the reaction to be immaculately dry, and this requirement was easier to meet with acetonitrile through the use of molecular sieves. Burfield *et al.*<sup>3</sup> showed that the same method was not suitable when using acetone due to the

catalytic effect of the molecular sieves that caused the production of water *in-situ* through an aldol reaction. As a result, for this preliminary work acetonitrile was used to avoid this effect.

### 3.1.2 Selection of Compatible Vinyl Moiety

Selection of the vinyl moiety required a few specific criteria to be met: a vinyl moiety, a hydroxyl group, and some form of linker between the two.

Firstly, for the living radical technique of RAFT polymerisation, the monomer would require the vinyl moiety during the polymerisation process because it propagates the radical, as discussed in Chapter 1, Section 1.6.1.1. Further, the choice was made to use a methacrylate as the vinyl source to increase the stability of the propagating radical as methacrylates are more activated monomers due to the presence of the methyl and ester moieties attached to the vinyl. These properties allow the propagating radical to be stabilised, increasing its lifetime which may also assist with polymerisation as the extended lifetime of the radical can compensate for the steric hindrance of the conjugated nucleotide.

When using the phosphoramidite coupling method, a hydroxyl moiety is required for the conjugation to the nucleotide. The two options for achieving this were a hydroxyl or a carboxylic acid. For later work, following the polymerisation of the vinyl-nucleotide bioconjugate monomer, it would have been more preferable to use the carboxylic acid as it was more soluble than the hydroxyl in water. However, the carboxylic acid would have lowered the pH significantly more than the hydroxyl, and the lower pH would cause the removal of the protecting groups from the nucleobase and the 5' hydroxyl as they were susceptible to acid catalysed hydrolysis.<sup>4</sup> For this reason a hydroxyl moiety was chosen.

The vinyl moiety was the most important component of this project as an incompatible group connecting the vinyl to the nucleotide could prevent polymerisation altogether. The first

requirement was the presence of a hydroxyl group for the phosphoramidite coupling to the nucleotide. Additionally, it was important to consider the solvent compatibility with the phosphoramidite for the coupling reactions, and the water for DNA interaction studies with the final bioconjugate. These factors ruled out many of the common monomers for RAFT polymerisation such as styrene or vinyl acetate. The two most appropriate classes of monomer were therefore methacrylates and methacrylamides as these have multiple derivatives that are soluble in both acetonitrile and water.

There are two main issues with these compounds to consider; cleavage of the linker, and off site reactions. Both the ester and the amide would be susceptible to acid catalysed hydrolysis, though there is no explicit use of acids strong enough to achieve this in the workup through the phosphoramidite method. There is a risk of dehydration, converting the amide to a nitrile, caused by the use of trifluoroacetic anhydride for the removal of the DMT protecting group as the method is presented in literature.<sup>5</sup> This reaction occurring would lead to removal of nucleotides from the final polymer and even partial removal would result in uneven spacing, in turn effecting the binding behavior.

The methacrylamide has the potential to undergo an off target coupling reaction by creating a second nucleophilic site on the monomer for the coupling of the phosphoramidite which was undesirable for this experiment. Though it is not nucleophilic enough to proceed under the initial conditions outlined as this procedure was unknown, having it present may have limited options when adjusting the reaction conditions. The dehydration and off target reactions lead to the selection of the ester, and thereby methacrylate, as the monomer of choice.

To give the vinyl moiety some spacing from the alkyl backbone during the polymerisation process, the vinyl source chosen for the work outlined in this chapter was hydroxyethyl methacrylate (HEMA) shown in Figure 3.3(iii). When HEMA was coupled to the C1 (Figure

3.3(i-ii)), it resulted in the monomer 5'-dimethoxytrityl-*N*-benzoyl-2'-deoxycytosine,3'-[(2-cyanoethyl)-(ethyl methacrylate)]-phosphite (**C2**).

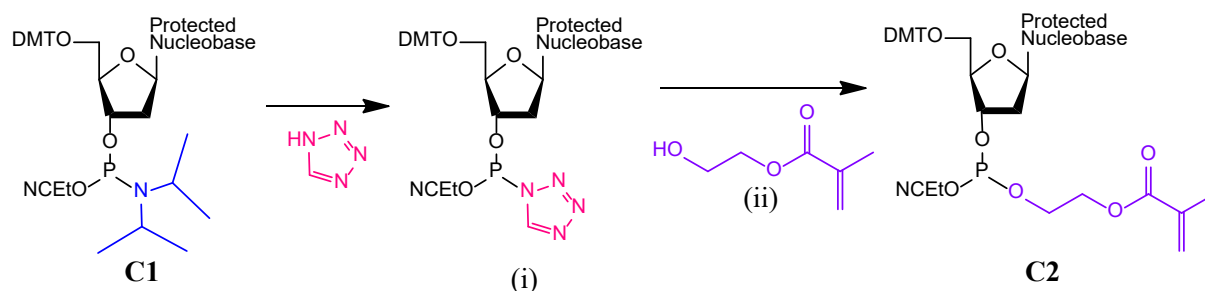


Figure 3.3 Coupling of the protected **C1**, (i) the activated phosphoramidite intermediate to (ii) HEMA resulting in the **C2** monomer.

The option to add a PEG linker between the alkyl backbone and the nucleotide would result in more degrees of freedom for the nucleotide compared to the shorter ethyl provided by HEMA. For the future application of the polymers synthesised in this project enzymatic compatibility or another method for the creation of ribose phosphate backbone from the alkyl polymer could more easily skip a unit in the sequence if the distance given by the PEG linker was greater than the base separation along the chain. Based on this information the decision was made to keep the linker between the nucleotide and the alkyl backbone to that given by the HEMA.

A risk with an alkyl polymer synthesised by radical polymerisation is its low solubility in aqueous systems. This can be overcome by the addition of a polyethylene glycol side group, or using a block-copolymer instead. However, both of these are incompatible with the goal of this project.

The use of a block-copolymer could cause the formation of vesicles or other secondary structures driven by the difference in solubility of each block. This would introduce a competing factor with the formation of structures driven by the selective binding of the

nucleobases, and is used as a method for controlling  $M_w$  and  $\mathcal{D}$  in other polymerisation techniques.

### 3.1.3 Activation of the Nucleotide Phosphoramidite

The first step of the phosphoramidite coupling method is activation, which converts the phosphoramidite into a reactive intermediate. The most common activator for single nucleotide phosphoramidite coupling is tetrazole, as discussed in Chapter 1, Section 1.4.3. In literature tetrazole has been shown to be most effective with primary hydroxyls such as that found in HEMA.<sup>6</sup>

Tetrazole was used in this study and underwent substitution with the diisopropyl amine, Figure 3.4 (blue), on the phosphoramidite to form the semi-stable intermediate as shown in Figure 3.4 (ii). The initial activation of the phosphoramidite was a rapid reaction that protonates the phosphoramidite.<sup>7</sup> The tetrazole was then, in turn, substituted with the hydroxyl moiety, resulting in the **C3** monomer.

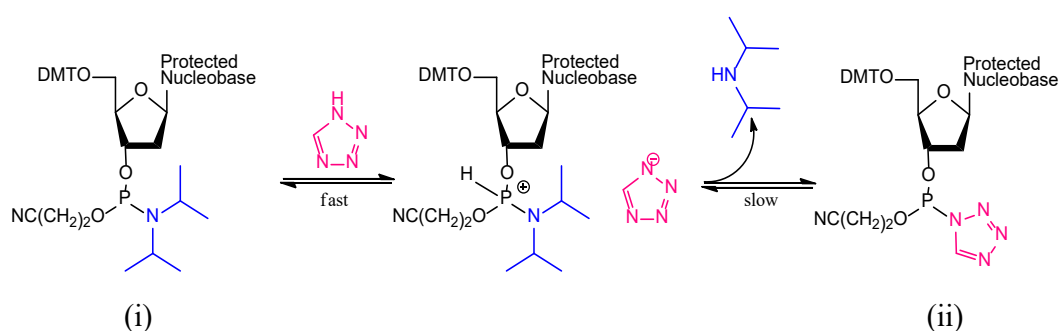


Figure 3.4 Mechanism for the activation of (i) a phosphoramidite, substituting the diisopropylamine (blue) with tetrazole (pink) resulting in (iii) an activated phosphoramidite.<sup>7</sup>

The tetrazole is subsequently regenerated when it is substituted with the monomer, completing the coupling.

### 3.1.3.1 Quenching the Activator

Following the coupling of the bioconjugate, the reaction needed to be quenched to prevent further addition of water to the **C3** by the activator during the following phase extraction as otherwise it would lead to the coupled vinyl moiety being replaced with water.<sup>8</sup> To quench the coupling reaction a solution containing triethylamine (TEA), ethyl acetate (EtOAc), and dichloromethane (DCM) at a ratio of 45:45:10 v/v EtOAc:DCM:TEA is added to the coupling solution. This combination of solvents has been shown by Dahl *et al.*<sup>8</sup> to quench the phosphoramidite coupling reaction while maintaining the successfully coupled phosphite product in solution.

### 3.1.3.2 Oxidation

Oxidation of phosphite to phosphate was required to convert the protected phosphoramidite into the nucleotide monophosphate. This step was necessary as the  $\text{PO}_4^-$  anion formed in the process was more soluble in water, which was required to determine if the vinyl-nucleotide bioconjugate was compatible with DNA systems.

When oxidising phosphite to phosphate, the ideal oxidant was something that would provide a rapid and selective reaction. In literature,  $\text{I}_2$  has been used with a mixture of pyridine, THF and water using the method outlined in Figure 3.5.<sup>9</sup> This was not an option for the synthesis used in this project because the  $\text{I}_2$  would add across the alkene bond which would remove the active group for the living radical polymerisation. Therefore, an alternative method had to be found.

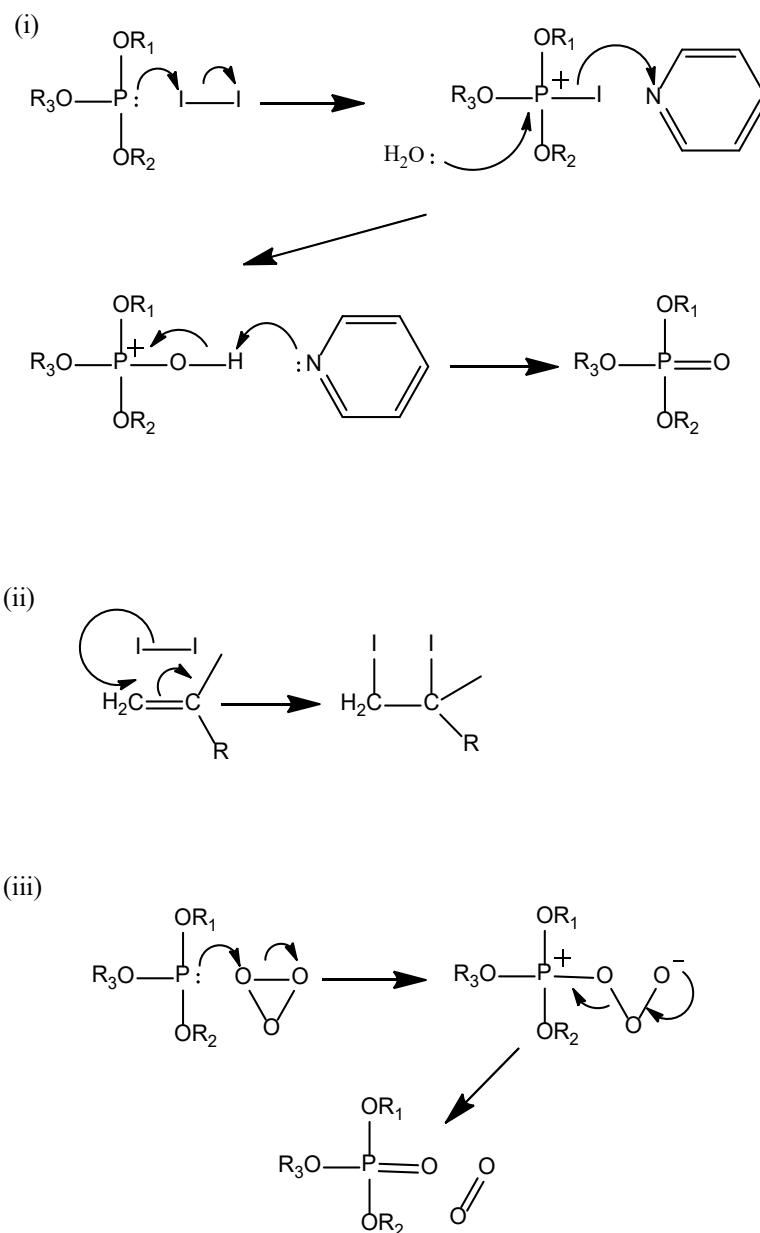


Figure 3.5 (i) Oxidation of phosphite to phosphate using  $I_2$ /pyridine/ $H_2O_2$  (ii) the halide addition to an alkene, and (iii) oxidation of phosphite by ozone present in air.

Methods have been reported using alternative oxidants, such as ethyl(methyl)dioxirane.<sup>10</sup> However, many of these such as *N*-bromosuccinimide-dimethyl sulfoxide and *t*-butyl hydroperoxide were also capable of acting as radical initiators<sup>11,12</sup> which makes them unsuitable as they may cause polymerisation of the vinyl moiety. Further literature studies

found no other suitable oxidative compounds reported for the oxidation of phosphite to phosphate for phosphoramidite coupling method.

Based on work by Dennison *et al.*<sup>13,14</sup> with phosphorous compounds, compressed air was trialled as it had several obviously favourable properties: notably, it uses oxygen gas which acts as a mild oxidant, meaning that during the short exposure required the oxygen degradation of the nucleic acid components of the **C3** would not take place. There was limited evidence directly showing the use of compressed air as a method for oxidation of phosphorous, e.g., Bolduc and Goe<sup>15</sup> demonstrated the oxidation of phosphite with O<sub>2</sub> under UV light using a dye sensitiser. More recently, Martin *et al.*<sup>16</sup> have shown that the oxidation of phosphite can occur rapidly in the presence of atmospheric gases, specifically ozone, oxygen, nitroxides and/or hydroxyl radicals.

More common than the deliberate oxidation of phosphite to phosphate using atmospheric gasses, was the use of alkyl phosphates as antioxidants. These are compounds that undergo sacrificial oxidation to protect another compound. Notably to this work is the previous use of alkyl phosphites to protect synthetic polymers.<sup>17,18</sup>

Further, due to the phase extraction method employed to isolate the **C3** the solution needed to be dried. The use of compressed air also increased the rate of evaporation of the solvent effectively increasing the rate of isolation and reducing the amount of remaining solvent to be removed during freeze drying.

### **3.2 Synthesis of HEMA-Nucleotide Bioconjugate**

The following sections outline the analytical methods used to confirm the synthesis of the DMT-dC-CE-EMA phosphoramidite monomer, as described in Chapter 2, Section 2.4.1.1. The methods employed for this analysis were NMR spectroscopy using <sup>1</sup>H and <sup>31</sup>P methods.



To carry out the conjugation, 5'-dimethoxytrityl-*N*-benzoyl-2'-deoxycytosine,3'-[(2-cyanoethyl)-(*N,N*-diisopropyl)]-phosphoramidite (**C1**) was treated with tetrazole and HEMA in dry acetonitrile to perform the coupling procedure. The full process is discussed in Chapter 2 Section 2.4.1.1. Following this procedure the resulting mixture was solvent extracted to isolate the 5'-dimethoxytrityl-*N*-benzoyl-2'-deoxycytosine,3'-[(2-cyanoethyl)-(oxyethyl methacrylate)]-phosphite monomer (denoted hereafter as **C3** monomer). This was then dried under a flow of compressed air to oxidise the 5'-dimethoxytrityl-*N*-benzoyl-2'-deoxycytosine,3'-[(2-cyanoethyl)-(oxyethyl methacrylate)]-phosphate monomer (denoted hereafter as **C3** monomer).

#### 3.2.1.1 Proton Nuclear Magnetic Resonance (<sup>1</sup>H NMR) Spectroscopy

Support for the successful attachment of HEMA to the **C1** was shown using <sup>1</sup>H NMR spectroscopy. Samples were prepared at 5 mg/mL in deuterated acetonitrile following oxidation and drying. The results are shown in Figure 3.6(i and ii) illustrating the **C1** and the **C3** monomer, respectively. The specific experimental parameters are presented in Chapter 2, Section 2.5.2.1. Full peak allocations are presented in Appendix 1.

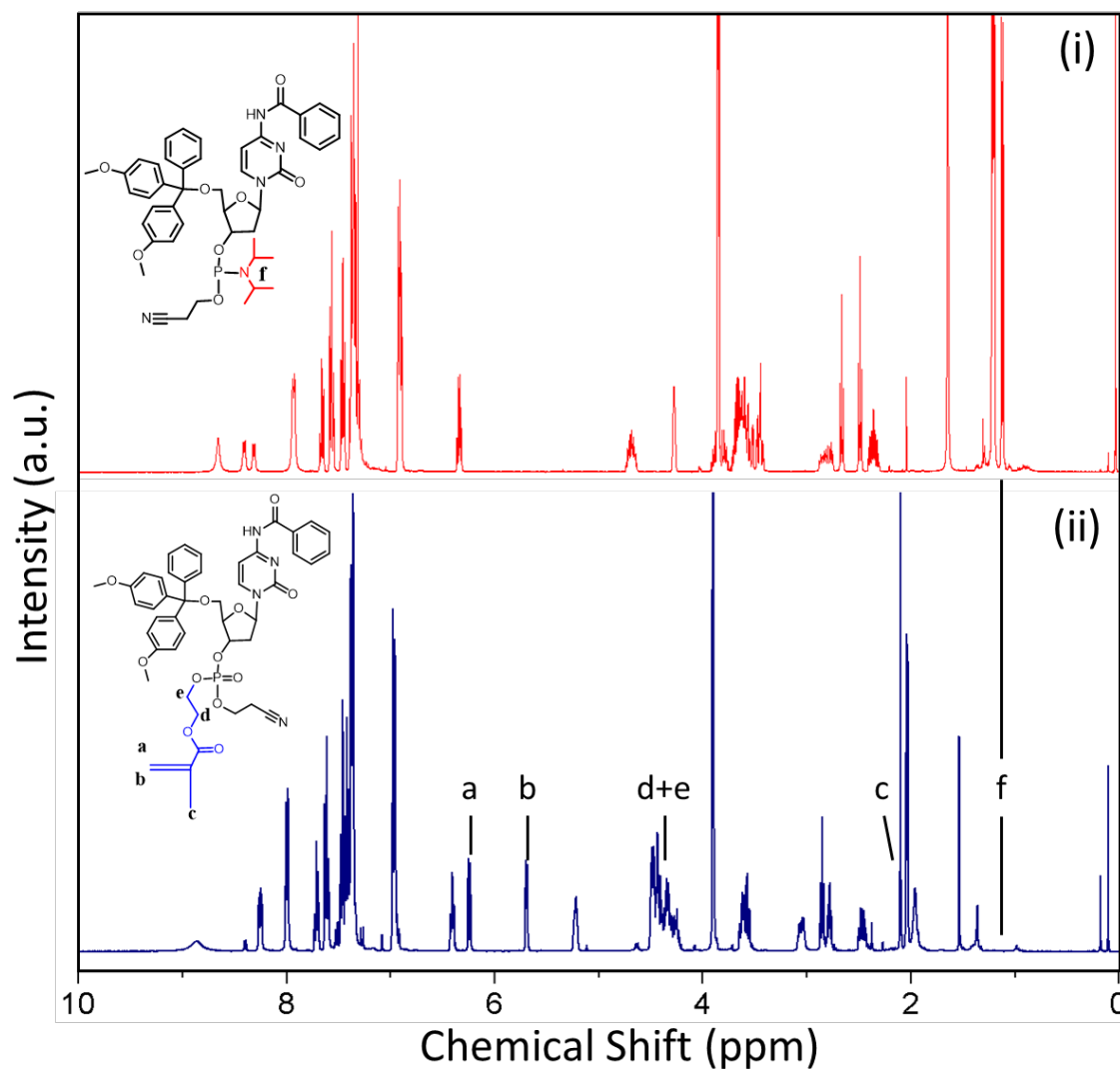


Figure 3.6  $^1\text{H}$  NMR spectra of (i) **C1** and (ii) **C3** monomer, showing the appearance of peaks (a-e) associated with HEMA and the disappearance of peak (f) associated with the diisopropyl amine (inset (i, red)) Spectra acquired in deuterated acetonitrile at 600 MHz. Full peak attributions can be found in Appendix 1.

The attachment of the HEMA to the **C1** was carried out through the substitution of the DIPA group. The removal of this peak in the **C3** monomer would indicate that the tetrazole activator had removed the DIPA.

The peak attributed to DIPA moiety was present in the **C1** spectrum ( $((\text{CH}_3)_2\text{CH-N})$  doublet,  $\delta = 1.2$  ppm,  $^3J_{\text{HH}} = 10.35$  Hz); this magnitude of splitting was expected for  $^3J_{\text{HH}}$  coupling.<sup>19</sup> This peak was notably absent in the spectrum of the **C3** monomer which is more clearly shown in Figure 3.7.

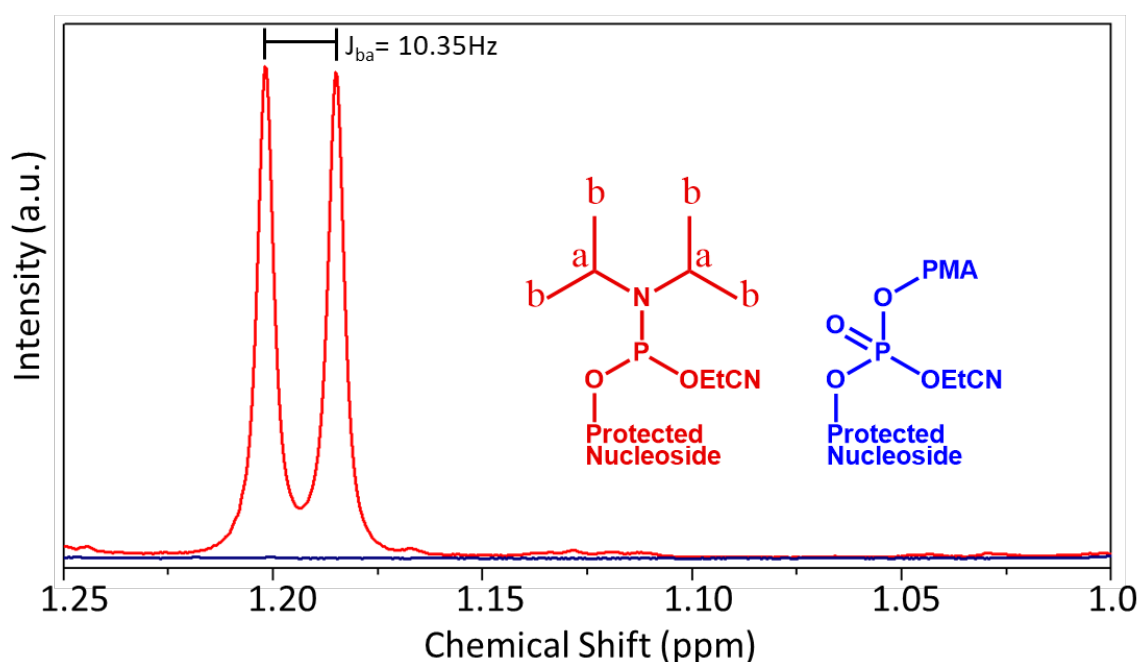


Figure 3.7  $^1\text{H}$  NMR spectra of the **C1** (red), and **C3** monomer (blue), showing the region from 1 ppm to 1.25 ppm. Spectra acquired in deuterated acetonitrile at 600 MHz.

The presence of HEMA moiety coupled to the **C3** monomer was seen as the presence of a pair of peaks at 6.25 ppm and 5.70 ppm (Figure 3.6(ii, a and b)). This area is expanded in Figure 3.8, showing the peaks associated with the *cis* and *trans* protons of the alkene group.<sup>20</sup>

The peak associated with the *trans* proton of the **C3** (Figure 3.8(inset, a)) shows a doublet caused by coupling to the adjacent *trans* proton,  $^2J_{\text{ab}} = 10.9$  Hz. This was within the expected 5-15 Hz range for  $^2J_{\text{HH}}$  germinal coupling as reported by Cahill *et al.*<sup>21</sup>

The 5.70 ppm peak associated with the *cis* proton to the methyl group (Figure 3.8(b)) shows two couplings. This major coupling seen from the *cis* proton was to the adjacent *trans* proton

( $^2J_{\text{HH}} = 8.9 \text{ Hz}$ ). Due to the fixed rotation of the alkene group an additional minor coupling was seen between the *cis* proton and the spatially adjacent methyl protons ( $^4J_{\text{HH}} = 1.77 \text{ Hz}$ ). The signal attributed to this methyl group appeared as a sharp peak at 2.10 ppm (Figure 3.6ii (c)).

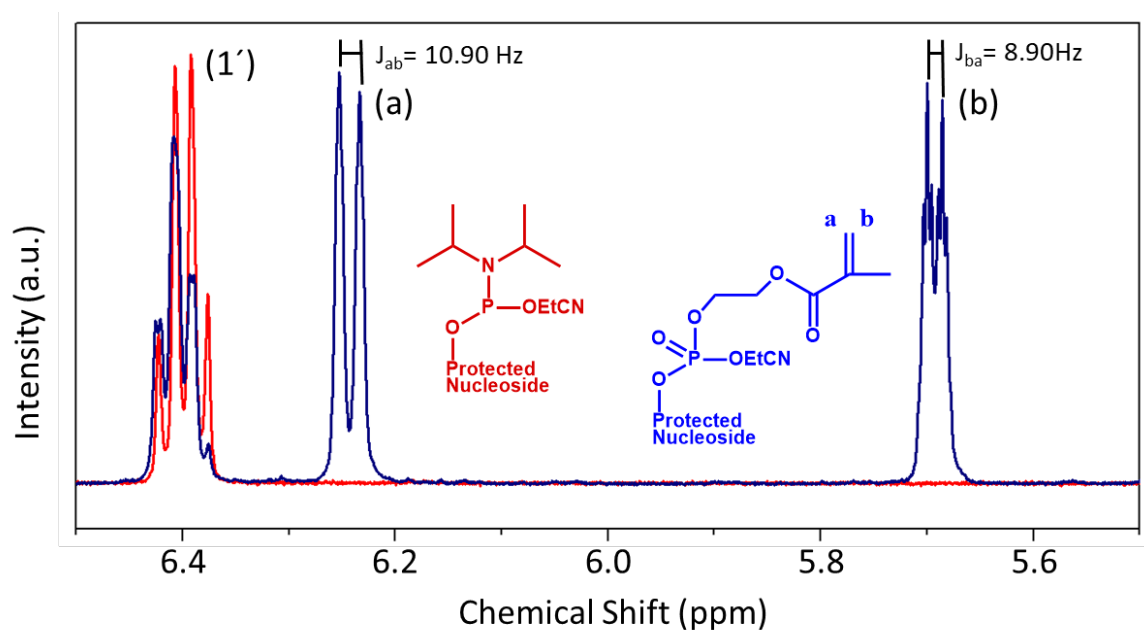


Figure 3.8  $^1\text{H}$  NMR spectra of the 5.5 ppm to 6.5 ppm region of **C1** (red) and **C3** monomer (blue), showing the appearance of peaks (a and b) associated with the *cis* and *trans* protons of the alkene (inset). In addition the peak associated with the 1' proton on the ribose is also visible in this region. Spectra acquired in deuterated acetonitrile at 600 MHz.

The coupling is further supported by the integration ratio between the peak at HEMA moiety *trans* proton (6.2 ppm) and the 1' proton (6.4 ppm) integrating to 1 and 0.9 respectively. This indicates that at the very least there is no excess of HEMA in the solution that could undergo a competing polymerisation during the following stages.

### 3.2.1.2 Phosphorous Nuclear Magnetic Resonance ( $^{31}\text{P}$ NMR) Spectroscopy

To confirm the oxidation of the **C1** from the P(III) oxidation state to the **C3** monomer P(V) oxidation state  $^{31}\text{P}$  NMR spectroscopy was used. The specific parameters are presented in Chapter 2, Section 2.5.2.1

For this work the important difference was caused by the oxidation following the phosphoramidite coupling. Prior to coupling the **C1** was significantly deshielded the phosphorous in the P(III) oxidation state. Following successful oxidation to the P(V) oxidation state of the **C3** monomer there was a significant upfield shift that can be seen in Figure 3.9 as the difference in peak location between the red to blue spectra.

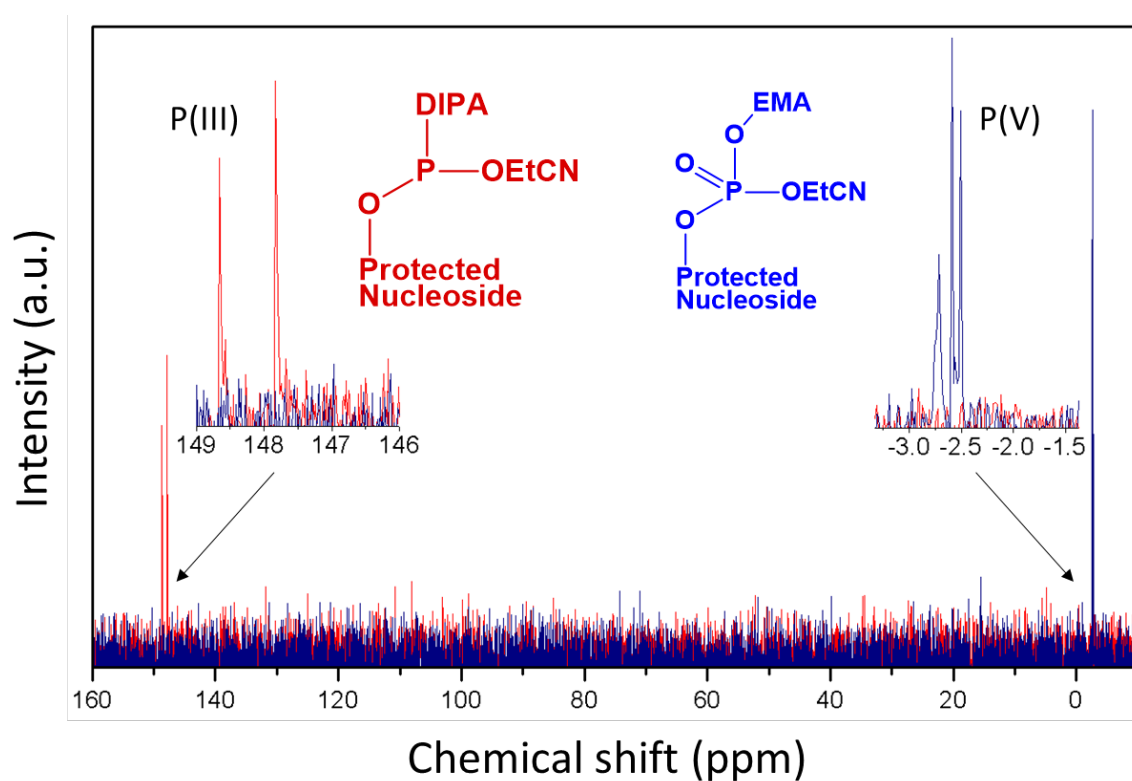


Figure 3.9  $^{31}\text{P}$  NMR spectra of the -10 ppm to 160 ppm region of **C1** (red, P(III)) and **C3** monomer (blue, P(V)) Spectra acquired pulse decoupled in deuterated acetonitrile at 600 MHz.

The result of the NMR for the **C1** (Figure 3.9, red) showed a pair of peaks at 148.7 ppm and 147.8 ppm. This would lead to a coupling constant of  $J = 540$  Hz. This value would be beyond possible  $^1J$  coupling values and suggests the computer pulse decoupling has not worked successfully. Due to the infrequent use of  $^{31}\text{P}$  spectroscopy is likely the CPD had not been calibrated, resulting in the peak splitting seen. The potential for the sample to be contaminated with another phosphite is unlikely as the supplier reported purity  $>98\%$  by HPLC and the sample was used directly as supplied. The similar shift and symmetry suggests that this may be due to deuterium induced peak splitting<sup>22</sup> or another effect as similar peak splitting has been previously reported in  $^{31}\text{P}$  spectra for cysteine deoxynucleotide phosphites.<sup>23,24</sup>

The spectra for **C3** monomer (Figure 3.9, blue) shows a triplet peak (-2.71 ppm, t,  $J = 58.43$  Hz). This was attributed to the P(V) oxidation state of the **C3** monomer following oxidation. The splitting of the peak was attributed to the chiral isomers at the phosphate position. The asymmetry seen in this peak was therefore assigned to  $J_{\text{PH}}$  coupling between the phosphorous and the protons on the deoxyribose ring in one of these isomers.

### 3.3 Polymerisation of the C3 Monomer

Following the synthesis of the **C3** monomer, it was polymerised using the RAFT method for radical polymerisation. This method introduces a mediator in the form of a RAFT agent that mediates the polymerisation to reduce the  $\bar{D}$  of the resulting polymers. The  $\bar{D}$  is discussed in more detail in Chapter 1, Section 1.5.2.

Radical polymerisation is a method that generates polymers through the conversion of the alkene moiety of the monomer into a long chain alkane through addition of a radical; this process is discussed in Chapter 1, Section 1.5.3. As previously mentioned, uncontrolled radical polymerisation results in polymers of varying lengths, which in turn causes the properties of

the polymer mixture to be less well defined.<sup>21</sup> Despite this, radical polymerisation was however chosen because it requires an alkene moiety, and this requirement limits the polymerisation sites within the complicated **C3** monomer to the conjugated HEMA.<sup>25</sup> As a result, the polymerisation could be directed to the specific alkene site.

Using an alternative method for polymerisation could introduce conflicting groups. Using RAFT polymerisation avoids this undesirable scenario due to the fact that the only moiety compatible with radical polymerisation present in **C3** monomer is from the conjugated HEMA. Comparatively, if condensation polymerisation was chosen, then both the phosphate, alcohol, and amine groups would have all been competitive sites for the polymerisation<sup>21</sup> which likely would have resulted in polymers that were branched and lacked structural uniformity.

To improve the uniformity of the polymers formed a controlled version of radical polymerisation was used. Introduction of this control required the addition of a mediator which regulates the growth of the chains, as discussed in Chapter 1, Section 1.5.4. Three specific techniques were considered: nitroxide-mediated polymerisation (NMP), atom transfer radical polymerisation (ATRP) and RAFT.

NMP was excluded because the nitroxide radical that was needed to propagate the active chains, requires high temperatures (above 100 °C) which would cause thermal degradation of the nucleotides.<sup>26,27</sup> ATRP, on the other hand, uses metallic compounds that could complex to the nucleobases. This complexation occurs due to the aromatic nature of the nucleobase, and the protecting groups, blocking the metallic ions in solution, which prevents the necessary

change in oxidation state of the metallic ion used to mediate the polymerisation which would cause retardation.<sup>28</sup>

The thiol chemistry that provides the mediation of RAFT polymerisation is less sensitive to complexation, and due to the solubility and reactivity being primarily determined by the secondary functional groups it could be applied over a wide range of conditions.<sup>29</sup> This made RAFT the most viable option for the polymerisation of nucleotide-vinyl polymers.

The RAFT agent was able to act as a mediator during the polymerisation but still required a radical source, the initiator. For this purpose, AIBN was chosen, the radical generation mechanism is shown in Figure 3.10. The main reason for this choice was that AIBN activates above room temperature, with a 10 h half-life at 65 °C, while still allowing the temperature to remain low enough, below 90 °C, to not cause rapid thermal degradation of the nucleotide.<sup>30</sup>

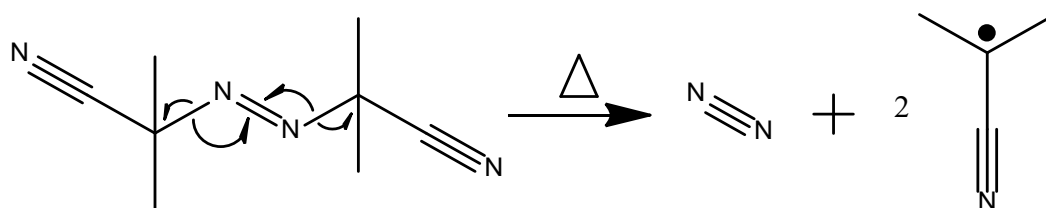


Figure 3.10 Thermal decomposition of AIBN into N<sub>2</sub> and the isobutyronitrile radical.<sup>31</sup>

#### 3.3.1.1 Selection of RAFT Agent

The RAFT agent mediates the polymerisation to control the *D* and molecular weight of the polymers formed. It was used to ensure that the polymers formed from the **C3** monomer would be of similar molecular weight and therefore share similar properties. If the *D* varied greatly between chains it could lead to inconsistent properties, such as broad melting peaks or solubilities. This would make the analysis of the polymer and its interactions with DNA difficult to perform, as different chains would act differently.



Not all RAFT agents were able to mediate all monomers, each showing different compatibilities with monomers, as discussed in Chapter 1, Section 1.6.1.2. For the polymerisation of the **C3** monomer, the 4-cyano-4-(phenylcarbonothioylthio) pentanoic acid *N*-succinimidyl ester (NHS-RAFT) agent was chosen based on compatibility with methacrylate monomers as well as shared solubility with the monomer.

The HEMA coupled to the **C1** was a methacrylate, which had been shown to work well with dithiobenzoates so this was the first class of RAFT agents tested.

To conduct the polymerisation in solution, the RAFT agent was required to share similar solvent compatibility as the **C3** monomer. By this point it was known that **C3** monomer was soluble in several organic polar solvents including acetonitrile, DMSO, DCM, DMF and THF. To accomplish similar solubility, 2-cyanopentanoic acid was chosen as the R group on the RAFT agent. The pentanoic acid provided similar solubility to the nucleotide as it was organic with an ionisable carboxylic acid group allowing it to be solvated in aqueous solutions. To act as a RAFT agent, it also required for cyanoethyl to be an electron withdrawing group and assist in the stabilisation of the radical intermediate of the dithiobenzoate, as discussed in Chapter 1, Section 1.6.1.2.

To prevent the removal of the DMT protecting group from the **C3** monomer during the polymerisation the carboxylic acid group needed to be protected. This was achieved through the use of the NHS protected version of the RAFT agent. In the absence of the NHS group the DMT moiety would be cleaved by the pentanoic acid Z-group present. This would generate a primary alcohol at the 5' position which would in turn be susceptible to condensation reactions with the pentanoic acid Z-group of the RAFT agent, or the phosphate on the **C3** monomer.

### 3.3.2 Polymerisation of **C3** Monomer

Following the synthesis of the **C3** monomer, it was tested to determine whether it was compatible with RAFT mediated polymerisation, as intended. To do this the polymerisation was conducted using the method outlined in Chapter 2, Section 2.4.1.2, simplified in Figure 3.11, giving a [C3]:[RAFT-NHS]:[AIBN] of [100]:[1.5]:[1] (M/M/M). This ratio was chosen based on the provided literature and discussion with Boron Molecular.<sup>32</sup> As this sample was diluted in acetonitrile and only allowed to progress for 3.5 h the conversion factor was expected to be low, with full conversion resulting in a theoretical DP of 36. This resulted in the formation of poly(2-(5'-dimethoxytrityl-*N*-benzoyl-2'-deoxycytosine-monophosphate)oxyethyl methacrylate) (denoted hereafter as poly(DMT-dC-CE-EMA))

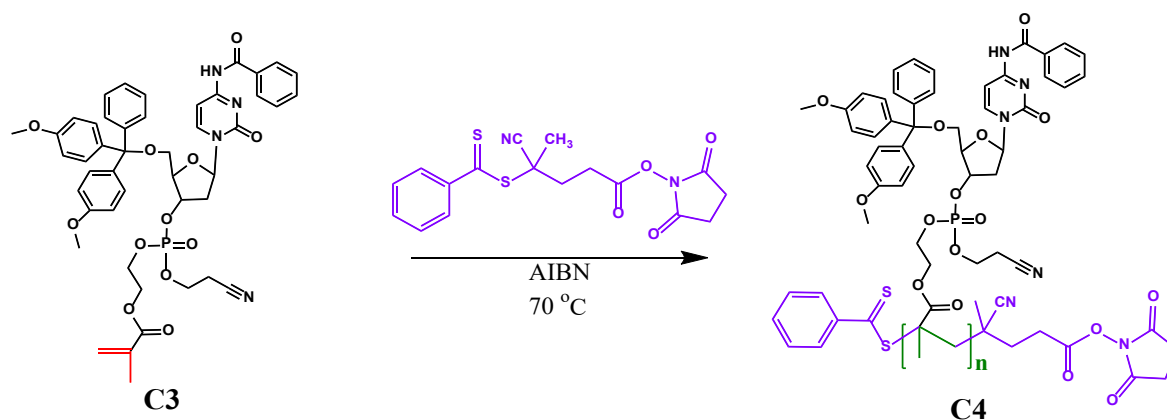


Figure 3.11 General scheme for the polymerisation of (i) **C3** monomer to (ii) **C4** using the RAFT agent 4-cyano-4-(phenylcarbonothioylthio)pentanoic acid *N*-succinimidyl ester and AIBN (ii) showing the active vinyl group (red) converted to the alkyl backbone (blue).

To quench the polymerisation the reaction mixture was precipitated by the addition of 5 °C water. This method was used to quench the reaction for a number of reasons: the presence of a non-solvent causes the polymer to precipitate from solution, preventing further propagation. Water was chosen as both poly(hydroxyethyl methacrylate) (poly(HEMA)) and nucleotide phosphoramidites were insoluble in it. Further, using cold water to decrease the temperature would slow any reaction that was occurring and inhibited the generation of further radicals.

This method had been tested with poly(HEMA) and found to form a white powder that could be isolated by filtration. When conducted with the product of the C3 polymerisation the resulting C4 resulted in a clear, colourless gel with no further precipitate (Figure 3.12(a)) indicating complete conversion or incorporation of monomer into the gel. Based on later discussion in section 3.3.4 it is possible that the monomer had become uncoupled phosphate and as a result of being water soluble.

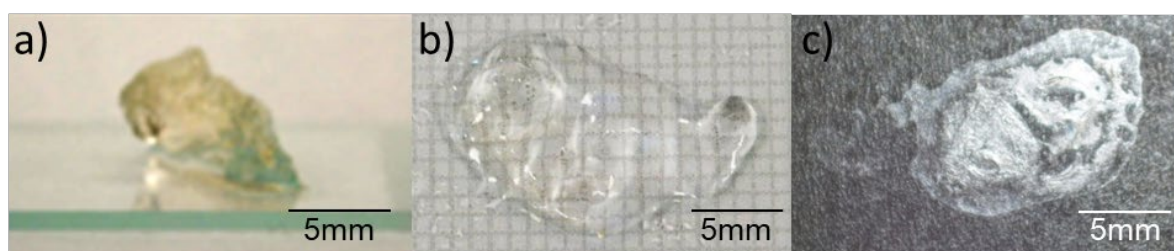


Figure 3.12 C4 gel swollen with (a) water or (b) DMSO and, (b) dried at 60 °C.

The formation of a gel from a polymer can be attributed to a number of factors.<sup>33-37</sup> Notable for this project were concentration, molecular weight, and cross-linking. Gels from high concentration polymer solutions result from mechanical entanglement: higher molecular weights of a polymer were associated with longer polymer chains, increasing the ability for mechanical entanglement at lower concentrations.<sup>38</sup> The solubility of the polymer in a given solvent can also affect the concentration at which this mechanical entanglement occurs.<sup>39</sup> For the C4 the theoretical maximum DP of 36 on its own is too low to expect mechanical entanglement, however the additional complexity and mass provided by the phosphoramidite significantly increases the possibility.

Due to the formation of a gel, the techniques ideally suited for determining the composition and properties of a polymer were no longer available, notably solution NMR spectroscopy, size exclusion chromatography and mass spectrometry. This was because these methods all require

the solvation of the polymer analyte to measure its properties. As a gel it was insoluble, displaying swelling behaviour in some solvents, and as such other techniques were found. For this thesis they were qualitative and quantitative solution studies to determine the binding between chains that caused the formation of the gel, and FTIR spectroscopy to determine if the nucleotide unit had been retained in the gel.

### 3.3.3 Investigating Solvent Effect on C4

Following polymerisation of the C3 monomer, the C4 gel that formed was tested in a number of other solvents. This was done to determine the cause of the gel formation, whether by mechanical, electrostatic, or covalent forces. In the case of a cytosine rich system there is a broader scope for the electrostatic interaction in the form of *i*-motifs, these are stacked cytosine-cytosine non-canonical pairs. These are able to form only in aqueous systems, so the same alternating solvent that would prevent electrostatic interactions would also reduce the formation of the *i*-motifs.

If the C4 gel was able to be dispersed in any solvent it would have ruled out covalent bonding as covalent gels will only swell. If the gel swells in a solvent and then disperses it would indicate a mechanical entanglement that is overcome by reducing the concentration. If the gel is formed by electrostatic forces, then a solvent that destabilises these forces should disperse the gel at low concentrations.

The C4 was first dried and then swollen in water to ensure no acetonitrile from the polymerisation remained. The C4 sample was placed into a gross excess of DMSO. This resulted in the C4 gel shrinking as it ejected the absorbed water, before again expanding in the

DMSO. The resulting DMSO swollen **C4** gel was less rigid and had poorly defined edges, Figure 3.12(b), compared to the water swollen **C4** gel.

The active rejection of the water from the polymer indicates a mechanical change a structural change within the gel that made it hydrophobic in the presence of DMSO as solvent displacement alone would not cause the gel to shrink and re swell. Due to the different solubilities of the backbone this was hypothesised to be the result of the hydration of the nucleotide moiety in water combined with the contraction of the hydrophobic regions shown in Figure 3.13(red). This in turn restricted the movement of the polymer, leading to a more rigid structure in water.

When the **C4** was then exposed to DMSO the whole structure became hydrated thereby allowing the hydrophobic regions to relax. This allowed more flexibility in the repeating units, leading to the decreased rigidity seen in Figure 3.12 (b).

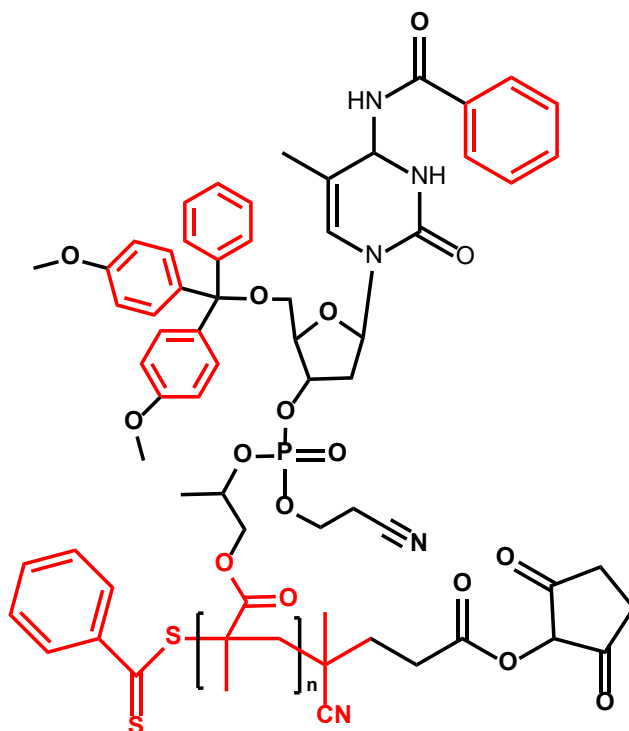


Figure 3.13 Structure of the **C4**, indicating hydrophobic moieties in red.

### 3.3.3.1 Quantitative Solvent-Gel Analysis

Following the qualitative analysis of the polymer-solvent interactions of the **C4** further experiments were conducted to determine the mechanism for the cross-linking between polymers. To do this the **C4** was dried (Figure 3.12 (c)) and divided into fragments, each being exposed to a gross excess of a solvent: water, DMSO, THF, CH<sub>3</sub>OH, or acetonitrile. If the **C4** gel was forming as the result of secondary binding, then it would be expected that at low concentrations the gel should be solvated. If it remained a gel, then it was more likely that the bonding between chains was covalent.

Following exposure to a solvent the **C4** sample was decanted, briefly blown with compressed air to remove surface solvent, and weighed. The mass ratio of solvent to gel was then calculated by the increase in mass of the gel following absorption of solvent compared to the initial weight. Details of the method are presented in Chapter 2, Section 2.5.1.2. The result of these

tests is shown in Table 3.1, with the solubility of DNA and poly(HEMA) included for reference.

**Table 3.1:** Solubility of the C4 gel in different solvents compared to the DNA and poly(HEMA) based on a single sample per measurement.

Solvent	DNA solubility <sup>40</sup>	Poly(HEMA) solubility	C4 gel		
			Dry mass, mg	Solvent mass (absorbed), mg	Swelling degree (%)
DMSO	Soluble at low $M_w$	Soluble	1.1	67.8	6200
H <sub>2</sub> O	Soluble at all $M_w$	Gel	2.5	257.7	10000
MeOH	Soluble at low $M_w$	Soluble	0.6	33.6	5600
THF	-	Insoluble	Insoluble		
Acetonitrile	Partially soluble	Insoluble	Insoluble		

From these results, it was apparent that none of the solvents were able to solvate the C4, even with the gross excess of solvent used. This indicated that polymer was unlikely to be forming due to electrostatic binding between chains. If the gel was forming from electrostatic interactions one of the solvents would have interfered with the electrostatic binding causing the C4 chains to solvate instead of only swelling. This experiment was primarily done to investigate if there was a way to solvate the gel for better analysis so it was not replicated for multiple samples.

One of the variables that was not considered at this stage was the pH, as all samples were analysed in neat solvent. This was not tested as the presence of an acid, or base, could have chemically altered the repeating unit, leading to a change in solubility without clarity on the cause (i.e. was it due to the disruption of electrostatic interactions or the removal of the functional groups). This was not investigated because the purpose of the project was not to

investigate the properties of this homopolymer gel, and as such it falls beyond the scope of the project.

If the C4 was mechanically entangled due to the molecular length then the low concentration of gel used would be expected to dissolve the gels. As all the C4 gels remained solid through the process, this indicates that mechanical entanglement was not the source of the gel formation. This left the covalent binding between the C4 chains as the most likely cause of the gel formation.

The magnitude of the degree of swelling found for the solvents DMSO, H<sub>2</sub>O and CH<sub>3</sub>OH was significantly higher than that found for other gels in literature.<sup>33,41</sup> For example the poly(ethylene glycol)/poly(L-lactic acid) alternating copolymer synthesised by Huh *et al*,<sup>41</sup> chosen for its similarly high complexity, was found to have a maximum swelling degree of 250%.

These high results were attributed to the small masses used and the balances available. As a result, the swelling magnitude could not be determined with a high degree of accuracy. However, the correlation between the swelling degree and the solubility of DNA indicates that the HEMA moiety determined if the gel was able to form, as the non-solvents for poly(HEMA) were also non-solvents for the C4. After that the nucleotide moiety affects the mass of solvent absorbed, with better nucleotide compatibility indicated by better solvation of DNA, leading to a higher swelling degree.

### 3.3.3.2 ATR-FTIR Spectroscopy

The gel-solvent analysis of the C4 had shown that the gel acted as if the nucleotides had been incorporated. Further analysis using ATR-FTIR spectroscopy was conducted to confirm that the cytosine nucleotide had been retained. ATR-FTIR spectroscopy was chosen as it did not



require the solvation of the **C4**. The samples were first dried to remove excess solvent, and the results of the spectroscopy are shown in Figure 3.14, with the fingerprint region of  $500\text{ cm}^{-1}$  to  $2000\text{ cm}^{-1}$  expanded in Figure 3.15. Notable peaks are listed in Table 3.2.

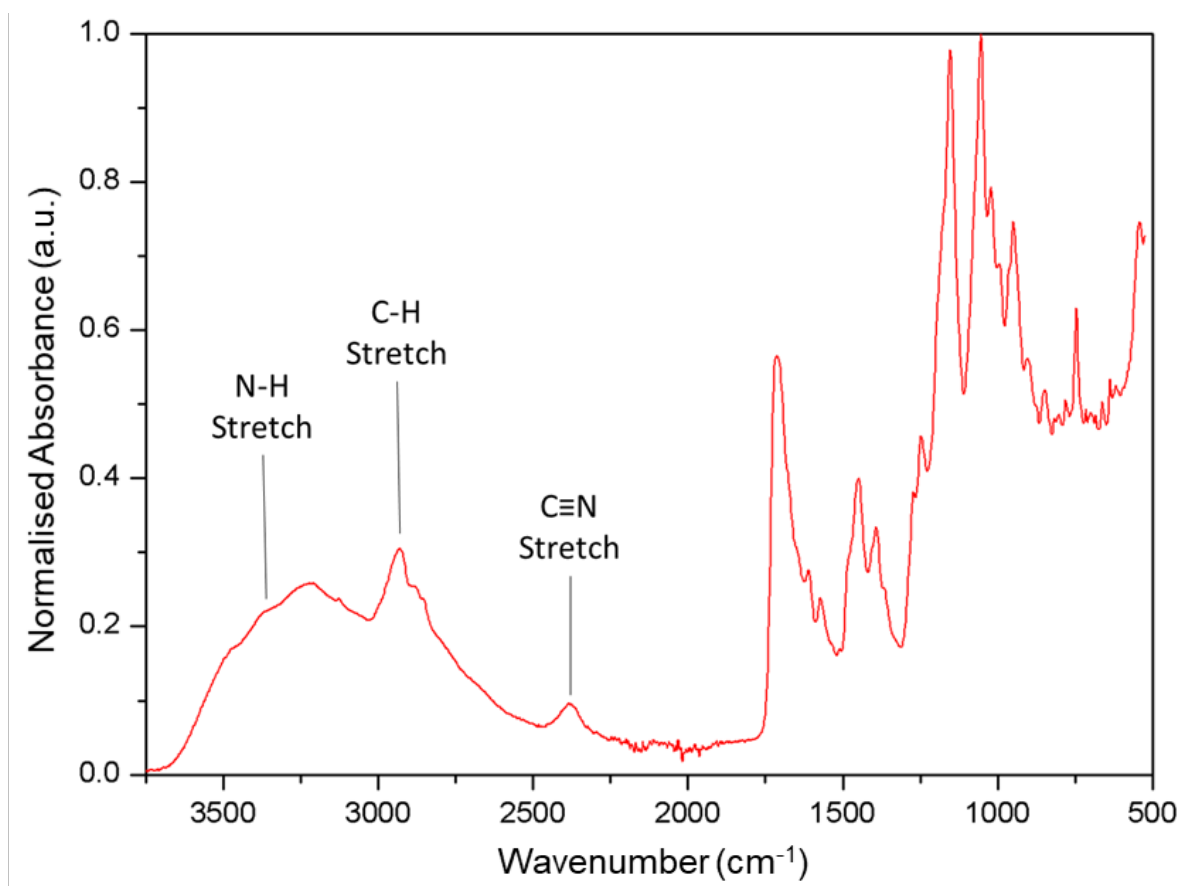


Figure 3.14 Normalised ATR-FTIR spectrum of the **C4** gel.

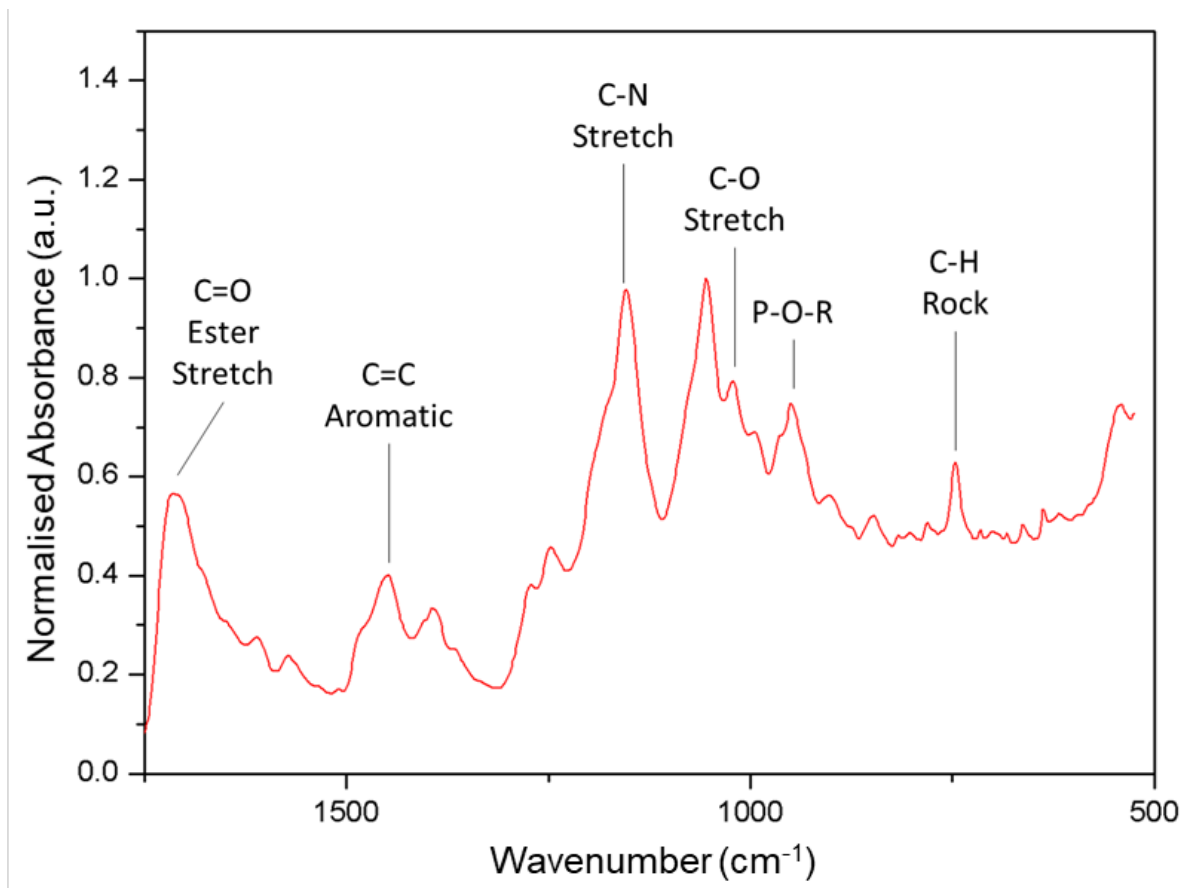


Figure 3.15 ATR-FTIR spectra of C4 gel in the fingerprint region 500-2000  $\text{cm}^{-1}$ .

**Table 3.2:** IR peak correlations.<sup>42</sup> Molecular structure of idealised poly(DMT-dC-P-EMA) included for reference.

Peak ( $\text{cm}^{-1}$ )	Functional group <sup>38</sup>
3380	N — H stretch
3243	O — H stretch
2935	C — H stretch
2393	C $\equiv$ N stretch
1718	C = O Ester stretch
1452	C = C Aromatic
1151	C—N stretch
1052	C—O stretch
950	P—O—R
748	C—H rock

The peaks present at  $3380\text{ cm}^{-1}$  and  $1151\text{ cm}^{-1}$  were associated with nucleobase amines. This indicated that the cytosine moiety of the **C4** had been incorporated into the gel and was not cleaved during its formation.<sup>39</sup> Further evidence that the full nucleotide had been incorporated into the **C4** gel was seen from the presence of the  $950\text{ cm}^{-1}$  peak associated with the phosphate moiety.<sup>43</sup>

The presence of the peak at  $2393\text{ cm}^{-1}$  associated with a  $\text{C}\equiv\text{N}$  stretch indicated that the cyanoethyl protecting group was still present on the phosphates that make up the **C4** gel. This showed that the gel was unlikely to have formed from hydrolysis as the conditions required would result in the removal of the cyanoethyl protecting group.

The presence of the broad peak centred at  $3250\text{ cm}^{-1}$  indicated the O-H stretch, associated with adsorbed water.<sup>40</sup> This indicated that the **C4** gel was hygroscopic and absorbed water from the air.

#### 3.3.4 Determining the Structure of the **C4** Gel

At this point in the experiment the solvent analysis and ATR-FTIR spectroscopy showed that the **C4** gel formed during the polymerisation was associated with strong binding between the polymer chains, and that the nucleotide unit was retained within the gel.

The broad insolubility of the **C4** gel in multiple solvents suggested covalent cross-linking of the polymer chains. Of the moieties that were present, the phosphate was the more reactive and susceptible to hydrolysis and other reactions due to the expanded octet of the P(V) oxidation state, confirmed in Section 3.2.1.2.

As the phosphate was still protected within the gel, the possibility of hydrolysis, or similar reaction, to create the cross-linking unit was not possible. As a result, it was hypothesised

that the cross-linking unit was a diene spontaneously formed (Figure 3.16) by the **C3** monomer in solution. This hypothesis was formed based on the work reported by Grondahl *et al.*<sup>45</sup> where they showed that phosphates in solution underwent substitution without hydrolysis. In their work they showed that monomers bearing primary ester link between the phosphate and the alkyl substituent was susceptible to the substitution. To this project the appearance of the peak associated with the formation would have appeared in the <sup>31</sup>P NMR spectrum had it occurred while stored, but it is proposed that it would have occurred primarily during the heating of the **C3** for the polymerisation, or during the polymerisation between repeating units. Thus, the diene formed within the **C4** could act as a cross-linking agent due to the presence of two alkene moieties each able to be incorporated into a different strand, creating a covalent link between the two polymer chains. As this process created more dienes, more cross linkers were present, eventually resulting in the **C4** gel.

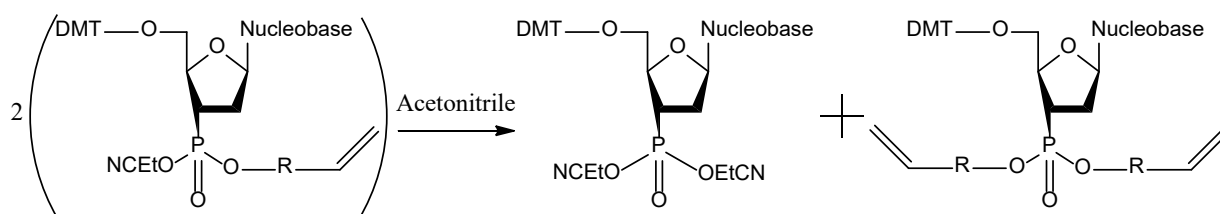


Figure 3.16 Proposed by-product reaction caused by the solvation of vinyl-nucleotide bioconjugate for extended periods, resulting in the diene impurity that would act as the cross-linking agent and subsequently leading to the gel formation.

### 3.4 Conclusion

This chapter has shown that using the phosphoramidite method to couple a hydroxyl bearing vinyl monomer, HEMA, to a cytosine protected nucleotide was possible. The resulting attempt to polymerise this vinyl functionalised nucleotide, **C3**, resulted in an insoluble gel unsuitable for further applications. This was hypothesised to be the result of the primary alcohol of the

HEMA being able to undergo substitution while solvated. This hypothesis was tested by utilising a sterically hindered secondary alcohol, namely 2-hydroxypropyl methacrylate, to prevent the substitution as presented in the following chapter.

### 3.5 References

- (1) Venkatesan, N.; Kim, S. J.; Kim, B. H. Novel Phosphoramidite Building Blocks in Synthesis and Applications toward Modified Oligonucleotides. *Curr. Med. Chem.* **2003**, *10* (19), 1973–1991.
- (2) Gaytán, P. Chemical Synthesis of Oligonucleotides Using Acetone as a Washing Solvent. *Biotechniques* **2009**, *47* (2), 701–702.
- (3) Burfield, D. R.; Smithers, R. H. Desiccant Efficiency in Solvent Drying. 3. Dipolar Aprotic Solvents. *J. Org. Chem.* **1978**, *43* (20), 3966–3968.
- (4) Bolton, P. D. Hydrolysis of Amides. Ii. Substituent Effects in Dilute Acid and Alkali. *Aust. J. Chem.* **1966**, *19* (6), 1013–1021.
- (5) Brown, R. S.; Bennet, A. J.; Slebocka-Tilk, H. Recent Perspectives Concerning the Mechanism of H<sub>3</sub>O<sup>+</sup>- and Hydroxide-Promoted Amide Hydrolysis. *Acc. Chem. Res.* **1992**, *25* (11), 481–488.
- (6) Berner, S.; Mühlegger, K.; Seliger, H. Studies on the Role of Tetrazole in the Activation of Phosphoramidites. *Nucleic Acids Res.* **1989**, *17* (3), 853–864.
- (7) Nurminen, E. J.; Mattinen, J. K.; Lönnberg, H. Kinetics and Mechanism of Tetrazole-Catalyzed Phosphoramidite Alcoholysis. *J. Chem. Soc. Perkin Trans. 2* **1998**, *0* (7), 1621–1628.

- (8) Dahl, B. H.; Nielsen, J.; Dahl, O. Mechanistic Studies on the Phosphoramidite Coupling Reaction in Oligonucleotide Synthesis. I. Evidence for Nucleophilic Catalysis by Tetrazole and Rate Variations with the Phosphorus Substituents. *Nucleic Acids Res.* **1987**, *15* (4), 1729–1743.
- (9) Maier, M. A.; Choi, Y.; Gaus, H.; Barchi, J. J.; Marquez, V. E.; Manoharan, M. Synthesis and Characterization of Oligonucleotides Containing Conformationally Constrained Bicyclo[3.1.0]Hexane Pseudosugar Analogs. *Nucleic Acids Res.* **2004**, *32* (12), 3642–3650.
- (10) Masanori, K.; Akira, H.; Shinya, O.; Mamoru, H.; Mitsue, A.; Rie, K.; Hayakawa, Y. Ethyl(Methyl)Dioxirane as an Efficient Reagent for the Oxidation of Nucleoside Phosphites into Phosphates under Nonbasic Anhydrous Conditions. *Org. Lett.* **2001**, *3* (6), 815–818.
- (11) Uzagare, M. C.; Padiya, K. J.; Salunkhe, M. M.; Sanghvi, Y. S. NBS-DMSO as a Nonaqueous Nonbasic Oxidation Reagent for the Synthesis of Oligonucleotides. *Bioorg. Med. Chem. Lett.* **2003**, *13* (20), 3537–3540.
- (12) Pérez-Rentero, S.; Garibotti, A. V.; Eritja, R. Molecules Solid-Phase Synthesis of Oligodeoxynucleotides Containing N4-[2-(t-Butyldisulfanyl)Ethyl]-5-Methylcytosine Moieties. *Molecules* **2010**, *15*, 5692–5707.
- (13) Dennison, G. H.; Johnston, M. R. Mechanistic Insights into the Luminescent Sensing of Organophosphorus Chemical Warfare Agents and Simulants Using Trivalent Lanthanide Complexes. *Chemistry - A European Journal*. John Wiley & Sons, Ltd April 20, 2015, pp 6328–6338.

- (14) Dennison, G. H.; Sambrook, M. R.; Johnston, M. R. Interactions of the G-Series Organophosphorus Chemical Warfare Agent Sarin and Various Simulants with Luminescent Lanthanide Complexes. *RSC Adv.* **2014**, *4* (98), 55524–55528.
- (15) Bolduc, P. R.; Goe, G. L. Singlet Oxygen Oxidation of Phosphites to Phosphates. *J. Org. Chem.* **1974**, *39* (21), 3178–3179.
- (16) Martin, P.; Tuazon, E. C.; Atkinson, R.; David Maughan, A. Atmospheric Gas-Phase Reactions of Selected Phosphorus-Containing Compounds. *J. Phys. Chem. A* **2002**, *106* (8), 1542–1550.
- (17) Schwetlick, K.; Pionteck, J.; Winkler, A.; Hähner, U.; Kroschwitz, H.; Habicher, W. D. Organophosphorus Antioxidants: Part X—Mechanism of Antioxidant Action of Aryl Phosphites and Phosphonites at Higher Temperatures. *Polym. Degrad. Stab.* **1991**, *31* (2), 219–228.
- (18) Schwetlick, K. Mechanisms of Antioxidant Action of Phosphite and Phosphonite Esters. In *Mechanisms of Polymer Degradation and Stabilisation*; Springer Netherlands: Dordrecht, 1990; pp 23–60.
- (19) Pregosin P.S.; Rügger, H; 2.1 - Nuclear Magnetic Resonance Spectroscopy, *Comprehensive Coordination Chemistry II*, 2003, 2, 1-35
- (20) Robinson, K. L.; Khan, M. A.; De Paz Báñez, M. V.; Wang, X. S.; Armes, S. P. Controlled Polymerization of 2-Hydroxyethyl Methacrylate by ATRP at Ambient Temperature. *Macromolecules* **2001**, *34* (10), 3155–3158.
- (21) Cahill, R.; Cookson, R. C.; Crabb, T. A. Geminal Coupling Constants in Methylene Groups-II. J in CH<sub>2</sub> Groups  $\alpha$  to Heteroatoms. *Tetrahedron* **1969**, *25* (19), 4681–4709.

- (22) Kupriyanov, V.V.; Steinschneider, A.Ya.; Ruuge, E.K.; Smirnov, V.N.; Saks, V.A.; <sup>31</sup>P-NMR spectrum of phosphocreatine: Deuterium-induced splitting of the signal, *Biochemical and Biophysical Research Communications*. **1983**, 114 (3), 1117-1125
- (23) Weinrich, T.; Jaumann, E. A.; Scheffer, U. M.; Prisner, T.F., Gobel, M. W.; Phosphoramidite building blocks with protected nitroxides for the synthesis of spin-labeled DNA and RNA. *Beilstein J. Org. Chem.* **2018**, 14, 1563–1569
- (24) Meher, G.; Efthymiou, T.; Stoop, M.; Krishnamurthy, R; Microwave-Assisted Preparation of Nucleoside-Phosphoramidites, *Chemical Communications*, **2014**, 50, 7463-7465
- (25) Mayadunne, R. T. A.; Rizzardo, E.; Chiefari, J.; Krstina, J.; Moad, G.; Postma, A.; Thang, S. H. Living Polymers by the Use of Trithiocarbonates as Reversible Addition-Fragmentation Chain Transfer (RAFT) Agents: ABA Triblock Copolymers by Radical Polymerization in Two Steps. *Macromolecules* **2000**, 33 (2), 243–245.
- (26) Schuerch, C.; Some Steric Factors in Vinyl Polymerization. *Annu. Rev. Phys. Chem.* **1962**, 13, 195–220.
- (27) Puts, R. D.; Sogah, D. Y. Control of Living Free-Radical Polymerization by a New Chiral Nitroxide and Implications for the Polymerization Mechanism. *Macromolecules* **1996**, 29 (9), 3323–3325.
- (28) Ma, J. W.; Smith, J. A.; McAuley, K. B.; Cunningham, M. F.; Keoshkerian, B.; Georges, M. K. Nitroxide-Mediated Radical Polymerization of Styrene in Miniemulsion: Model Studies of Alkoxyamine-Initiated Systems. *Chem. Eng. Sci.* **2003**, 58 (7), 1163–1176.
- (29) Clark, A. J.; Battle, G. M.; Heming, A. M.; Haddleton, D. M.; Bridge, A. Ligand



- Electronic Effects on Rates of Copper Mediated Atom Transfer Radical Cyclisation and Polymerisation. *Tetrahedron Lett.* **2001**, *42* (10), 2003–2005.
- (30) Moad, G.; Rizzardo, E.; Thang, S. H. Radical Addition-Fragmentation Chemistry in Polymer Synthesis. *Polymer*. Elsevier March 3, 2008, pp 1079–1131.
- (30) Van Hook, J. P.; Tobolsky, A. V. The Thermal Decomposition of 2,2'-Azo-Bis-Isobutyronitrile. *J. Am. Chem. Soc.* **1958**, *80* (4), 779–782.
- (31) Charton, N.; Feldermann, A.; Theis, A.; Stenzel, M. H.; Davis, T. P.; Barner-Kowollik, C. Initiator Efficiency of 2,2'-Azobis(Isobutyronitrile) in Bulk Dodecyl Acrylate Free-Radical Polymerizations over a Wide Conversion and Molecular Weight Range. *J. Polym. Sci. Part A Polym. Chem.* **2004**, *42* (20), 5170–5179.
- (32) RAFT General Procedures, Boron Molecular, accessed 20 February 2016, <[http://www.boronmolecular.com/index.php?route=information/information&information\\_id=52](http://www.boronmolecular.com/index.php?route=information/information&information_id=52)>
- (33) Sasaki, S.; Suzuki, A. Factors Influencing the Swelling and Elution Properties of Poly(Vinyl Alcohol) Cast Gels. *Polym. Adv. Technol.* **2016**, *27* (3), 318–324.
- (34) Madkour, A. E.; Grolman, J. M.; Tew, G. N. Synthesis of Hydrogels via Ring-Opening Metathesis Polymerization: Factors Affecting Gelation. *Polym. Chem.* **2011**, *2* (1), 114–119.
- (35) Lvov, Y.; Ariga, K.; Ichinose, I.; Kunitake, T. Formation of Ultrathin Multilayer and Hydrated Gel from Montmorillonite and Linear Polycations. *Langmuir* **1996**, *12* (12), 3038–3044.

- (36) Kim, Y.; Faqih, M. .; Wang, S. . Factors Affecting Gel Formation of Inulin. *Carbohydr. Polym.* **2001**, *46* (2), 135–145.
- (37) Abend, S.; Lagaly, G. Sol–Gel Transitions of Sodium Montmorillonite Dispersions. *Appl. Clay Sci.* **2000**, *16* (3–4), 201–227.
- (38) Porter, R. S.; Johnson, J. F. The Entanglement Concept in Polymer Systems. *Chem. Rev.* **1966**, *66* (1), 1–27.
- (39) Charlesby, A. Gel Formation and Molecular Weight Distribution in Long-Chain Polymers. *Proc. R. Soc. London. Ser. A. Math. Phys. Sci.* **1954**, *222* (1151), 542–557.
- (40) Nakano, S.-I.; Sugimoto, N. The Structural Stability and Catalytic Activity of DNA and RNA Oligonucleotides in the Presence of Organic Solvents. *Biophys. Rev.* **2016**, *8* (1), 11–23.
- (41) Huh, K. M.; Bae, Y. H. Synthesis and Characterization of Poly(Ethylene Glycol)/Poly(L-Lactic Acid) Alternating Multiblock Copolymers. *Polymer (Guildf)*. **1999**, *40* (22), 6147–6155.
- (42) Stuart, B. H. *Infrared Spectroscopy: Fundamentals and Applications*; Analytical Techniques in the Sciences; Chichester, UK, 2004.
- (43) Kyogoku, Y.; Lord, R. C.; Rich, A. An Infrared Study of Hydrogen Bonding between Adenine and Uracil Derivative in Chloroform Solution. *J. Am. Chem. Soc.* **1967**, *89* (2), 496–504.
- (44) Pereira, R.; Tojeira, A.; Vaz, D. C.; Mendes, A.; Bártolo, P. Preparation and Characterization of Films Based on Alginate and Aloe Vera. *Int. J. Polym. Anal.*

*Charact.* **2011**, *16* (7), 449–464.

- (45) Grøndahl, L.; Suzuki, S.; Wentrup-Byrne, E. Influence of a Diene Impurity on the Molecular Structure of Phosphate-Containing Polymers with Medical Applications. *Chem. Commun. (Camb)*. **2008**, No. 28, 3314–3316.

# Chapter 4: Synthesis of The Poly(2-(2'-deoxyguanosine-monophosphate)oxypropyl methacrylate)): a Guanine Rich Methacrylate Polymer

## 4.1 Synopsis

*This chapter describes the design, synthesis and characterisation of the 5'-dimethoxytrityl-N-isobutyryl-2'-deoxyguanosine,3'-[(2-cyanoethyl)-(oxypropyl methacrylate)]-phosphate monomer, henceforth referred to as **DMT-dG-CE-PMA phosphate monomer**, building on the methods and conclusions presented in Chapter 3.*

*Synthesis of DMT-dG-CE-PMA phosphate monomer was achieved through the coupling of 2-hydroxypropyl methacrylate (HPMA) with a protected 5' guanosine (G) monophosphate. Following the synthesis of the DMT-dG-CE-PMA phosphate monomer, it was polymerised using reversible addition-fragmentation chain transfer (RAFT) polymerisation and subsequently deprotected to form poly(2-(2'-deoxyguanosine-monophosphate)oxypropyl methacrylate), referred to as **poly(dG-P-PMA)**.*

## 4.2 Introduction

This chapter builds on Chapter 3 which showed the synthesis of 5'-dimethoxytrityl-N-benzoyl-2'-deoxycytosine,3'-[(2-cyanoethyl)-(oxyethyl methacrylate)]-phosphate monomer (**C3** monomer) using a phosphoramidite coupling approach. This approach was chosen for a number of reasons, discussed in more depth in Chapter 3.

The phosphoramidite coupling method used in Chapter 3 was further developed for this chapter, resulting in the procedure shown in Figure 4.1. The phosphoramidite coupling approach started with a protected nucleotide phosphoramidite, Figure 4.1(i); the nucleotide phosphoramidite was then activated with the imidazole derivative 4,5-dicyanoimidazole (DCI), the activator. The activator reacts with the phosphoramidite moiety to form the activated intermediate phosphoramidite, Figure 4.1(ii). This chapter utilised 4,5-dicyanoimidazole instead of the tetrazole used in Chapter 3 for the reasons discussed in Section 4.2.5. The activated phosphoramidite intermediate targets virtually any hydroxyl moiety, coupling it to the nucleotide and forming a nucleotide phosphite, Figure 4.1(iii), and the coupling also regenerates the activator allowing the latter to act as a catalyst. The final step in the coupling is the conversion of the phosphite into a phosphate. This step was conducted in order to control the oxidation of the phosphite, rather than allowing it to react uncontrollably during the following polymerisation process.

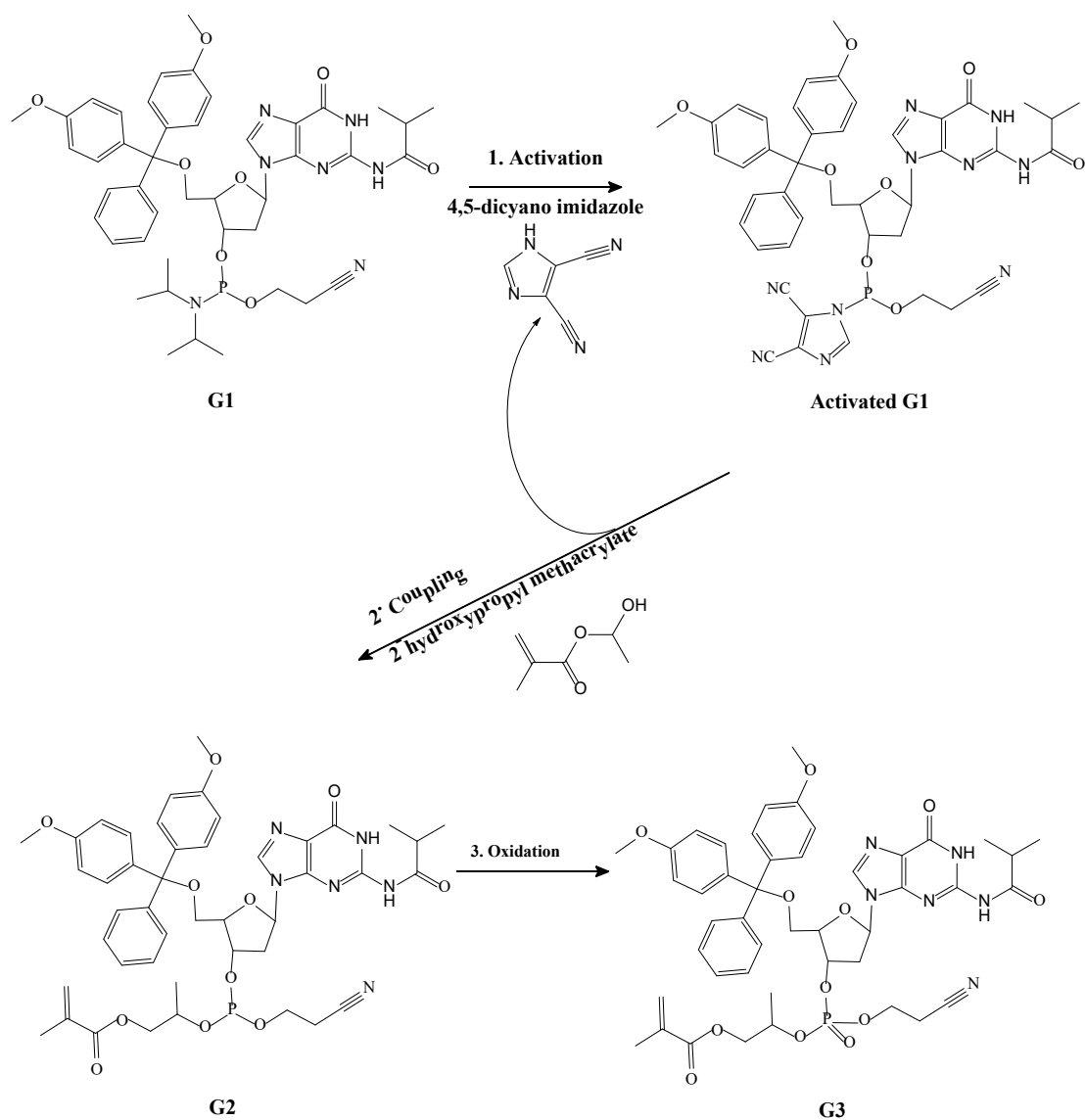


Figure 4.1 Overview for the conversion of **G1** starting material through the activation with DCI to form the activated **G1** intermediate. This in turn was coupled to HPMA to form a **G2** monomer and then oxidised to form the **G3** monomer. The DCI required for the activation (step 1) is regenerated during the coupling step (step 2) allowing it to act as a catalyst.

#### 4.2.1 Maintaining the Use of the Phosphoramidite Coupling Method

As the method in Chapter 3 had synthesised the **C3** monomer successfully, the use of a phosphoramidite method was retained. This also meant that a nucleotide phosphoramidite would still be used as the nucleotide source for the coupling reaction.

Most important to this thesis, and the reason it was still used in this chapter, was the high yields achievable through the phosphoramidite coupling method compared to other methods of nucleotide coupling. Yield was important as producing polymers, which is the ultimate goal of the work done for this thesis, required a significant amount of material. Alternative methods, such as the H-phosphonate method discussed in Chapter 1 Section 1.4.2, have been shown in literature to result in lower yields.<sup>1</sup>

#### **4.2.2 Determining the Phosphoramidite Isomer to be Used**

As discussed in Chapter 3, Section 3.2.1 there are 2 classes of nucleotide phosphoramidite which are distinguished from each other based on the location of the phosphorus moiety on the sugar ring, whether it is attached to the 5' or 3' carbon, Figure 4.2.

In Chapter 3, the 3' phosphoramidite was chosen because it had the phosphorus connected to the ribose through a more stable secondary alcohol, compared to the 5' which connects through a primary alcohol. This difference causes the 3' phosphoramidite to be less susceptible to hydrolysis. This property is important since hydrolysis of the phosphate would cause the nucleoside to detach, effectively removing any selective binding functionality from the vinyl bioconjugate. Based on this, the phosphoramidite method we used in this chapter still relied on the 3' phosphoramidite similarly to the previous Chapter 3.

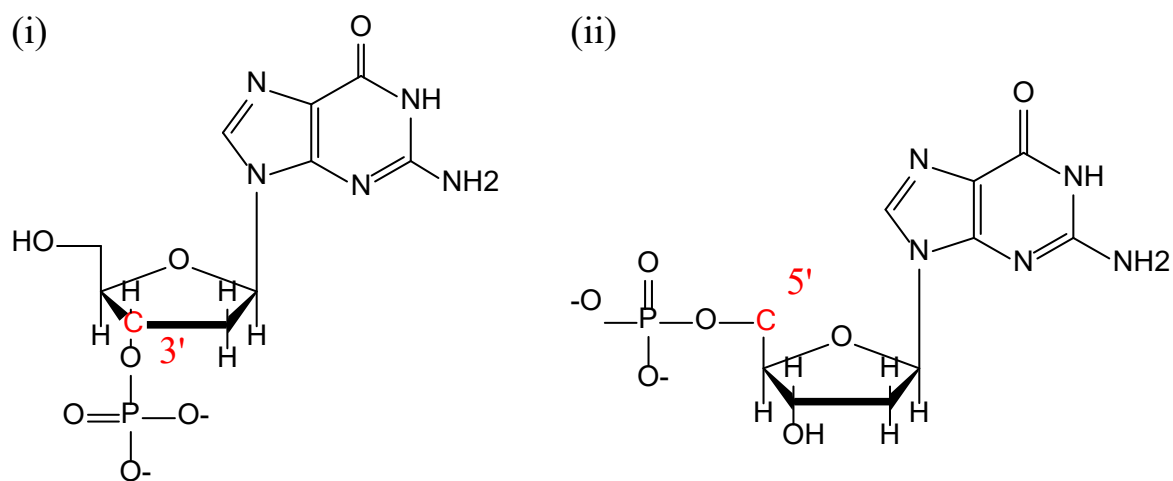


Figure 4.2 (i) 3'-deoxy guanosine monophosphate and (ii) 5'-deoxy guanosine monophosphate isomers.

### 4.2.3 Preventing the Formation of a Gel

In Chapter 3 we used cytosine as the nucleotide, coupling it to hydroxyethyl methacrylate to form the **C3** monomer. This polymerisation resulted in the monomer forming a gel which was undesirable consistency for the end product. The exact nature of the gel could not be determined from the data collected, though it was hypothesised to be due to covalent linkages between polymer chains caused by the formation of a diene. For that reason the synthesis of the nucleotide functionalised monomer was changed in an effort to prevent gel formation by limiting any sources of unwanted inter-chain bonding.

If the gel was forming due to secondary bonding, there are a number of sites where it could be possibly happening. Least critical to the success of the project was the nucleobase component, which had been cytosine. If the secondary bonding between polymer strands occurred through the deoxyribose or phosphate moieties, however, that would prevent the use of any nucleotide going forward.



#### 4.2.4 Changing the Nucleobase

As discussed in Chapter 3 Section 3.4.4 the formation of a gel from the **C4** may have been the result of intermolecular secondary bonding from the formation of *i*-motifs 3.3.3. To rule this out as a possibility, the nucleobase used as a model for the generation for a nucleotide functionalised polymer was changed from cytosine to guanine.

Thymine phosphoramidites were excluded as a model because they do not bear any protecting group on the nucleobase moiety, meaning that they may act differently to the protected nucleobases. Specifically of note, the conditions for the removal of the protection group with ammonium hydroxide could not be tested as there is no protecting group present, and the potential difference in solubility this may cause.

Adenine was not chosen as it contained the benzoyl protecting group which had also been present in cytosine that was used previously; if this aromatic group had been involved in the intermolecular binding it was more likely to occur when using adenine. Guanine sits in between thymine and adenine in this regard, bearing the non-aromatic isobutyryl protecting group.

Guanine can also form secondary structures known as G-quartets, as discussed in Chapter 1, Section 1.2.5.1. Similar to cytosine, G-quartets form through non-canonical bonding; on the other hand, literature shows that G-quartets, unlike cytosine, form around large cations, such as  $K^+$  or  $Mg^{2+}$ . As none of the compounds being used contained such ions, this was not considered an issue in this experiment.

#### 4.2.5 Changing the Vinyl Moiety

The possible covalent route for the cross-linking was the formation of a diene impurity, as described in Chapter 3 Section 3.4.4, and previously presented by Grøndahl *et al.*<sup>2</sup> The reaction as it pertains to this project is shown in Figure 4.3. In their work Grøndahl *et al.* showed the

dienes could form due to the exchange of the vinyl moieties on phosphates while solvated.<sup>2</sup> This exchange could occur with the **C3** monomer when solvated during the polymerisation in which case the resulting DMT-dG-PMA-PMA phosphate diene would contain two vinyl groups, each of which could be incorporated into a separate chain, thereby acting as a cross-linking agent.

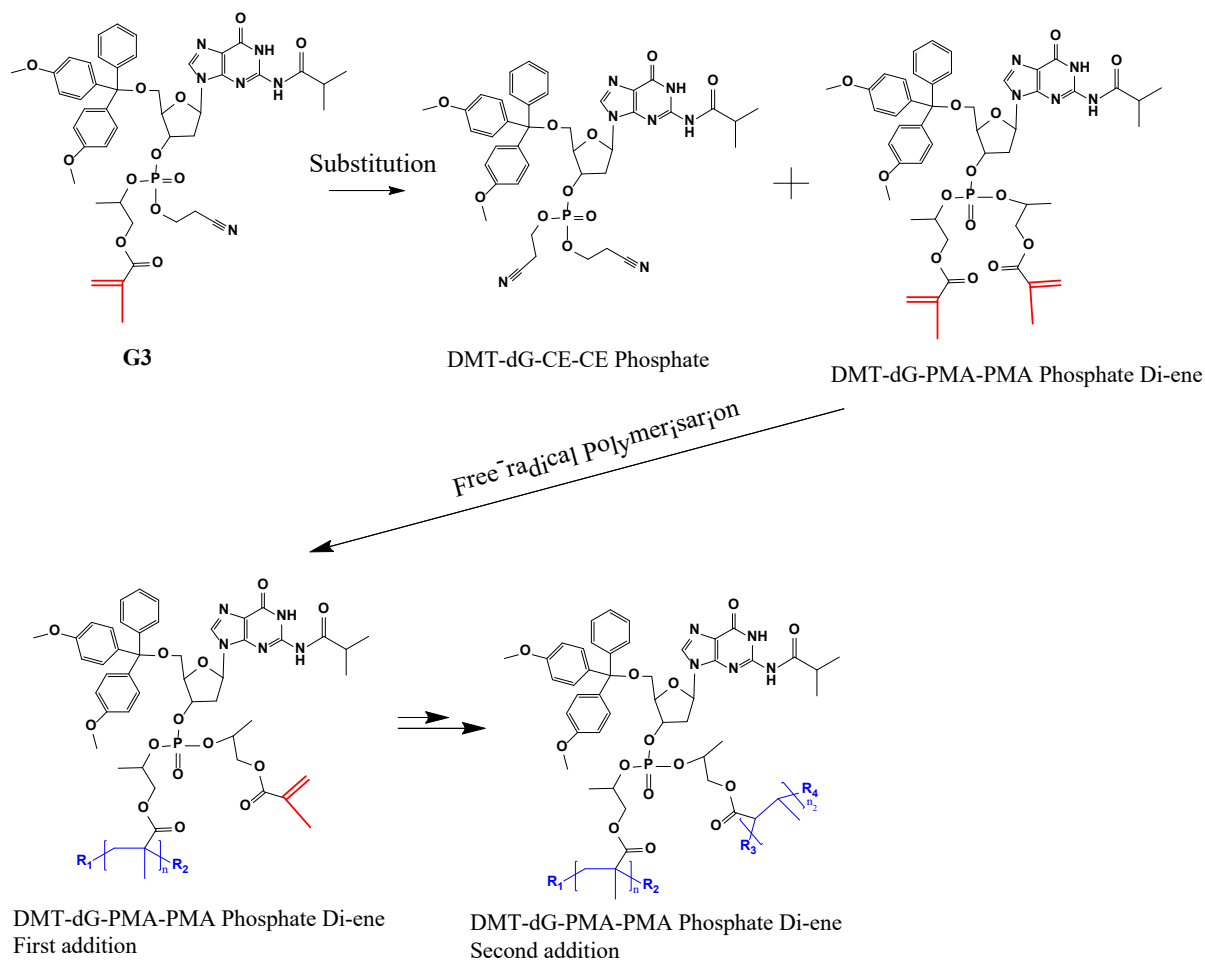


Figure 4.3 Formation of the diene impurity from **G3** monomer in solution, followed by polymerisation creating the first addition, and leading to cross-linking with the second addition. For clarity active vinyl groups are shown in red. Polymerised vinyl groups shown in blue.

To mitigate the formation of the diene, the vinyl containing moiety was changed from HEMA to 2-hydroxypropyl methacrylate (HPMA). The HPMA structure was similar to that of HEMA, with the addition of a methyl group converting it from a primary to a secondary alcohol. This change was hypothesised to minimise the formation of the diene through the decreased reactivity and steric hindrance provided by the adjacent methyl group.

As a result of the change to HPMA, however, the activator also needed to be changed. Tetrazole, the activator used in Chapter 3, has been shown in literature to undergo the coupling more efficiently with primary alcohols; as a result the activator was changed to 4,5-dicyanoimidazole (DCI). DCI was chosen as in literature it had been shown to produce higher coupling yields with sterically hindered phosphoramidite compared to tetrazole.<sup>3</sup> This improvement in yield is explained by the increased nucleophilicity of DCI.<sup>3</sup> This allows it to be regenerated more easily during the coupling step (Figure 4.1).

The oxidation process that follows the coupling phase of the experiment was done in the same way as described in Chapter 3 since using of HPMA as the vinyl source still prohibited the use of I<sub>2</sub> or pyridine as an oxidant due to the risk of halide addition, as discussed in Chapter 3 Section 3.2.3.2.

### **4.3 Analysis of DMT-dG-CE-P-PMA Phosphite and Phosphate**

The following sections outline the analytical methods used to confirm the synthesis of **G2** and **G3** monomers, as described in Chapter 2 Section 2.5.2.1. The methods employed were ESI-MS and NMR Spectroscopy using both <sup>1</sup>H and <sup>31</sup>P variations of the method.

#### **4.3.1 Electrospray Ionisation Mass Spectrometry (ESI-MS)**

ESI-MS was used as the primary method for determining the successful synthesis of **G2** monomer. This technique was chosen because it can provide an accurate mass measurement

for all the components within the mixture, which can be compared to the theoretical mass of the products in our calculations.<sup>4</sup> As a result, it also gives a reasonable idea of not only how pure a sample is (based on what  $m/z$  are present) but what impurities might be present.<sup>5</sup> ESI-MS is less sensitive to impurities compared to other techniques, such as NMR spectroscopy,<sup>6</sup> since ESI-MS gives each molecule a dedicated signal despite impurities. For contrast, 1D NMR spectroscopy maps all chemical environments for a given sample, which then need to be interrogated to determine the source of each signal.<sup>6</sup>

Due to the ionisation method used, the **G2** and phosphate monomers form adducts with the cations present, notably  $H^+$  and  $Na^+$ , and with solvent molecules attached through electrostatic interactions. This is evident as a series of peaks following the molecular ion represent these adducts on the resulting spectrogram.

To perform the ESI-MS analysis, samples of the **G2** monomer were freeze-dried from the DCM phase prior to evaporation and oxidation. This resulted in the formation of a white powder which was prepared for ESI-MS at 1 mg/mL in acetonitrile. Measurements were then taken under positive ion mode; the result is shown in Figure 4.4. The theoretical mass value for **G2** monomer was calculated as 882.3  $m/z$ . Following oxidation the DMT-dG-CE-P-PMA phosphate monomer was calculated theoretically to be 899.3  $m/z$ .

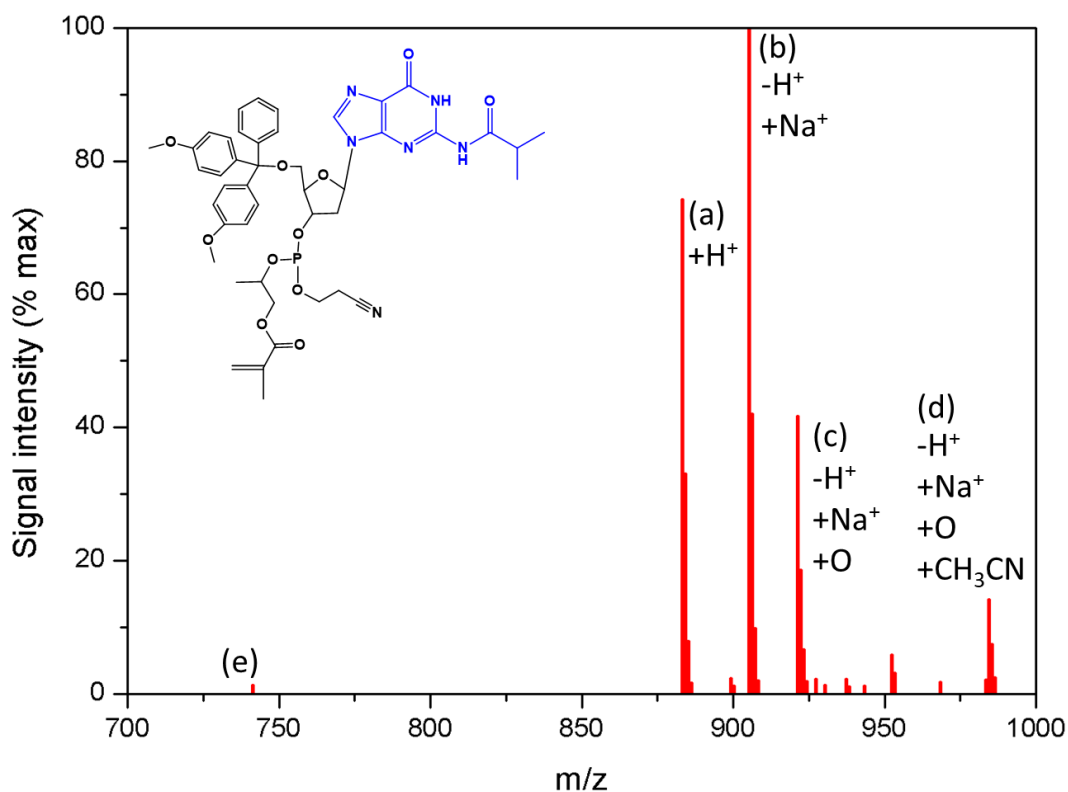


Figure 4.4 ESI-MS spectrum of the final product showing the following peaks: (a) **G2** (molecule shown inset), (b) **G2** sodium adduct, (c) **G3** monomer sodium adduct, and (d) **G3** monomer disodium + acetonitrile adduct.

The ESI-MS spectrum showed the presence of a peak at 883 m/z (Figure 4.4(a)) which was consistent with the theoretical value of 882.3 m/z for **G2** with the H<sup>+</sup> adduct. Figure 4.4(b) also shows the sodium adduct of **G2** at 905 m/z, evident from the 23 m/z difference.

A third major peak was also seen at 921 m/z (Figure 4.4(c)). This matched the theoretical value of 921.3 m/z for the sodium adduct of **G3** monomer. It was complemented by the peak at 985 m/z (Figure 4.4(d)) which matched the theoretical value of 985.34 m/z expected for the **G3** monomer disodium + acetonitrile adduct.

The presence of these four peaks indicated successful coupling of the HPMA to the **G1** starting material by the substitution of the diisopropylamine group (DIPA). However, the spectrum also indicated a mixture of **G2** and phosphate was produced.

The **G1** starting material, with a theoretical  $m/z$  of 839.38, appears as a trace peak in the **G2** spectrum (Figure 4.4(e)). This indicated virtually complete conversion during the phosphoramidite coupling.

In addition to these major peaks, each is shadowed by a series of diminishing peaks of increasing  $m/z$  due to the presence of different isotopes within the molecule.<sup>7</sup> For all of the elements present in the **G2** and phosphate monomers, the major isotope for each element is also the lightest which means that the statistically most common  $m/z$  is also the lightest.

### 4.3.2 Nuclear Magnetic Resonance (NMR) Spectroscopy

NMR spectroscopy analysis was chosen as the secondary analysis method to confirm the synthesis of the **G3** monomer. Firstly,  $^1\text{H}$  NMR (proton) spectroscopy was used to confirm the substitution of the diisopropylamine group with HPMA on the phosphorus. Following this  $^{31}\text{P}$  NMR was used to determine the successful conversion of the phosphorus from the P(III) oxidation state of the **G1** starting material to the P(V) oxidation state of DMT-dG-CE phosphate monomer.

#### 4.3.2.1 Proton Nuclear Magnetic Resonance ( $^1\text{H}$ NMR) Spectroscopy

Support for successful conjugation of HPMA to the DMT-dG-CE-phosphoramidite was shown using  $^1\text{H}$  NMR spectroscopy. Samples were prepared at 5 mg/mL in deuterated acetonitrile following oxidation and drying. Figure 4.5(i and ii) shows the obtained  $^1\text{H}$  NMR spectra of the **G1** starting material, and the **G3** monomer, respectively.

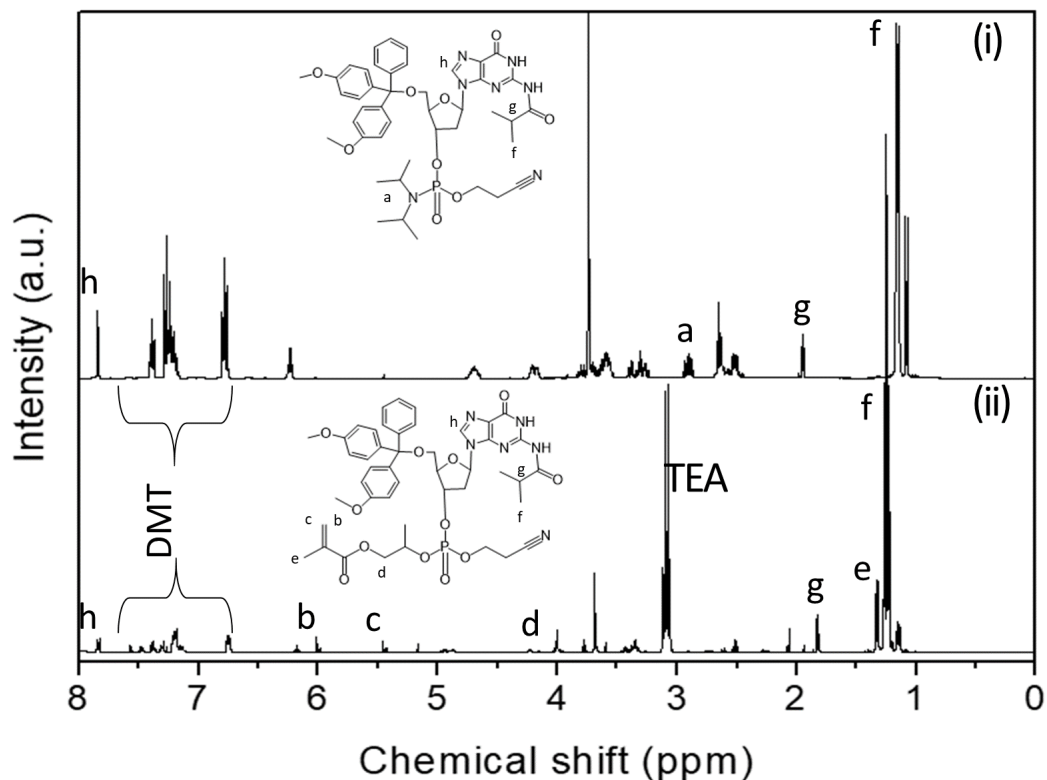


Figure 4.5 <sup>1</sup>H NMR spectra of (i) **G1** starting material and (ii) the bioconjugate **G3** monomer.

Spectra acquired in deuterated acetonitrile at 400 MHz, with triethylamine residue (TEA).

Full peak attributions can be found in Appendix 2.

The removal of the diisopropylamine group was required for the addition of the HPMA moiety. If it still appeared in the spectrum of **G3** monomer (Figure 4.5(ii)), it would indicate that the HPMA was only mixed with the **G1** (Figure 4.5(i)) and had not been coupled.

The peak attributed to the DIPA moiety was present in the **G1** spectrum ( $((\text{CH}_3)_2\text{CH}-\text{N}$  multiplet,  $\delta = 2.9$  ppm,  $^3J_{\text{HH}}=9.9$  Hz), but was noticeably diminished in the spectrum for DMT-dG-CE-PMA phosphoramidite (Peak a in Figure 4.5) indicating near complete conversion. This is more clearly shown in Figure 4.6. This splitting of 9.9 Hz is in the expected range for  $^3J$  coupling.

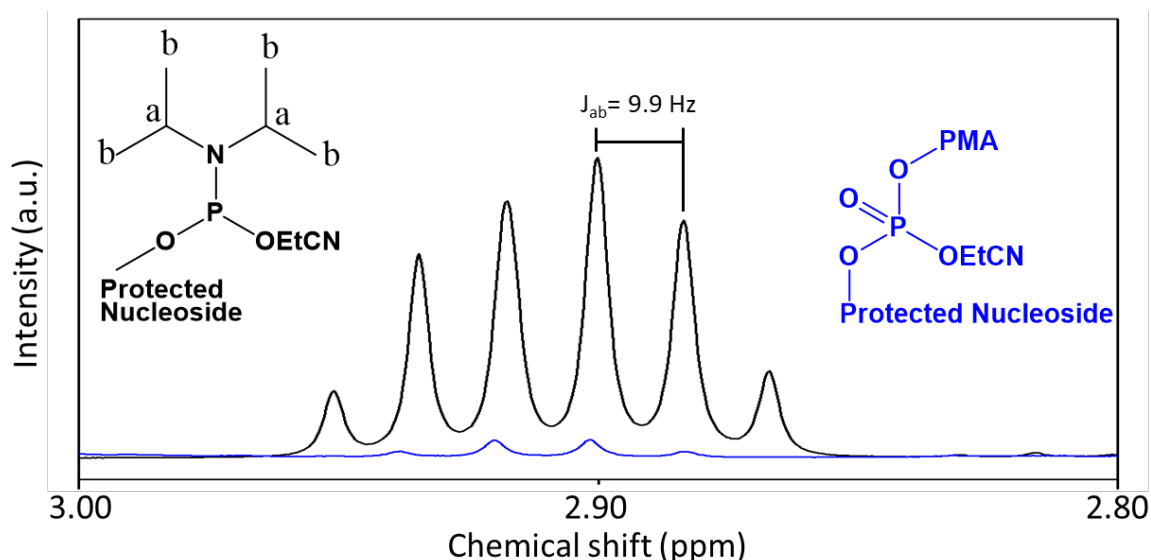


Figure 4.6  $^1\text{H}$  NMR spectra region from 3 ppm to 2 ppm showing the **G1** (black) and the **G3** monomer (blue). Spectra acquired in deuterated acetonitrile at 400 MHz.

The presence of the HPMA moiety was seen as the appearance of peaks at  $\delta = 6$  ppm and  $\delta = 5.45$  ppm (Figure 4.5(peaks b and c)). These peaks (expanded in Figure 4.7(peaks a and b), were attributed to the *cis* and *trans* protons on the alkene group respectively. Both of these peaks appear to show asymmetric splitting,  $^2J_{ab}=13.4$  Hz and  $^2J_{ba}=12.4$  Hz, however this was due to the different isomers formed at the secondary alcohol (Figure 4.7 (inset, arrow)).

The additional peak shown in this region, at 6.2 ppm, was caused by the 1' proton on the deoxyribose ring. In both samples the main coupling was to the 2' protons, causing the distinct triplet ( $^3J_{1'2'}=12$  Hz). The **G1** showed additional splitting ( $^4J_{1'3'}=1.8$  Hz) which was not present in the **G3** monomer sample and was therefore hypothesised to be due to the conformation of the HPMA moiety reducing the coupling below the resolution of the NMR spectrometer.



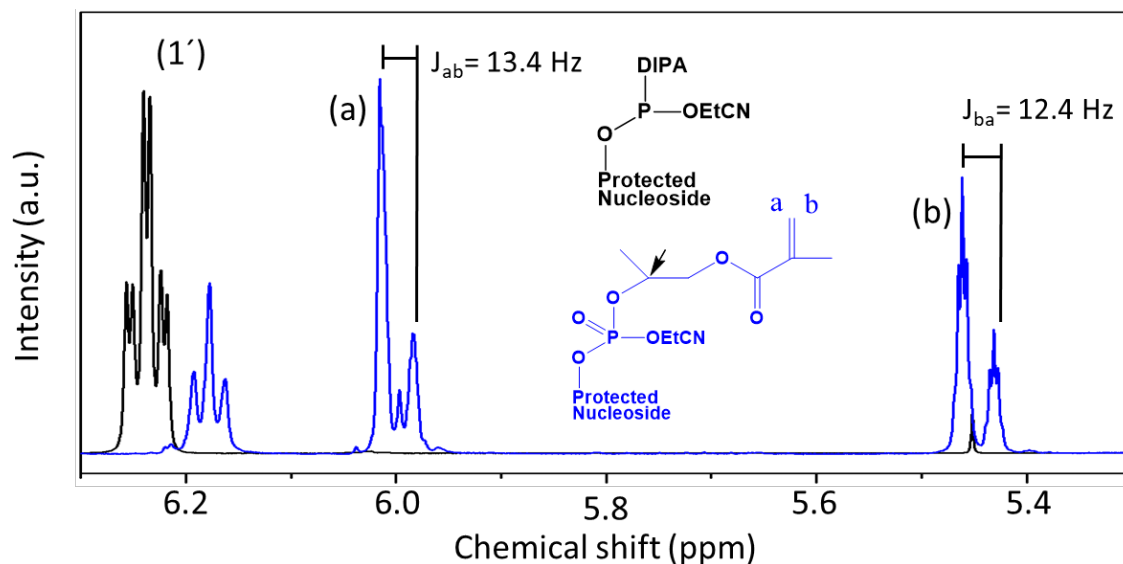


Figure 4.7  $^1\text{H}$  NMR of the 6.3 ppm to 5.3 ppm region for **G1** (black) **G3** (blue). Spectra acquired in deuterated acetonitrile at 400 MHz.

#### 4.3.2.2 Phosphorous Nuclear Magnetic Resonance ( $^{31}\text{P}$ -NMR) Spectroscopy

Confirmation of the phosphorus oxidation from the P(III) state of **G1** to the P(V) oxidation state of **G3** was achieved using solution  $^{31}\text{P}$  NMR spectroscopy.

In this case, the P(III) oxidation state significantly deshields the phosphorus, leading to the peaks being considerably downfield of those associated with the P(V) state for all phosphate compounds. As a result, the oxidation of the phosphorus leads to an upfield shift of  $\sim 120$  ppm.<sup>8,9</sup> This can be seen in Figure 4.8 as the difference in peak location between (i) and (ii).

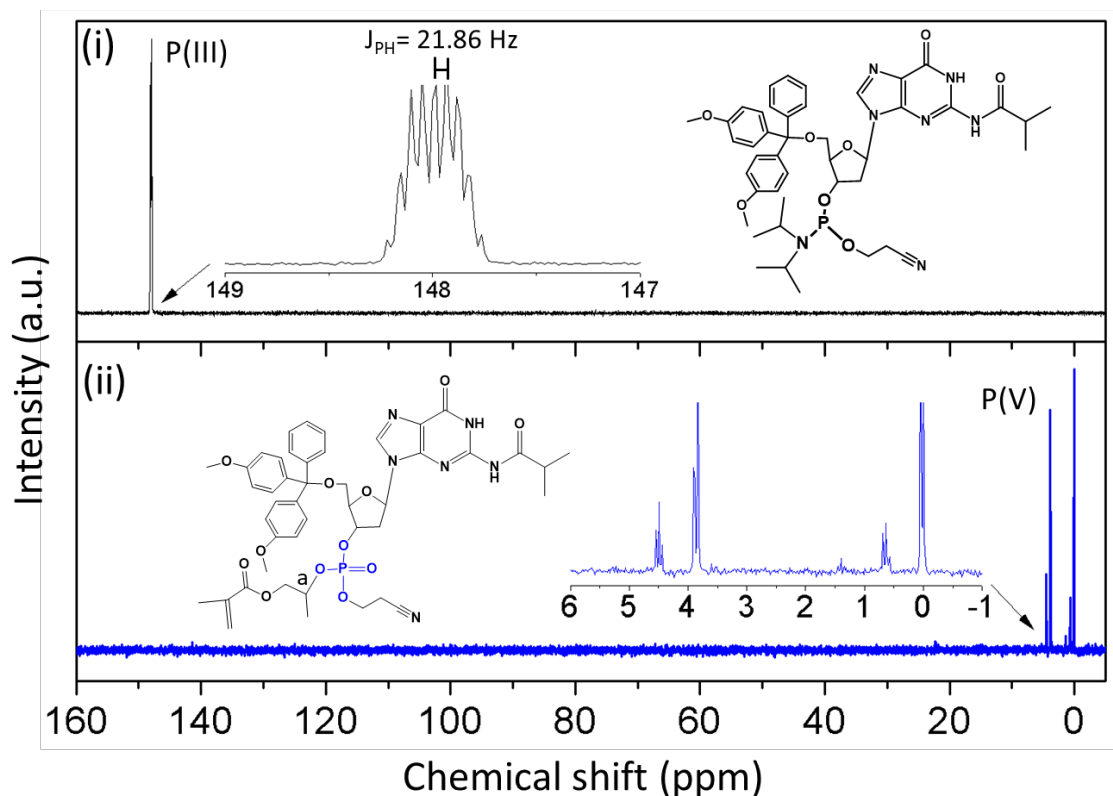


Figure 4.8  $^{31}\text{P}$  NMR spectra of (i) **G1** starting material and (ii) **G3** monomer with (inset) the 6 ppm to 1 ppm region. Spectra acquired in deuterated acetonitrile at 400 MHz.

This result showed a peak at  $\delta = 148$  ppm (multiplet  $^3J_{\text{PH}}=21.86$  (Figure 4.8(i)), associated with the P(III) oxidation state of the **G1**. This splitting was caused by the  $^3J_{\text{PH}}$  heteronuclear coupling with the protons on the cyanoethyl, DIPA, and nucleoside.

The **G3** monomer does not show this peak, indicating the complete conversion of the phosphoramidite. The peaks present are a pair of split peaks at  $\delta = 0$  ppm and  $\delta = 4$  ppm, centred on  $\delta = 2$  ppm (Figure 4.8(ii)).<sup>10</sup> These are associated with the chiral states of the phosphate that were formed following the oxidation from the deshielded P(III) state to the shielded P(V) state of the phosphate. The chiral centre of note is the phosphate itself and the proton on the oxypropyl group (Figure 4.8(ii, inset a)).

These results from the  $^1\text{H}$  and  $^{31}\text{P}$  NMR spectroscopy analysis show that the **G1** has been converted to a phosphate, and that the HPMA has been incorporated. The splitting and shifts present in these spectra support the conclusion that the **G3** monomer has been synthesised. This further supports the results of the ESI-MS analysis discussed in Section 4.3.1, showing the successful synthesis of the **G3** monomer.

#### 4.4 Polymerisation of **G3** monomer

Following the synthesis of **G3** monomer, it was polymerised using the same RAFT method as the HEMA variant discussed in Chapter 3. Polymerisation included the use of azobisisobutyronitrile (AIBN) as the initiator, and 4-cyano-4-(phenylcarbonothioylthio)pentanoic acid *N*-succinimidyl ester (NHS-RAFT) as the RAFT mediator. This polymerisation resulted in the formation of poly(2-(5'-dimethoxytrityl-*N*-isobutyryl-2'-deoxyguanosine-monophosphate)oxypropyl methacrylate), or **G4**, as shown in Figure 4.9.

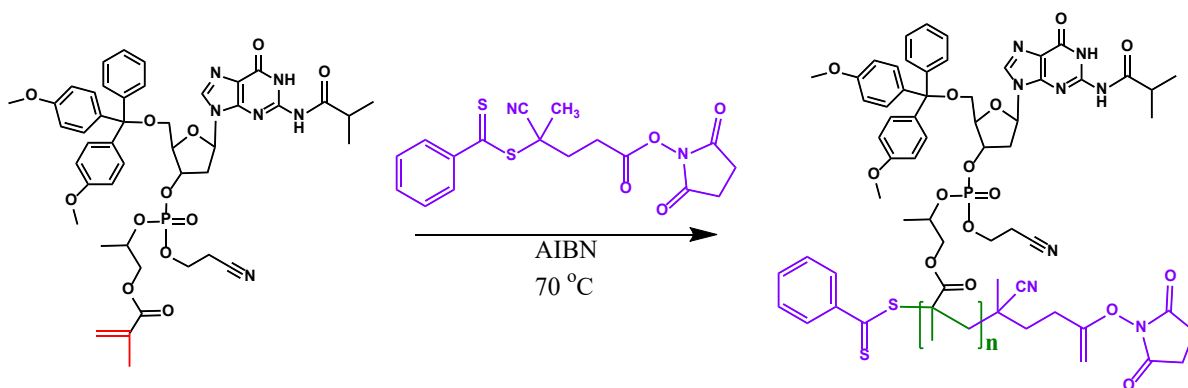


Figure 4.9 Polymerisation of **G3** monomer showing the starting vinyl group (red) converted to the alkyl group (green) and the incorporation of the NHS-RAFT agent (purple).

As discussed in Chapter 3 Section 3.4, the three components necessary for the synthesis of the polymer by RAFT mediated polymerisation were the initiator used to begin the polymerisation, namely AIBN, the monomer which forms the bulk of the polymer (**G3** monomer), and the RAFT mediator which helps to control the polymer synthesis (NHS-RAFT).

#### 4.4.1 Preliminary Testing for RAFT Polymerisation of G3 Monomer

Following selection of the NHS-RAFT agent, the polymerisation was tested to determine if the **G3** monomer was able to undergo RAFT mediated polymerisation without forming a gel. To do this, the polymerisation was conducted with a relatively high concentration of the initiator and RAFT agent compared to the monomer, specifically a molar ratio of 20:4:1 monomer: RAFT agent: initiator.

The **G4** was isolated from solution using a phase extraction with water, resulting in a white precipitate. The mixture was then centrifuged and the solid **G4** collected. It is worth noting that the **G4** synthesised in acetonitrile often separated from solution as the reaction cooled down, and formed a second phase with high viscosity, approaching the properties of a gel. This phenomenon was presumably caused by the decrease in solubility of higher  $M_w$  **G4** in the acetonitrile as the polymerisation progressed.

This **G4** was unlike the **C4** gel described in Chapter 3. The **G4** was able to be dispersed in THF where the **C4** gel previously described in Chapter 3 only had only swelled in the same solvent. Further, when exposed to water the **G4** instead precipitated to a loose white powder, where the **C4** gel had absorbed the water.

To determine the  $M_w$  and  $D$  of the **G4**, the sample was analysed by SEC. Due to the compatibility of the available columns, the **G4** sample was first freeze-dried to remove excess acetonitrile and washed again with water, then freeze-dried a second time to remove any residual solvents. The resulting **G4** powder was solvated in THF at 1 mg/mL and measured using SEC with a refractive index (RI) detector and polystyrene standards, Figure 4.10 and Table 4.1.

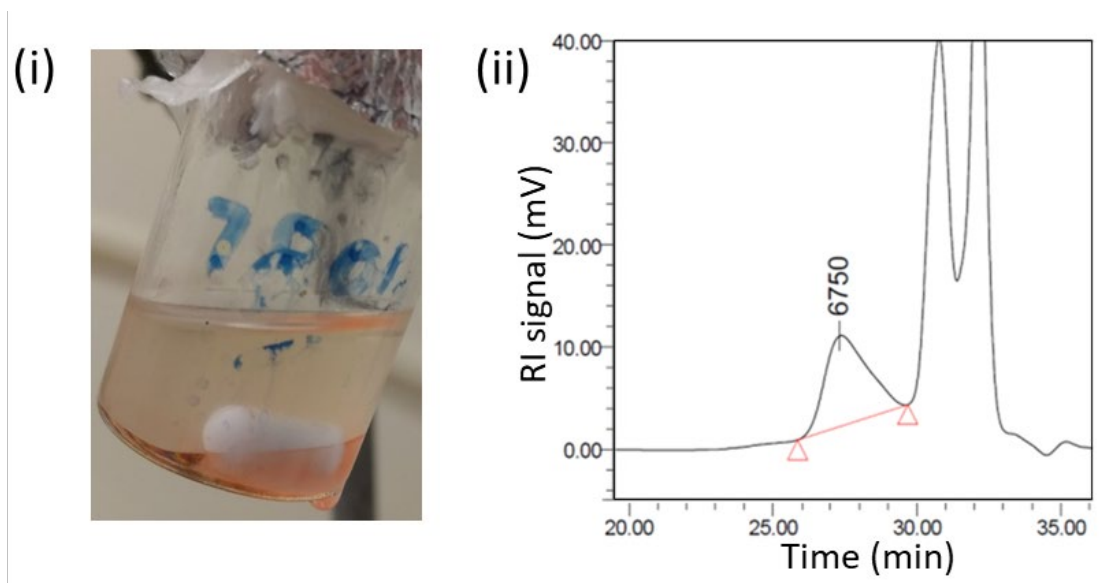


Figure 4.10 (i) Photo showing the phase separation of **G4** upon cooling of the polymerisation mixture, and (ii) DRI chromatogram and results of the 24 h polymerisation of **G4**, showing the formation of a polymer, 6750 Da. at 27.5 min attributed to the **G4**. Additional peaks at 31 min is attributed to the monomer and 32.5 min to DMT residue in solution.

**Table 4.1:** Results of polymerisation of **G3** monomer over 24 h.

	<b>24 h Polymerisation</b>
$M_n$	5090 Da
$M_w$	6060 Da
MP	6750 Da
DP	7.08 units
$\bar{D}$	1.12

The SEC result showed a  $M_w$  of 6060 Da indicating a DP of 7 (Figure 4.11) and thus essentially an oligomer. This was determined by subtracting the  $M_w$  of the NHS-RAFT unit (376.45 Da) and dividing the remaining  $M_w$  by the  $M_w$  of the **G3** monomer (882 g/mol). This increase in molecular weight showed that the **G3** monomer had undergone radical polymerisation. The DP is higher than that expected based on the starting molar ration of 5:1 monomer: CTA, which would give a theoretical maximum DP of 5. This could be caused by a number of factors. Most

apparent is that the PMMA standards used for SEC are not a perfect analogue to the **G4** as there may be a difference in solubility or the formation of aggregates that causes them to migrate faster through the column. Based on this alone the DP and  $M_w$  can not be accurately determined.

For the **G4** the  $D$  of 1.1 found showed that the polymers were relatively uniform in length compared to a non-mediated polymerisation. There is sufficient data to suggest that the polymerisation has proceeded under RAFT mediation as the reported low  $D$  is consistent with the standard bounds of  $D < 1.2$ .<sup>11</sup> This was calculated within the processing software based on the formulas shown in Chapter 1, Section 1.5.2.

The peaks at 31 minutes (880 Da) and 32.5 minutes (303 Da) were determined to be residual monomer monomer and DMT respectively. This indicates the incomplete conversion of the monomer which is not ideal, a more complete analysis of the maximum attainable  $M_w$  for the monomer is presented in Section 4.5.2. Importantly there is a large peak attributed to the presence of free DMT in solution indication the partial degradation of the monomer or polymer. As this is the removal of a protecting group, just earlier than anticipated in the procedure, it was not considered an impedance in the continuation of the project.

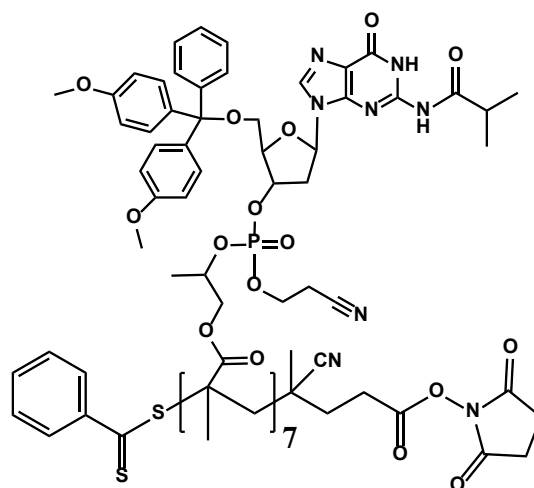


Figure 4.11 Structure of the **G4** heptamer. Note that following polymerisation it has not been treated in a way that would remove the NHS protecting group.

#### 4.4.2 Confirmation of polymerisation of DMT-dG-CE-P-PMA Phosphate by $^1\text{H}$ NMR

Confirmation of the polymerisation of **G3** to the **G5** was conducted using  $^1\text{H}$  NMR spectroscopy in deuterated acetonitrile resulting in the spectra shown in Figure 4.12.

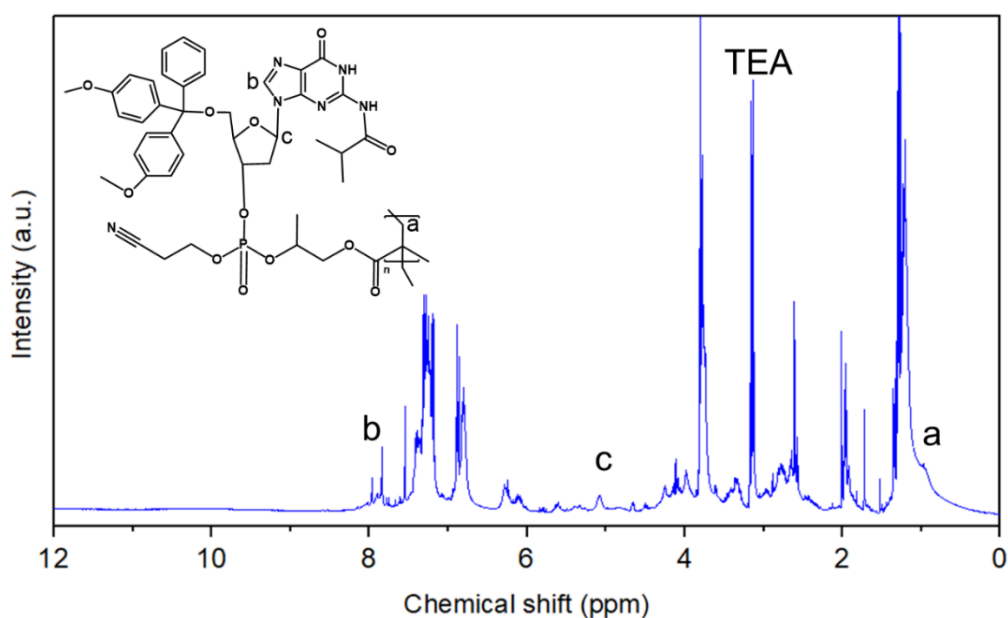


Figure 4.12  $^1\text{H}$  NMR spectra of **G4** in deuterated acetonitrile with majority noted peak allocation indicating (a) polymerisation, (b) nucleobase retention and, (c) the ribose connection between them. Spectra acquired in deuterated acetonitrile at 400 MHz.

Polymerisation was observed as the disappearance of the vinyl peak at  $\delta = 5.6$  ppm associated with the alkene group that is converted into the alkyl backbone during the polymerisation. This then creates a broad shoulder peak at approximately 1 ppm from the polymer backbone (Figure 4.12(a)). The peak associated with the C8 proton on the guanine nucleobase is present at 7.8 ppm (Figure 4.12(b)) indicating that the nucleobase has been retained with the polymer. Confirmation that the nucleobase remains attached to the polymer through the ribose is shown by the presence of the broad peak at  $\delta = 5.1$  ppm from the proton on the C2 carbon of the ribose unit (Figure 4.12(c)).

The general broadening of peaks across the spectrum suggests that a polymer has been formed, as this behaviour is indicative of the multiple similar chemical states caused by each repeating unit. This further supports the conversion and synthesis of a polymer under these conditions.

#### 4.4.3 Solvent Effect on Polymerisation of G3 Monomer

Following successful polymerisation of the **G3** monomer in acetonitrile, the polymerisation was tested in dimethylformamide (DMF) to investigate what effect the solvent had on the polymerisation. This was done to determine if further polymerisations should be conducted in a different solvent.

This effect of the solvent on the rate and conversion of the polymerisation can come from the solvent affecting the energy required for propagation which leads to differences in the rate constant as a result. Working out the specific reaction values was beyond the scope of this thesis, but determining what effect the solvent had qualitatively was a necessity.

To determine the solvent effect on polymerisation, the polymerisation of **G3** with NHS-RAFT and AIBN was prepared for both solvents (acetonitrile and DMF) and run concurrently. For these polymerisations two samples of 0.1 g **G3** monomer with NHS-RAFT and AIBN at a



molar ratio of 100:1:0.3 were prepared and solvated in 10 mL of either dry DMF or dry acetonitrile.

The resulting mixtures were degassed with dry N<sub>2</sub>, followed by heating to 70 °C for 2 h under inert atmosphere. This 2 h period was shorter than the test polymerisation shown previously in Section 4.4.1, for two reasons. Firstly, it introduced a second piece of evidence to further show the compatibility of the NHS-RAFT to provide mediation under different conditions. If the RAFT mediation of the polymerisation was effective, then it should be effective over differing time scales.

Secondly, by using a shorter time period for the polymerisation, any effects of the phase separation (seen in Figure 4.10(i)) would be less likely to affect the result. If the longer polymer chains decreased in solubility, it would affect the rate of the polymerisation as this process would effectively remove them from the reaction. By decreasing the polymerisation time the polymer synthesised would have a lower M<sub>w</sub> resulting in better solubility and preventing this influence.

During this time there was a slight change in colour of the DMF sample, losing the pink hue associated with the NHS-RAFT agent, Figure 4.13. This yellowing can be attributed to the presence of free amines in the DMF that can cleave the RAFT agent. Following the 2 h period, the polymerisation was thermally quenched by placing it into liquid nitrogen, before exposing it to air.

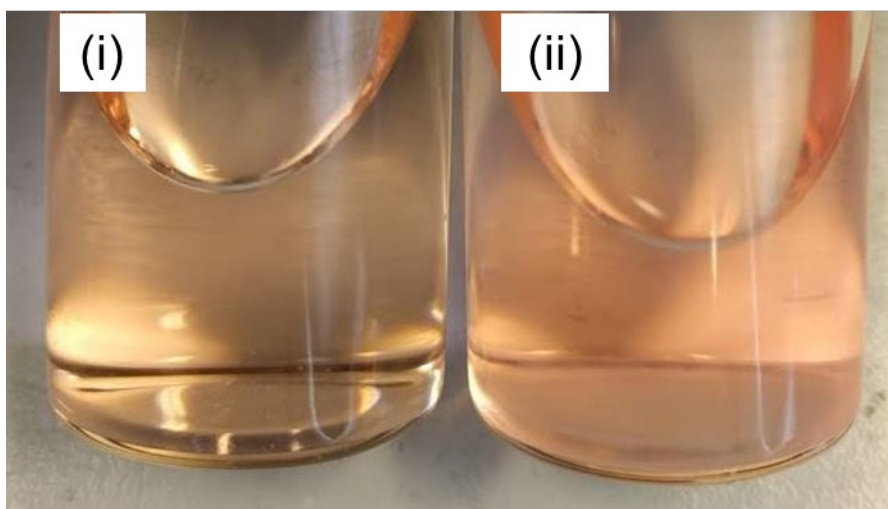


Figure 4.13 Difference in solution hue of the **G5** reaction mixture with (i) DMF and, (ii) acetonitrile as solvent after 2 h.

To analyse the polymerisation, the samples were dried by evaporation at ambient temperature with compressed air to remove residual solvent. The samples were then solvated in THF at 1 mg/mL for analysis by SEC, Figure 4.14. Freeze-drying was not an option as the sample synthesised in DMF was incompatible with the equipment available. The results are shown in Table 4.2.

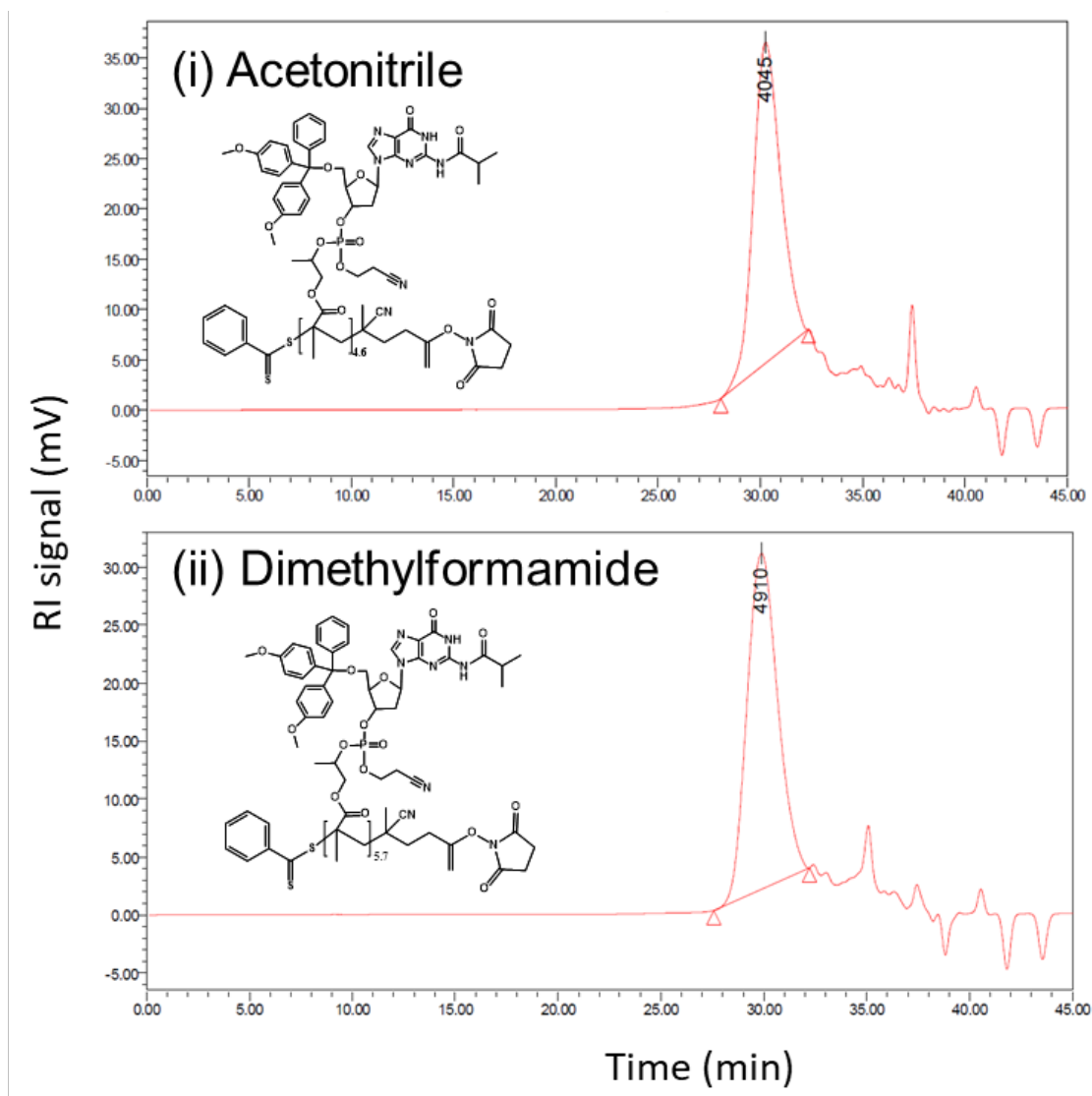


Figure 4.12 DRI chromatograms of **G4** polymerised for 2 h using either (i) acetonitrile, or (ii) dimethylformamide as the solvent. Numbers shown indicate the  $M_w$  at maximum.

**Table 4.2:** Results of polymerisation in different solvents over 2 h.

	Acetonitrile	Dimethylformamide
$M_w$ (Da)	4054	5003
DP (units)	4.6	5.7
$\bar{D}$	1.12	1.14

The DRI chromatogram showed that the 2 h polymerisation in DMF resulted in a higher measured molecular weight (5033 Da) compared to that achieved with acetonitrile (4054 Da) over the same 2 h period. As with the previous sample the  $M_w$  reported can not be considered

accurate but does still allow for conclusions to be drawn on the relative rate of reaction. The higher  $M_w$  represents that roughly one additional **G3** monomer unit had been incorporated per chain. As the polymerisation was conducted over the same period, this suggested that the DMF increased the rate of polymerisation.

Comparing the two polymerisations, there was also a change in the  $D$ . DMF showed a slightly higher  $D = 1.14$  compared to the  $D = 1.12$  for acetonitrile. The difference in  $D$  between the two solvents was small. In practice, it showed that the NHS-RAFT was roughly as effective at mediating the polymerisation when solvated in DMF as compared to acetonitrile. The experiment was conducted once, so there is no reported error, and the method for measuring the  $D$  is subjective, so this result did not provide a distinction between the two solvents. Due to the DMT-dG-CE-P-PMA phosphate monomer being prepared in acetonitrile, the decision was made to use acetonitrile as the solvent for further polymerisations as it was at this point a known value in the reaction procedure and the impact of a single addition was considered minor at the cost of possible degradation.

#### **4.5 Kinetics for the Polymerisation of G3 Monomer**

The two methods for measuring the rate of polymerisation considered for this project were *in-situ* and *ex-situ* measurements.

*In-situ* measurements have the benefit of being able to measure the direct conversion of monomer to polymer by the change in NMR spectrum peak intensity of specific groups. In this project it was the conversion of the monomer's alkene group to the polymer's alkane as the polymerisation progresses. This allows direct measurement of the conversion rate and degree of polymerisation but does not give insight to the mass properties on an individual strand basis, i.e., the method describes how much monomer was converted but not the  $D$  or the  $M_w$  of the

product. These values were collected following completion of the polymerisation using SEC, following the same method as used in Section 4.4.2.

*Ex-situ* measurements require removal of a fraction of the mixture as a sample to study at specific time increments during the reaction. Due to the removal of solution the number of samples that can be measured was limited by the volume of solution. Further, under normal laboratory conditions, there was a high risk of contamination by air due to repeated interactions with the solution, however, such risk can be minimised with the use of a glove box or similar isolation equipment. For this thesis *ex-situ* samples were collected using the automated Chemspeed SWING robotic synthesis platform based at CSIRO Clayton, Victoria, Australia. The Chemspeed SWING robotic synthesis platform is an automated system that operates under a dry nitrogen atmosphere and can collect samples automatically using a syringe pump. The machine is shown, and procedure described, in Chapter 2, Section 1.5.2.3.2.

#### 4.5.1 *In-situ* $^1\text{H}$ Nuclear Magnetic Resonance (NMR) Spectroscopy Kinetic Measurements

The kinetics of the polymerisation were measured *in-situ* using an NMR spectrometer by pinch sealing the reaction solution in glass NMR tubes, which had been previously backfilled with nitrogen. The benefit of this method was that the number of data points was only limited by the time it took for each individual measurement to be made (2.5 min), as the total volume of solvent (1 mL) was maintained throughout the reaction. In principle, this method allowed for more consistent analysis because once the reaction was sealed it could not be contaminated. This seal prevented oxygen or water entering the system and quenching the reaction, as is a risk with *ex-situ* measurements.

The disadvantage to using NMR spectroscopy as a method for measuring the kinetics of polymerisation was the need of a deuterated solvent, which meant that any significant scale of

polymerisation became prohibitively expensive. Further, deuterated solvents can influence the kinetics of a reaction of this type through the difference in the stabilisation of the radical intermediate created during the propagation phase of the polymerisation, changing the chiral preference of subsequent monomer additions.<sup>12</sup>

Samples for the NMR *in-situ* spectra kinetics measurements were first prepared by dissolving the **G3** monomer (1 g) into deuterated acetonitrile (6 mL) with NHS-RAFT (60 mg) and AIBN (8.5 mg) for a molar ratio of 20:4:1, replicating the ratio used in Section 4.1. This volume was then degassed with dry N<sub>2</sub> and divided into 5 sealed NMR tubes under inert atmosphere. In order to do this, 2 syringes were sealed into the end of the NMR tube by melting the glass and pinching it closed. The syringe-modified NMR tube was then purged with N<sub>2</sub> for 10 min to ensure there was no oxygen remaining. The polymerisation mixture (1 mL) was then added to the tube and the other end of the tube was sealed by melting and pinching it shut with pliers, fusing the glass.

The sample compartment within the NMR instrument was then heated to 70 °C while containing a ceramic spinner and one of the five samples of the polymerisation mixture, denoted as the "locking sample". This locking sample was used to maintain the NMR phase lock as the instrument was heated. This was needed as the heating of the solvent affects the shift, which can result in the instrument failing to achieve a successful lock. If this lock was not obtained the samples would not be comparable.

The heating was completed in 10 °C increments, with a 15 min hold time to equilibrate at each temperature increment. This procedure was required to ensure the non-magnetic alloys used in the NMR probe were not damaged by sudden temperature change. Locking and shimming was also conducted at each of the equilibration points to ensure that the instrument auto-lock and shim could account for the effects of higher temperature on the chemical shift.

When the temperature had equilibrated at 70 °C, the locking sample was removed and replaced with the sample of **G3** monomer polymerisation mixture to be analysed. A series of <sup>1</sup>H NMR spectra were acquired using 16 scans. This process required 2.5 min per time increment, with a 10 min delay between each set of the scans, resulting in the time separation of 12.5 min between each data point. This process was then repeated a total of 4 times, the fifth sample having been used as the locking sample.

When taking *in-situ* measurements the conversion would normally be measured by comparing the decrease in the integration of the alkene peak associated with the **G3** monomer at 5.4 ppm (Figure 4.7(b)) with the appearance of the peak associated with the polymer at 1.2 ppm. However, in the case of the **G4** an additional peak at 1.8 ppm associated with the formation of the alkyl backbone overlaps with the signals from the nucleotide moiety.

The increased temperature appeared to affect the lock and shim enough that it caused a downfield shift of the 5.4 ppm peak associated with the alkene to 5.6 ppm. As a result, a method was developed to measure the decrease in the integration of the vinyl peak at 5.6 ppm (shown in Figure 4.7(b)).<sup>13</sup>

To measure the conversion the integration of the 5.6 ppm peak was measured over time (Figure 4.13(i)). To do this the ratio of this peak had to be normalised to the 3.1 ppm peak associated with the triethylamine residue from the isolation of the **G3** monomer. The integration ratio of the 5.6 ppm vinyl peak was then plotted against time to determine the kinetics of the polymerisation Figure 4.15.

Over the first 3 time points (37.5 min) there was a steep upward trend. Based on prior literature this represented the rapid decomposition of the AIBN initiator and its first addition to the **G3** monomer.<sup>14</sup>

Following the first addition there was a plateau until 100 min. This was attributed to the first addition of the **G3** monomer reacting preferentially with the NHS-RAFT, rather than propagating with other monomers in solution. This created the macro-RAFT agent, as shown in Figure 4.16(inset). This phenomenon has been previously discussed in Chapter 1, Section 1.5.4.

Following this, from 147.5 min there was a linear trend during the propagation phase of the reaction. Here, the macro-RAFT agent reacts with the **G3** in solution, incorporating it into the propagating chains through addition to the alkene group. This causes the decrease in the alkene concentration as it was converted to the alkyl backbone of the polymer. The mechanism for this process is shown in Chapter 1, Section 1.6.

Over the 4 runs the results showed a low level of variance (indicated by the consistent error bars) and linear growth over the remainder of the 850 min period, indicating that the polymerisation was progressing under RAFT mediation.



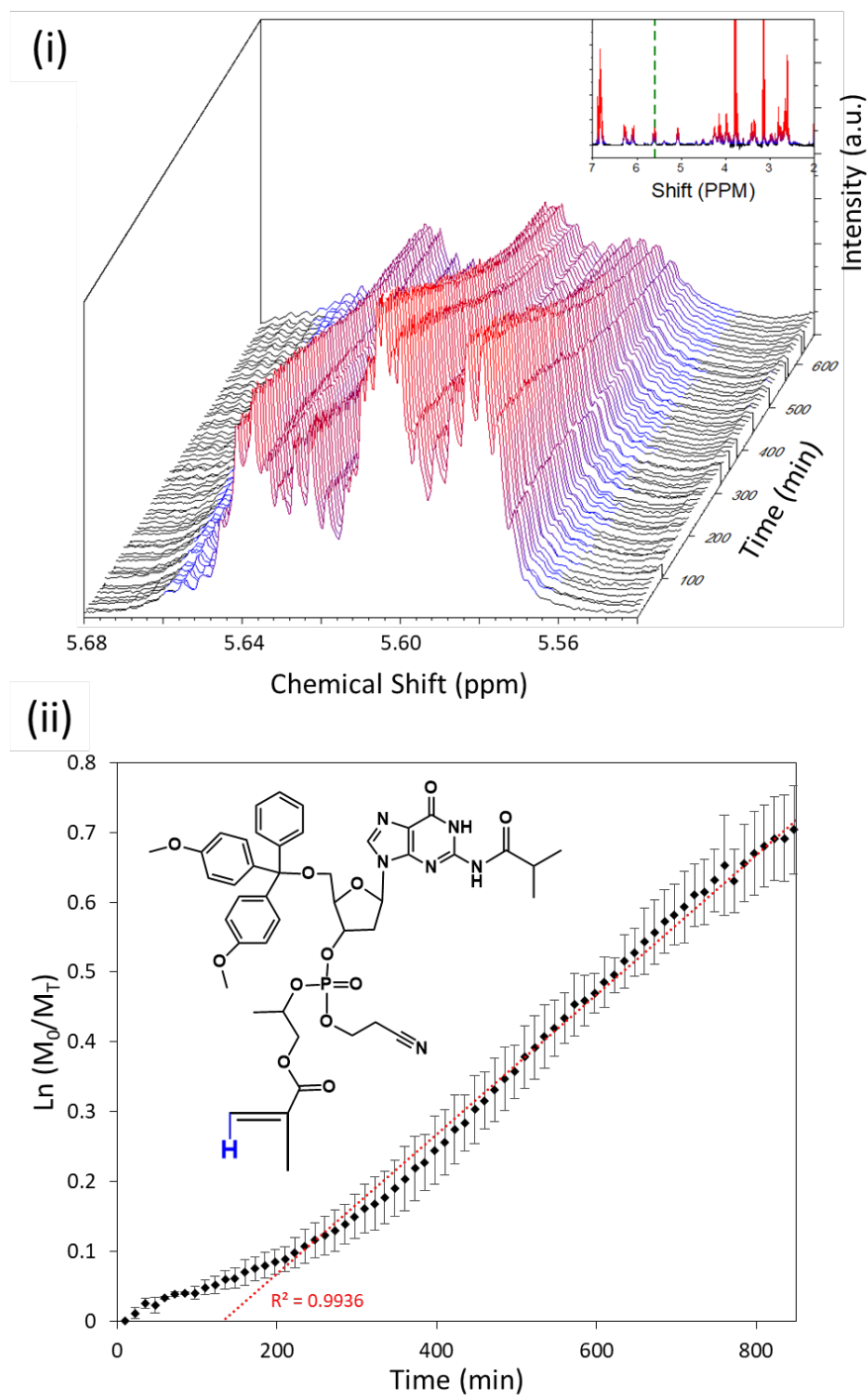


Figure 4.15 (i) Waterfall graph showing the decrease in magnitude of the 5.6 ppm peak associated with the vinyl proton as the polymerisation of **G3** with stacked spectrums (inset) and, (ii) kinetic measurements of the conversion of **G3** monomer, calculated using the peak ratio of the 5.6 ppm peak associated with the vinyl proton (blue) average of 4 samples. Linear fit from 147.5 minutes shown in red. Spectra acquired in deuterated acetonitrile at 400 MHz.

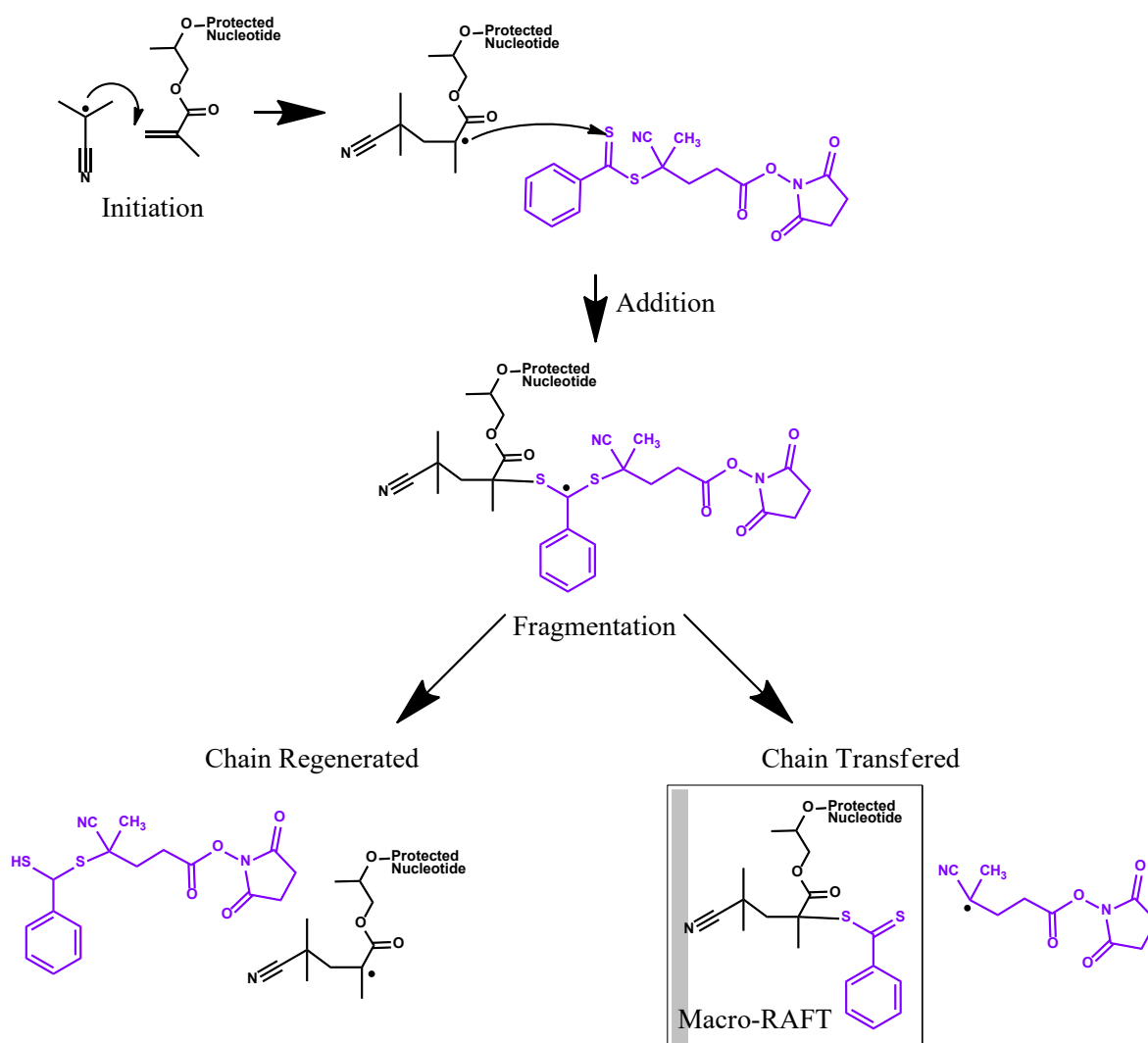


Figure 4.16 Stages in the first addition during the RAFT polymerisation of **G3** monomer through the stages of initiation, addition, and fragmentation. This process is reversible as the radical group created by the transferred chain can recombine with the dormant chain, the one not containing the radical. The transfer of the thiol to the propagating chain generates the macro-RAFT agent.

#### 4.5.2 *Ex-situ* Kinetics Determined by Size Exclusion Chromatography.

For the *ex-situ* kinetic measurements, the experiments were conducted on a Chemspeed SWING robotic synthesis platform, shown in more detail in Chapter 2, Section 2.5.2.3.2. This is an automated system used for running arrays of experiments simultaneously and is typically

used for formulation variations. For measuring the polymerisation of **G3** monomer it allowed for the reaction to be run both in triplicate and simultaneously.

The Chemspeed system was required for *ex-situ* measurements as the inert atmosphere could not be maintained using the conventional lab setup. When the polymerisation was conducted using manual syringing with positive N<sub>2</sub> pressure only the first sample could be consistently acquired. Following this the reaction solution would turn dark brown to black as if burning. Potentially this could be overcome using an alternative methodology, but as the Chemspeed was available and able to perform more consistently it was chosen instead.

To measure the polymerisation, **G3** monomer was prepared with the NHS-RAFT and AIBN in a molar ratio of 100:1:0.25 in acetonitrile. This ratio was substantially higher in monomer than that used for the *in-situ* kinetics, discussed in Section 4.5.1. The choice to use this ratio was made so that the automated system could determine if there was maximum molecular weight achievable with acetonitrile as the solvent. By testing with acetonitrile this would indicate if the solvent limited not only the rate, as discussed in Section 4.4.1, but the M<sub>w</sub> achievable.

Based on the molar ratio 100:1:0.25 of **G3** monomer: NHS-RAFT: AIBN, the calculated maximum M<sub>w</sub> for the resulting polymers was 78 kDa. This is provided by Equation 4.1 and based on full conversion of the monomer into polymer, complete reaction with the RAFT agent, and complete decomposition of the initiator.

$$\textit{Theoretical } M_w = \frac{[\textit{Monomer}]}{[\textit{Initiator}] + [\textit{RAFT Agent}]} \quad \text{Equation 4.1}$$

The **G3** monomer samples were polymerised in triplicate at 70 °C with 1 mL samples collected at each time point. Following the collection of all time points, the 1 mL **G4** samples were freeze-dried for 24 h until the pressure equilibrated at 0.019 mbar. The **G4** samples were then

solvated in 1.5 mL DMF each and analysed using SEC against PMMA standards. The results of these measurements were then collected and plotted, as shown in Figure 4.17.

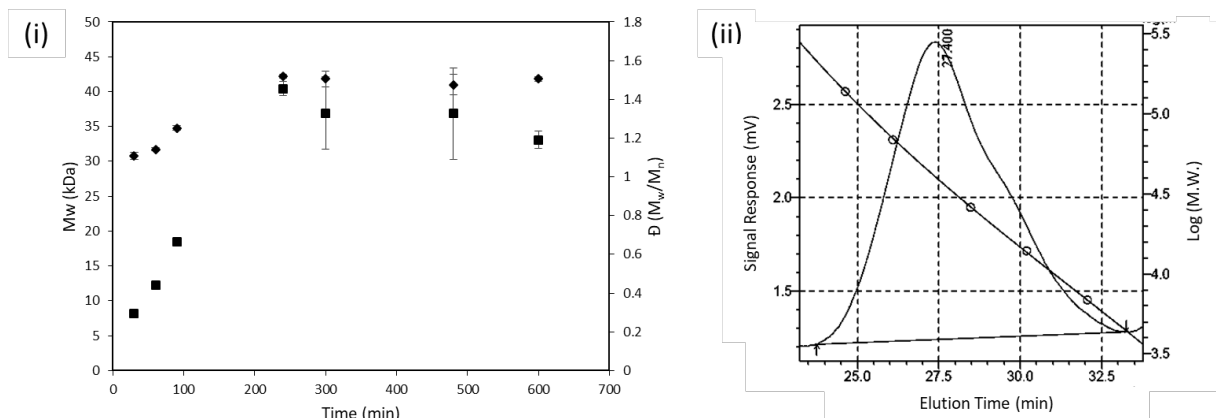


Figure 4.17 (i)  $M_w$  of **G4** (square) and the corresponding  $D$  (diamond) over time calculated from SEC and, (ii) example DRI chromatogram for the 240 min sample of **G4**. Further example DRI chromatograms can be found in Appendix 3.

These results showed that initially there was a noticeable increase in  $M_w$  between 0 and 240 min as the polymerisation progressed. Following the initial increase achieving a maximum  $M_w$  of 40 kDa, equivalent to a DP of 43, there was an 18% decrease in  $M_w$  over the subsequent 360 minutes. This indicates that the polymerisation had stopped and that the product may have been undergoing thermal degradation, likely partial deprotection of some repeating units based on the results presented in section 4.4.1.

Over the first hour of polymerisation the  $D$  appears to remain below the threshold for RAFT polymerisation to be controlled ( $D < 1.2$ ) and the  $M_w$  has increased above that seen in Section 4.4.1. Following this time however the  $D$  begins to rise to over 1.5. The change in  $D$  over time indicates that there is a loss of control for the polymerisation, potentially caused by the change in solubility of the polymer inhibiting the ability for the chain addition step based on other results. Further, the increased variance in the  $D$  at 300 minutes and 480 minutes matched the

increased variance in the  $M_w$  at these time points, further supporting the partial decomposition of the polymer. As the SEC indicated the conversion of  $M_w$  and not  $M_n$

These observations suggested that the maximum  $M_w$  achievable by this method was a DP of 43. Combined with the results of the bulk polymerisation, being able to reach higher molecular weights will likely require further optimisation of the solvent system, either adjusting concentration or changing the solvent entirely, which could in turn need the RAFT agent and possibly initiator to be altered.

#### **4.6 Activation of the Guanine Nucleobase in G4**

Following the successful synthesis of **G4**, the activation of the nucleobase functionality was required to investigate the binding properties of the nucleobase. This was done through the two step process: deprotection and detritylation.

The proper, deprotection, removes the cyanoethyl group from the phosphate and the isobutyryl from the guanine. The latter, detritylation, removes the dimethoxytrityl protection from the 5' hydroxyl on the ribose. Completion of these steps results in poly(2- (2'-deoxyguanosine monophosphate)- methacrylate), or **G6**; the process is summarised in Figure 4.18.

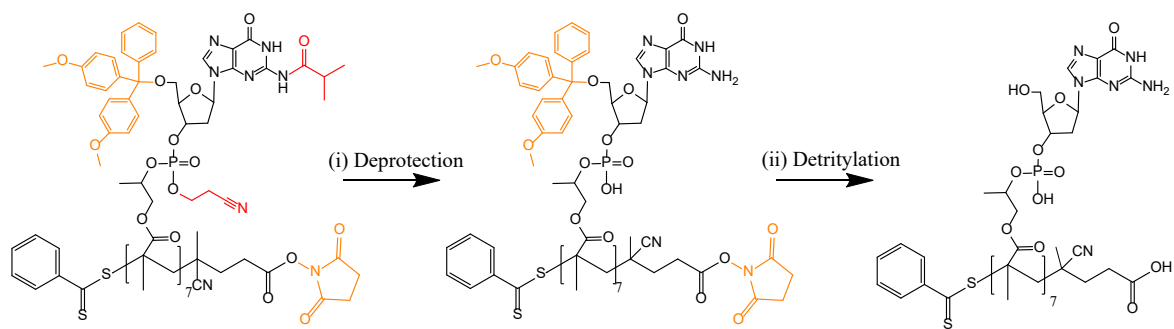


Figure 4.18 Process for the conversion of **G4** into **G6** through (i) deprotection removing the CE protecting groups shown in red and, (ii) detritylation removing the groups shown in orange.

#### 4.6.1 Deprotection

Deprotection of the polymer refers to the removal of the cyanoethyl protecting group from **G4** generating acrylonitrile (shown in Figure 4.19(i)) and the removal of the isobutyryl protection from the guanine (Figure 4.19(ii)). The deprotection was performed by treating **G4** with a gross excess of 30% ammonia at 50 °C. This high concentration of ammonia was important as lower concentrations result in incomplete deprotection. The reaction was monitored by the solvation of the polymer in the aqueous media. As the **G4** was deprotected the formation of the phosphate significantly changes the solubility as it is able to form the phosphate anion. For low molecular weights the **G5** was completely solvated; for higher  $M_w$  the solution formed a white suspension, shown in Figure 4.19(iii).

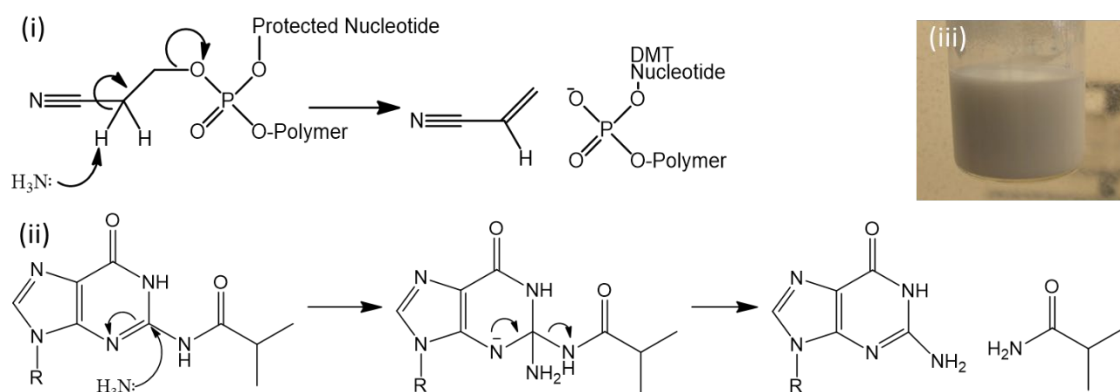


Figure 4.19 (i) Mechanism for the removal of the cyanoethyl protecting group by ammonia resulting in acrylonitrile and **G5** and (ii) mechanism for the removal of isobutyryl protection from guanine using ammonia (iii) the white colloidal suspension of **G5** generated.

#### 4.6.2 Detritylation

Detritylation is the removal of the dimethoxytrityl (DMT) protecting group from the 5' carbon, generating the hydroxyl moiety. This step was conducted with addition of glacial acetic acid and resulted in bright orange solution, as shown in Figure 4.20(i and ii). The benefit of using this method was that it also removed any remaining protection from the nucleobase in the form of dimethylformamide. The choice of acetic acid was made as it was easier and safer to work with than trichloroacetic acid (TCA) that would have given similar results otherwise. TCA has been used in literature because the detritylation process is typically carried out between phosphoramidite additions during DNA synthesis. The anhydrous conditions for detritylation required the use of a dry solvent, normally acetonitrile. As a result of the detritylation being conducted following complete synthesis, rather than between cycles, exposure to water was not an issue as the presence of water does not pose a risk to further reactions in this case. The mechanism for the removal of the DMT group is shown in Figure 4.20(iii)

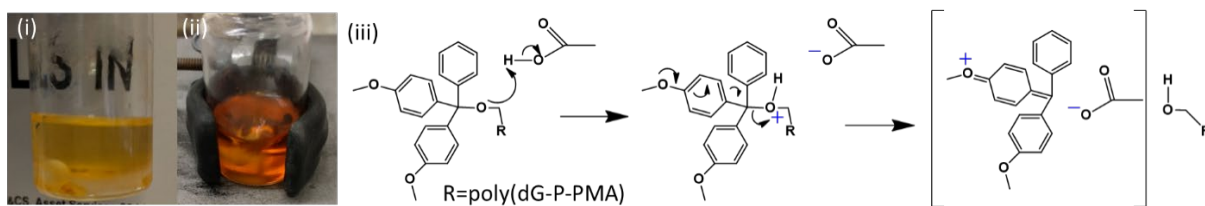


Figure 4.20 The orange colour produced as a result of the acetic acid addition to the **G5** from (i) immediately after addition to (ii) 5 min after addition with (iii) the mechanism for this conversion.

Exposure to acetic acid during the detritylation step also results in the removal of the NHS protecting group from the NHS-RAFT unit of the polymer and converting it into the pentatonic acid.

#### 4.6.2.1 Neutralisation Agents

At this stage of the experiment the **G6** was solvated at pH <3 as a result of the acetic acid used during the detritylation. The solution therefore needed to be neutralised to ensure that the guanine was not cleaved.

To perform the neutralisation the **G6** solution was treated with an acetate counter ion which was provided in the form of either sodium or lithium acetate. The addition of the acetate caused a loss of colour as the orange DMT cation was converted to dimethoxytrityl acetate, a colourless compound.

#### 4.6.3 **Isolation**

Isolation of **G6** was performed to remove residual monomer and salts during the deprotection and detritylation phases. To achieve this, the **G6** mixture following detritylation was precipitated into propan-2-ol and chilled to -20 °C for 14 h. This method for desalting was chosen based on the literature for isolation of DNA synthesised using similar approaches.



Under these conditions DNA has been shown to precipitate at most  $M_w$  and even lower concentrations where ethanol is ineffective. In this work however, early instances where sodium acetate had been used in the detritylation step no precipitate formed. Instead the solution turned slightly opaque. Further investigation of this solution and its subsequent characterisation is presented and discussed in more depth in Chapter 5. The result was that the colloid was attributed to the formation of G-quartets, discussed in Chapter 1, Section 1.2.5.1, with the sodium cation.

To overcome this lithium acetate was used resulting in the polymerisation and isolation of **G6** from any residual monomer by centrifugation. The **G6** was then repeatedly washed with pure water to complete the desalting (removal of acetate and excess lithium). Final isolation of the polymer was achieved by drying the precipitate, which resulted in a solid white compound.

At this point it was found that the **G6** was limited in that it was insoluble in water, requiring the addition of propan-2-ol as a cosolvent. Polymers at all  $M_w$  tested appeared to be soluble in 10:1 water: propan-2-ol v/v, with the solutions appearing cloudy at other ratios tested. A test with acetic acid showed that it could allow for the solvation of the polymer without a secondary solvent, but the concentration of acetic required acid and the subsequent pH may damage the polymer so no further work was conducted to improve its solubility.

#### 4.6.4 Confirmation of Nucleobase Activation

Confirmation of the conversion of **G4** (Figure 4.21(i)) to the **G6** (Figure 4.21(ii)) was conducted using  $^1\text{H}$  NMR spectroscopy in deuterated dimethyl sulfoxide. Due to the low solubility of the polymer, the spectrum showed low signal-to-noise. However, it can be noted that the spectrum was simpler following deprotection compared to the **G4** suggesting that the polymer has now had bulky moieties removed resulting in fewer proton signals.

The removal of the DMT and CE protecting groups resulted in a change in solvent compatibility between the **G4** and **G6**. As a result the **G4** was collected in deuterated acetonitrile, while **G6** had to be collected in deuterated DMSO. This had a small effect on the proton chemical shift. It is notable that while both of these spectra were recorded under the same conditions the signal to noise ratio is significantly higher for the **G6** which is attributed to the low solubility.

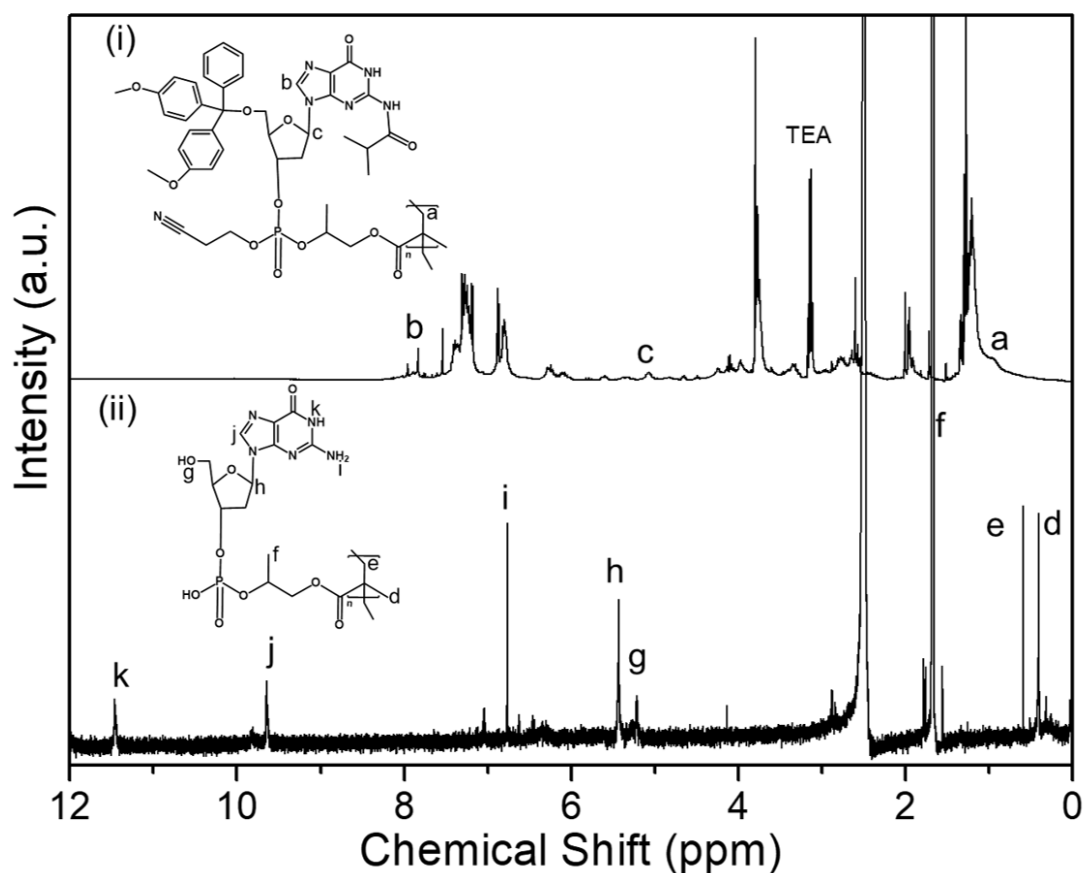


Figure 4.21 <sup>1</sup>H NMR spectra of (i) **G4** in deuterated acetonitrile and (ii) **G6** in deuterated DMSO. Spectra acquired in deuterated acetonitrile at 400 MHz.

The removal of the aromatic DMT groups caused the methacrylic backbone peaks to be up-shifted in the **G6** sample compared to the protected **G4**. As a result, the methyl peak from the alkyl backbone was observed at approximately  $\delta = 0.4$  ppm (Figure 4.22(ii, peak d)) and the

two ethylene protons were now observed at approximately  $\delta = 0.6$  ppm (Figure 4.22(ii, peak e)). The propyl linkage between the phosphate and the methacrylic backbone was seen as a series of peaks around  $\delta = 1.7$  ppm (Figure 4.20(ii, peak f)).

The activated guanosine units were observed as the appearance of peaks from the ribose and guanine. For the ribose, peaks were observed at  $\delta = 5.2$  ppm (C5'-OH) and  $\delta = 5.4$  ppm (H-2') (Figure 4.22(ii, peaks g and h respectively)). Finally, for guanine, peaks were observed at  $\delta = 6.7$  ppm (NH<sub>2</sub>),  $\delta = 9.6$  ppm (H-8) and  $\delta = 11.5$  ppm (NH) (Figure 4.22(ii, peaks i, j and k respectively)). These results confirmed the presence of the guanosine monophosphate nucleotides on the propyl methacrylate backbone.

#### 4.7 Conclusion.

This chapter showed the successful use of HPMA as a vinyl source in the generation of the vinyl functionalised nucleotide, **G3** monomer, using the phosphoramidite coupling method previously described in Chapter 3.

The polymerisation of the **G3** monomer using the RAFT polymerisation method resulted in polymers of low dispersity ( $D < 1.2$ ) indicating that the RAFT method was successful. This was further reinforced through the use of different conditions and reagent ratios of monomer: RAFT agent: initiator where the dispersity remained below the 1.2 threshold. This indicated the NHS-RAFT agent was able to mediate the polymerisation in acetonitrile. This resulted in a protected **G4** polymer.

Activation of the guanine moiety was achieved using similar deprotection procedures to synthetic DNA and resulted in the activated **G6** polymer. However this polymer formed a colloid which is investigated further in the following Chapter 5.

## 4.8 References

- (1) Roy, S.; Caruthers, M. Synthesis of DNA/RNA and Their Analogs via Phosphoramidite and H-Phosphonate Chemistries. *Molecules* **2013**, *18* (11), 14268–14284.
- (2) Grøndahl, L.; Suzuki, S.; Wentrup-Byrne, E. Influence of a Diene Impurity on the Molecular Structure of Phosphate-Containing Polymers with Medical Applications. *Chem. Commun. (Camb)*. **2008**, No. 28, 3314–3316.
- (3) Vargeese, C.; Carter, J.; Yegge, J.; Krivjansky, S.; Settle, A.; Kropp, E.; Peterson, K.; Pieken, W. Efficient Activation of Nucleoside Phosphoramidites with 4,5-Dicyanoimidazole during Oligonucleotide Synthesis. *Nucleic Acids Res.* **1998**, *26* (4), 1046–1050.
- (4) Smith, P. B.; Snyder, A. P. Electrospray Ionization Tandem Mass Spectrometry of Mixtures: Deconvolution by Parent-Ion Scans. *Rapid Commun. Mass Spectrom.* **1992**, *6* (6), 373–375.
- (5) Qian, K.; Edwards, K. E.; Diehl, J. H.; Green, L. A. Fundamentals and Applications of Electrospray Ionization Mass Spectrometry for Petroleum Characterization. *Energy and Fuels* **2004**, *18* (6), 1784–1791.
- (6) Emwas, A. H. M. The Strengths and Weaknesses of NMR Spectroscopy and Mass Spectrometry with Particular Focus on Metabolomics Research. *Methods Mol. Biol.* **2015**, *1277*, 161–193.
- (7) de Hoffmann, E. Mass Spectrometry. In *Kirk-Othmer Encyclopedia of Chemical Technology*; John Wiley & Sons, Inc.: Hoboken, NJ, USA, 2005.
- (8) Ugi, I.; Jacob, P.; Landgraf, B.; Rupp, C.; Lemmen, P.; Verfürth, U. Phosphite Oxidation

- and the Preparation of Five-Membered Cyclic Phosphorylating Reagents via the Phosphites. *Nucleosides and Nucleotides* **1988**, 7 (5–6), 605–608.
- (9) Masanori, K.; Akira, H.; Shinya, O.; Mamoru, H.; Mitsue, A.; Rie, K.; Hayakawa, Y. Ethyl(Methyl)Dioxirane as an Efficient Reagent for the Oxidation of Nucleoside Phosphites into Phosphates under Nonbasic Anhydrous Conditions. *Org. Lett.* **2001**, 3 (6), 815–818.
- (10) Li, Y.; Raushel, F. M. Differentiation of Chiral Phosphorus Enantiomers by <sup>31</sup>P and <sup>1</sup>H NMR Spectroscopy Using Amino Acid Derivatives as Chemical Solvating Agents. *Tetrahedron Asymmetry* **2007**, 18 (12), 1391–1397.
- (11) Moad, G.; Rizzardo, E.; Thang, S. H. Radical Addition-Fragmentation Chemistry in Polymer Synthesis. *Polymer*. Elsevier March 3, 2008, pp 1079–1131.
- (12) Green, M. M.; Peterson, N. C.; Sato, T.; Teramoto, A.; Cook, R.; Lifson, S. A Helical Polymer with a Cooperative Response to Chiral Information. *Science (80-. )*. **1995**, 268 (5219), 1860–1866.
- (13) Scales, C. W.; Vasilieva, Y. A.; Convertine, A. J.; Lowe, A. B.; McCormick, C. L. Direct, Controlled Synthesis of the Nonimmunogenic Hydrophilic Polymer, Poly(N-(2-Hydroxypropyl)Methacrylamide) via RAFT in Aqueous Media. *Biomacromolecules* **2005**, 6 (4), 1846–1850.
- (14) Foster, J. C.; Radzinski, S. C.; Matson, J. B. Graft Polymer Synthesis by RAFT Transfer-To. *Journal of Polymer Science, Part A: Polymer Chemistry*. John Wiley & Sons, Ltd September 15, 2017, pp 2865–2876.

# Chapter 5: Formation of G-quartets Utilising Nucleotide Functionalised Synthetic Polymers

## 5.1 Synopsis

*This chapter outlines the characterisation of poly(2-(2'-deoxyguanosine-monophosphate)oxypropyl methacrylate), referred to as **poly(dG-P-PMA)**, colloidal solutions following their synthesis as presented in Chapter 4.*

*The poly(dG-P-PMA) colloid was found to form as a result of sodium acetate being present, indicating the formation of G-quartet based secondary structures, as determined by circular dichroism and melting studies.*

## 5.2 Introduction

This chapter builds on some of the results described in Chapter 4. Specifically the formation of a colloidal solution from poly(2-(2'-deoxyguanosine-monophosphate)oxypropyl methacrylate) (**G6**) following isolation. This **G6** colloid formed during the desalting procedure discussed in Chapter 4 Section 4.6.3, and was attributed to the presence of sodium acetate (NaOAc) during the isolation.

The investigation of the **G6** colloid and its properties forms the basis for this chapter. First the specific characterisation of the **G6** samples that formed the colloid will be presented, followed by an investigation of causes for the colloid forming. This will include the effect of different salts, lithium acetate (LiOAc), NaOAc and potassium acetate (KOAc), as they relate to the secondary structures of **G6**.

The nature of the **G6** suspension was determined using scanning electron microscopy (SEM) and dynamic light scattering (DLS). This determined that the colloid led to the formation of spherical particles in solution, and that the formation of these particles was solvent dependant.

This led to the hypothesis that G-quartets were influencing the formation of the particles. The formation of secondary structures within nucleic acids was not a new phenomenon. The DNA double helix was most notable of these but others, such as the *i*-motif and G-quadruplex discussed in Chapter 1 Section 1.2.5, have been shown to form in both natural and synthetic systems.<sup>1-3</sup> Based on this hypothesis, experiments were conducted using circular dichroism (CD) spectroscopy, fluorescence microscopy and melting behaviour of the **G6** to determine if G-quartets were the cause of particle formation.

### 5.2.1 Size Exclusion Chromatography (SEC) of G6

The **G6** samples used in this chapter were all derived from the same batch of synthesised **G4**. This batch was synthesised using the method presented in Chapter 2, Section 2.4.2.2. Prior to deprotection and detritylation SEC showed that this batch of **G4** was a hexamer, a polymer 6 units in length, shown in Figure 5.1.

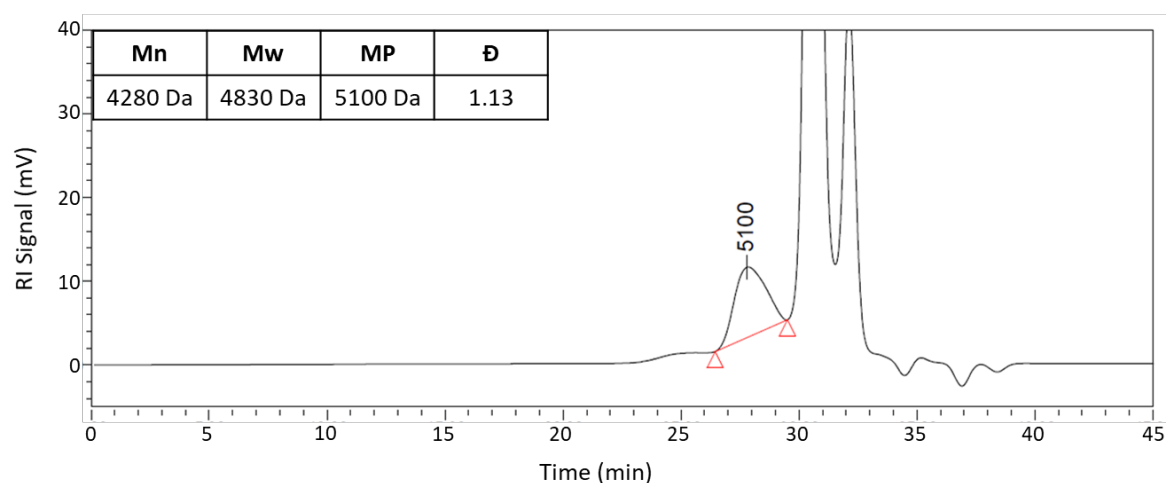


Figure 5.1 DRI chromatogram of **G4** hexamer prior to deprotection, with specific results inset. Note, the large peaks at 30.5 min and 32 min were attributed to cleaved DMT and residual monomer, respectively, based on their elution time and the corresponding  $M_w$ .

Following deprotection and detritylation (Figure 4.17 and 4.18, respectively), the **G6** was again analysed with SEC using a 10 mM TRIS-HCl (trisaminomethane/hydrochloric acid) aqueous buffer to account for the change in solubility caused by the removal of the dimethoxytrityl (DMT) protecting group, at a loading of 1 mg/mL. The mass of the **G6** was found to have increased significantly. This elution time exceeded the calibration and measurement capabilities of the SEC columns available at the time.

SEC works based on the same separation principle as any chromatography technique, differing affinity to either the mobile phase solvent or stationary phase column causes different



compounds to separate. In the case of SEC this is due to the porosity of the stationary phase in the column and the hydrodynamic diameter and solvent dimensions of the analyte, in this case the polymer. A smaller diameter leads to greater binding and therefore a longer elution time indicates a lower  $M_w$ . The rapid elution of the **G6** sample therefore showed that the  $M_w$  of the samples was higher following deprotection. An increase in  $M_w$  from the removal of the protecting groups did not appear to make sense, as similar methods are used in the synthesis of ssDNA to near quantitative levels. The more likely possibility was that the polymer had formed a larger secondary structure.

This was hypothesised to be due to the secondary interactions of the **G6** causing the formation of larger structures. These larger structures could simulate the effect of a higher mass polymer, preventing the binding to the column which prevents the technique from being effective. This supported the hypothesis that **G6** was forming particles in solution. Due to this being a homopolymers it was not going to be the result of a canonical duplex forming between the nucleobases.

### 5.3 Formation of G6 Particles

The formation of the colloidal **G6** occurred following the detritylation of the **G5**. For the detritylation procedure the **G5** was treated with an excess of with acetic acid, and subsequently neutralised with sodium acetate.

In practice most Brønsted-Lowry acids of high pKa would have worked. In literature trichloroacetic acid in dry DCM was typically used as it maintain the anhydrous conditions required for the next coupling stage in the DNA synthesis. As the **G6** synthesis was now completed the presence of water was not an issue, allowing for the use of acetic acid instead.

This also minimises the risk of depurination occurring due the higher pKa for acetic acid (4.76 compared to the 0.51 of trichloroacetic acid).

As the detritylation reaction requires a low pH simply using a stoichiometric (1:1) ratio of repeating unit to acetic acid would have resulted in incomplete deprotection.<sup>4</sup> Following exposure to acid the **G6** required neutralisation to prevent acid catalysed degradation of the nucleotide moiety of the **G6**. This resulted in an aqueous solution containing sodium salts that were normally removed through column extraction, precipitation, or filtration.<sup>5,6</sup>

Due to the novel structure of **G6**, phase extraction was chosen as the isolation method as it would require less workup than other methods. This method of isolation was consistent with those used for the isolation of short chain oligonucleotides and DNA by precipitation.<sup>7,8</sup> Isolation of nucleic acids with salt precipitation works by screening the charge on the phosphate allowing it to aggregate in solution.<sup>9</sup>

The process for the desalting of **G6** was to precipitate it into propan-2-ol in a ratio of 5:1 (v/v) propan-2-ol:water (Chapter 2, Section 2.4.2.4). Instead of precipitating the **G6** formed a cloudy white suspension, shown in Figure 5.2(a). This **G6** suspension resisted separation using centrifugation and remained suspended following 2 weeks at -10 °C.

At this point it was determined that potentially the addition of a vinyl moiety may have changed the solubility of the **G6** significantly compared to DNA. In an attempt to reverse the formation of the colloid and solvate the **G6**, a fraction of the 5:1 suspension was added to enough MilliQ water to invert the ratio to 1:15 (v/v) propan-2-ol:water, Figure 5.2(b). This dispersion also remained as a suspension for the 2 weeks at -10 °C. Following drying and resolution of the samples 100% water and propan-2-ol solutions resulted in a similar appearance though could be centrifuged.

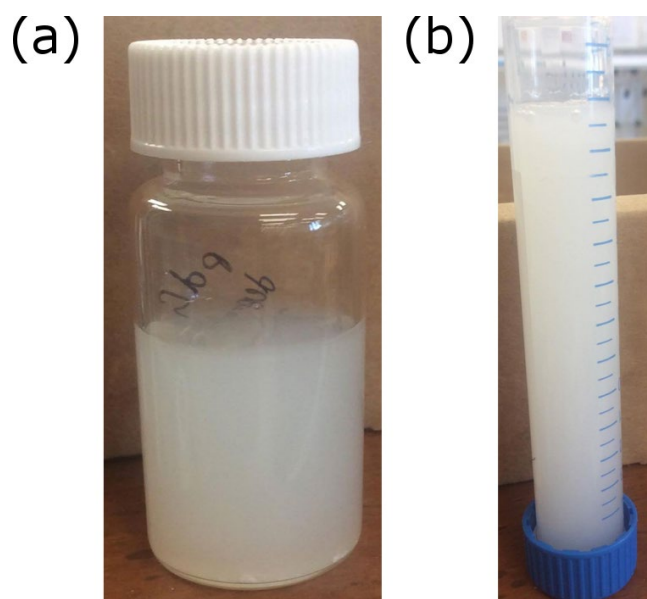


Figure 5.2 Sample of **G6** following deprotection and detritylation as isolated using NaOAc in propan-2-ol:water (a) 5:1 and (b) 1:15 (v/v).

From the stability of the **G6** samples in solution it was hypothesised that surface charged particles had formed, and that this surface charge prevented the aggregation required for precipitation. The oxypropyl methacrylate moiety (Figure 5.(red)) was known to be insoluble in water and propan-2-ol, and to aggregate to itself.<sup>10</sup> The cause of the particle formation was unclear at this time as both solutions appeared visually similar, but the generation of the phosphate moiety (Figure 5.3(green)) may have had some impact, generating a negative surface charge.

Alternatively, the nucleobases were mildly basic, and within the **G6** structure were the most exposed groups (Figure 5.3(green)). This, combined with their hydrophilicity, may have resulted in them being pushed away from the hydrophobic alkyl backbone, creating a positive surface charge.

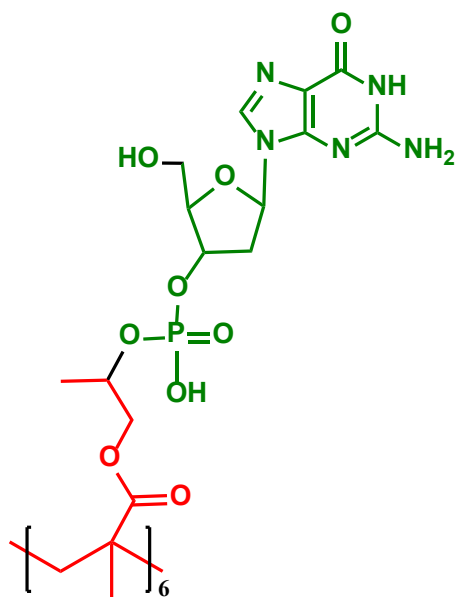


Figure 5.3 Structure of **G6** showing the hydrophilic nucleotide based region known to be water soluble in isolation (green) and the comparatively hydrophobic region known to be water insoluble in isolation (red).

### 5.3.1 Scanning Electron Microscopy (SEM) of G6 Particles

Following the formation of the white suspension, SEM was used to investigate the nature of the suspension. At this point it had been determined that it was acting as a colloid in terms of its solubility, and SEM was thought to give some insight into the particle size. It would not show what the interactions were directly, but the shape of the particles could indicate if they were forming uniformly or if they were disorganised agglomerates.

The limitation of using SEM for solution particle analysis was that it is not a solution-based technique. As a result, the **G6** samples were prepared in such a way as to preserve any structures that had formed while removing the solvent matrix. This procedure involved freeze drying the samples onto a silicon wafer using the method described in Chapter 2, Section 2.5.3.1. Images of the **G6** particles isolated from 5:1 (v/v) propan-2-ol:water deposited onto silicon are shown in Figure 5.4.

Samples of **G6** in 5:1 (v/v) propan-2-ol:water solution, at a loading of 100 mg/mL were drop cast onto a silicon wafer and imaged using SEM on a Phenom<sup>®</sup> benchtop scanning electron microscope (Figure 5.4).

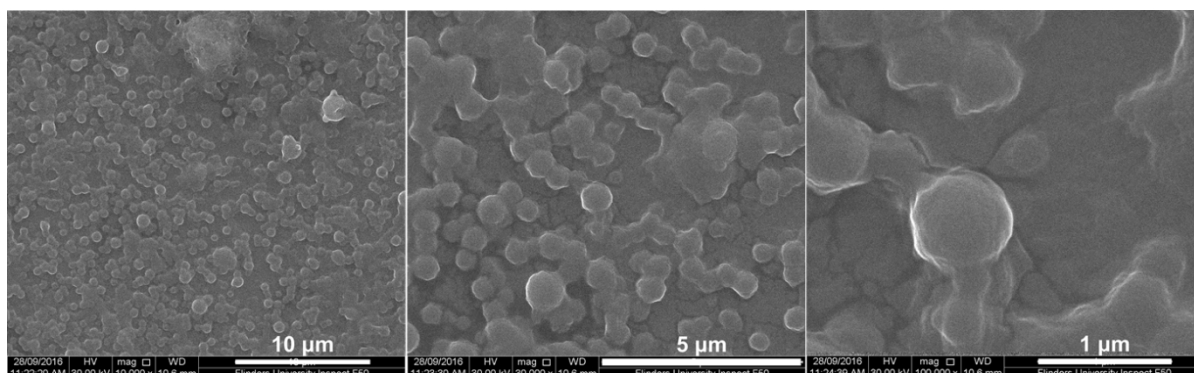


Figure 5.4 SEM images of the **G6** isolated in propan-2-ol:water 5:1 (v/v) at various magnification.

These SEM images show the **G6** had formed into particles approximately 0.5 μm in size. These **G6** particles appear to have formed bridges connecting them to each other. This could have been the result of the isolation technique with the lower temperatures causing a forced precipitation of the **G6**.

In this case the **G6** has bound to the silicon surface and rapidly precipitated as the result of cooling. This had then changed the structure of the **G6** resulting in the formation of polymer monoliths. Similar structures have been seen in a number of surface grafted polymers, most notably in the work of Li *et al.*<sup>4</sup> Their work synthesised multiblock thermo-responsive poly(2-(2-methoxyethoxy)ethyl methacrylate-co-oligo(ethylene glycol) methacrylate (poly(MEO2MA-co-OEGMA)), with the monoliths formed from non-grafted samples shown in Figure 5.5.

**Image Removed Due to Copyright Restrictions.**

**See Reference: 10.1021/am403510g**

Figure 5.5 Non-grafted polymer monoliths of poly(2-(2-methoxyethoxy)ethyl methacrylate (MEO2MA)-co-oligo(ethylene glycol) methacrylate at differing magnification. Taken from

*Li et al*<sup>10</sup>

Following these measurements the same batch of the **G6** was used to prepare samples with the solvent ratio of 1:15 (v/v) propan-2-ol:water using the same method (Figure 5.6). This ratio was not chosen deliberately but was an attempt to force the precipitation of the **G6** by changing the major solvent from propan-2-ol to water.

These SEM images showed the **G6** formed particles of more irregular size, where some larger particles have collapsed or deformed in such a way as to suggest they were hollow. This was consistent with the formation of polymersomes.<sup>10</sup> These are vesicle macrostructures similar to liposomes caused by a difference in solubility or amphiphilic nature within the polymer.<sup>10</sup> Typically these are seen with block copolymers and surfactants.<sup>10</sup>

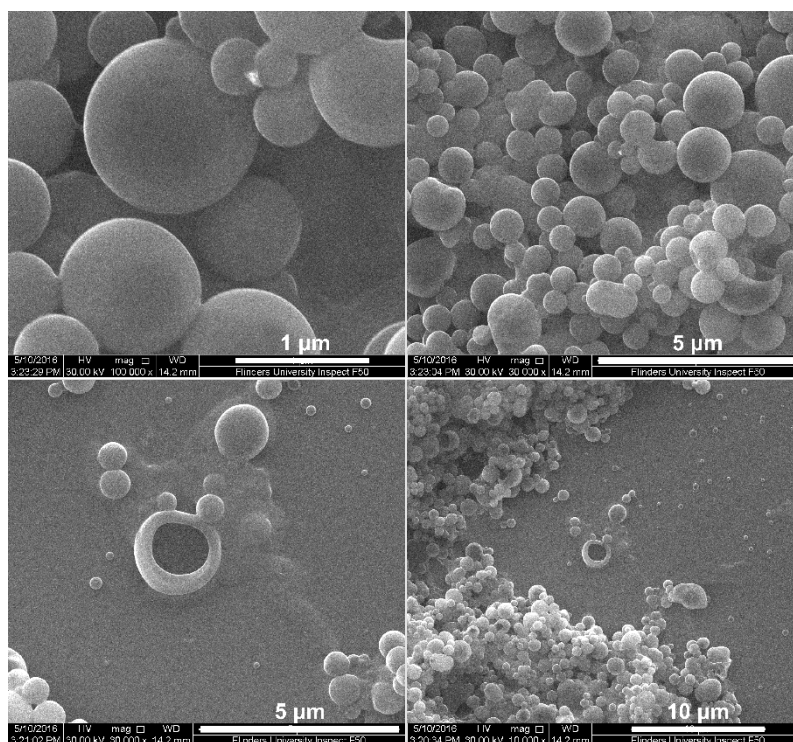


Figure 5.6 SEM images of the **G6** isolated in propan-2-ol:water 1:15 (v/v) at various magnifications.

Based on the chemical structure of the **G6**, there was a distinct hydrophobic region in the **G6** caused by the long chain alkyl backbone. If the difference in hydrophobicity was sufficient it would have driven the formation of a sheet-like structure, as shown in Figure 5.7. This sheet represents the cross section of the **G6** polymersomes.

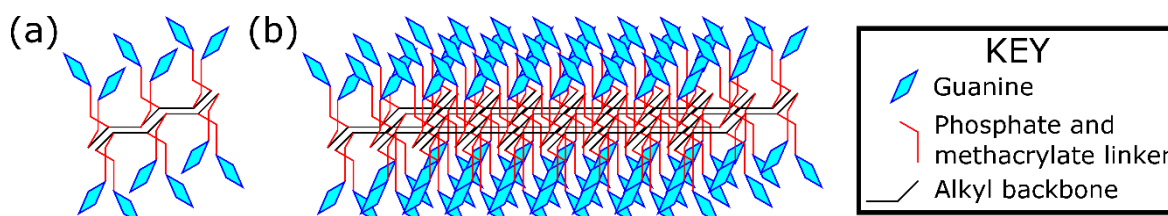


Figure 5.7 Proposed general structure of **G6** in propan-2-ol:water 1:15 (v/v) (a) sheet 'unit' and (b) sheet cross section of polymersome wall.

It was then plausible that in the propan-2-ol:water 5:1 (v/v) solution both this hydrophobic region and the nucleotide component were insoluble leading to the formation of monoliths. When the **G6** was then solvated in propan-2-ol:water 1:15 (v/v) this hydrated and partially solvated the nucleotide unit, creating the polymersomes as a way to stabilise the sheets at lower concentrations, removing the sheet edge. If the structure proposed in Figure 5. was accurate then the polymersomes would be covered in guanine.

Further, the change in size and shape between the two sets of **G6** samples indicates that the particles are dynamic. This indicates that unlike the poly(DMT-dC-CE-P-PMA) discussed in Chapter 3 these polymers had not cross-linked. If the **G6** had cross-linked the structure of the particles would not have been able to change, and would instead have undergone a swelling and gelation.

### **5.3.2 Particle Sizing of G6 Particles by Dynamic Light Scattering (DLS)**

Following the SEM investigation the particles were further analysed using DLS. For this the samples were made to a loading of 1:10 that used for the SEM as a lower loading was required for clear measurements. The results are shown in Figure 5.8.



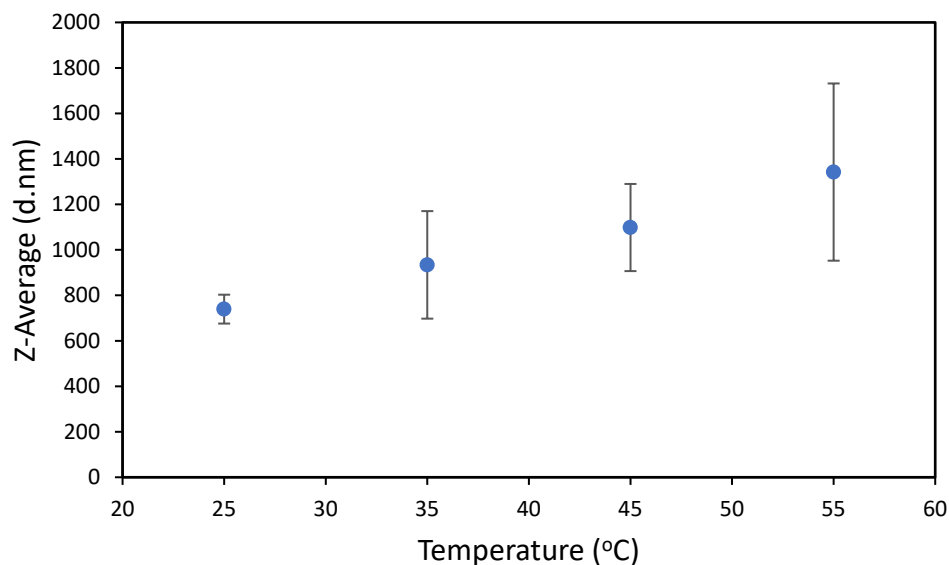


Figure 5.8 DLS measurements showing the particle size of **G6** in 15:1 (v/v) water:propan-2-ol as isolated with NaOAc.

This DLS shows that the particles at room temperature were 726 nm in size with a small amount of variance. The recorded diameter increases by 40% to 1017 nm with heating to 65 °C. The relatively uniform size at room temperature, increasing upon heating is consistent with the hypothesis that these are dynamic particles. The increase in temperature changes the stability of the particles causing them to merge and form larger particles. As the temperature approaches that the polymer was forming particles that expanded upon heating.

These dimensions were significantly smaller than those determined by SEM, further supporting the hypothesis that these are dynamic particles. The reason for the change in size comparing the two methods was attributed to the effect of the decreasing solubility in the cold solvent required for SEM, which would be consistent with the trend for the particles to be smaller at a lower temperature.

## 5.4 Determining the Presence of G-quartets and the G-quadruplex Structure.

The structure proposed for the formation of **G6** sheets may generate a guanine rich surface. As a result, the next stage was to investigate if G-quartets, Figure 1.8, were influencing the formation of these particles and if these quartets were stacking to form G-quadruplex structures Figure 5.9. To do this CD was used. When used for DNA, this method can be used to determine the secondary structure based on the induced chirality of the nucleobase in relation to the ribose, and its interaction with the adjacent bases.<sup>11</sup> It had previously been shown in literature that CD was able to determine not only the presence of G-quartets, but their relation to one another based on the conformation of the deoxyguanosine into either the *syn*- or *anti*- position, as shown in Figure 1.13.<sup>12</sup>

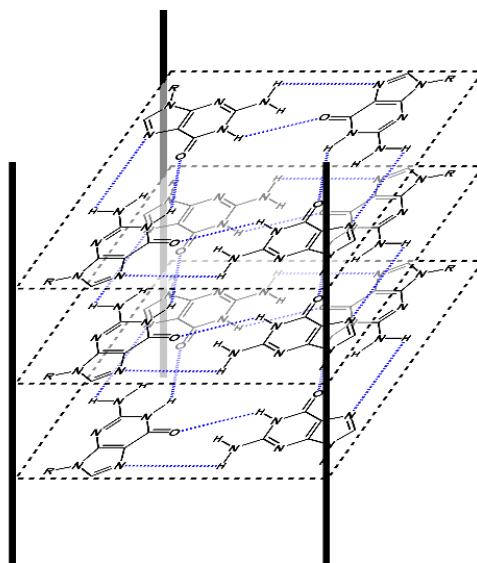


Figure 5.9 The stacking of G-quartets to form a G-quadruplex. Image adapted from Tóthová *et al.*<sup>12</sup>

To determine the nature of the binding within the **G6** particles, they were isolated using the method described previously, Chapter 2, Section 2.4.2.4, using LiOAc and prepared in 10:1 (v/v) water:propan-2-ol at 10 µg/mL loading. Two additional samples were prepared from this batch prepared with added NaOAc and KOAc salts. This was done as larger monovalent cations

have been shown to increase the formation and stability of G-quartets.<sup>13,14</sup> The samples were then analysed using a full spectrum scan at 4 s nm<sup>-1</sup> dwell-time between 180 nm and 340 nm. The results were shown in Figure 5.10.

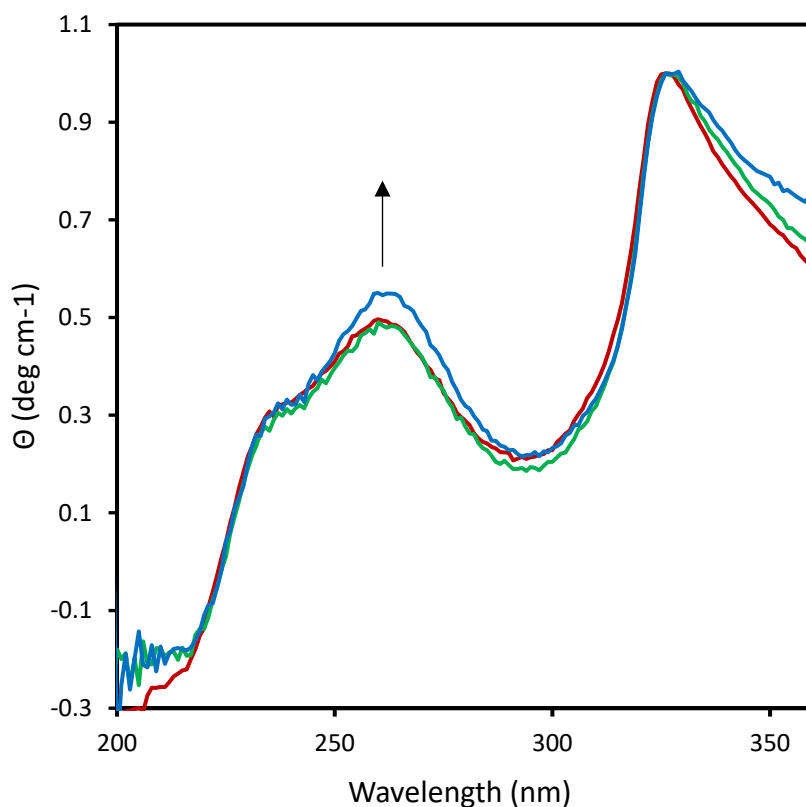


Figure 5.10 Circular dichroism measurements of **G6** in 10:1 (v/v) water:propan-2-ol as isolated with LiOAc (red) and with added NaOAc (green) and KOAc (blue) normalised to the 325 nm peak.

All three **G6** samples show a large peak at 325 nm. It was hypothesised that was caused by the tacticity of the propyl methacrylate moiety, consistent with that seen from other alkyl polymers.<sup>15-17</sup> This is iso or syndiotactic structure would be apparent over the length of the polymer and may be induced by the nucleotide sidechain, forming a sterically locked helix around the alkyl-backbone.<sup>4</sup>

The two peaks relevant to the formation of G-quadruplexes were 261 nm, and the shoulder at 240 nm.<sup>18</sup> These peaks were caused by the guanine moiety which as a pair is associated in literature with the formation of a G-quadruplex containing stacked *anti*-G-quartets.<sup>12,19</sup> The increase in the peak 261 nm peak (Figure 5.10 (arrow)) with the addition of KOAc shows greater formation of G-quartets as would be expected for their increased stability.<sup>20</sup> This was attributed to the larger valence shell of the K<sup>+</sup> cation being better able to stabilise the charge distribution across the G-quartet.<sup>20</sup> This increased stabilisation allowed some quartets to form that were too far separated to be stabilised by the smaller sodium cation.

This data showed that the **G6** polymersomes found in section 5.3 are able to form G-quadruplexes. Further, similar to those found in DNA the **G6** G-quartets are increasingly stabilised by the presence of potassium cations.

## 5.5 Testing for DNzyme Properties with TMB Oxidation

In addition to circular dichroism the oxidation of 3,3',5,5'-tetramethylbenzidine (TMB) was typically used as a method to determine the presence of G-quartets within DNA systems.<sup>21</sup> This was possible as ferric chloride heme (hemin) (figure 5.11) forms a complex with G-quadruplexes with is then able to demonstrate a peroxidase mimicking activity, a so-called a DNzyme as presented in Chapter 1, Section 1.3.3. This in turn accelerates the oxidation of TMB which causes a change in colour, from colourless to blue, that can be measured with UV-vis spectroscopy, specifically by measuring the peak at 450 nm.<sup>22</sup> The mechanism for this process is shown in Figure 5.12. However as the peroxidase mimicking activity is not required for the oxidation to occur the rate of oxidation needs to be compared to the background rate. Seeing a similar rate acceleration in the presence of **G6** would therefore suggest the presence of G-quadruplexes and the ability for the **G6** to act as a DNA analogue in this reaction.

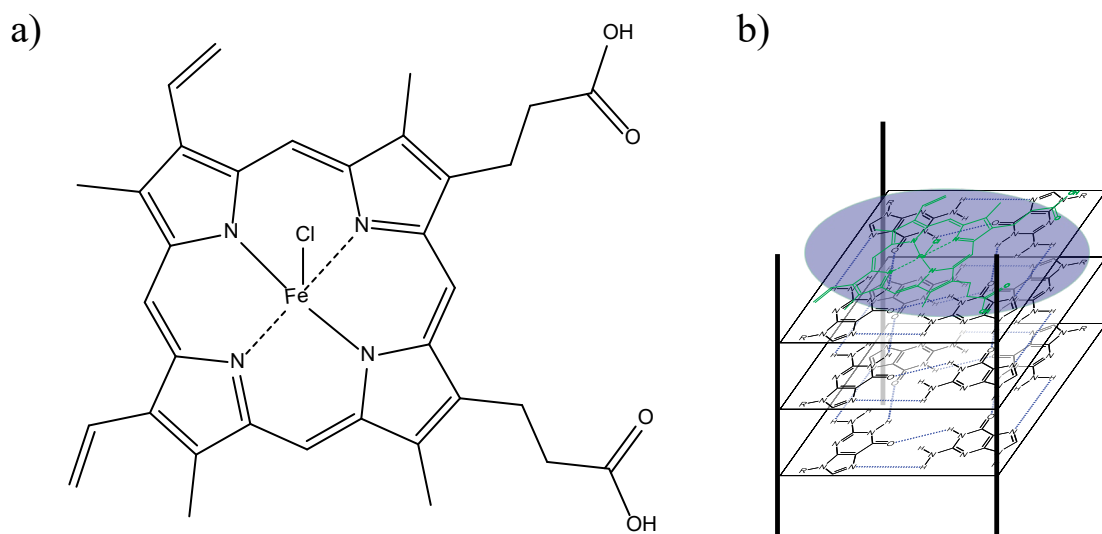


Figure 5.11 (a) Structure of ferric chloride heme (hemin), and (b) the hemin stacked on a g-quadruplex

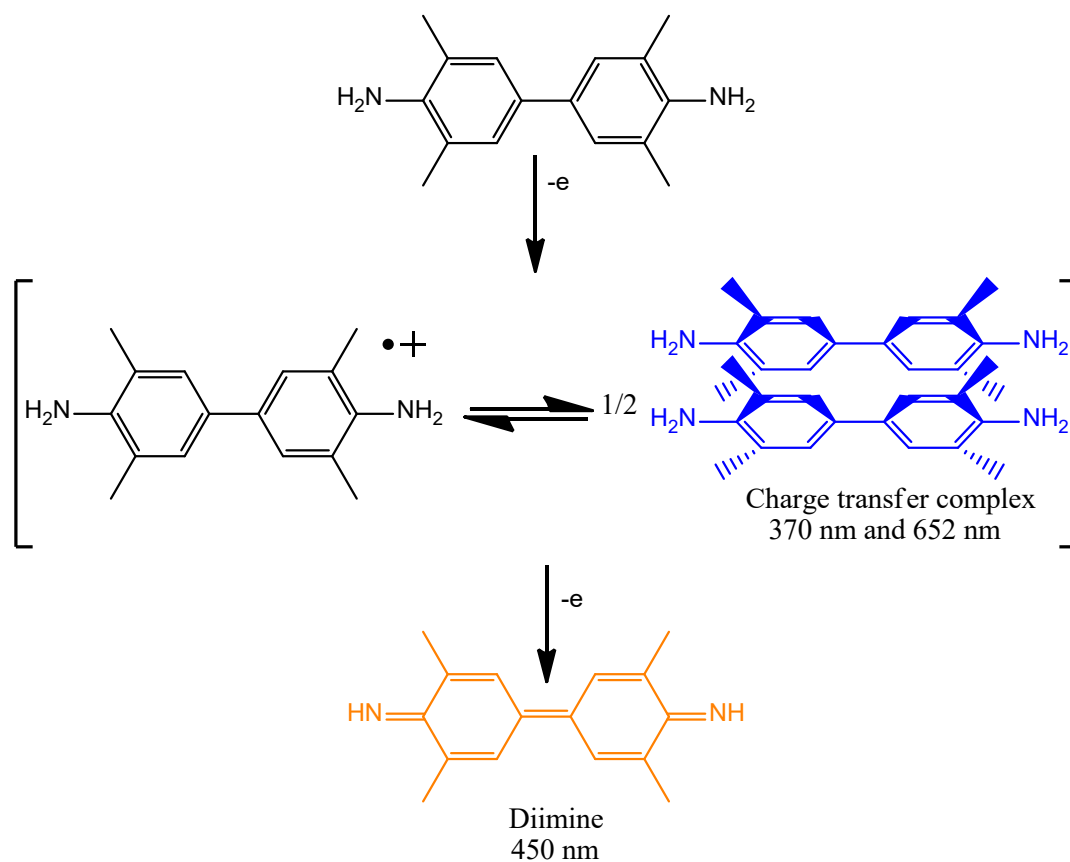







Figure 5.12 Oxidation of TMB caused by the G-quadruplex/Hemin DNzyme with absorption wavelengths shown. Adapted from Stefan *et al.*<sup>23</sup>

### 5.5.1 Bulk testing of DNAzyme Activity

The first test of the **G6** for DNAzyme activity was conducted on a 1 mL scale and investigated using qualitative observation. Specifically, if the presence of the **G6** acted as a DNAzyme and caused the production of the blue TMB charge transfer complex then this would be visible without instrumentation. If the **G6** sample turned a darker shade of blue than the negative control in the same timeframe this would indicate the TMB charge transfer complex had formed. As the samples were run concurrently a difference in the shade of blue would indicate a difference in the rate of oxidation, with darker shades indicating more rapid oxidation. This was done prior to quantitative analysis to ascertain if the **G6** particles interfered with the oxidation.

For these measurements a negative control solution containing hemin and TMB was prepared and divided into 5 samples as outlined in Chapter 2, Section 2.5.3.2. The positive control was made by adding the known G-quadruplex forming sequence (G3T2)3G3T20 (hereafter referred to as GQ DNA). The primary analyte was the **G6** sample. Two additional samples were also included containing the polymer prior to deprotection **G4** (as synthesised in Chapter 4, Section 4.6.3), and following deprotection of the **G4**, respectively. The inclusion of **G4** and **G5** was to determine if incomplete deprotection had any effect on the oxidation caused by the **G6**. After the addition of the polymer solutions the samples were left at ambient conditions for 1 h to progress, the results were shown in Table 5.1.

**Table 5.1:** Results of TMB oxidation tests, all samples contain hemin, TMB, 10 mM TRIS-HCl in addition to the listed reagent.

Reagent	Result
No further addition (negative control)	
GQ DNA (positive control)	
<b>G6</b>	
<b>G5</b>	
<b>G4</b>	

The results of this test gave several key insights. Firstly, the evolution of the blue colour in both the positive and negative control samples indicated that the oxidation of TMB occurs without the presence of the GQ DNA to act as a DNAzyme.

Secondly, samples containing **G6** and **G5** show significantly less colour. The reduction in the rate of oxidation compared to the negative control rate suggests that some component of the reaction is being removed, either the TMB or the hemin.

Both of these samples contain an active guanine moiety, compared to the **G4** which still has the protecting group present. This suggested that the presence of the activated guanine moiety on these vinyl based polymers decreased the rate of oxidation below the negative control. This indicated that either the TMB or the hemin had been removed from the reaction. As it was

previously reported that the hemin binds to g-quartets and these two polymers have available guanines to form these quartets. This would suggest the G-quartets are forming polymersomes or a similar structure and reducing the availability of the hemin for oxidation of the TMB.

### 5.5.2 Analysis of DNAzyme activity using UV-Vis spectroscopy

Following the bulk measurements of the DNAzyme activity, the experiment was repeated with more detailed measurements using UV-Vis spectrometry. Due to the relatively limited supply of the **G6** the experiment was first performed with just the GQ DNA positive control and negative control solutions to determine the required concentration and experimental parameters. To do this 1  $\mu\text{L}$  of hemin was combined with 18.5  $\mu\text{L}$  of 0.4 M TMB and 985  $\mu\text{L}$  of 10 mM TRIS-HCl buffer as the stock solution. For the positive control an additional 0.1  $\mu\text{L}$  of the 0.6 mM GQ DNA solution was added as this sequence would accelerate the oxidation of TMB above the background rate of the negative control. The results of these measurements were shown in Figure 5.13. The results of the UV-Vis measurements of TMB oxidation showed a clear distinction between the negative control solutions (Figure 5.13(black)) and the positive controls with GQ DNA (Figure 5.13(blue)). This difference represents a high discrimination between the samples.



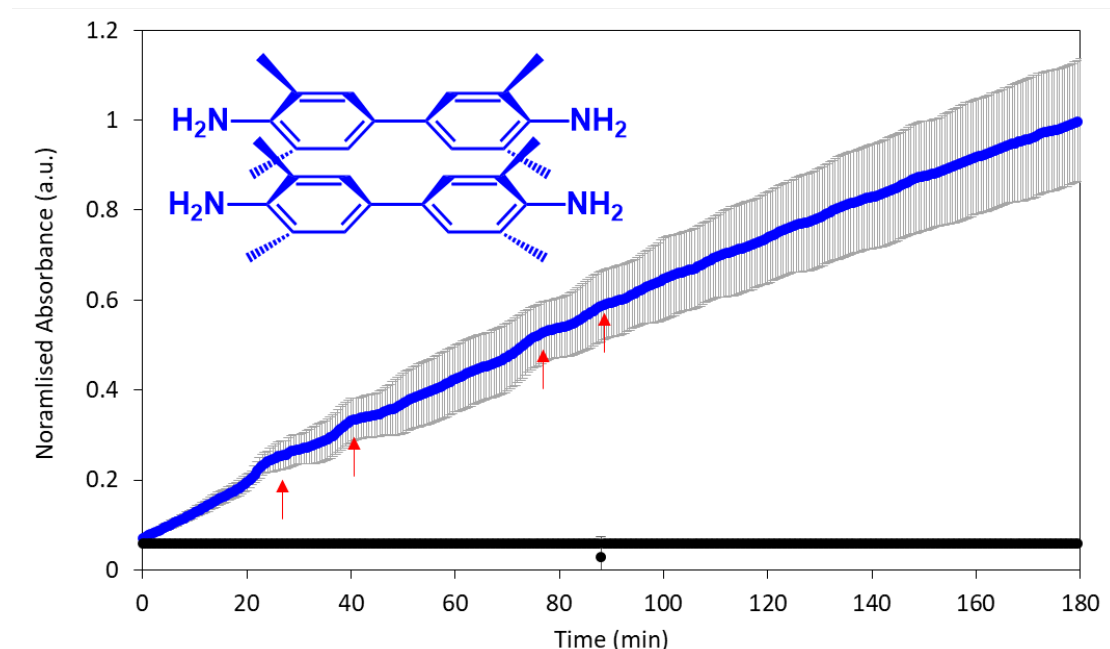


Figure 5.13 UV-Vis measurements at 450 nm for acceleration in the oxidation of TMB by hemin/G-quadruplex complex. Positive controls of TMB/Hemin/GQ DNA (blue) and negative control of TMB/Hemin (black) with non-linear behaviour (red arrows). Samples measured in triplicate.

The limitation of this method was immediately visible within the positive control as these samples showed a high degree of variance between replicates (Figure 5.13(blue)). Further, several local peaks were seen between 20 and 100 minutes (indicated by the red arrows in Figure 5.13). Based on the timing and the thermal sensitivity of the reaction this behaviour was attributed to the air-conditioning in the laboratory. For this reason, the decision was made to instead use a plate reader and measure multiple samples simultaneously. This affords a lower sensitivity but ensures that all samples were exposed to the same temperature gradients.

To replicate the experiment samples were prepared in a 96-well plate. A Bulk solution of the TMB/Hemin negative control was prepared and 140  $\mu\text{L}$  added to each of 15 wells. 10  $\mu\text{L}$  of analyte was then added to make the final volume 150  $\mu\text{L}$ . As a positive control the GQ DNA

sequence was again used. Poly(HPMA) and the **G6** were made to equivalent molar concentrations based on the number of repeating units, i.e., as the **G6** was a hexamer it was prepared at 6 times the concentration of the GQ DNA, a 38-mer, to account for its shorter length. By measuring this it was hoped to see an acceleration in the rate of TMB oxidation for samples capable of forming G-quadruplex, such as those believed to be present in the **G6** system. The results of these measurements were shown in Figure 5.14.

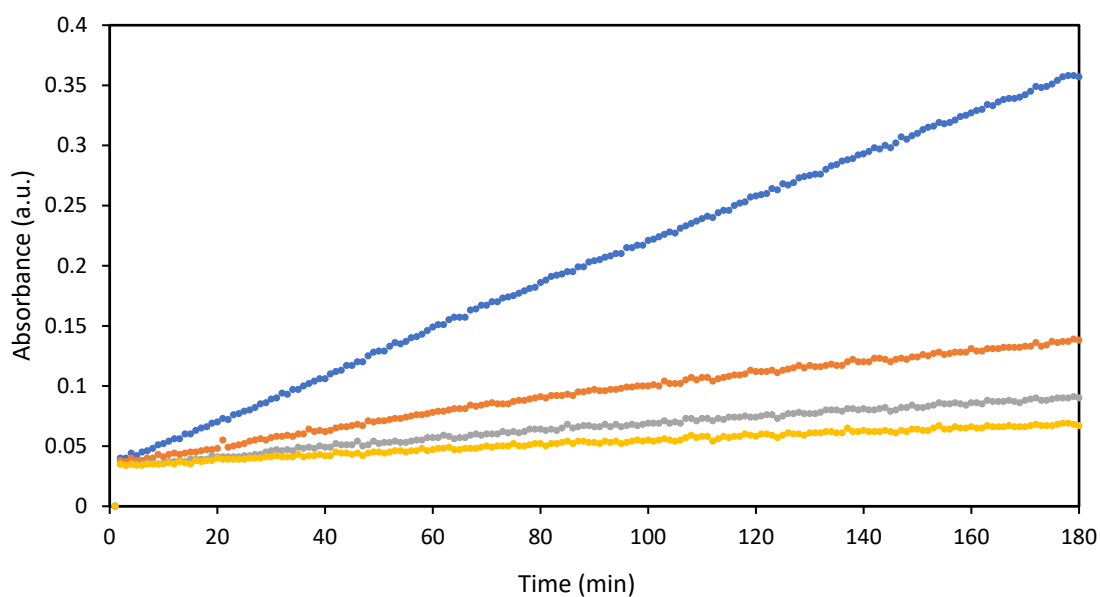


Figure 5.14 UV-Vis measurements at 450 nm for TMB oxidation of the positive GQ DNA control (blue), poly(HPMA) (orange), negative control (grey) and **G6** (yellow).

This result showed that the presence of **G6** does not increase the rate of TMB oxidation. Further, it can be seen that there was a slight decrease in rate compared to the negative control. In combination with the batch TMB oxidation observations it appeared that **G6** does not act as a DNAzyme. In addition, these results showed that **G6** slows the rate of oxidation. This could be due to a fraction of the hemin being bound within the **G6** polymersome core, thus preventing the complex from interacting with the TMB in solution.

## 5.6 Properties of G6 Particles

### 5.6.1 Particle Sizing by Dynamic Light Scattering (DLS)

Following the measurements of peroxidase mimicking activity it was clear that there was no increase in activity provided by the addition of hemin, but the potential decrease suggested possible binding of the particles to the hemin. To test this, samples of the **G6** were combined with hemin and their diameters measured using DLS. The hypothesis was that the addition of hemin to the **G6** particles would shield the surface charge of the particles, thereby decreasing the hydrodynamic diameter.

To this end, samples were prepared of **G6** with addition of different amounts of hemin solution. 1 mL samples were prepared from 0.166  $\mu\text{M}$  **G6** hexamer (equivalent to 1  $\mu\text{M}$  of the repeating unit) with additions of between 0 and 16  $\mu\text{L}$  of hemin solution resulting in a final concentration of between 0 and 8X. For comparison, a solution of the protected **G4** hexamer was also used. The results are shown in Figure 5.15.

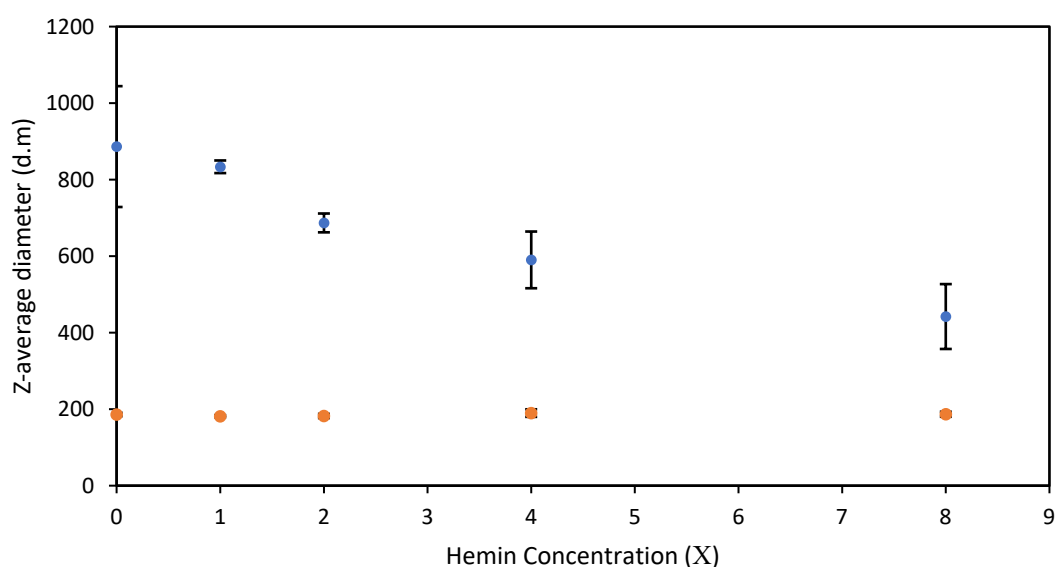


Figure 5.15 DLS measurements of Z-average particle diameter of **G6** (blue), and its protected form **G4** (orange).

From this data it can be seen that the protected **G4** had a smaller hydrodynamic diameter than the **G6** following deprotection. This was consistent with the **G4** having a lower solubility, and the DMT groups being hydrophobic. This causes the surface of the particles to be ‘hard’ and separated from the solution, compared to the deprotected version which is better able to hydrate.

Further, the **G6** particle’s hydrodynamic diameter decreased with increasing additions of the hemin solution. It was hypothesised that as the hemin was added to the **G6** particles it coordinated to the surface, similarly to its complexation with G-quartets. The result is the screening of the guanine with the less soluble porphyrin, thereby decreasing the hydrodynamic diameter. Full investigation would have required zeta potential analysis which was unavailable at the time.

Zeta potential measurements may have indicated if the presence of the larger  $\text{Fe}(3^+)$  present in the hemin was able to effectively screen the particles to prevent aggregation, compared to the  $\text{K}^+$  or  $\text{Na}^+$  present in a g-quadruplex.

### 5.6.2 Melting Behaviour of G6 Particles.

Melting measurements were conducted to determine the stability of the G-quadruplexes created within **G6** and the effect of addition of  $\text{K}^+$  ions. This was done as the increased stability of G-quartets provided by  $\text{K}^+$  ions should increase the melting point of the G-quadruplex. To measure the melting behaviour CD was used as the melting of the G-quadruplexes could be measured by the decrease in optical rotation of the 261 nm peak associated with the stacked *anti*-G-quartets.

For these measurements 1  $\mu\text{g/mL}$  **G6** was prepared with both untreated and treated with 25 mM KOAc. Measurements were taken as described in Chapter, 2 Section 2.5.3.5. These measurements were obtained at 261 nm with samples heated from 25  $^{\circ}\text{C}$  to 85  $^{\circ}\text{C}$  and then cooled to obtain a heating cycle and determine if the particles reformed. The results of this method are shown in Figure 5.16.

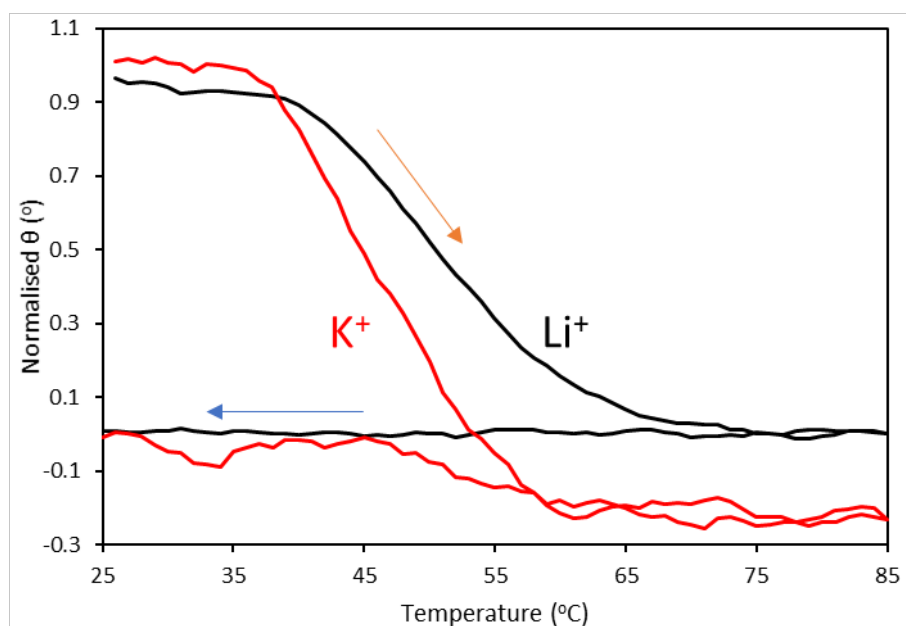


Figure 5.16 Circular dichroism measurement at 261 nm of **G6** samples in 10:1 (v/v) water:propan-2-ol as isolated in LiOAc (black) and with 25  $\mu\text{M}$  KOAc (red), normalised.

Heating indicated by orange, and cooling with blue.

These measurements showed an initial decrease in rotation as the samples were heated and that this did not recover upon cooling. This suggested that 85  $^{\circ}\text{C}$  was above the upper critical solution temperature (UCST), causing the **G6** to precipitate into a hydrophobic structure as a whole, preventing the reformation of the G-quadruplexes upon cooling.

This was most evident for the **G6** sample as isolated with LiOAc. For this sample the increase in temperature caused a decrease in the optical rotation to 0 $^{\circ}$ . This indicated a generally disordered structure with no preference for the induced chirality of the guanine in a G-

quadruplex. When the **G6** with LiOAc was cooled the angle of optical rotation remained at 0°, indicating that there were no G-quadruplexes present. The lack of recovery to a higher angle of rotation suggested that the process was non-reversible, and that the G-quadruplexes were not reformed. This was likely due to the polymer passing its UCST and undergoing a major structural change which prevented the reformation of the G-quadruplex.

The **G6** treated with KOAc showed a distinctly different result. Firstly, the optical rotation decreased in rotation more rapidly, reaching a minimum at ~60 °C compared to the ~70 °C for the **G6** sample, as isolated (i.e., no KOAc). Further, the optical rotation decreased beyond the 0° and began to show negative rotation, i.e., *anti*-clockwise. This could indicate that the presence of the K<sup>+</sup> ions stabilises a different conformation of the nucleotide as the G-quartet melts.

As with the **G6** sample without KOAc, the optical rotation measured returns to 0° rotation, indicating that this was a non-reversible process. Further, as the optical rotation returned to 0° this indicated that the high temperature structure was only stable at the increased temperature, and was the result of the KOAc. This indicated that the negative rotation seen at high temperatures could be the result of surface attachment between particles that precipitated above the UCST. This would in turn mean that as the temperature decreased the particles partially solvated causing the G-quadruplexes to separate.

## 5.7 ATTO 550 Fluorescence Measurements

To determine the chemical properties of the **G6**, fluorescence measurements were chosen. This was because the confinement of fluorescent dyes within nanodomains had been shown as a method for investigating the melting behaviour and structure of polymer particles.<sup>24,25</sup>

For the measurements of the **G6** polymersomes ATTO 550 was chosen as it was slightly hydrophobic. This was chosen so that localised binding of the dye within the **G6** polymersomes would indicate that they contain a hydrophobic core. This in turn would mean that the alkyl backbone was preferentially orientated inward within the particles. The specific properties of the ATTO dye were listed in Table 5.1.

**Table 5.1:** Fluorescent properties of ATTO 550

Absorption wavelength, $\lambda_{\text{abs}}$	Molar attenuation, $\epsilon_{\text{max}}$	Emission wavelength, $\lambda_{\text{fl}}$	Quantum yield, $\eta_{\text{fl}}$	Fluorescence-lifetime, $\tau_{\text{fl}}$
554 nm	120000 M <sup>-1</sup> cm <sup>-1</sup>	576 nm	80%	3.2 ns

### 5.7.1 Melting Behaviour of G6 as measured with ATTO 550

The melting behaviour of the particles treated with ATTO 550 fluorescent dye was analysed using the fluorescence detector on a Q-gen® real time PCR machine, as discussed in Chapter 2 Section 2.5.3.6. To do this 100  $\mu\text{L}$  samples of the 1  $\mu\text{g}/\text{mL}$  **G6**, which had been isolated in LiOAc, were prepared in 10:1 (v/v) water:propan-2-ol with the addition of 2  $\mu\text{L}$  of the ATTO 550 dye. This was then divided into 4 x 25  $\mu\text{L}$  tubes so that an average could be taken. This process was then repeated for samples made with an addition of KOAc to make a concentration of 24  $\mu\text{M}$ . The samples were then heated from 30  $^{\circ}\text{C}$  to 95  $^{\circ}\text{C}$ , and the change in fluorescence measured. The results of are shown in Figure 5.17.

Figure 5.17 shows an increase in fluorescence with heating, and that both **G6** samples showed similar magnitude increases. As the samples were loaded with the same concentration of ATTO 550 this indicated that the particles were releasing the dye in roughly the same quantity. This suggests that the dye, initially bound within the **G6** particles, was quenching the fluorescence. When the particles were heated they undergo a change causing the release of the dye, allowing it to fluoresce in solution.

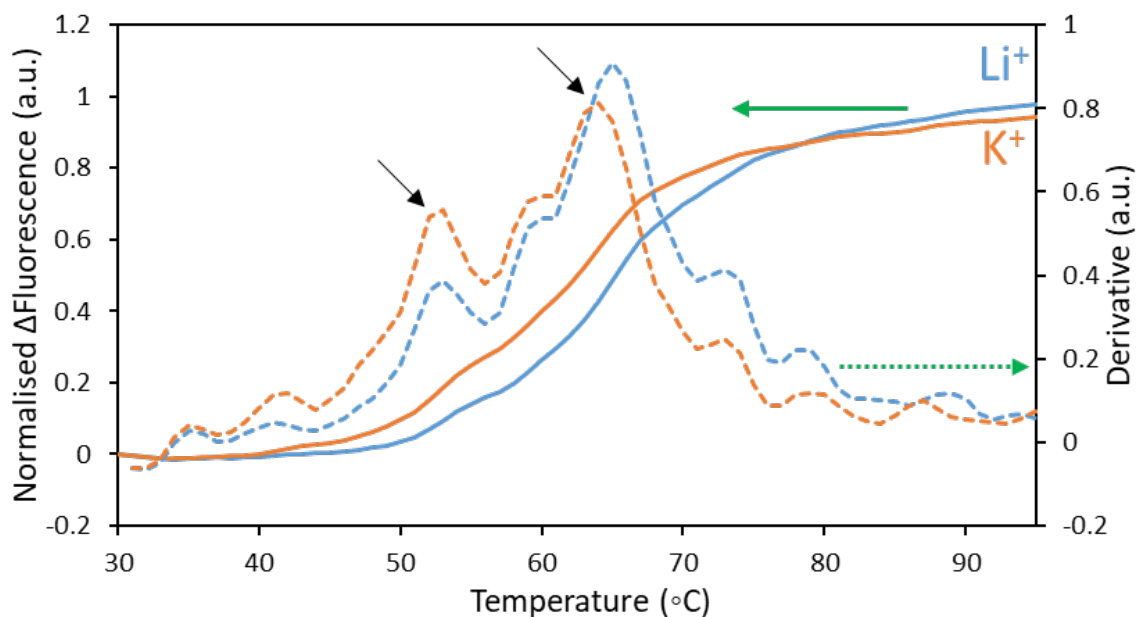


Figure 5.17 Change in fluorescence intensity of ATTO 550 treated **G6** measured with heating, average of 4 samples. Particles isolated with LiOAc (solid blue) and treated with 25  $\mu\text{M}$   $\text{K}^+$  ions (solid orange), normalised to the 95  $^{\circ}\text{C}$  untreated maximum fluorescence and the derivative of the melting curves (dashed).

Further, the derivative curves show that there were two peaks (Figure 5.15, black arrows) associated with the melting at 52  $^{\circ}\text{C}$  and  $\sim 65$   $^{\circ}\text{C}$ . For the  $\text{K}^+$  ion treated samples, there was a higher fraction melting at the first point and a slight decrease in the second melting point. This suggests that the presence of the  $\text{K}^+$  ions effects the stability, with the melting of the  $\text{K}^+$  ion treated **G6** particles appearing at a lower temperature than those without the treatment. This was attributed to the first melting occurring as the particles disperse, with the second being caused by the particles themselves melt. The stronger binding of the  $\text{K}^+$  increased the number of aggregated particles, and thereby the proportion of the ATTO dye that was trapped within the particle aggregates. Due to the lower density of binding sites the aggregates have a lower melting point than the particles, meaning that it presented as the lower melting point peak.



### 5.7.2 Optical Imaging of G6 with ATTO 550

Confocal laser scanning fluorescence microscopy (CLSM) was then used to investigate the G6 particles and their uptake of ATTO 550. Due to its slight hydrophobic nature any specific confinement of the ATTO 550 dye within the particles could provide information on their structure.<sup>24</sup> If the ATTO 550 was confined to the particle core it would indicate that the core was hydrophobic and therefore the nucleotide component (being hydrophilic) was pushed onto the surface of the particles.

Further, it allowed for specific visualisation of the particles without the issue of diffraction. This was because CLSM focuses on a plane, limiting the distortion caused by the solvent.<sup>26</sup> Samples were prepared containing G6, and poly(HPMA) as a control, in the 10:1 (v/v) water:propan-2-ol solvent. The samples were prepared with at 1 mg/mL concentrations of the respective polymer with 1x ATTO 550 dye. These solutions were then treated with no salt, or 25  $\mu$ M NaOAc, or 25  $\mu$ M KOAc, as shown in Figure 5.18.

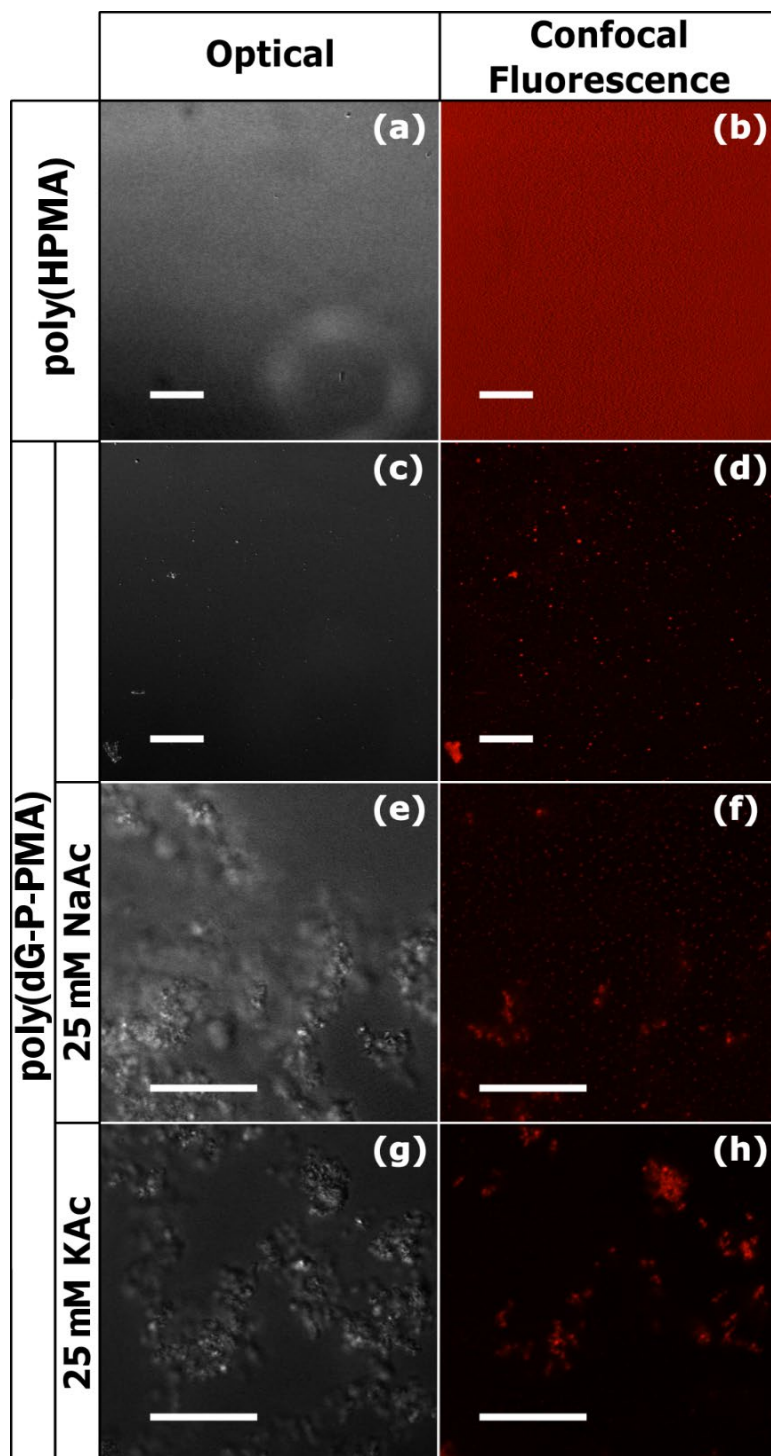


Figure 5.18 Optical and CLSM images of ATTO 550 stained (a and b) poly(HPMA), (c and d) G6 as isolated with LiOAc, and (e and f), as isolated with LiOAc and added Na<sup>+</sup> ions and (g and h) and as isolated with LiOAc and added K<sup>+</sup> ions (25 mM), respectively. Note the excitation laser output for poly(HPMA) had been amplified 10x. Scale bars indicate 20  $\mu$ m.

These images showed the poly(HPMA) samples (Figure 5.18(a and b)) showed no confinement of the ATTO 550 dye seen as the uniform distribution of the fluorescence across the field of view. This was in contrast to all samples containing **G6** where the ATTO 550 dye had been confined within the particles, as indicated by the red colour.

Of interest was the confinement of the ATTO 550 in samples containing **G6**. In all these the ATTO 550 had been confined to the particles, indicating the presence of a hydrophobic region capable of confining the dye, and that this does not quench the fluorescence of the ATTO 550 dye.

Further, the presence of NaOAc and KOAc, Figure 5.18(e-h), led to aggregation of the **G6** particles compared to those isolated using LiOAc, Figure 5.18(c, d). These aggregates appeared rigid in solution, based on how they move as blocks in solutions and collided inelastically. This suggested some form of electrostatic binding between the particles. Based on the previous CD measurements, this was likely due to the formation of inter-particle G-quartets (Figure 5.19).

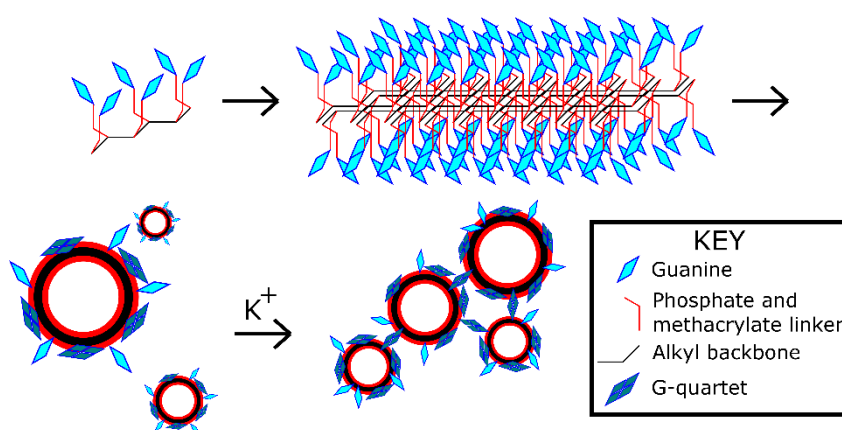


Figure 5.19 Proposed pathway for the formation of **G6** particles and their interactions with  $K^+$  ions. Starting with the polymer, forming sheets, becoming micelles with G-quartets on the surface, and forming inter-particle G-quartets.

## 5.8 Conclusion

This chapter has shown that the samples of **G6** found in Chapter 4 formed polymersomes. These macrostructures were the result of the hydrophobic alkyl backbone of the polymer and the hydrophilic nucleotide groups interacting with the solvent to create a bilayer.

This led to the hypothesis that the polymersomes would have a guanine rich surface. Investigation with circular dichroism showed that G-quartets were formed and subsequently stacked to form G-quadruplexes. This led to an investigation of the effect of stabilising cations which showed that the addition of Na<sup>+</sup> and K<sup>+</sup> ions stabilised the formation of inter-polymersome binding. From this it could be determined that further study on alkyl polymer-DNA interactions, such as that covered in Chapter 6, should avoid the use of guanine containing polymers to avoid the competitive formation of G-quartets.

## 5.9 References

- (1) Li, W.; Wu, P.; Ohmichi, T.; Sugimoto, N. Characterization and Thermodynamic Properties of Quadruplex/Duplex Competition. *FEBS Lett.* **2002**, *526* (1–3), 77–81.
- (2) Simonsson, T. G-Quadruplex DNA Structures Variations on a Theme. *Biol. Chem.* **2001**, *382* (4), 621–628.
- (3) Zhu, J.; Kim, Y.; Lin, H.; Wang, S.; Mirkin, C. A. PH-Responsive Nanoparticle Superlattices with Tunable DNA Bonds. *J. Am. Chem. Soc.* **2018**, *140* (15), 5061–5064.
- (4) Cahill, R.; Cookson, R. C.; Crabb, T. A. Geminal Coupling Constants in Methylene Groups-II. J in CH<sub>2</sub> Groups  $\alpha$  to Heteroatoms. *Tetrahedron* **1969**, *25* (19), 4681–4709.
- (5) Berner, S.; Mühlegger, K.; Seliger, H. Studies on the Role of Tetrazole in the Activation

- of Phosphoramidites. *Nucleic Acids Res.* **1989**, *17* (3), 853–864.
- (6) Caruthers, M. H. Gene Synthesis Machines: DNA Chemistry and Its Uses. *Science* **1985**, *230* (4723), 281–285.
- (7) Klassen, R.; Fricke, J.; Pfeiffer, A.; Meinhardt, F. A Modified DNA Isolation Protocol for Obtaining Pure RT-PCR Grade RNA. *Biotechnol. Lett.* **2008**, *30* (6), 1041–1044.
- (8) Tamkovich, S. N.; Laktionov, P. P.; Rykova, E. Y.; Vlassov, V. V. Simple and Rapid Procedure Suitable for Quantitative Isolation of Low and High Molecular Weight Extracellular Nucleic Acids. In *Nucleosides, Nucleotides and Nucleic Acids*; Taylor & Francis Group, 2004; Vol. 23, pp 873–877.
- (9) Feig, M.; Pettitt, B. M. Sodium and Chlorine Ions as Part of the DNA Solvation Shell. *Biophys. J.* **1999**, *77* (4), 1769–1781.
- (10) Li, M.; Qi, L.; Shen, Y.; Li, Y.; Chen, Y. Thermoresponsive oligo(ethylene glycol)-based polymer brushes on polymer monoliths for all-aqueous chromatography. *ACS Appl Mater Interfaces.* **2013**, *5* (23), 12441-12448.
- (11) Protozanova, E.; Macgregor, R. B. Circular Dichroism of DNA Frayed Wires. *Biophys. J.* **1998**, *75* (2), 982–989.
- (12) Tóthová, P.; Krafčíková, P.; Víglaský, V. Formation of Highly Ordered Multimers in G-Quadruplexes. *Biochemistry* **2014**, *53* (45), 7013–7027.
- (13) Nagesh, N.; Chatterji, D. Ammonium Ion at Low Concentration Stabilizes the G-Quadruplex Formation by Telomeric Sequence. *J. Biochem. Biophys. Methods* **1995**, *30* (1), 1–8.

- (14) Kaiser, C. E.; Gokhale, V.; Yang, D.; Hurley, L. H. Gaining Insights into the Small Molecule Targeting of the G-Quadruplex in the c-MYC Promoter Using NMR and an Allele-Specific Transcriptional Assay. *Topics in current chemistry*; **2012**; Vol. 330, pp 1–21.
- (15) Pini, D.; Iuliano, A.; Salvadori, P.; Zuliano, A.; Salvadori, P. Synthesis and CD Spectra of Isocyanide Polymers: Some New Aspects about Their Stereochemistry. *Macromolecules* **25**, 6059–6062.
- (16) Jin, Y. J.; Seo, K. U.; Choi, Y. G.; Teraguchi, M.; Aoki, T.; Kwak, G. Annealing-Induced Circular Dichroism Enhancement in Luminescent Conjugated Polymers with an Intramolecular Stack Structure. *Macromolecules* **2017**, *50* (17), 6433–6438.
- (17) Chen, L.-C.; Mao, Y.-C.; Lin, S.-C.; Li, M.-C.; Ho, R.-M.; Tsai, J.-C. Induced Circular Dichroism of Stereoregular Vinyl Polymers. *Chem. Commun.* **2012**, *48* (30), 3668.
- (18) Ilc, T.; Šket, P.; Plavec, J.; Webba da Silva, M.; Drevenšek-Olenik, I.; Spindler, L. Formation of G-Wires: The Role of G:C-Base Pairing and G-Quartet Stacking. *J. Phys. Chem. C* **2013**, *117* (44), 23208–23215.
- (19) Haider, S. M.; Neidle, S.; Parkinson, G. N. A Structural Analysis of G-Quadruplex/Ligand Interactions. *Biochimie* **2011**, *93* (8), 1239–1251.
- (20) Kan, Z.; Yao, Y.; Wang, P.; Li, X.; Hao, Y.; Tan, Z. Molecular Crowding Induces Telomere G-Quadruplex Formation under Salt-Deficient Conditions and Enhances Its Competition with Duplex Formation. *Angew. Chemie Int. Ed.* **2006**, *45* (10), 1629–1632.
- (21) Stefan, L.; Denat, F.; Monchaud, D. Insights into How Nucleotide Supplements Enhance the Peroxidase-Mimicking DNAzyme Activity of the G-Quadruplex/Hemin System.

*Nucleic Acids Res.* **2012**, *40* (17), 8759–8772.

- (22) Li, W.; Li, Y.; Liu, Z.; Lin, B.; Yi, H.; Xu, F.; Nie, Z.; Yao, S. Insight into G-Quadruplex-Hemin DNAzyme/RNAzyme: Adjacent Adenine as the Intramolecular Species for Remarkable Enhancement of Enzymatic Activity. *Nucleic Acids Res.* **2016**, *44* (15), 7373–7384.
- (23) Golub, E.; Freeman, R.; Willner, I. A Hemin/G-Quadruplex Acts as an NADH Oxidase and NADH Peroxidase Mimicking DNAzyme. *Angew. Chemie* **2011**, *123* (49), 11914–11918.
- (24) ATTO GmbH. Fluorescent Labels and Dyes. *Fluoresc. Labels Dye. Cat.* **2013**, *49*, 1–45.
- (25) Jana, B.; Bhattacharyya, S.; Patra, A. Perspective of Dye-Encapsulated Conjugated Polymer Nanoparticles for Potential Applications. *Bull. Mater. Sci.* **2018**, *41* (5), 122.
- (26) Jang, J.; Lim, B. Facile Fabrication of Inorganic-Polymer Core-Shell Nanostructures by a One-Step Vapor Deposition Polymerization. *Angew. Chemie - Int. Ed.* **2003**, *42* (45), 5600–5603.

# Chapter 6: Interactions of Nucleotide Functionalised Synthetic Polymers with DNA Using Poly(2-(2'-deoxythymine-monophosphate)oxypropyl methacrylate) as a Model System.

## 6.1 Synopsis

*This chapter outlines the principles for the binding of a thymine functionalised homopolymer, poly(dT-P-PMA) (T6) with dA ssDNA. This interaction will be considered initially from a computational model with further insight provided from UV and fluorescence spectroscopy measurements.*

*This chapter describes the synthesis characterisation of 5'-dimethoxytrityl-N-isobutyryl-2'-deoxythymine, 3'-[(2-cyanoethyl)-(2-oxypropyl methacrylate)]-phosphate, hence forth referred to as the T3 monomer (T3), using the methodology developed in the previous Chapter 4. Following the synthesis of the T3 monomer, it was polymerised using reversible addition-fragmentation chain-transfer (RAFT) method resulting in poly(dT-P-PMA).*

*This poly(dT-P-PMA)(T6) was then tested with a complementary sequence of monoadenine deoxyribose nucleic acid (dA ssDNA) to investigate the binding properties of the two complementary polymers.*



## 6.2 Introduction

This chapter outlines the application of the method for the synthesis of a nucleotide functionalised alkyl polymer, presented in Chapter 4, as it applies to the nucleotide thymine. Subsequently the interactions of the **T6** with the complementary single stranded DNA (ssDNA) adenine homopolymer was investigated using a number of fluorescence binding dyes. Firstly the interaction of the SYBR Safe dye was used as a model for the optimisation of the analysis process, before applying the method to further dyes, namely dsGreen, Yo-Pro-1 Iodine and SYBR Green II. The interaction and binding preferences of these dyes was then used to illicit the binding structure of the DNA-**T6** complex.

### 6.2.1 Choice of Nucleobases

For studying model nucleobase pairing interactions between the alkyl DNA-polymer and native ssDNA there were a number of factors to be considered. Based on the work reported in Chapter 5, guanosine was excluded due to the high risk of competing G-quartet formation. This also ruled out the guanine-cytosine pairing, leaving the adenosine-thymine (A-T) pairing the most straightforward to study.

There are additional benefits to the A-T base pairing for this investigation. Firstly, the deprotection of thymine was simpler than for the other nucleobases as it does not contain the benzoyl or butryl protecting groups present in the other bases.<sup>1</sup> This lack of protecting group means that the thymine present in the alkyl polymer will be active independent of the efficiency of the deprotection. This was important as the protection of a single nucleotide in the polymer chain may dramatically lower the melting point as it separates the binding regions.<sup>2</sup>

Following the selection of the nucleobase pair the next factor to consider was the length of both the alkyl DNA polymer and the native ssDNA polymer. It is well known that the length of a

DNA sequence is directly linked to its melting point.<sup>3</sup> Thus, for this chapter the ideal length needed must be high enough to form a duplex at room temperature, ~25 °C, while also being within the range of the critical solution temperature of the alkyl polymer which appeared to be in the range of 65 °C based on the data presented in Chapter 5, Section 5.7.1 on the melting behaviour of the polymersomes.

The melting point of the complementary A-T duplex for differing lengths was determined using the calculators provided by DNA suppliers IDT DNA technologies® and Sigma-Aldrich®. Here, the target melting point was chosen as 40 °C. This was chosen as it was above 25 °C which will be used for the binding experiments, with additional clearance to account for some variance in the melting point caused by the presence of salts in the solution which can alter the melting point.<sup>4</sup> Based on the IDT DNA technologies® calculator this was an adenine ssDNA sequence 23 units in length. The specific melting point as calculated was 40.8 °C at 0.25 μM dA ssDNA with 50 mM sodium chloride. The proposed **T6**-dA ssDNA pairing is shown in Figure 6.1. In this structure the narrowly separated C-C backbone of the **T6** is shorter and less hydrophilic than the dA ssDNA causing it to stretch away from the base pair similar to a polymer brush.

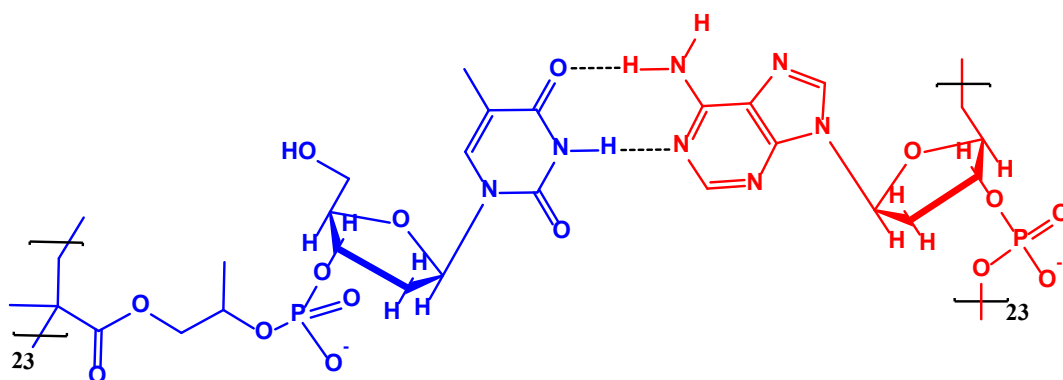


Figure 6.1 Proposed binding of **T6** 23-mer (blue) interacting with dA ssDNA 23-mer (red).

## 6.3 Synthesis of Target T6

For the analysis of the T6 binding interaction, the polymer first had to be synthesised using the method developed in Chapter 4, with adjustments to account for use of the thymine phosphoramidite and the targeted 23-mer.

### 6.3.1 Synthesis of T3 Monomer

The method for the synthesis of the thymine-methacrylate monomer utilised the conjugation of 2-hydroxypropyl methacrylate (HPMA) to the protected thymine nucleotide phosphoramidite.<sup>5</sup> The method for this coupling is outlined in Chapter 2, Section 2.4.2.1. The isolated product was then analysed using electrospray ionisation mass spectrometry (ESI-MS) using the same method discussed in Chapter 4, Section 4.3.1. The results are shown in Figure 6.2.

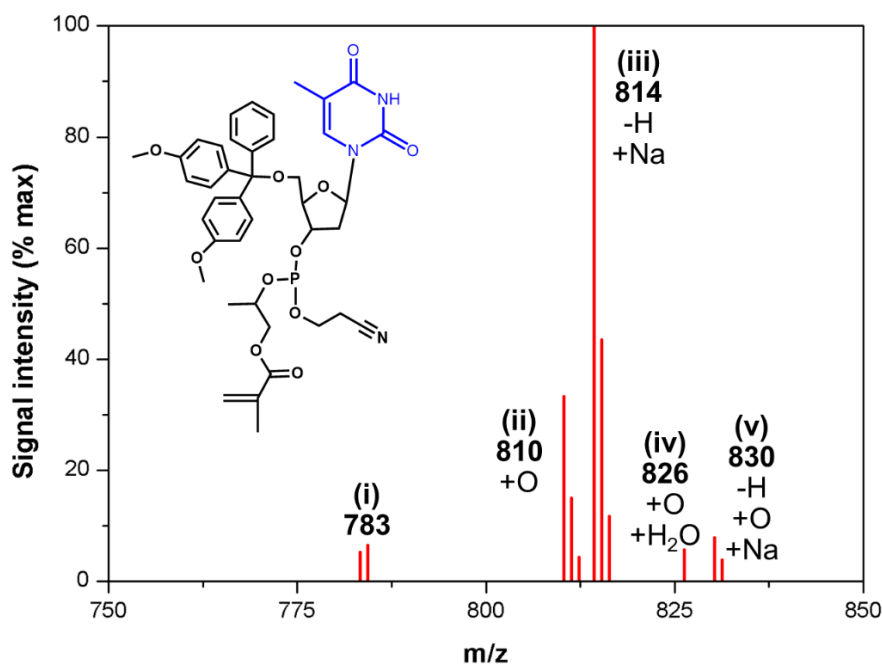


Figure 6.2 ESI -MS spectrum of T2 monomer showing the following peaks: (i) T2 monomer (molecule shown inset), (ii) T3 monomer, (iii) T2 monomer sodium adduct, (iv) T3 monomer water adduct, and (v) DMT-dT-CE-PMA sodium adduct.

The ESI-MS spectrum showed the presence of a peak at 783 m/z (Figure 6.2(i)). This was assigned as **T3**, which has a theoretical value of 788.8 m/z. This means that the theoretical value was lower than the measured by 5 m/z. This was attributed to the presence of a Li<sup>+</sup> ion adduct, rather than the H<sup>+</sup> ion normally used to generate the charged molecule.

The peak present at 810 m/z (Figure 6.3(ii)) was attributed to the DMT-dT-P-PMA phosphate monomer which has a theoretical value of 804.8 m/z. As with the previous peak this was 5 m/z lower than the experimental result.

The largest peak was seen at 814 m/z (Figure 6.2(iii)). This peak was attributed to the **T2** monomer sodium adduct. This complex has a theoretical value of 810.78 m/z.

Above this point are two smaller peaks at 826 m/z and 830 m/z (Figure 6.2(iv and v)). The first of these was attributed to the **T3** monomer with water adduct, consistent with the theoretical value of 821.8 m/z. The second was associated with the **T3** monomer sodium adduct, consistent with the theoretical value of 16 m/z higher than the peak attributed to the **T2** monomer due to the presence of the additional oxygen contributing the total 16 m/z.

The consistent difference of 5 m/z from the theoretical values suggests an error in the calibration of the instrument, though the separation between peaks matches the expected values. Further, the presence of these five peaks indicated successful synthesis of the **T2** monomer, in combination with its oxidised form. This was considered sufficient to then continue to the polymerisation method.

In addition to MS of the monomer, <sup>1</sup>H NMR was also conducted to confirm the identity of the **T2** monomer, Figure 6.3. Full peak allocation is presented in Appendix 4. The integration of the peaks associated with the *trans* and *cis* protons at  $\delta=5.6$  ppm and  $\delta=6$  ppm respectively

(Figure 6.3(a and b)) can be seen and integrate to the peak at  $\delta = 6.2$  associated with the 1' proton on the deoxyribose ring. The additional splitting is due to the combination of the T2 P(III) and some T3 in the (PV) state caused by oxidation during preparation.

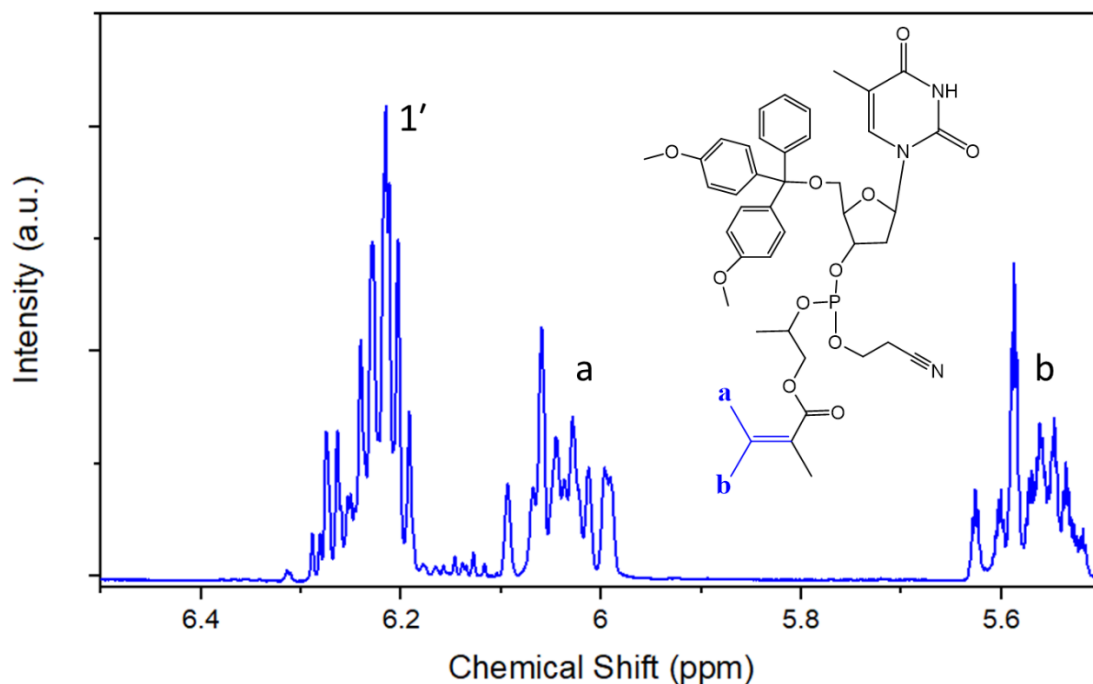


Figure 6.3  $^1\text{H}$  NMR of the 6.5 ppm to 5.5 ppm region for **T2** (inset) with **T3** present. Spectra acquired in deuterated acetonitrile at 600 MHz.

### 6.3.2 Synthesis of Polymer

The synthesis of the **T6** used the same method developed in Chapter 4, with the concentration of **T3** monomer increased to four times the concentration of guanine bioconjugate which resulted in the hexamer discussed in Chapter 5. Assuming similar conversion this would have resulted in a 24-mer of the **T6**. This increased length compared to the 23-mer desired was chosen as the target to account for the decreased rate of polymerisation caused by the longer polymer chain becoming less soluble. This behaviour was previously discussed in Chapter 4, Section 4.4.1.

The time period of the polymerisation was reduced to 4 h due to the formation of a precipitate at this time. This indicated that the polymer forming was at the limits of its solubility in acetonitrile, and further polymerisation may have resulted in a gel similar to that found in Chapter 3.

The resulting **T4** was then deprotected and detritylated to form the **T6**. This was analysed using SEC to determine its molecular weight, using PMMA standards, the result shown in Figure 6.4 and described in Table 6.1

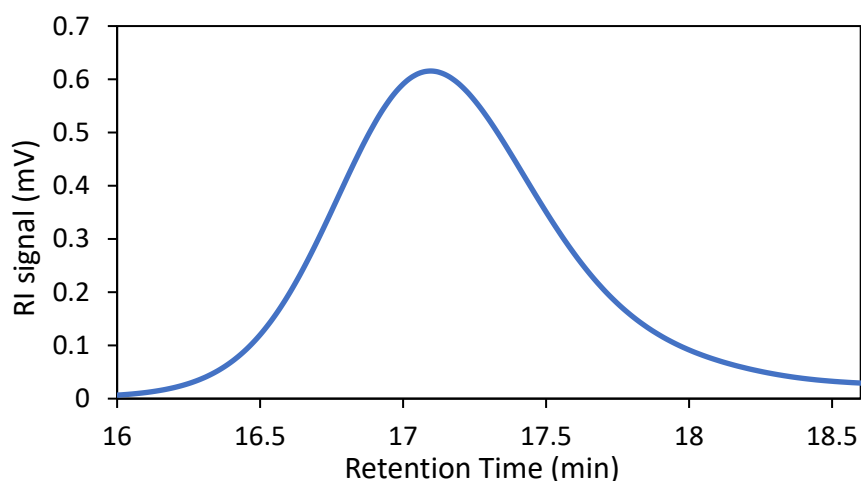


Figure 6.4 DRI chromatogram of **T6** following 4 h polymerisation, showing the formation of a polymer, 9364 Da.

**Table 6.1:** SEC results for the measurement of **T6**.

	<b>24 h Polymerisation</b>
<b>M<sub>n</sub></b>	7800 Da
<b>M<sub>w</sub></b>	9400 Da
<b>MP</b>	9000 Da
<b>DP</b>	21 units
<b>D</b>	1.2

The SEC result showed the **T6** had a  $M_w$  of 9364 Da. This showed that the **T6** chains formed were approximately 21 units in length. This was determined by dividing the  $M_w$  of the **T6** (9364 Da) by the  $M_w$  of the dT-P-PMA repeating unit (447.3 Da).

The  $M_w$  found was below the targeted  $M_w$  of 10281 Da for the **T6** 23-mer. Based on the formation of the precipitate this was close to, if not, the maximum  $M_w$  attainable using this polymerisation method. For this reason, it was decided to progress using the **T6** 21-mer and measure its interaction with the dA ssDNA 23-mer.

For a length of 21 base pairs the expected melting point of the duplex was 38.2 °C based on the IDT DNA technologies calculator. This temperature still fits within the intended temperature range, discussed in Section 6.2.1.

## **6.4 Computer Modelling of T6**

To validate the proposed binding of **T6** to dA ssDNA computer modelling was conducted using Ascalaph designer running on the FIREFLY computational chemistry algorithms. This program was chosen as Ascalaph was open access software based on the same fundamental protocols, definitions, and code parameters as other programs such as PC GAMES (UK) and PC GAMES (US). Further, its open file standards make it more accessible for integrating structures from other programs, notably for this project ChemDraw Ultra 12.0.1076.

Modelling was conducted on a consumer level workstation running a 4.02 GHz Intel 4790k quad-core 8 thread CPU and nVidia 970 TI GPU. This combination was chosen as Ascalaph was CPU bottlenecked with limited multithread optimisation and the 4790k was the highest speed CPU based on single core performance available at the time.<sup>6</sup>

#### 6.4.1 Modelling of Selective Binding Interactions Between T6 and dA ssDNA

Pentamers of T6 and dA ssDNA were generated in Chemdraw ultra 14, converted to the .mol2 format and imported into Ascalaph designer. This method was chosen as Chemdraw allows for rapid generation of complex structures, where Ascalaph designer was optimised for generation of DNA and protein structures. Further, using the 2 dimensional visualisation of the structure makes proofreading easier. From here the molecules were converted to 3 dimensional structures using the quick optimisation tool and checked for correct stereocenters at the 2', 3' and 5' positions. The program was then optimised a further 2 times to relieve stress on the structure generated by this conversion.

The binding state simulation was run initially at 1 K to reduce energy generated from the optimisation, followed by 2 optimisations at 50 K. This was essential as running the simulation immediately at 50 K resulted in the molecules breaking apart and crashing the simulation. Once a stable state for the model had been found as a starting point the simulation was run for 100,000 iterations using the hybrid Lui Storey and conjugate descent method (LS&CD) for optimising the structure.<sup>6-8</sup> The resulting optimised dimer structure is shown in Figure 6.5.

This showed that there was a level of binding and orientation seen between some of the nucleobases, specifically 5' terminal group of the dA ssDNA, located in the lower right of Figure 6.5(i) as indicated. The T6 strand on the left appears to be fanning out more, a result of the shorter base separation caused by the alkyl backbone as hypothesised. As a result of this measurement it was determined that binding between the complementary bases was possible, but that the duplex structure formed would need to somehow account for this difference in base separation.



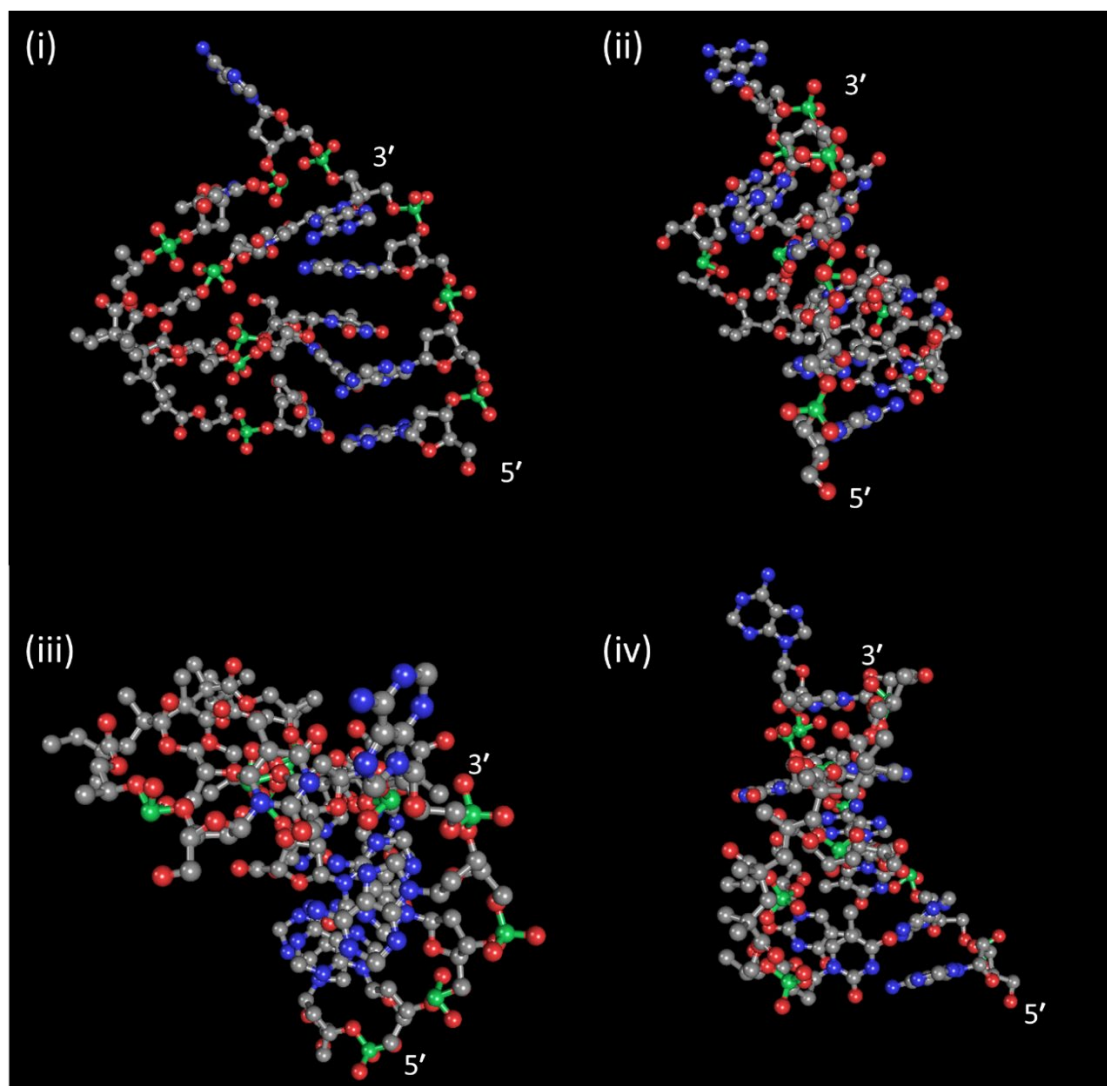


Figure 6.5 Optimised structural model of **T6** and dA ssDNA pentamers following 100,000 iterations. Directionality of the dA ssDNA shown. Angles provided are (i) groove, (ii) **T6** front, (iii) top, and (iv) dA ssDNA front.

The binding nature of the polymer can not be determined from this calculation however as the specific interactions between nucleobases remains unclear. It can be seen in Figure 6.5(i) that the separation of the base pairs leads to a binding ratio of approximately 1:1, as they are aligned, but due to them not being coplanar the binding may be driven partially by non-specific electrostatic forces.

#### 6.4.2 Modelling of Long-strand T6

Following modelling of the **T6** and dA ssDNA duplex using the pentamers, a larger model was prepared to determine the conformation of larger **T6** molecules. This modelling was required to ascertain if the thymine functionality would be available for binding to ssDNA as the effect of the hydrophobic backbone may become more dominant at higher molecular weights, causing the polymer to become insoluble. Similar behaviour was seen in other polymers, notably pHEMA.<sup>9,10</sup>

The 21-mer of the **T6** structure was imported as a 2D file from Chemdraw® as it had been with the dimer combination tested in Section 6.4.1. Following the short optimisation to remove clashes and overlap, the molecule was optimised using the same hybrid LS&CD method. This time the optimisation was carried out for 10,000 iterations at each of 70 K, 180 K and 273 K before being run at 100,000 iterations at 300 K, room temperature. The result of the optimisation, Figure 6.6, shows the formation of a spiral like structure.

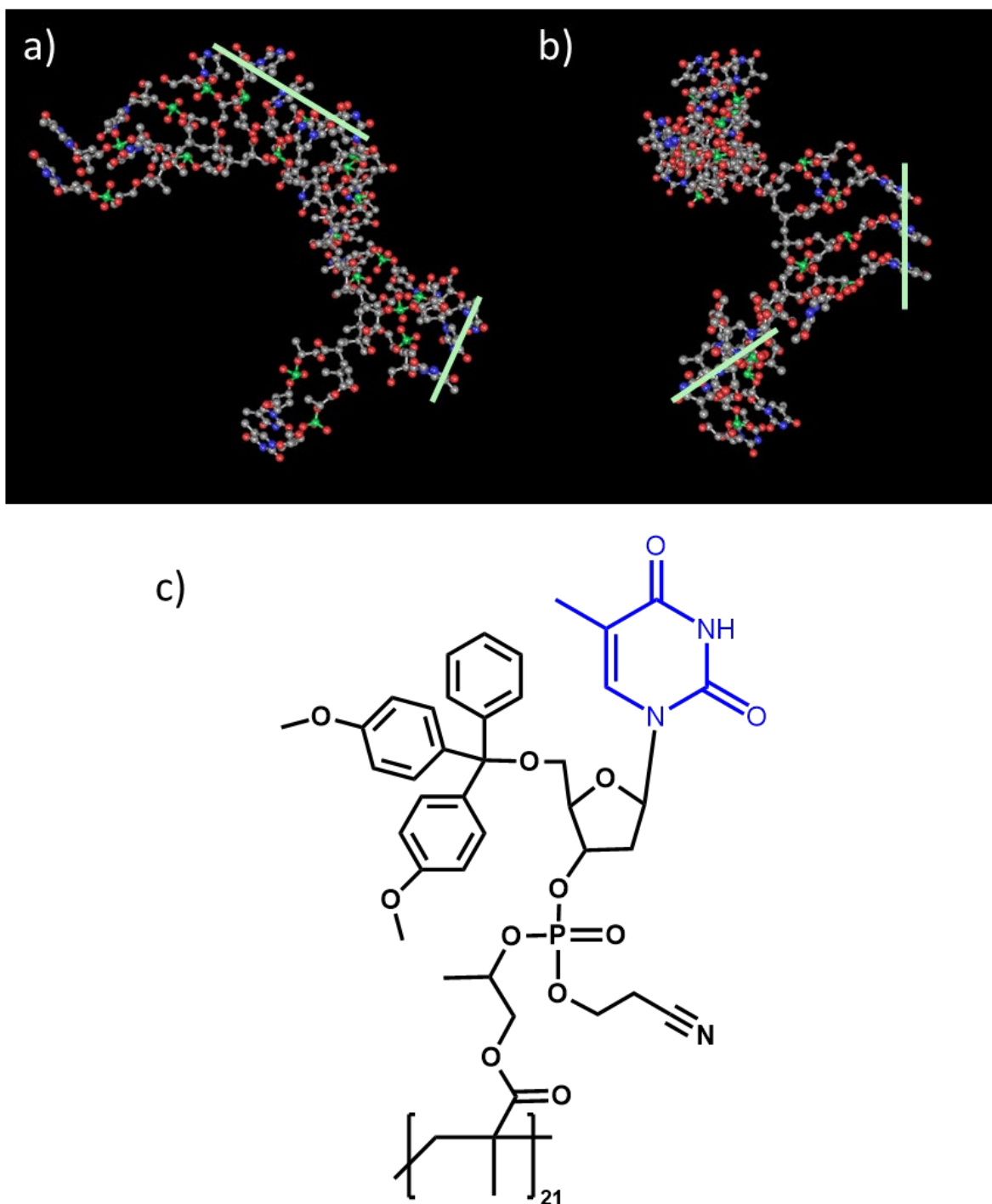


Figure 6.6 Molecular structure of the **T6** 21-mer following optimisation, (a) at 0° and (b) 90° rotation around the vertical axis, with light green bars indicating linearly aligned nucleobases.

(c) showing the structure of **T6**.

As expected the shorter separation between nucleotides caused by the alkyl backbone, seen in the previous section, results in the nucleotides fanning out. Short runs of the nucleobases appear to be linearly stacking, indicated in Figure 6.6(a and b) with the green lines. This means that the thymine was available for base pairing.

Importantly, it shows that **T6** does not form a dense particle. Overall there was a clear curve to the structure, arching away from the nucleobases, compacting the alkyl backbone on itself. The resulting orientation breaks up the nucleotide sections.

## 6.5 Analysis by UV-Vis spectroscopy of DNA

The absorbance of nucleotides in solution as measured by UV-vis spectroscopy is commonly used to determine the concentration of DNA in solution<sup>11</sup> due to the consistent absorption at 260 nm. This peak is associated with the heterocycle aromatic rings that make up the nucleobase moiety.<sup>12</sup> It has been shown that the formation of a standard double helix results in lower absorption of UV light due to interactions between complementary bases.<sup>13</sup>

It was hypothesised that measuring the decrease in absorbance caused by the formation of a duplex would be able to show that hybridisation was occurring between the dA ssDNA and the **T6**. This would occur as a result of the hybridised adenine to thymine decreasing the absorbance at 260 nm associated with free nucleotides in solution.<sup>11</sup> This technique was reported by Tinco,<sup>14</sup> and others have since applied to non-canonical DNA systems.<sup>15,16</sup>

To determine the level of hybridisation, the dA ssDNA was combined with samples of **T6** as described in Chapter 2, Section 2.5.4.1, such that the net concentration of nucleobases in solution remained constant. The absorbance versus **T6**/dA ssDNA concentration ratios are shown in Figure 6.7. The hybridisation would therefore appear as an inverted peak, minimum absorbance occurring at the ratio of the dA ssDNA to **T6** that resulted in the greatest hybridisation.

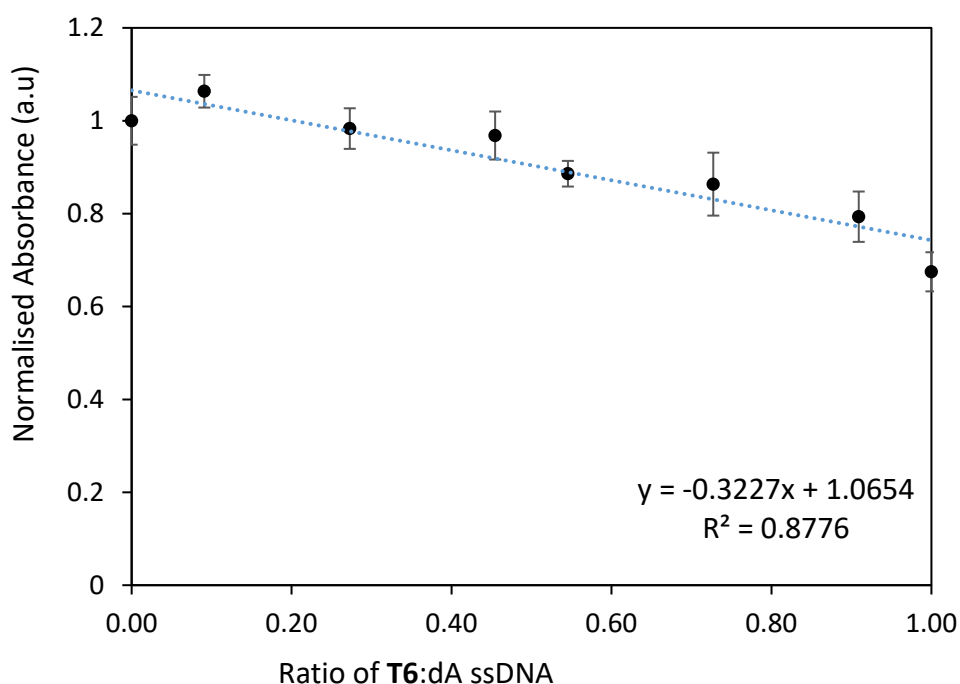


Figure 6.7 The absorbance with increasing ratio of **T6** to dA ssDNA at 260 nm, average of 4 samples, in 10 mM TRIS-HCl buffer.

The data showed that increasing ratio of **T6** to the dA ssDNA in solution resulted in an overall decrease in absorption, and that this was approximately linear. This decrease could not be determined to be caused by binding, as it was consistent with what would be expected for the dilution of the higher absorbing dA ssDNA by the lower absorbing **T6** sample. Therefore this does not show direct evidence of the hybridisation occurring between the two strands.

This experiment did show that the equivalent concentration of **T6** resulted in a decrease in absorption of 32.5% compared to the dA ssDNA. This gives two important pieces of information. Firstly, that the **T6** still shows absorption in the 260 nm region associated with DNA, indicating nucleobase functionality was still present. Secondly, if there was any binding to form a duplex it was not significantly effecting the absorption of either compound. This does not explicitly rule out the formation of base pairs, but it does show that they may not form a traditional double helix.

## **6.6 Determination of Duplex Formation Using Fluorescent Dyes**

The determination of DNA hybridisation is frequently measured by the addition of intercalator dyes.<sup>17,18</sup> These dyes bind to DNA as described in Chapter 1, Section 1.4.5. As a result, they were used to interrogate some of the binding properties of the dA ssDNA-**T6** duplex that would be formed. If the dyes show the same fluorescence response when exposed to the dA ssDNA-**T6** duplex that is seen with the dAdT dsDNA this would show that the binding is almost identical. Conversely, no change in fluorescence response to the dA ssDNA-**T6** duplex would indicate no binding is present. An intermediate result would indicate an alternative binding site has formed.

There are a number of possible dyes that can be used to illicit binding properties of DNA that will be considered in this chapter including the SYBR<sup>(R)</sup> range of dyes and Yo-Pro-1 Iodine. Four stains were tested, namely SYBR Safe, dsGreen (equivalent to SYBR Green I), Yo-Pro-1 and SYBR Green II.

Throughout this section the concentration of the fluorescent dyes will be referred to in terms of “X” for concentration. Due to the proprietary nature of the dyes, unfortunately, there was no direct conversion for this measure into standardised units, such as mM or g L<sup>-1</sup>. Through this

chapter the provided concentrations of dye before dilution was 10,000X dye in dimethyl sulfoxide (DMSO). Based on the result presented in Chapter 3, Section 3.4.3.1, DMSO may affect the solubility of the nucleotide functionalised alkyl polymer. However, as the dye was diluted below 1/100 of the original concentration, the interaction of the DMSO was deemed insignificant.

For measuring the fluorescence, a Qiagen® Rotor-Gene Q real time PCR instrument was used. This instrument was chosen because it was a high throughput system able to measure 72 samples at low volumes (20 µL) meaning that replicates can be conducted in a single run to minimise variation between measurements. Further, it was designed for use with the dyes used in this section, specifically the SYBR binding dyes.

One limitation of this method was that the fluorescence detector can be over saturated for some samples, requiring the automatic adjustment of the signal gain. As a result, the gain was recorded with the data, and samples that saturated the detector are noted. These samples exceed the detection limit the Rotor-Gene Q. This automatic adjustment of gain was limited to 10, raising it further could have introduced artefacts and reduce reproducibility between runs by amplifying secondary effects, for example additional fluorescence from the plastic of the PCR tubes.

#### **6.6.1 Binding and Properties of SYBR Safe® DNA stain**

The most common series of dyes used in DNA staining was the SYBR series produced by Thermo Fisher Scientific. For the initial round of testing SYBR Safe® was chosen for its relative versatility as it could be used in a wide range of tests including being free in solution, added into precast gels or added into gels post-electrophoresis. The structure of SYBR Safe is shown in Figure 6.8. SYBR Safe was primarily used as a dsDNA dye for measuring the

formation of dsDNA during hybridisation processes.<sup>19</sup> This was possible due to its higher quantum yield when confined between the stacked bases of dsDNA compared to ssDNA.

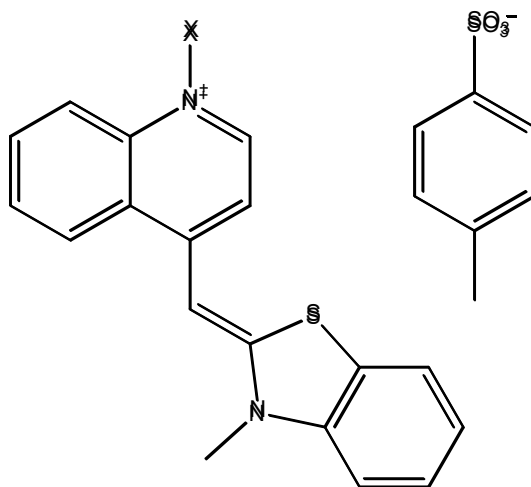


Figure 6.8 Structure of SYBR Safe dye.

### 6.6.2 Optimisation of T6 Concentration for Investigation of Dye Binding

The first step in preparing for the dye measurements was to optimise the concentration of **T6**. Optimising the concentration of the **T6** was required for a number of reasons. As was seen in Chapter 5, the nucleotide functionalised polymers are able to form particles, and due to the limited solubility of the alkyl backbone, it was considered important to minimise the probability that the **T6** would precipitate after binding to the dA ssDNA. If the duplex became insoluble and precipitated then this could significantly affect the fluorescence measurements. In addition, the batch process for synthesis of **T6** meant that getting all the measurements from the same batch was important, as a separate batch of **T6** may have a different  $M_w$  and dispersity.

Samples of the **T6** 21-mer were prepared in MilliQ water at concentrations between 1  $\mu$ M and 1 mM to determine the optimum concentration for the fluorescent dye binding studies, with each concentration prepared in quadruplicate. For these measurements the concentration of SYBR Safe was maintained constant at 5X concentration. This concentration was chosen based on previous work from Bou *et al.*<sup>20</sup> investigating similar polymer DNA properties. These **T6**



samples were heated from 25 °C to 99 °C and their fluorescence measured at 1 °C intervals on the Qiagen® Rotor-Gene Q real time PCR instrument. The results are shown in Figure 6.9.

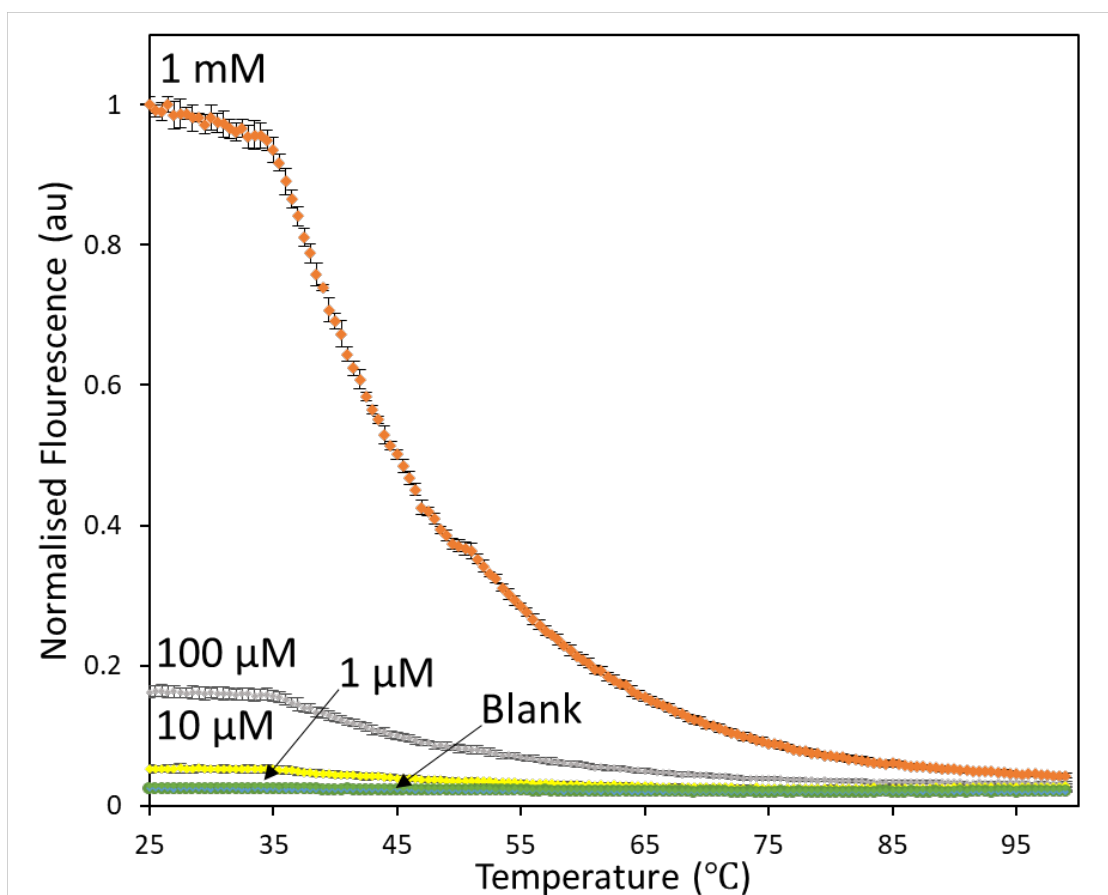


Figure 6.9 Normalised fluorescence of 5X SYBR Safe (blue) and with T6 at 1 mM (orange), 100 µM (grey), 10 µM (yellow) and 1 µM (green). Samples run in quadruplicate at gain 10.

The first note from this data was that the fluorescence begins to sharply decline at 35 °C. This temperature was consistent across the 1 mM, 100 µM and 10 µM concentrations, measured with only its magnitude changing between samples. The 1 µM sample appeared to be only slightly above the background SYBR Safe fluorescence (<1%) meaning that it was unsuitable for further measurements.

Importantly all samples decrease to similarly low levels, <1.5% at higher temperatures. This suggested that the dye was no longer confined, as the confinement of the dye causes the fluorescence.

The 10  $\mu\text{M}$  solution appears to show the best balance of analyte consumption to fluorescence yield, giving 5% of the fluorescence from the 1 mM sample for only 1% of the **T6**. As a result, 10  $\mu\text{M}$  solutions of **T6** was chosen for further work. Further, this concentration produced high enough signal above the background to discriminate any decrease in fluorescence caused by the binding of dA ssDNA.

### 6.6.3 Optimisation of the SYBR Safe Concentration.

Following the optimisation of the **T6** concentration the next step was to optimise the concentration of the SYBR® Safe dye. Following the thermal profile seen in the **T6** optimisation, there were a few important considerations for this process. Primarily, the high gain required to produce that signal meant that the separation between blank and sample needed to be maximised both in magnitude and error. Further, the distinct thermal profile seen means that this profile needed to be maintained for investigating the melting behaviour of any **T6**-dA ssDNA duplex.

To do this samples of SYBR Safe were prepared with and without the 10  $\mu\text{M}$  **G6**. The concentration of SYBR Safe was varied between 0 and 12.5X in 2.5X increments. The fluorescence of these samples was measured using a Q-gen® real time PCR machine at 25 °C and again at 99 °C (Figure 6.10(a and b, respectively)).

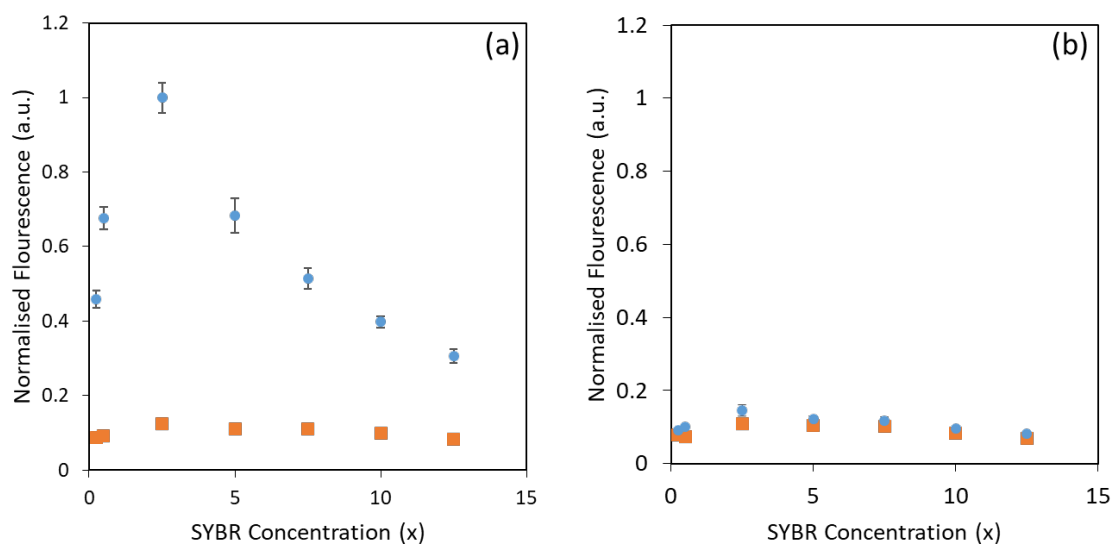


Figure 6.10 Normalised fluorescence of SYBR Safe with 10  $\mu\text{M}$  **T6** (blue) and without (orange) at (a) 25 °C and (b) 99 °C. Samples run in quadruplicate at gain 10, error bars are displayed in both plots though fit within the marker for some data points.

These results showed that the greatest difference in fluorescence between samples with and without **T6** occurs at a SYBR Safe concentration of approximately 2.5X. This result was unexpected as the presence of more dye would be expected to create a higher fluorescence signal. The reason this was not the case may be due to an increase above the critical micelle concentration of the SYBR safe dye, partially attributed to the dye having a relatively low affinity for the **T6**. This means that at the lower concentrations there was an increase in fluorescence with increasing concentration as a result of there being more dye bound to the **T6**. When the concentration increases enough the dye begins forming secondary structures competitively with the dye binding to **T6**. This may be in part due to the DMSO required to solvate the dye initially increases in concentration with the dye and improves the solubility of the **T6**. A decrease in fluorescence of 85% for the 2.5X sample between 25 °C and 99 °C, with all samples decreasing to a similar level.

As with the measurements in Section 6.6.2 this was attributed to the non-confinement of the dye at higher temperatures. This was supported by the same decrease observed in the samples not containing **T6**.

From these results it was observed that the best concentration for discrimination between the blank and the **T6** sample was at 2.5X and as a result it was this concentration that was used for further SYBR dye measurements.

#### 6.6.4 Effect of Sodium Chloride on SYBR Interaction

Sodium chloride (NaCl) can play a significant role in the conformation of DNA, being a major contributor to the conversion between A-, B-, and C- forms of the double helix (see Chapter 1, Section 1.3.2 for further details). Similarly, the presence of NaCl can affect the solubility of DNA and methacrylate polymers.

To ensure this was not an issue, samples of 10  $\mu\text{M}$  **T6** and 2.5X SYBR safe were prepared with NaCl concentrations between 5 mM and 1 M (see Chapter 2, Section 2.5.4.3 for experimental details), in quadruplicate. These samples were then heated from 25 °C to 99 °C and their fluorescence measured at 1 °C intervals. If the presence of the NaCl was impeding the binding of the SYBR safe dye there would be a significant change in the melting curve, as the dye would not be released because it had not bound to the duplex formed. The results are shown in Figure 6.11.

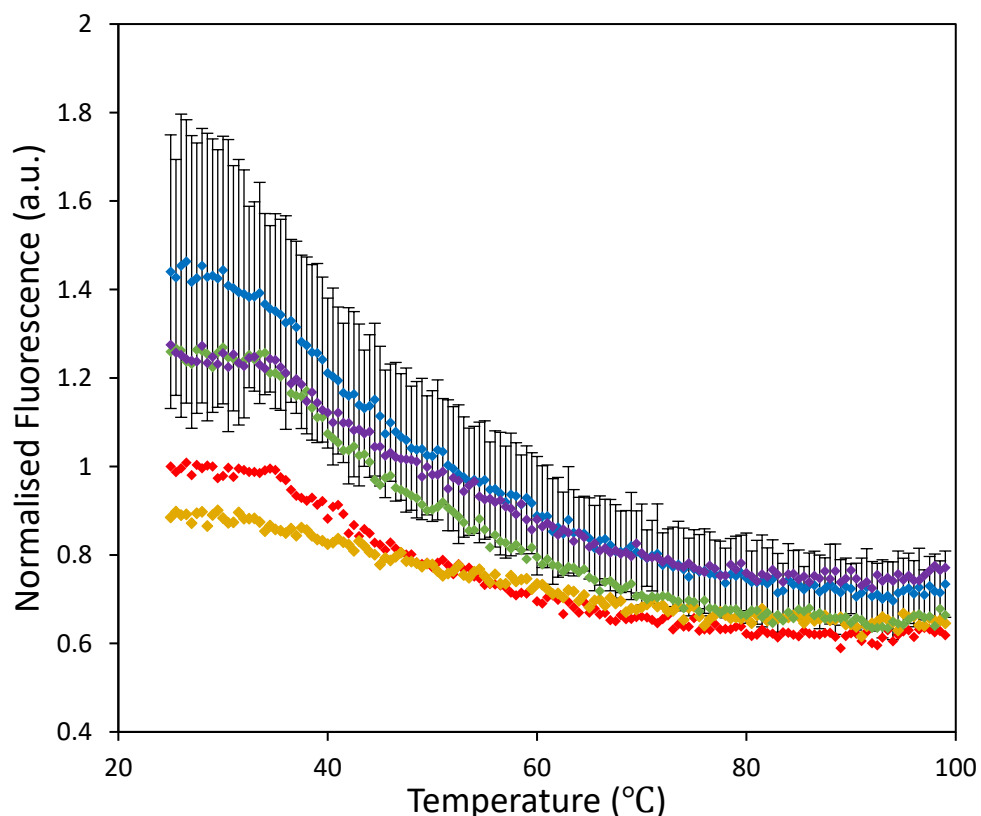


Figure 6.11 Normalised fluorescence of 2.5X SYBR Safe with 10  $\mu$ M **T6** with the addition of different loadings of NaCl ; 5 mM (purple), 10 mM (blue), 20 mM (green), 50 mM (yellow), and 100 mM (red). Samples run in quadruplicate at gain 10. Error bars included for the 10 mM NaCl sample are similarly representative of all samples.

Most importantly these measurements showed a low reproducibility between samples as indicated by the large error bars. This demonstrated that the addition of sodium chloride interfered with the binding and stabilisation between the **T6** and SYBR safe dye. This could be due to the destabilisation of the SYBR Safe ion pair, or the change in solubility of **T6**. For this reason, no NaCl was added to further experiments.

### 6.6.5 Effect of Pre-annealing on Fluorescence

The final parameter to check was if pre-annealing the **T6** would affect the binding of the SYBR Safe dye. The annealing process involved heating the samples and then rapidly cooling them to generate specific conformations. These measurements were also conducted in TRIS-HCl buffer as this would be required for the addition of ssDNA in subsequent sections.

To do this, four 100  $\mu\text{L}$  samples of 10  $\mu\text{M}$  **T6** were prepared in 10 mM TRIS-HCl buffer then heated to either 45  $^{\circ}\text{C}$  or 95  $^{\circ}\text{C}$  from room temperature, held at that temperature for 15 min, before being cooled. SYBR Safe 2.5X was then added (see Chapter 2, Section 2.5.4.2, for experimental details). These temperatures were chosen as 45  $^{\circ}\text{C}$  was above the 35  $^{\circ}\text{C}$  seen in Section 6.6.2 Figure 6.9 where the fluorescence rapidly drops. The 95  $^{\circ}\text{C}$  point was chosen as a maximum temperature control to prevent boil off of the solvent. This heating process was conducted using a generic PCR heating block before measuring the samples on the Rotor-Gene Q. The measurements are shown in Figure 6.12.

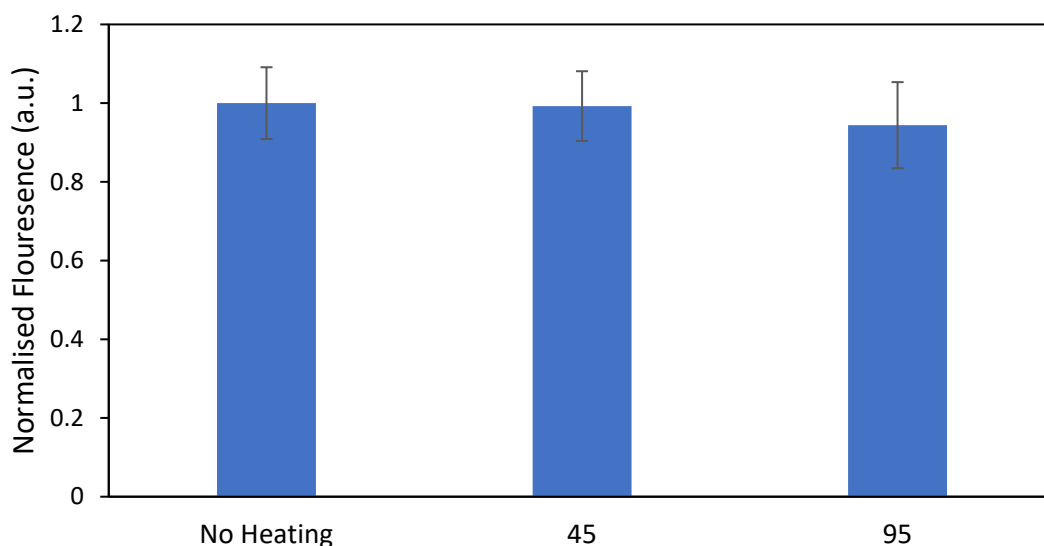


Figure 6.12 Normalised fluorescence of SYBR Safe with **T6** following annealing at temperatures indicated.

These results demonstrated that the interaction of **T6** with SYBR Safe was not affected significantly by annealing the sample before the addition of SYBR Safe. This shows that any structures that may have been formed by the heating of **T6** were not retained upon cooling, allowing the **T6** to be available to bind dA ssDNA.

## **6.7 Comparison of Binding Interactions of dA ssDNA with Complementary Polymers**

Following the optimisation of the various concentration parameters, measurement of the interactions between **T6** and the complementary dA ssDNA were conducted. The dyes are all reported in the same concentration units (X) which was designed to be detected using the same instrumental parameters (i.e., 1X SYBR SAFE should have a similar signal intensity to 1X SYBR Green II). In addition optimisation of the process was considered beyond the scope of the project so the process used for optimising SYBR Safe was not repeated for each of the remaining dyes.

Further, to exclude effects of the alkyl polymer backbone an additional sample of poly(acrylic acid) (pAA) was used. This was chosen due to pAA having a significantly improved solubility in water compared to pHPMA while still retaining an alkyl backbone. The effect of the ionisable acid was considered acceptable within this approximation to compare to the ionisation of the phosphate. The pKa of pAA is reported to be 4.5<sup>21</sup> which puts in in the range of reported pKa for adenosine of between ~3.6-4.3.<sup>22</sup>

Finally, a dT ssDNA 23-mer was also tested with each of the binding dyes. This sequence was chosen as it was complementary to the dA ssDNA 23-mer, and provided a positive control for the formation of double stranded DNA and the associated hybridisation

### 6.7.1 Interactions with SYBR Safe Dye

The first dye tested was SYBR Safe. This dye binds to dsDNA, leading to its confinement and an increase in fluorescence. For this experiment the signal increase for the combination of **T6** with dA ssDNA would indicate the formation of a double helix with base pair stacking similar to that seen in traditional double stranded DNA systems. For that reason the combination of dT ssDNA and dA ssDNA was also measured, as this would hybridise to form dsDNA.

Samples were prepared at 10  $\mu\text{M}$  with 2.5X SYBR Safe in 10 mM TRIS-HCl buffer, full experimental details are presented in Chapter 2, Section 2.5.4.4. The samples to undergo hybridisation have a loading of 10  $\mu\text{M}$  of the duplex to account for hybridisation, i.e. 10  $\mu\text{M}$  dA ssDNA and 10  $\mu\text{M}$  dT ssDNA results in 10  $\mu\text{M}$  dAdT dsDNA. Fluorescence was measured at 25  $^{\circ}\text{C}$  with the results shown in Figure 6.13.

As expected, Figure 6.13 shows that the combination of dA ssDNA and dT ssDNA resulted in far greater fluorescence than any other sample, exceeding the detection limit of the instrument at the maximum permitted gain settings. This showed that the SYBR Safe has an increased quantum yield in the presence of dsDNA.

Interestingly the fluorescence of the SYBR Safe in the presence of **T6** is 290% that seen in the dA ssDNA and 241% greater than that seen in dT ssDNA alone. This suggests that the **T6** only sample confines the SYBR Safe dye, but the insertion does not lead to a dramatically higher fluorescence state.



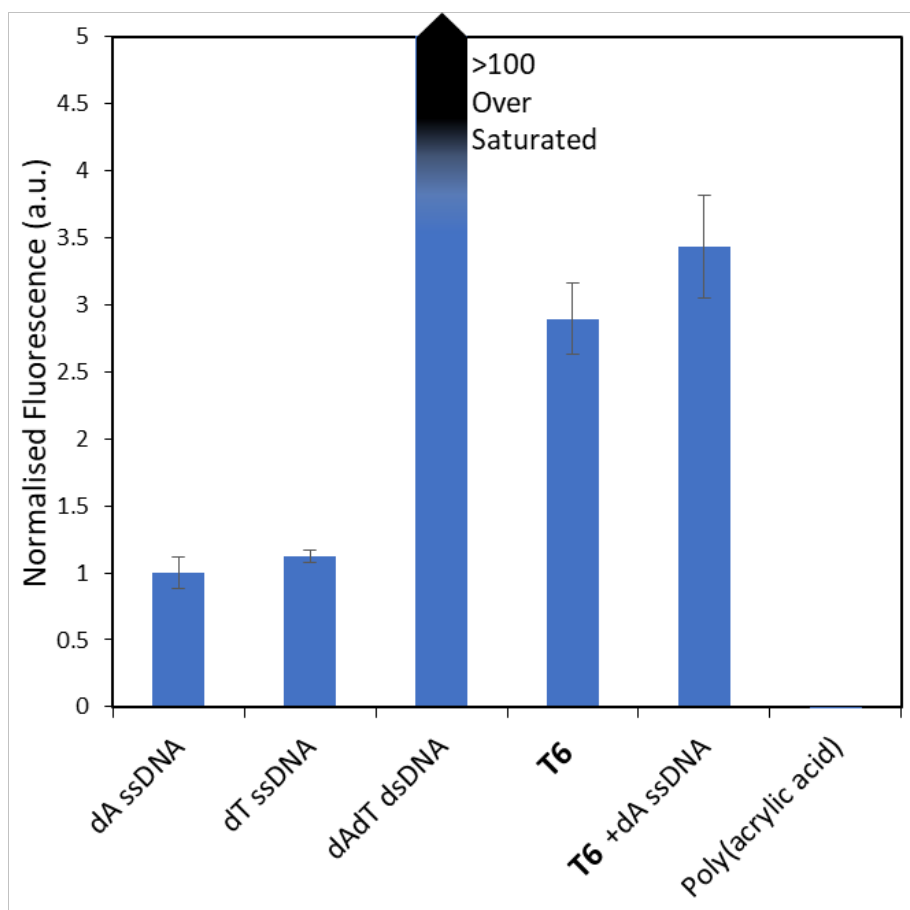


Figure 6.13 Background corrected fluorescence of samples treated with SYBR Safe containing ssDNA and **T6** in combinations shown. Samples normalised to dA ssDNA and run in quadruplicate at gain 10, 25 °C.

The measured fluorescence of the dA ssDNA + **T6** sample was significantly lower than the fluorescence measured for dsDNA. This indicated that any hybridisation was not in the same conformation as dsDNA. This result was therefore consistent with the findings of Section 6.4.2.

The lack of fluorescence signal for the pAA shows that the confinement provided by the **T6** does not come solely from the hydrophobic alkyl backbone of the polymer.

### 6.7.2 Interactions with dsGreen

Following testing with SYBR Safe the experiment was repeated with dsGreen, Figure 6.14. dsGreen was more sensitive to dsDNA than SYBR Safe being both an intercalator and a minor groove binder with both binding sites causing fluorescence (see Chapter 1, Section 1.4.5 for

further details).<sup>23</sup> The experimental conditions were the same as the Section 6.6.1 with the only change being the substitution of the dye. These results are presented in Figure 6.15.

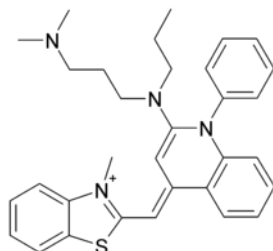


Figure 6.14 Structure of dsGreen.

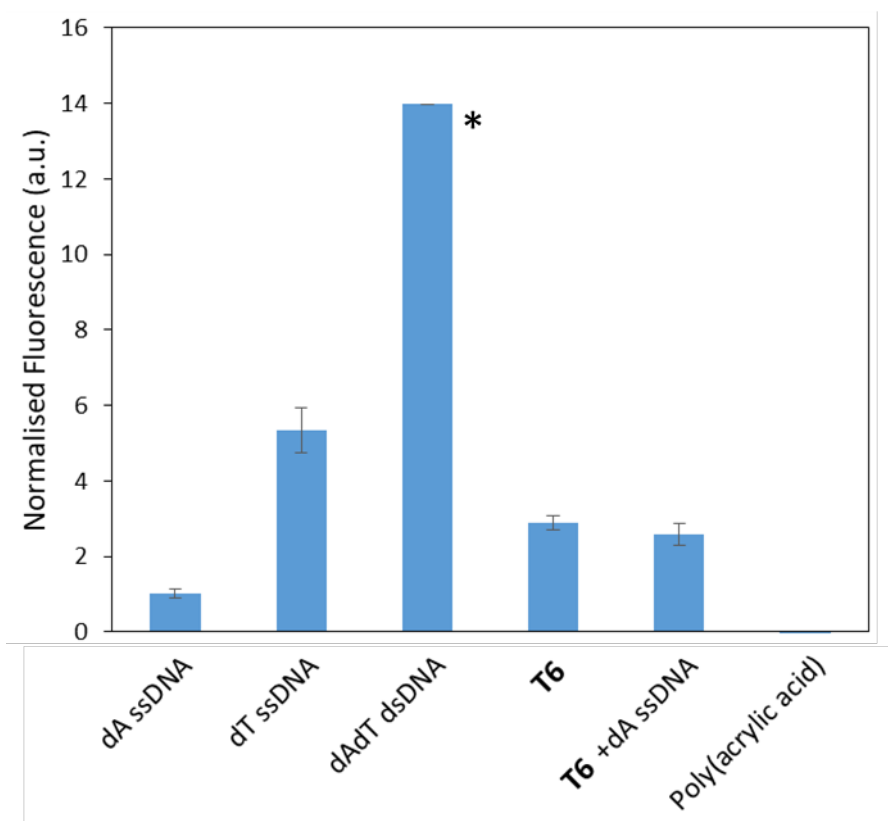


Figure 6.15 Background corrected fluorescence of samples treated with dsGreen containing ssDNA and **T6** in combinations shown. Samples normalised to dA ssDNA and run in quadruplicate at gain 10 at 25 °C. Samples marked \* indicate oversaturation of the detector.

These results show, again, that the dsDNA (A-T) creates a much stronger fluorescent signal than any of the individual single stranded component. The overall response from the samples

was significantly higher than the recorded measurements for SYBR Safe, roughly an order of magnitude, showing that the dsGreen gives better detection of the dsDNA.

The data shows that the affinity for dsGreen was higher towards thymine than adenine, based on the increased fluorescence for both dT ssDNA and **T6** compared to dA ssDNA. This was likely due to the 6 membered heterocycle pyrimidine being better able to bind the dye than the larger 9 membered heterocycle purine, as reported by Somoza *et al.*<sup>22</sup> Similar selectivity for cytosine dyes, the class dsGreen belongs too, was reported by Agbavwe *et al.* who attributed this to the difference in the ability to undergo  $\pi$ - $\pi$  stacking.

The detector was once again saturated with the signal from dAdT dsDNA indicating that the canonical duplex has a stronger affinity for the dye. The combination of **T6** with dA ssDNA also did not lead to an increase in fluorescence, within the margin of error the combination caused a decrease of 11%. This may suggest that the addition of the dA ssDNA causes the removal of bound dsGreen from the **T6**. This further suggests that a complex structure was forming between the dA ssDNA and **T6** which was in turn binding the dye, but based on the magnitude of fluorescence it was not able to increase the quantum yield to the extent of equivalent dsDNA.

### 6.7.3 Interactions with Yo-Pro-1 Dye

The next dye tested was Yo-Pro-1 iodide (Yo-Pro), Figure 6.16. Yo-Pro was a mono-intercalating dye that binds between base pairs at a 1:3 spacing of Yo-Pro:base pairs. It has been shown by Biebricher *et al.*<sup>17</sup> that this leads to a higher fluorescent yield with dsDNA due to the more rigid structure of the double helix. For these measurements the same concentration of analyte was used as for the previous SYBR dyes, 10  $\mu$ M, but the Yo-Pro iodide concentration was lowered to 1X compared to the 2.5X used for SYBR dyes. The fluorescence was then measured using the Q-gen® real time PCR machine. The results are shown in Figure 6.17.

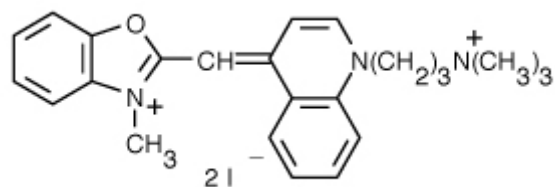


Figure 6.16 Structure of Yo-Pro iodide.

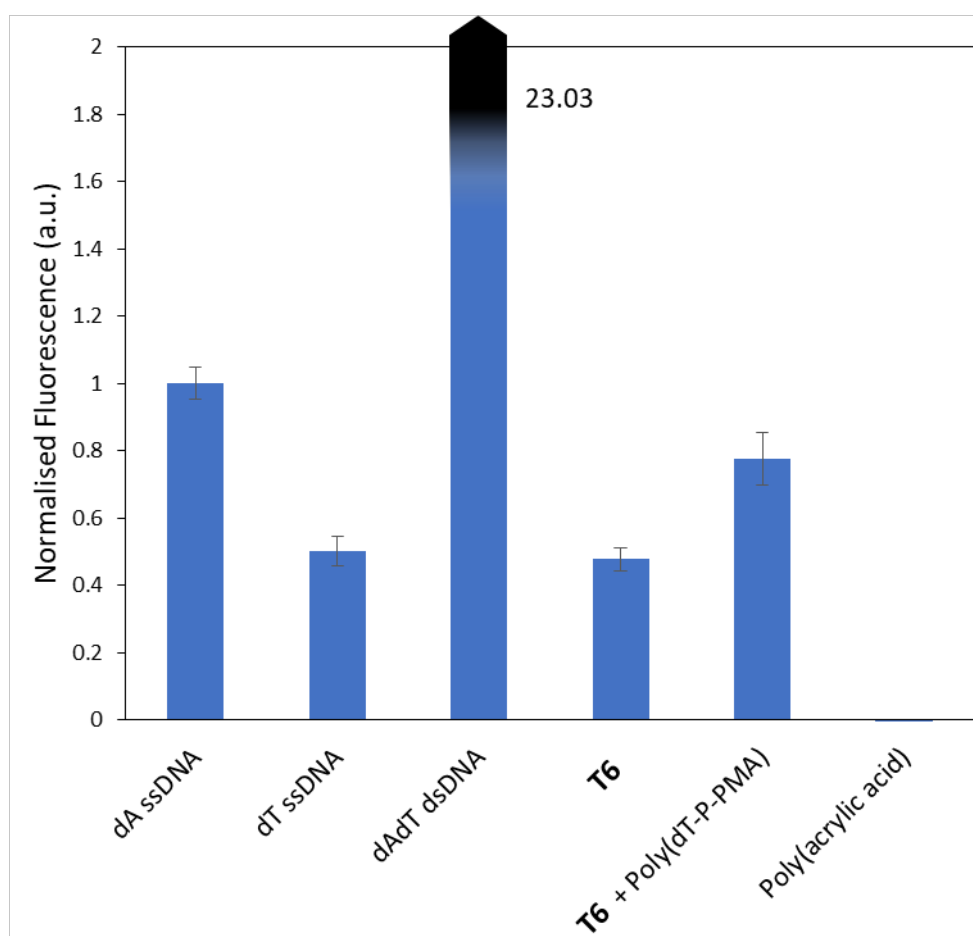


Figure 6.17 Background corrected fluorescence of samples treated with Yo-Pro iodide ssDNA and **T6** in combinations shown. Samples normalised to dA ssDNA and run in quadruplicate at gain 2.67, 25 °C.

The first important thing to note with these samples was the magnitude of the signal intensity. Due to the high fluorescence intensity the gain on the photomultiplier was lowered to 2.67, compared to 10 for SYBR stains, to get the same signal intensity for the dA ssDNA. This can

be attributed to the higher efficiency of the Yo-Pro when bound. Further, the signal intensity for the pAA standard remained at 0, indicating that again, as with SYBR, there was no fluorescence caused by binding to the alkyl backbone of the vinyl based polymers.

As with SYBR, Yo-Pro shows the highest fluorescence with the dsDNA sample, greater than the sum of the two individual ssDNA samples. Distinctly though it now shows a statistically significant increase in fluorescence for the dA ssDNA compared to dT ssDNA indicating a possible preference in binding. Somoza *et al.* have reported that this behaviour is present in guanine and adenine rich sequences of ssDNA due to the increased rigidity caused by the size of the purine nucleobases.<sup>24</sup> When the dA ssDNA was combined with **T6** again the fluorescence decreased compared to the dA ssDNA by itself.

#### 6.7.4 Interactions with SYBR Green II

The major difference between SYBR Green II and the other dyes tested was that it was considered selective for ssDNA and RNA. There was no available structure for SYBR Green II as it was a trade secret. It was also the only dye tested that was of unknown binding, but this selectivity has been demonstrated experimentally.<sup>25</sup> As with SYBR Safe the dye was prepared at a 2.5X loading with 10  $\mu$ M of each analyte tested, the results of the fluorescent measurements shown in Figure 6.18.

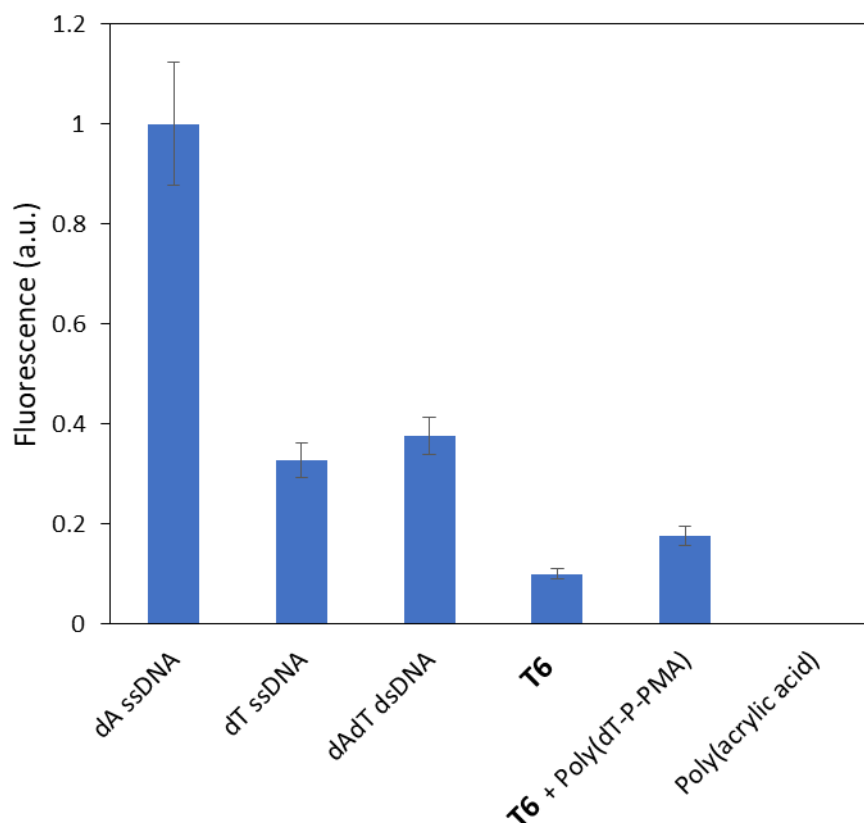


Figure 6.18 Background corrected fluorescence of samples treated with SYBR Green II containing ssDNA and **T6** in combinations shown. Samples normalised to dA ssDNA and run in quadruplicate at gain 10, 25 °C.

The sample containing dA ssDNA showed the highest fluorescence. This was due to the adenine being a purine, containing a larger aromatic structure. This in turn was able to bind to the SYBR Green II more effectively as reported in literature.<sup>26</sup> By comparison thymine samples (dT ssDNA and **T6**) have a lower fluorescence response because it was a smaller pyrimidine.

When the dA ssDNA was combined with a complementary nucleobase sequence (dT ssDNA or **T6**) the binding of the adenine by the thymine displaces the SYBR Green II dye, causing the fluorescence to decrease. This change indicates that there was successful hybridisation between the **T6** and dA ssDNA, but that it was not structurally comparable to that of dsDNA.

## 6.8 Structural Hypothesis

From the investigations into the binding of different fluorescent dyes it was hypothesised that the shorter spacing of bases in **T6**, and by extension all nucleotide functionalised alkyl-based polymers, causes a shorter space between rotations. This in turn leads to the ssDNA wrapping around the alkyl polymer in order to bind to it, creating an asymmetric helix as shown in Figure 6.19. This new structure prevents the binding of traditional dyes, but was detectable by measuring the decrease in fluorescence caused by the displacement of the ssDNA bound dye. This is unlikely to be a 1:1 binding as idealised in Figure 6.19, but rather a series of regions bound in this manner.

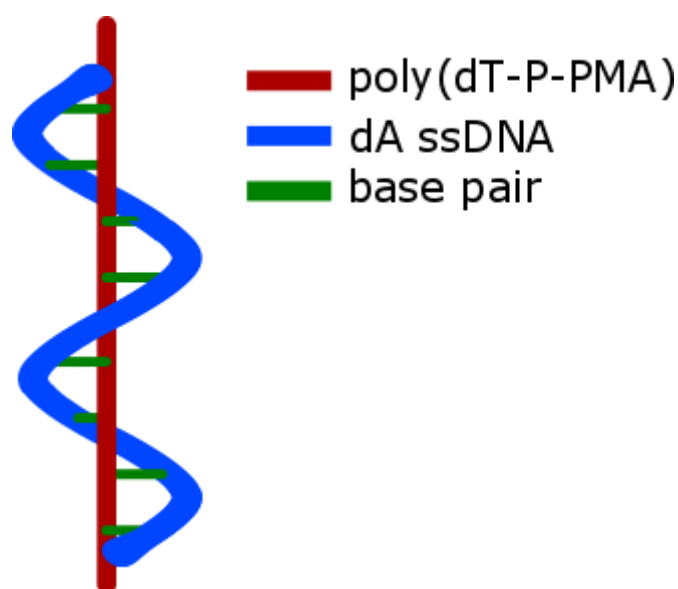


Figure 6.19 Proposed screw-like helix formed around **T6** by dA ssDNA.

## 6.9 Conclusion

From the information covered in this chapter it was possible to determine that there was binding occurring between the **T6** and a DNA structure containing its complementary nucleobase, namely dA ssDNA. However, the nature of this binding was not clear. The change in fluorescence of the dyes in the presence of **T6** following addition of dA ssDNA showed that

there was binding occurring between them. The magnitude of the change in fluorescence seen following the addition showed that the spacing of nucleotides does not offer the same confinement of the dye as it did for the similar complementary dsDNA under the same conditions. It was hypothesised that this was the result of the shorter spacing between bases in the **T6** caused by the shorter distance between repeating units in the polymer chain, compared to dT ssDNA equivalent, impairing the binding of the subsequent confinement of the dye which would have led to a higher fluorescence signal.

## 6.10 References

- (1) Caruthers, M. H. Gene Synthesis Machines: DNA Chemistry and Its Uses. *Science* **1985**, *230* (4723), 281–285.
- (2) Cahill, R.; Cookson, R. C.; Crabb, T. A. Geminal Coupling Constants in Methylene Groups-II. J in CH<sub>2</sub> Groups  $\alpha$  to Heteroatoms. *Tetrahedron* **1969**, *25* (19), 4681–4709.
- (3) Breslauer, K. J.; Frank, R.; Blocker, H.; Marky, L. A. Predicting DNA Duplex Stability from the Base Sequence. *Proc. Natl. Acad. Sci.* **1986**, *83* (11), 3746–3750.
- (4) Huguet, J. M.; Ribezzi-Crivellari, M.; Bizarro, C. V.; Ritort, F. Derivation of Nearest-Neighbor DNA Parameters in Magnesium from Single Molecule Experiments. *Nucleic Acids Res.* **2017**, *45* (22), 12921–12931.
- (5) Russell, M. A.; Laws, A. P.; Atherton, J. H.; Page, M. I. The Mechanism of the Phosphoramidite Synthesis of Polynucleotides. *Org. Biomol. Chem.* **2008**, *6* (18), 3270.
- (6) Zhang, L.; Zhou, W. Two Descent Hybrid Conjugate Gradient Methods for Optimization. *J. Comput. Appl. Math.* **2008**, *216* (1), 251–264.



- (7) Livieris, I. E.; Tampakas, V.; Pintelas, P. A Descent Hybrid Conjugate Gradient Method Based on the Memoryless BFGS Update. *Numer. Algorithms* **2018**, *79* (4), 1169–1185.
- (8) Yang, X.; Luo, Z.; Dai, X. A Global Convergence of LS-CD Hybrid Conjugate Gradient Method. *Adv. Numer. Anal.* **2013**, *2013*, 1–5.
- (9) Beers, K. L.; Boo, S.; Gaynor, S. G.; Matyjaszewski, K. Atom Transfer Radical Polymerization of 2-Hydroxyethyl Methacrylate. *Macromolecules* **1999**, *32* (18), 5772–5776.
- (10) Robinson, K. L.; Khan, M. A.; De Paz Báñez, M. V.; Wang, X. S.; Armes, S. P. Controlled Polymerization of 2-Hydroxyethyl Methacrylate by ATRP at Ambient Temperature. *Macromolecules* **2001**, *34* (10), 3155–3158.
- (11) Desjardins, P.; Conklin, D. NanoDrop Microvolume Quantitation of Nucleic Acids. *J. Vis. Exp.* **2010**, No. 45.
- (12) Bhushan, B. *Handbook of Nanomaterials Properties*; 2006; Vol. 44.
- (13) Gray, B. Basic Biochemical Methods. *Biochem. Educ.* **1985**, *13* (4), 186.
- (14) Xodo, L. E. Characterization of the DNA Triplex Formed by d(TGGGTGGGTGGTTGGGTGGG) and a Critical R · Y Sequence Located in the Promoter of the Murine Ki-Ras Proto-Oncogene. *FEBS Lett.* **1995**, *370* (1–2), 153–157.
- (15) Rosu, F.; Gabelica, V.; De Pauw, E.; Antoine, R.; Broyer, M.; Dugourd, P. UV Spectroscopy of DNA Duplex and Quadruplex Structures in the Gas Phase. *J. Phys. Chem. A* **2012**, *116* (22), 5383–5391.
- (16) Rhodes, W. The Symmetry and Spectral Properties of Helical Polynucleotides. *Radiat.*

*Res.* **1963**, 20 (1), 120.

- (17) Biebricher, A. S.; Heller, I.; Roijmans, R. F. H.; Hoekstra, T. P.; Peterman, E. J. G.; Wuite, G. J. L. The Impact of DNA Intercalators on DNA and DNA-Processing Enzymes Elucidated through Force-Dependent Binding Kinetics. *Nat. Commun.* **2015**, 6 (1), 7304.
- (18) Armitage, B. A. Cyanine Dye-DNA Interactions: Intercalation, Groove Binding, and Aggregation. *Top. Curr. Chem.* **2005**, 253, 55–76.
- (19) Gudnason, H.; Dufva, M.; Bang, D. D.; Wolff, A. Comparison of Multiple DNA Dyes for Real-Time PCR: Effects of Dye Concentration and Sequence Composition on DNA Amplification and Melting Temperature. *Nucleic Acids Res.* **2007**, 35 (19), e127.
- (20) Bou, S. J. M. C.; Connolly, A. R.; Ellis, A. V. High-Throughput Physicochemical Analysis of Thermoresponsive Polymers. *Polym. Chem.* **2018**, 9 (15), 1934–1937.
- (21) Michaels, A.S.; Morelos, O.; Polyelectrolyte adsorption by kaolinite. *Ind Eng Chem.* **1955**, 47,1801–1809
- (22) Thaplyal, P.; Bevilacqua, P.C.; Experimental Approaches for Measuring pKa's in RNA and DNA, *Methods Enzymol.* **2014**; 549: 189–219.
- (23) Zipper, H.; Brunner, H.; Bernhagen, J.; Vitzthum, F. Investigations on DNA Intercalation and Surface Binding by SYBR Green I, Its Structure Determination and Methodological Implications. *Nucleic Acids Res.* **2004**, 32 (12), e103–e103.
- (24) Agbavwe, C.; Somoza, M. M. Sequence-Dependent Fluorescence of Cyanine Dyes on Microarrays. *PLoS One* **2011**, 6 (7), e22177.

- (25) Law, J. C.; Facher, E. A.; Deka, A. Nonradioactive Single-Strand Conformation Polymorphism Analysis with Application for Mutation Detection in a Mixed Population of Cells. *Anal. Biochem.* **1996**, *236* (2), 373–375.
- (26) Section 8.1-Nucleic Acid Stains, The Molecular Probes Handbook, Thermofisher Technical Reference Library. Accessed online 2018-06-20.

## Chapter 7: Conclusion

### 7.1 Synopsis

*This aim of this thesis was to develop a method for the synthesis of alkyl based polymers bearing nucleotide functionality with a view to creating a DNA analogue.*

*Chapter 3 demonstrated the fundamental basis for the process through the phosphoramidite coupling method to generate the required class of monomer. Chapter 4 built on this to show that a polymer could be synthesised that contained guanine functionality. This polymer and its secondary interactions were further investigated in Chapter 5 with the determination that they formed complexes analogous to those found in DNA.*

*Chapter 6 applied the techniques and information gathered to determine that the thymine nucleotide polymer bioconjugate underwent binding to complementary DNA.*

## 7.2 Concluding Remarks and Future Work.

Chapter 1 presented the prior work on the convergence of biological nucleic acid and synthetic polymerisation techniques, demonstrating that nature has already achieved what artificial methods are still attempting to replicate (Section 1.5.2). The body of literature presented shows that achieving this through a hybrid method of combined biological and synthetic techniques has formed a foundation on which to build. The incorporation of nucleic acid fragments has already built a foundation for this work (Section 1.7). Building upon that, this thesis has developed a monomer possessing both nucleic acid and radical polymerisation compatible moieties. What has made this work unique is that it is the first to combine the full nucleic acid repeating unit, a nucleotide.

The work presented in Chapter 3 demonstrated the coupling method for attaching a vinyl moiety from a methacrylate, to a nucleotide in the form of 5'-dimethoxytrityl-N-benzoyl-2'-deoxycytosine,3'-[(2-cyanoethyl)-(N,N-diisopropyl)]-phosphoramidite (Section 3.3). This was achieved through the use of a modified phosphoramidite coupling method, created for this project. This resulted in the formation of the **C3** monomer. Confirmation of this coupling was achieved through the use of proton and <sup>31</sup>phosphorous nuclear magnetic resonance (NMR) spectroscopy. This was through the substitution of the diisopropyl amine peak at 1.2 ppm with a pair of peaks associated with the HPMA conjugation at 6.25 ppm and 5.7 ppm.

Subsequently the bioconjugate monomer was found to undergo radical polymerisation successfully, but testing resulted in the formation of a polymer-gel (Section 3.4). The remainder of the chapter investigated the formation of this gel, determining its characteristics and properties to prevent it happening in subsequent iterations of the procedure. Fourier transform infrared spectroscopy demonstrated that the nucleic acid functionality had been retained within the gel, ruling out hydrolysis of the nucleotide connection to the methacrylate. Testing with a

variety of solvents revealed that the most likely cause of the **C4** forming a gel was the diene caused by substitution of the methacrylate moieties while in solution.

Chapter 4 demonstrated how the limitations of the initial method could be overcome for the synthesis of a monomer capable of forming a stable polymer by adjusting the vinyl source to block the substitution that caused the diene to form (Section 4.2). This was achieved using a 2-hydroxypropyl methacrylate, and conjugating it to the 5'-dimethoxytrityl-*N*-isobutyryl-2'-deoxyguanosine,3'-[(2-cyanoethyl)-(diisopropyl)]-phosphoramidite, resulting in 5'-dimethoxytrityl-*N*-isobutyryl-2'-deoxyguanosine,3'-[(2-cyanoethyl)-(oxypropyl methacrylate)]-phosphate monomer. This conjugation was again confirmed through the use of proton and <sup>31</sup>phosphorous NMR spectroscopy (Section 4.3). The appearance of peaks 3.6 ppm and 5.3 ppm in the proton NMR spectrum combined with the removal of the 2.9 ppm peak associated with the substituted diisopropyl amine confirmed the conjugation. The <sup>31</sup>phosphorous NMR showed a shift from 148 ppm to the 2 ppm range indicating that the phosphorous had oxidised to the desired P(V) state of the phosphate.

The successful conjugation was further confirmed through the use of electrospray ionisation mass spectrometry where the peak at 883 m/z and the associated adducts further confirmed the conjugation.

Chapter 4 further demonstrated the compatibility of the **G3** monomer with radical polymerisation and the controlled growth that could be achieved (Section 4.4). Though preliminary experiments showed the formation of a stable suspension, further investigated in Chapter 5, the successful polymerisation was confirmed through size exclusion chromatography.

Additional investigation of the polymerisation of **G3** utilised both *in-situ* and *ex-situ* measurements to determine that the polymerisation was proceeding under RAFT mediated conditions (Section 4.5). The *in-situ* NMR spectroscopy methods demonstrated that the polymerisation of **G3** monomer initially begins under the expected RAFT control based on the distinct growth period, followed by a decrease as monomer availability in solution decreases. The addition of SEC as a technique showed that there is a distinct plateau in the rate of polymerisation at ~22 repeating units incorporated, indicating the maximum  $M_w$  attainable using this methodology.

Chapter 5 investigated the formation of particles from the **G6** in solution. It was found that these particles were forming as the result of g-quartets forming between the guanine units of the **G6** chains, resulting in the formation of g-quadruplexes (Section 5.3).<sup>1</sup> These g-quadruplexes were found to form more strongly in the presence of the monovalent potassium, consistent with the g-quadruplexes found in other DNA systems. The measurement of the structures formed using the ATTO 550 fluorescent dye with microscopy and melting analysis indicated the formation of a vesicle like structure with a hydrophobic shell and hydrophilic core (Section 5.5).

Finally, Chapter 6 investigated the formation of duplexes between the thymine functionalised homopolymer, **T6** and a complementary sequence dA ssDNA. Computer modelling using the Firefly computational modelling system demonstrated that the binding was possible, and introduced strain to the system forming a non-typical structure (Section 6.4). This was further supported through the investigation of the binding with fluorescence dyes, comparing their relative affinity to the canonical DNA duplex to that seen for the polymer-ssDNA duplex (Section 6.7).

### 7.3 Future Work

The synthesis of nucleotide functionalised polymers as presented in this thesis demonstrate a distinct method to those presented previously. The resulting polymers bare a structural similarity closer, to that seen in natural systems, and therefore should be further investigated in systems where this similarity may provide a benefit.

Most notably among these is enzymatic compatibility. The polymers presented here show that when a vinyl back bone is generated through a radical addition there remains a binding affinity for DNA, as presented in Chapter 6. The extension of this then would be to generate a ribose phosphate backbone using a polymerase enzyme and determine if this allows the radical polymerisation to be conducted afterwards. If possible, this presents a route for the synthesis of sequence-controlled polymers beyond what has been achieved to date.<sup>2</sup> Along this line then is the expansion of the monomer library, utilising different vinyl sources such as the amides considered in Chapter 3 Section 3.2.2, and non-natural nucleotides.

Utilising the current polymers though there is scope to investigate their binding and use as a scaffold in the synthesis of nanostructures. Previous literature has shown that DNA can be used to form structures through origami like folding,<sup>2,3</sup> but the potential to create these structures from more resilient alkyl polymers increases the range of potential applications.

The potential resilience of the alkyl based polymers able to bind DNA selectively could also increase the availability of DNA sensors. Currently the conditions required for the preservation of DNA restrict their possible application. The polymers presented here may assist in overcoming this as the alkyl based polymer would be incompatible with biological breakdown mechanisms, such as bacteria, and more thermally stable due to the carbon-carbon back bone.



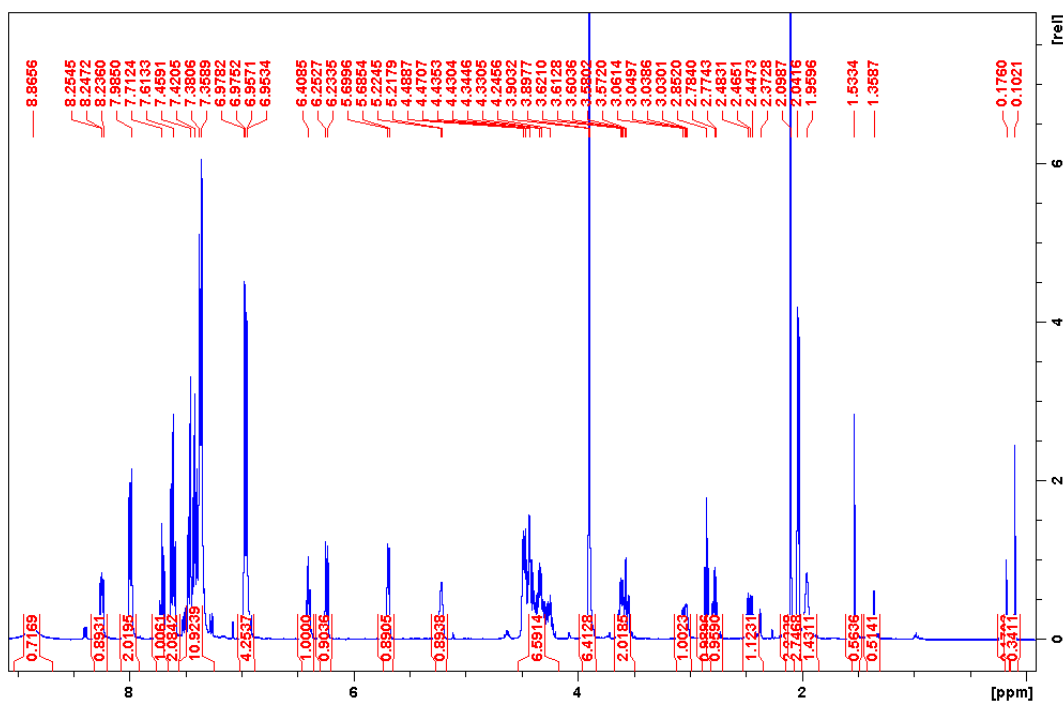
To determine if this is the case further work is required to investigate the biocompatibility of the polymers presented.

Overall, the work presented in this thesis is a significant step towards the use of biological processes for the synthesis of tailored artificial polymers over a broad range of applications.

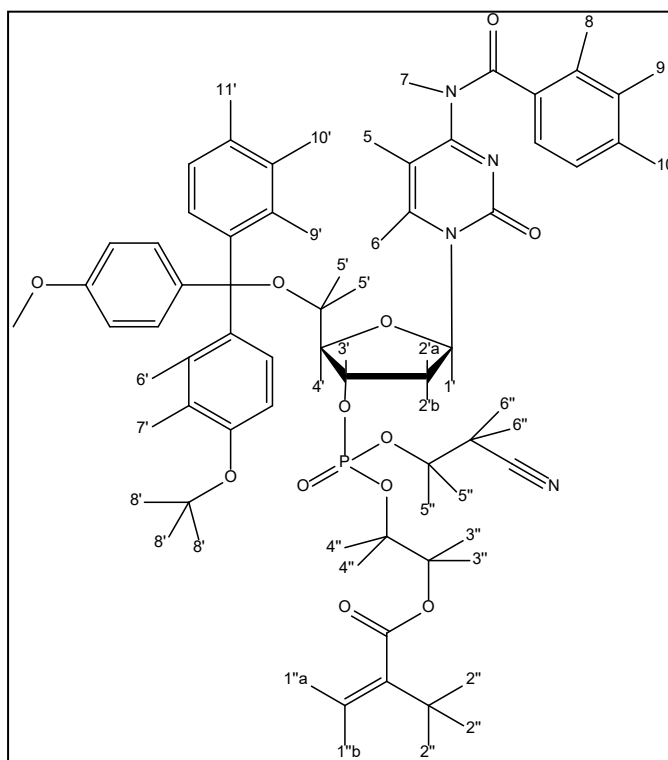
## 7.4 References

1. Wilson, M. J., Fenati, R. A., Williams, E. G. L., Ellis, A. V. *New J. Chem.*, **2018**, 42, 8815–8822.
2. Yang, D., Campolongo, M. J., Nhi Tran, T. N., Ruiz, R. C. H., Kahn, J. S., Luo, D. *Wiley Interdiscip. Rev. Nanomedicine Nanobiotechnology*, **2010**, 2, 648–669.
3. Kuzuya, A., Komiyama, M. *Nanoscale*, **2010**, 2, 310–322.

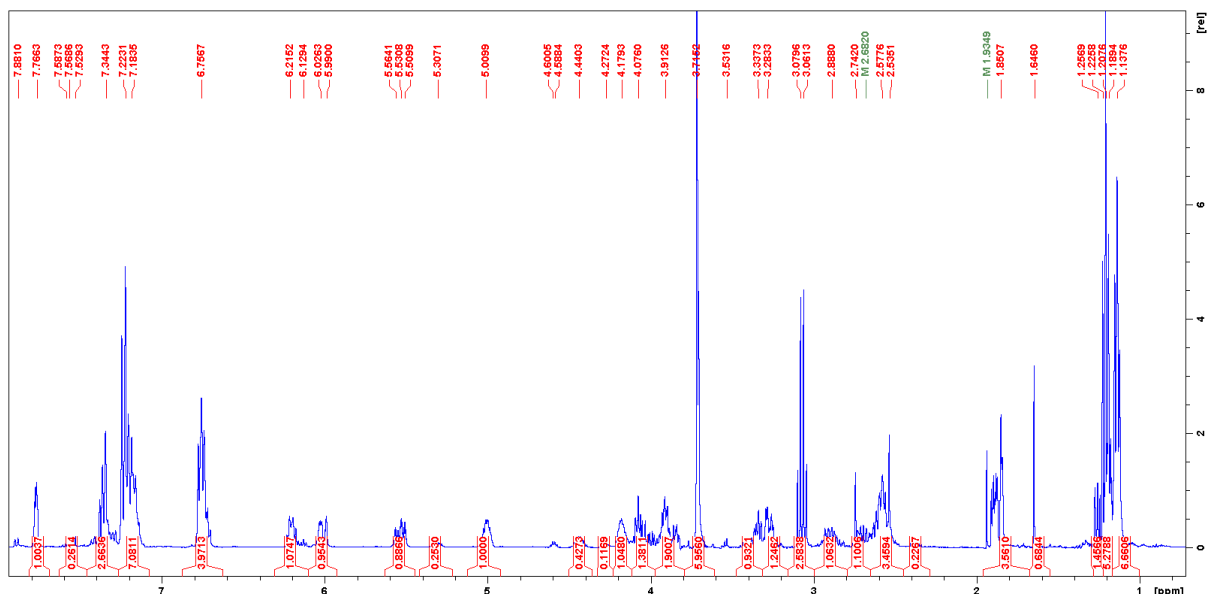
## Appendix 1: C3 <sup>1</sup>H NMR Peak Attributions



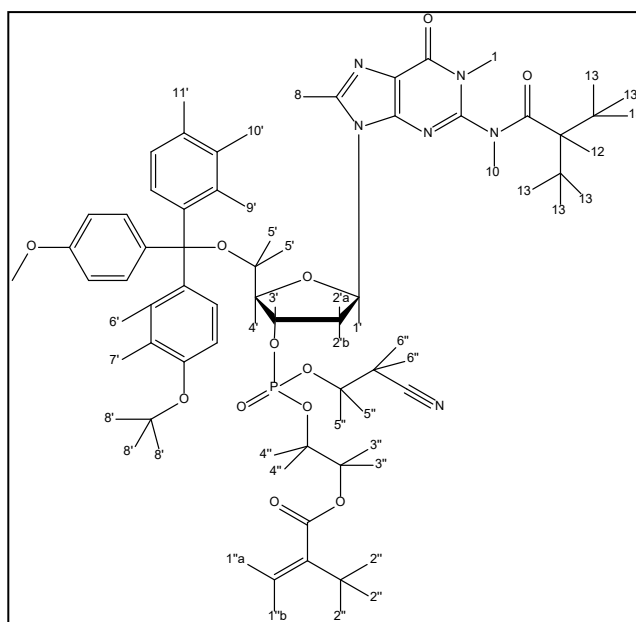
Proton Position	Shift (ppm)
5	8.8656
6	8.2472
8	7.985
9	7.7124
10	7.6133
11'	7.4591
9'	7.4205
10'	7.4205
6'	7.375
7'	6.9752
1'	6.4085
1''a	6.2527
1''b	5.6696
4'	5.2245
4''	4.4707
3''	4.4353
5''	4.3446
3'	4.2456
8'	3.9032
5'	3.6036
7	3.0386
2'a	2.4651
2'b	2.3728
6''	2.0987
2''	2.0416



## Appendix 2: G3 <sup>1</sup>H NMR Peak assignments

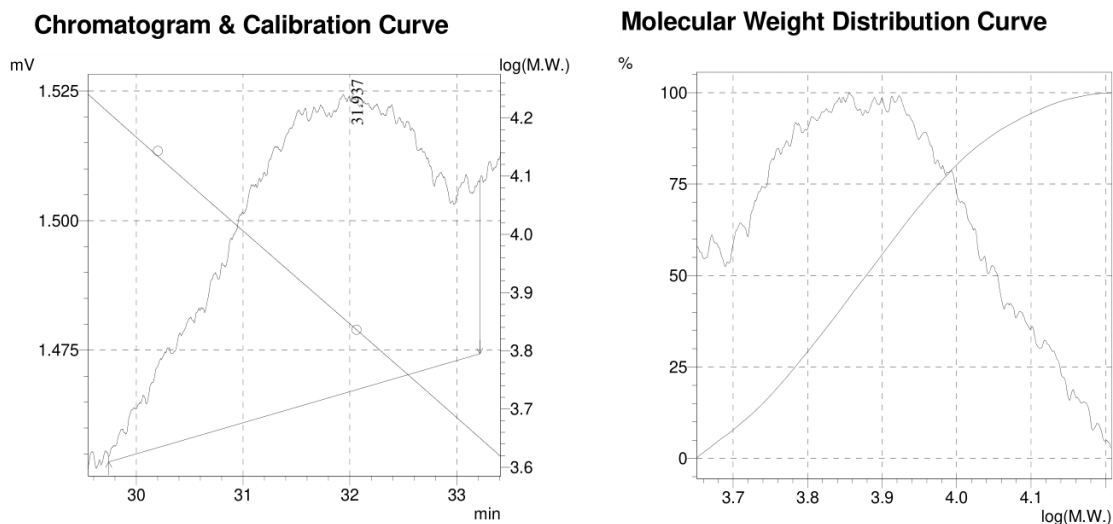


Proton Position	Chemical Shift (ppm)
8	7.7663
12	1.2569
13	1.1376
1'	6.2152
2'a	2.5351
2'b	2.5776
3'	4.076
4'	5.0099
5'	3.3373
6'	7.3443
7'	6.7567
8'	3.7152
9'	7.1835
10'	7.2231
1''a	5.5308
1''b	6
2''	1.8507
4''	4.4403
5''	4.1793
6''	3.9126



### Appendix 3: Example DRI chromatograms for the polymerisation kinetics of G3.

30 minutes.



#### GPC Calculation Results

Peak#: 1 (Detector B Channel 1)

[Peak Information]

	Time(min)	Volume(mL)	Molecular Weight	Height
Start	29.742	29.742	16177	1453
Top	31.937	31.937	7178	58
End	33.217	33.217	4468	1474

Area : 7810

Area% : 100.0000

[Average Molecular Weight]

Number Average Molecular Weight(Mn)	7339
Weight Average Molecular Weight(Mw)	8000
Z Average Molecular Weight(Mz)	8741
Z+1 Average Molecular Weight(Mz1)	9516
Mw/Mn	1.09008
Mv/Mn	0.00000
Mz/Mw	1.09255

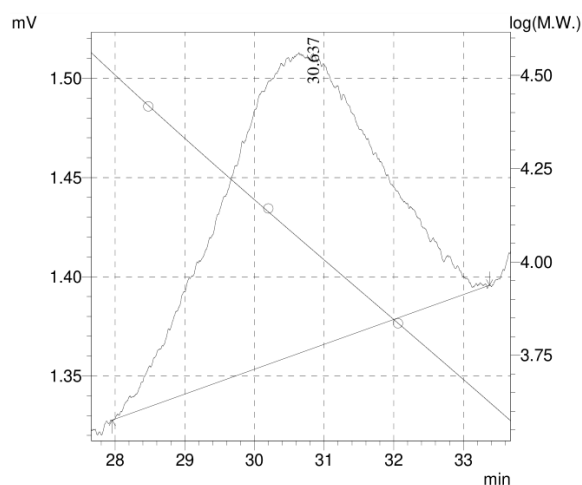
Detector B Channel 1

[Average Molecular Weight(Total)]

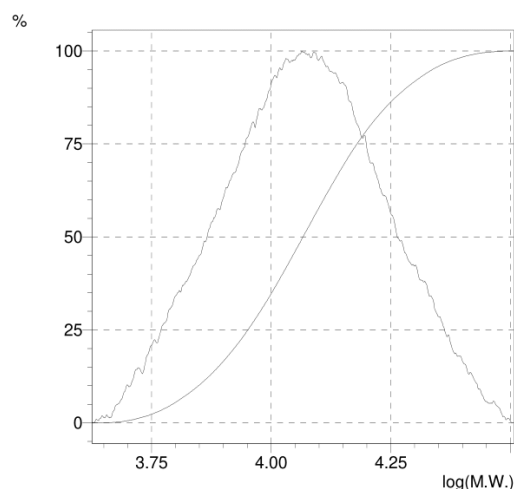
Number Average Molecular Weight(Mn)	7339
Weight Average Molecular Weight(Mw)	8000
Z Average Molecular Weight(Mz)	8741
Z+1 Average Molecular Weight(Mz1)	9516
Mw/Mn	1.09008
Mv/Mn	0.00000
Mz/Mw	1.09255

60 minutes.

### Chromatogram & Calibration Curve



### Molecular Weight Distribution Curve



### GPC Calculation Results

Peak#:1 (Detector B Channel 1)

[Peak Information]

	Time(min)	Volume(mL)	Molecular Weight	Height
Start	27.958	27.958	32225	1328
Top	30.637	30.637	11586	151
End	33.375	33.375	4211	1396

Area : 23811

Area% : 100.0000

[Average Molecular Weight]

Number Average Molecular Weight(Mn)	10867
Weight Average Molecular Weight(Mw)	12488
Z Average Molecular Weight(Mz)	14288
Z+1 Average Molecular Weight(Mz1)	16155
Mw/Mn	1.14913
Mv/Mn	0.00000
Mz/Mw	1.14416

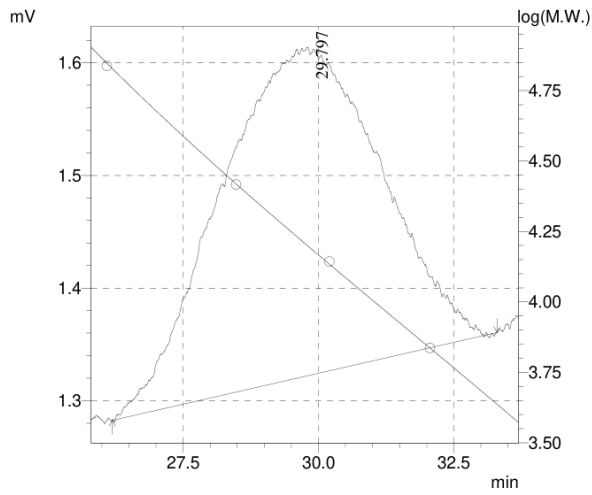
Detector B Channel 1

[Average Molecular Weight(Total)]

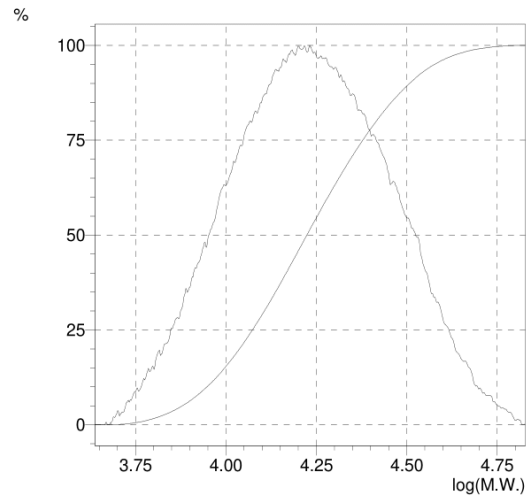
Number Average Molecular Weight(Mn)	10867
Weight Average Molecular Weight(Mw)	12488
Z Average Molecular Weight(Mz)	14288
Z+1 Average Molecular Weight(Mz1)	16155
Mw/Mn	1.14913
Mv/Mn	0.00000
Mz/Mw	1.14416

90 minutes.

**Chromatogram & Calibration Curve**



**Molecular Weight Distribution Curve**



**GPC Calculation Results**

Peak#: 1 (Detector B Channel 1)

[Peak Information]

	Time(min)	Volume(mL)	Molecular Weight	Height
Start	26.192	26.192	67361	1283
Top	29.797	29.797	15847	292
End	33.300	33.300	4331	1361

Area : 60386

Area% : 100.0000

[Average Molecular Weight]

Number Average Molecular Weight(Mn)	15003
Weight Average Molecular Weight(Mw)	18977
Z Average Molecular Weight(Mz)	23800
Z+1 Average Molecular Weight(Mz1)	28983
Mw/Mn	1.26489
Mv/Mn	0.00000
Mz/Mw	1.25415

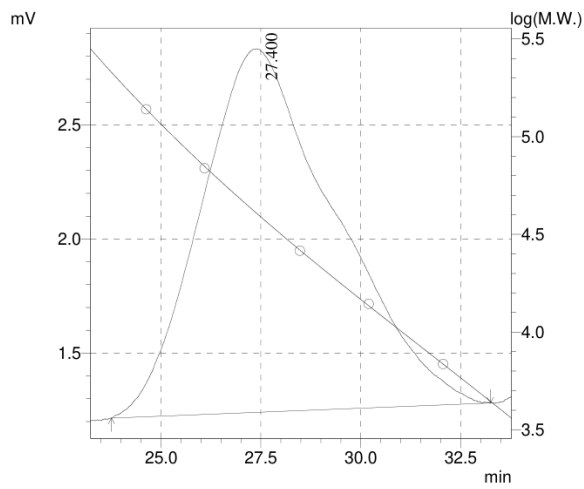
Detector B Channel 1

[Average Molecular Weight(Total)]

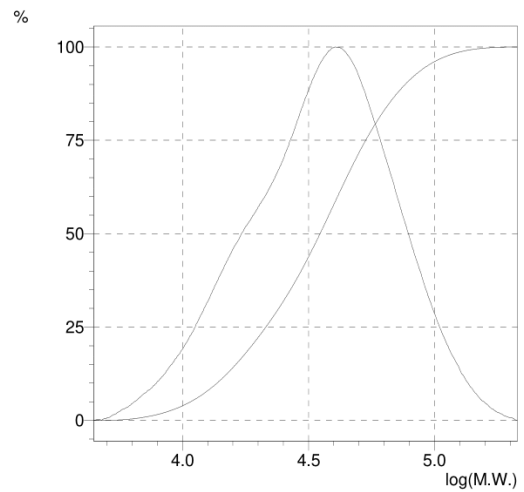
Number Average Molecular Weight(Mn)	15003
Weight Average Molecular Weight(Mw)	18977
Z Average Molecular Weight(Mz)	23800
Z+1 Average Molecular Weight(Mz1)	28983
Mw/Mn	1.26489
Mv/Mn	0.00000
Mz/Mw	1.25415

240 minutes.

### Chromatogram & Calibration Curve



### Molecular Weight Distribution Curve



### GPC Calculation Results

Peak#:1 (Detector B Channel 1)

[Peak Information]

	Time(min)	Volume(mL)	Molecular Weight	Height
Start	23.758	23.758	213525	1215
Top	27.400	27.400	40385	1593
End	33.242	33.242	4427	1281

Area : 372429

Area% : 100.0000

[Average Molecular Weight]

Number Average Molecular Weight(Mn)	26987
Weight Average Molecular Weight(Mw)	41177
Z Average Molecular Weight(Mz)	58685
Z+1 Average Molecular Weight(Mz1)	77622
Mw/Mn	1.52577
Mv/Mn	0.00000
Mz/Mw	1.42520

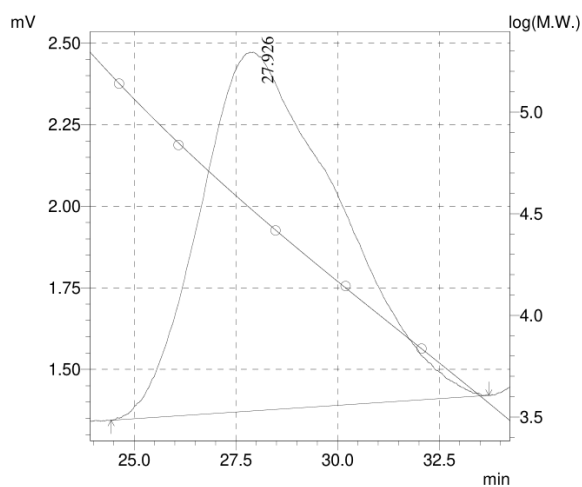
Detector B Channel 1

[Average Molecular Weight(Total)]

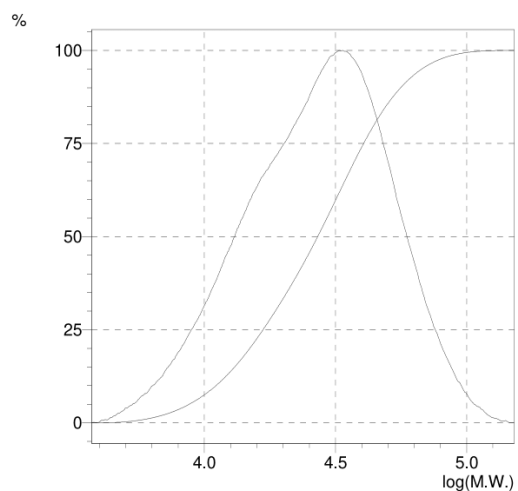
Number Average Molecular Weight(Mn)	26987
Weight Average Molecular Weight(Mw)	41177
Z Average Molecular Weight(Mz)	58685
Z+1 Average Molecular Weight(Mz1)	77622
Mw/Mn	1.52577
Mv/Mn	0.00000
Mz/Mw	1.42520

300 minutes.

### Chromatogram & Calibration Curve



### Molecular Weight Distribution Curve



### GPC Calculation Results

Peak#:1 (Detector B Channel 1)

[Peak Information]

	Time(min)	Volume(mL)	Molecular Weight	Height
Start	24.433	24.433	152067	1344
Top	27.926	27.926	32650	1099
End	33.717	33.717	3702	1421

Area : 258844

Area% : 100.0000

[Average Molecular Weight]

Number Average Molecular Weight(Mn)	21196
Weight Average Molecular Weight(Mw)	30981
Z Average Molecular Weight(Mz)	42401
Z+1 Average Molecular Weight(Mz1)	54154
Mw/Mn	1.46160
Mv/Mn	0.00000
Mz/Mw	1.36863

Detector B Channel 1

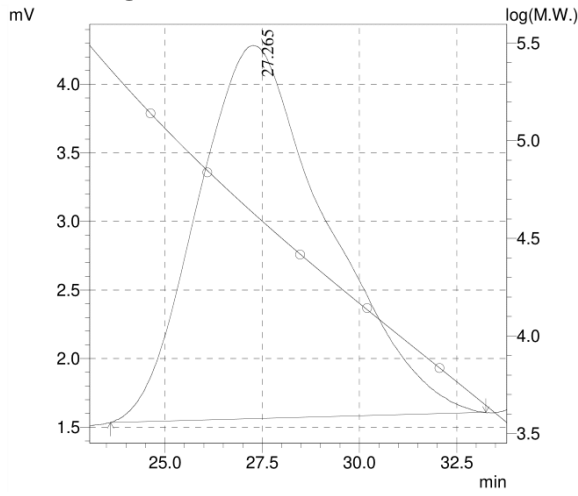
[Average Molecular Weight(Total)]

Number Average Molecular Weight(Mn)	21196
Weight Average Molecular Weight(Mw)	30981
Z Average Molecular Weight(Mz)	42401
Z+1 Average Molecular Weight(Mz1)	54154
Mw/Mn	1.46160
Mv/Mn	0.00000
Mz/Mw	1.36863

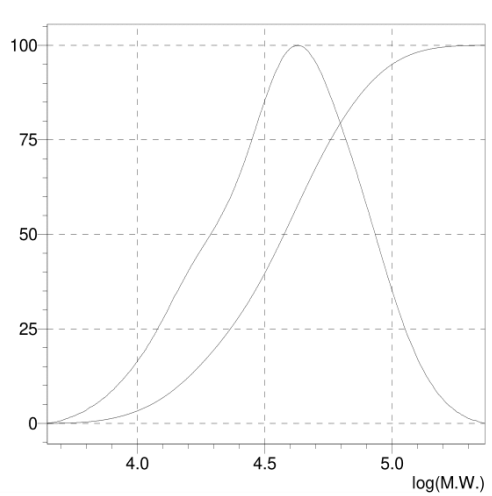


480 minutes

**Chromatogram & Calibration Curve**



**Molecular Weight Distribution Curve**



**GPC Calculation Results**

Peak#:1 (Detector B Channel 1)

[Peak Information]

	Time(min)	Volume(mL)	Molecular Weight	Height
Start	23.600	23.600	231783	1533
Top	27.265	27.265	42699	2722
End	33.250	33.250	4413	1607

Area : 633752  
Area% : 100.0000

[Average Molecular Weight]

Number Average Molecular Weight(Mn)	28817
Weight Average Molecular Weight(Mw)	44129
Z Average Molecular Weight(Mz)	62630
Z+1 Average Molecular Weight(Mz1)	82356
Mw/Mn	1.53133
Mv/Mn	0.00000
Mz/Mw	1.41926

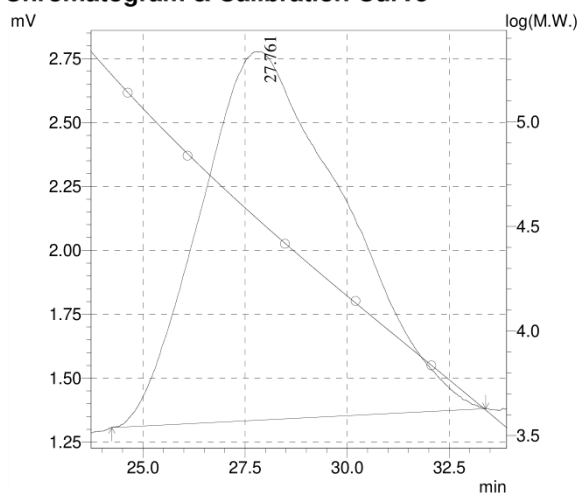
Detector B Channel 1

[Average Molecular Weight(Total)]

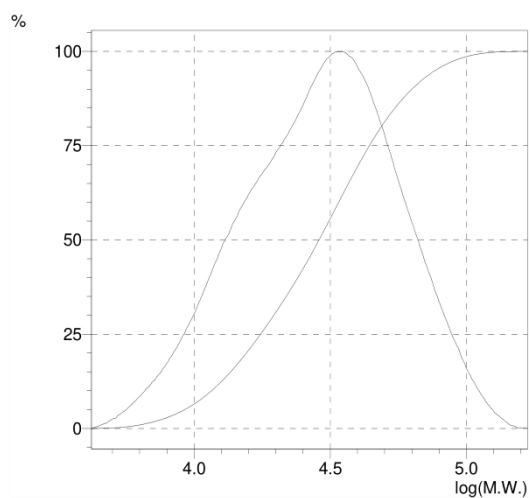
Number Average Molecular Weight(Mn)	28817
Weight Average Molecular Weight(Mw)	44129
Z Average Molecular Weight(Mz)	62630
Z+1 Average Molecular Weight(Mz1)	82356
Mw/Mn	1.53133
Mv/Mn	0.00000
Mz/Mw	1.41926

600 minutes.

### Chromatogram & Calibration Curve



### Molecular Weight Distribution Curve



### GPC Calculation Results

Peak#:1 (Detector B Channel 1)

[Peak Information]

	Time(min)	Volume(mL)	Molecular Weight	Height
Start	24.233	24.233	167870	1307
Top	27.761	27.761	34882	1442
End	33.392	33.392	4185	1381

Area : 354174

Area% : 100.0000

[Average Molecular Weight]

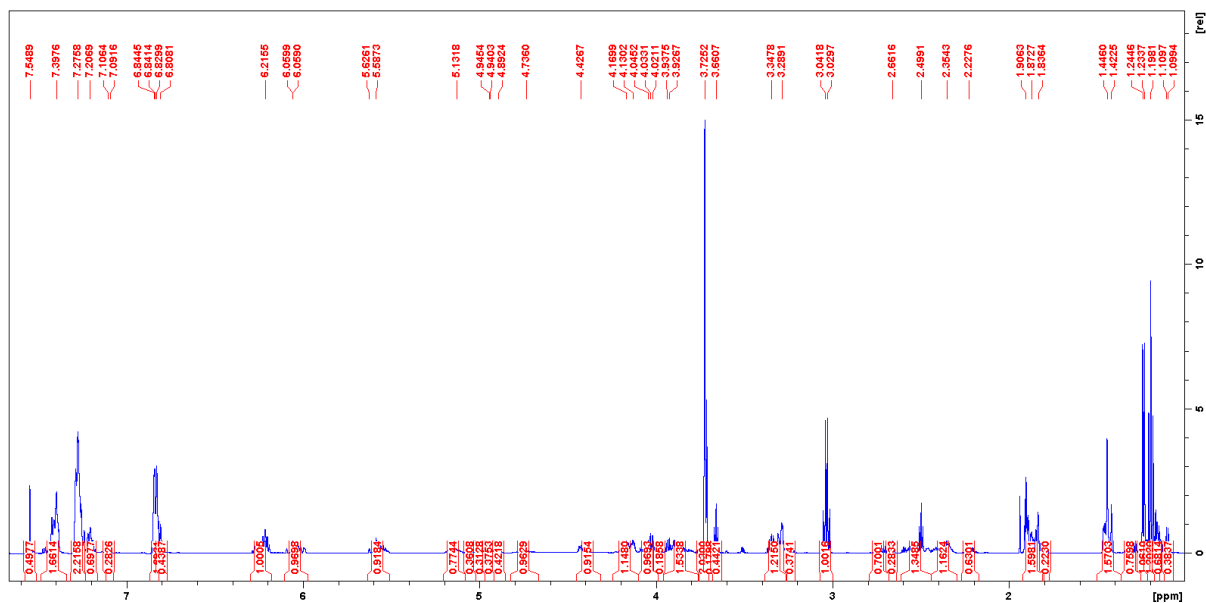
Number Average Molecular Weight(Mn)	22529
Weight Average Molecular Weight(Mw)	33793
Z Average Molecular Weight(Mz)	47598
Z+1 Average Molecular Weight(Mz1)	61846
Mw/Mn	1.49999
Mv/Mn	0.00000
Mz/Mw	1.40850

Detector B Channel 1

[Average Molecular Weight(Total)]

Number Average Molecular Weight(Mn)	22529
Weight Average Molecular Weight(Mw)	33793
Z Average Molecular Weight(Mz)	47598
Z+1 Average Molecular Weight(Mz1)	61846
Mw/Mn	1.49999
Mv/Mn	0.00000
Mz/Mw	1.40850

## Appendix 4: T3 <sup>1</sup>H NMR Peak Attributions



Proton Position	Chemical Shift (ppm)
6	7.5
9'	7.39
10'	7.28
11'	7.2
7'	6.8
1'	6.2
1''a	6.05
1''b	5.58
4'	5.1
5''	4.95
4''	4.736
3''	4.4
3'	4.17
8'	3.8
5'	3.72
6'	3.66
6''	2.73
2'a	2.5
2'b	2.35
2''	2.22
7	1.191

